



UNIVERSIDADE DE VIGO

FUENTES GLOBALES DE HUMEDAD: CARACTERIZACIÓN Y ESTUDIO DE SU VARIABILIDAD

Doctor of Philosophy thesis submitted by Rodrigo Alberto Castillo Rodríguez MSc
within the Programme of Doctor of Philosophy in Climate Sciences: Meteorology,
Physical Oceanography and Climate Change

Advised by Raquel Olalla Nieto Muñiz PhD
and Luis Gimeno Presa PhD

January 2015



UNIVERSIDADE DE VIGO

FUENTES GLOBALES DE HUMEDAD: CARACTERIZACIÓN Y ESTUDIO DE SU VARIABILIDAD

Doctor of Philosophy thesis submitted by Rodrigo Alberto Castillo Rodríguez MSc
within the Programme of Doctor of Philosophy in Climate Sciences: Meteorology,
Physical Oceanography and Climate Change

Advised by Raquel Olalla Nieto Muñiz PhD
and Luis Gimeno Presa PhD

The student PhD

The advisor

The advisor

Ourense, January 2015

Fuentes Globales de Humedad: caracterización y estudio de su variabilidad

Author: Rodrigo Alberto Castillo Rodríguez MSc

Advisor: Raquel Olalla Nieto Muñiz PhD

Advisor: Luis Gimeno Presa PhD

The following website contains updated information about this thesis and related topics:

<http://ephyslab.uvigo.es/tramo/>

Text printed in Ourense

First edition January 2015

Informe de los Directores

La Dra. Raquel Olalla Nieto Muñiz, Profesora Titular y el Dr. Luis Gimeno Presa, Profesor Catedrático ambos pertenecientes al Departamento de Física Aplicada, dentro del área de Física de la Tierra, de la Universidad de Vigo:

CERTIFICAN que:

La presente memoria *“Fuentes Globales de Humedad: caracterización y estudio de su variabilidad”*, resume el trabajo de investigación realizado, bajo nuestra dirección, por D. Rodrigo Alberto Castillo Rodríguez en el departamento de Física Aplicada dentro del programa de doctorado de **“Ciencias del Clima: Meteorología, Oceanografía Física y Cambio Climático”** de la Facultad de Ciencias de Ourense para optar al título de **“DOCTOR POR LA UNIVERSIDAD DE VIGO”**.

Y para que conste y en cumplimiento de la legislación vigente, firman el presente informe en Ourense, a 28 de Noviembre del 2014.

Fdo: Dra. Raquel Olalla Nieto Muñiz

Fdo: Dr. Luis Gimeno Presa

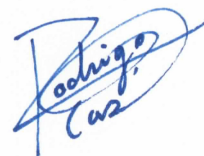
To my parents
and
my beloved departed grandfather
(1918-2008)

Acknowledgements

I would like to thank my advisors Raquel Olalla Nieto Muñiz PhD and Luis Gimeno Presa PhD for their encouragement in the development of this work. I also thank the EPhysLab for allowing me the opportunity to develop this research over the last few years. Thanks are also due to Anita R. Drumond PhD for her valuable contribution in this study and to Ana María Durán Quesada PhD, from whom I received important feedback at the beginning of this project. I also want to thank Orlando García Feal who provided helpful support with coding, data, and optimization. I also gratefully acknowledge the financial support provided by “Xunta de Galicia” through the CHEGA project (INCITE09.383.278), also by the Spanish Ministry responsible for Science for its contribution through the TRAMO project (CGL2012-35485); both these schemes were cofunded by FEDER. I also acknowledge the additional financial grant provided by the University of Costa Rica that made possible the work developed during the PhD Programme in Climate Sciences: Meteorology, Physical Oceanography and Climate Change at the University of Vigo, which allowed the preparation of the thesis herein presented. Finally I want to thank the support of my family, my Costa Rican friends, and all the people I have met during these years, but I would most especially like to thank The Most High.

Rodrigo CR

January 2015

A handwritten signature in blue ink, appearing to read 'Rodrigo CR', with a stylized flourish underneath.

Abstract

The current work is a climatological study and characterization of the global sources of moisture for continental precipitation based on a Lagrangian analysis technique. It consists of a synopsis of a series of articles published in specialist publications, thereby demonstrating the quality of the outcomes. The five key articles form the main structure of this research and it is these that address the crucial aspects of the atmospheric branch of the hydrological cycle, such as the characterization of the global sources of moisture, the interannual variability of the moisture transport, and the distribution of continental precipitation from oceanic moisture source regions. The study provides a robust identification of all major oceanic moisture sources as well as an assessment of their recent changes in amplitude, allowing three key scientific questions to be answered: (i) have the moisture source regions been stationary, or have they changed over the last three decades?, (ii) how do the changes in the intensity (more evaporation) and position of the sources affect the distribution of continental precipitation?, and (iii) what is the role of the main modes of climate variability such as ENSO, NAM and SAM in the variability of the moisture regions and the continental precipitation associated with each source? Moreover, by studying the potential influence on continental precipitation of the oceanic regions with higher evaporation minus precipitation rates in a future climate change scenario, this work is an analysis of the oceanic sources of continental precipitation linked to climate change. Finally, by using a catalogue to identify and characterize all the major moisture sources associated with the continental climatic regions based on two different regionalization schemes, this study provides a reliable and robust assessment of source-sink relationships in the atmospheric water cycle for regional climates, which is a requirement for understanding the major driving factor for extreme weather and climate events.

Resumen

El presente trabajo aborda un estudio detallado y una caracterización climatológica de las fuentes globales de humedad para la precipitación continental, basado en una técnica de análisis Lagrangiano. El corpus del trabajo está basado en una serie de artículos publicados en revistas especializadas, lo que demuestra la calidad de los resultados. Cinco artículos clave forman la estructura principal de esta investigación y son éstos los que abordan algunos aspectos cruciales de la rama atmosférica del ciclo hidrológico, como la caracterización de las fuentes globales de humedad, la variabilidad interanual del transporte de humedad, y la distribución de la precipitación continental debida a las principales fuentes de humedad oceánica. Este estudio proporciona una identificación robusta de las principales fuentes de humedad oceánica, así como una evaluación de sus recientes cambios en su amplitud, permitiendo dar respuesta a tres preguntas científicas clave: (i) ¿han sido las regiones fuentes de humedad estacionarias, o han cambiado a lo largo de las últimas tres décadas?, (ii) ¿cómo los cambios en la intensidad (mayor evaporación) y la posición de las fuentes afectan a la distribución de la precipitación continental?, y (iii) ¿cuál es el papel de los principales modos de variabilidad climática como ENSO, NAM y SAM en la variabilidad de las regiones fuentes de humedad, así como en la precipitación continental asociada a ellos?. Por otra parte, se aborda también el estudio de la influencia potencial en la precipitación continental de las regiones oceánicas con altas tasas de evaporación menos precipitación en un futuro escenario de cambio climático, lo que hace que este trabajo esboce un análisis de las fuentes oceánicas de precipitación continental relacionadas con el cambio climático. Por último, mediante el uso de un catálogo para identificar y caracterizar las principales fuentes de humedad asociadas con las regiones climáticas continentales basado en dos sistemas de regionalización diferentes, este estudio proporciona una evaluación fiable y robusta de las relaciones fuente-sumidero de humedad para los climas regionales, siendo éste un requisito para entender el factor impulsor de los fenómenos meteorológicos y climáticos extremos.

Resumo

O presente traballo aborda un estudo detallado e unha caracterización climatolóxica das fontes globais de humidade para a precipitación continental, baseado nunha técnica de análise Langrangiano. O corpus do traballo está baseado nunha serie de artigos publicados en revistas especializadas, o que demostra a calidade dos resultados. Cinco artigos clave forman a estrutura principal desta investigación e son estes os que abordan algúns aspectos cruciais da rama atmosférica do ciclo hidrolóxico, como a caracterización das fontes globais de humidade, a variabilidade interanual do transporte da humidade, e a distribución da precipitación continental debida ás principais fontes de humidade oceánica. Este estudo proporciona unha identificación robusta das principais fontes de humidade oceánica, así como unha avaliación dos seus recentes cambios de amplitude, permitindo dar resposta a tres preguntas científicas clave: (i) foron as rexións fontes de humidade estacionarias, ou cambiaron ao longo das últimas tres décadas?, (ii) como os cambios na intensidade (maior evaporación) e a posición das fontes afectan á distribución da precipitación continental?, e (iii) cal é o papel dos principais modos de variabilidade climática como ENSO, NAM e SAM na variabilidade das rexións fontes de humidade, así como na precipitación continental asociada a eles?. Por outra parte, abórdase tamén o estudo da influencia potencial na precipitación continental das rexións oceánicas con altas taxas de evaporación menos precipitación nun futuro escenario de mudanza climática, o que fai que este traballo esboce unha análise das fontes oceánicas de precipitación continental relacionadas co cambio climático. Por último, mediante o uso dun catálogo para identificar e caracterizar as principais fontes de humidade asociadas coas rexións climáticas continentais baseado en dous sistemas de rexionalización diferentes, este estudo proporciona unha avaliación fiable e robusta das relacións fonte-sumidoiro de humidade para os climas rexionais, sendo éste un requisito para entender o factor impulsor dos fenómenos meteorolóxicos e climáticos extremos.

Contents

List of Figures	xvii
List of Tables	xxi
List of Acronyms	xxiii
1 Introduction	1
1.1 Problem	2
1.2 Proposal	3
2 Objectives	5
3 Overall methodology	9
3.1 Oceanic moisture source regions	9
3.1.1 Major oceanic sources of continental precipitation	9
3.1.2 Oceanic sources of continental precipitation linked to climate change	10
3.2 Moisture sources for continental climatic regions	12
3.3 The choice of Lagrangian approach	14
3.4 Input data and simulations	16
3.5 Technique and Significance of Composites	19
3.5.1 Composites of the intensification for the major oceanic moisture sources	20
3.5.2 El Nino-Southern Oscillation (ENSO) composites for the major oceanic moisture sources	22

CONTENTS

3.5.3	Hemispheric annular modes composites for the major oceanic moisture sources	23
3.5.4	Composites for the continental climatic regions	25
4	Collection of publications	27
4.1	Estimating the temporal domain when the discount of the net evaporation term affects the resulting net precipitation pattern in the moisture budget using a 3-D lagrangian approach	31
4.2	Influence of the intensification of the major oceanic moisture sources on continental precipitation	41
4.3	The role of the ENSO cycle in the modulation of moisture transport from major oceanic moisture sources	49
4.4	The modulation of oceanic moisture transport by the hemispheric annular modes	63
4.5	A catalog of moisture sources for continental climatic regions	75
5	Summary and Conclusions	83
A	Further details of FLEXPART	97
A.1	Brief Review	97
A.2	Model Computing Aspects	98
A.3	Model Physical Aspects	99
A.3.1	Forward and backward modeling	99
B	Supporting Results	101
B.1	Influence of the intensification of the major oceanic moisture sources on continental precipitation	101
B.2	The role of the ENSO cycle in the modulation of moisture transport from major oceanic moisture sources	104
B.3	A catalog of moisture sources for continental climatic regions	106
C	Resumen General	119
C.1	Introducción	119
C.2	Objetivos	122
C.3	Metodología	124

CONTENTS

C.4 Colección de Publicaciones	130
C.5 Sumario y Conclusiones	131
References	145

List of Figures

3.1	Major oceanic moisture sources: Climatological annual vertically integrated moisture flux divergence (mm/yr) for the period 1980-2012 using data from ERA-Interim. Values greater than 250 mm/yr are shown in gray scale, with intervals between isolines of 250 mm/yr. Areas inside the red contour lines indicate the regions considered as moisture sources in the forward integrations.	10
3.2	Multimodel ensemble mean ($E - P$) change in moisture budget for 2046-1965 minus 1961-2000 for October-March, based on the data generated using 15 GCMs run as part of the Coupled Model Intercomparison Project phase 3 (Meehl et al., 2007) and used for the Intergovernmental Panel on Climate Change Fourth Assessment Report (IPCC AR4). Data provided by Richard Seager (Seager et al., 2010).	11
3.3	As Figure 3.2 for April-September.	11
3.4	Set of 35 continental climatic regions with similarities not only in terms of mean climate (1970-1999) but also in terms of projected changes in precipitation (2070-2099) [homogenous future change] defined by Mahlstein and Knutti (2010), [MKRs].	12
3.5	Set of 21 continental climatic regions widely used in IPCC reports representing different climatic regimes [homogenous current climate] defined by Giorgi and Francisco (2000), [GRs].	13

LIST OF FIGURES

- B.1 Values of $(E - P)$ integrated over 10 days for the period 1980-2000, calculated by forward tracking from the oceanic regions but excluding the moisture sources indicated in Figure 3.1. Only negative values less than -0.01 mm/day are plotted ($E - P < -0.01$ mm/day). The left and right columns are for the periods DJF and JJA, respectively. 101
- B.2 Values of $(E - P)$ integrated over 10 days for the period 1980-2000, calculated by forward tracking from the oceanic moisture sources indicated by the closed pink lines and identified by their acronym. Only negative values less than -0.01 mm/day are plotted ($E - P < -0.01$ mm/day). The left and right columns are for DJF and JJA, respectively. 102
- B.3 The composite differences in $(E - P)$ between the average of the five highest source intensity periods and the average of the five lowest intensity periods for DJF (left panels) and JJA (right panels). Each moisture source is shown on a separate pair of panels. The black contour lines indicate areas where absolute values of the differences greater than 0.01 mm/day are significant at the 90% confidence level, according to a bootstrap test that permutes the original time series 1000 times. 103
- B.4 Monthly composites of moisture sink areas detected for the ENSO phases for 1980-2012. The sources of moisture (bottom maps) are those detected in Figure 3.1. Only negative values of $(E - P)$ calculated by forward tracking from defined moisture sources greater than -0.05 mm/day are plotted for (left) El Niño episode and (right) La Niña phase. 104
- B.5 Climatology values of $(E - P)$ integrated over 10 days for the period 1980-2012, calculated by forward tracking from the oceanic regions but excluding the moisture sources indicated in Figure 3.1. Only negative values less than -0.05 mm/day are plotted ($E - P < -0.05$ mm/day). . . 105
- B.6 (a) Selected target continental climatic regions (CCRs) with homogeneous current climate (Giorgi regions). These regions are widely used in the IPCC reports and were identified by Giorgi and Francisco (2000). Items (b,c,d, and e) follow the same methodology of Figure 1 (Nieto et al. [2014b] and page 77 of this thesis) for the Northern Europe (NEU) region of analysis using a threshold of 0.1 mm/day. 106

LIST OF FIGURES

B.7	Sensitivity test. As Figure 1 (Nieto et al. [2014b] and page 77 of this thesis) using a threshold of 0.05 mm/day.	107
B.8	Sensitivity test. As Figure 1 (Nieto et al. [2014b] and page 77 of this thesis) using a threshold of 0.15 mm/day.	108
B.9	Sensitivity test. As Figure 1 (Nieto et al. [2014b] and page 77 of this thesis) using a threshold of 0.2 mm/day.	109
B.10	Sensitivity test. As Figure B.6 using a threshold of 0.05 mm/day.	110
B.11	Items (a,b,c,d, and e) follow the same methodology of Figure 2 (Nieto et al. [2014b] and page 79 of this thesis) for the Northern Europe (NEU) region of analysis using a threshold of 0.1 mm/day.	111
B.12	Sensitivity test. As Figure 2.a (Nieto et al. [2014b] and page 79 of this thesis) using different thresholds: (a) 0.05 mm/day, (b) 0.15 mm/day and (c) 0.2 mm/day.	111
B.13	Sensitivity test. As Figure B.11.a using a threshold of 0.05 mm/day. . .	112
B.14	The composite differences in $(E - P)$ between the average of the eight years with higher NAMI and the average of the eight years with lower NAMI for December-March. Only significant differences at the 90% confidence level are shown according to a bootstrap test that permutes the original time series 1000 times.	112

List of Tables

3.1	List of MKR regions used in this study.	13
3.2	As Table 3.1 for the GR regions.	14
3.3	Summary of the methods that make use of numerical water vapour tracers, taken from Gimeno et al. (2012).	15
3.4	Summary of the methods used to establish source-sink relationships for atmospheric water vapour, taken from Gimeno et al. (2012).	16
3.5	Upper (red colour) and lower (blue colour) years of the divergence intensity of the vertically integrated flux of moisture per unit area [$10^{-8} \cdot \frac{\text{mm}}{\text{yr} \cdot \text{m}^2}$] for boreal summer (JJA) during the period 1980-2000. Data: ERA-40.	21
3.6	As Table 3.5 for boreal winter (DJF).	22
4.1	Summary of the journal rank in category.	29
4.2	Summary of the impact and quality criteria of the journals of publication.	30
A.1	Output variables of the LPDM FLEXPART.	100
B.1	Annual values of $(E - P)_{1-10}$ (in mm/day) for the North Atlantic (NATL), Caspian (CAS) and Mediterranean (MED) sources of moisture for the NMEU/WA CCR and the $(\pm\sigma)$ standard deviation, using a threshold of 0.1 mm/day.	113
B.2	Annual values of $(E - P)_{1-10}$ (in mm/day) for the North Atlantic (NATL), Black Sea (BLACK) and Mediterranean (MED) sources of moisture for the NEU CCR and the $(\pm\sigma)$ standard deviation, using a threshold of 0.1 mm/day.	114

LIST OF TABLES

B.3	As Table B.1 but using the threshold of 0.05 mm/day to define the moisture sources (NATL, NORWEGIAN, MED, BALTIC and EAST). . . .	115
B.4	As Table B.1 but using the threshold of 0.15 mm/day to define the moisture sources (NATL, CAS and MED).	116
B.5	As Table B.1 but using the threshold of 0.2 mm/day to define the moisture sources (NATL and CAS).	117
B.6	As Table B.2 but using the threshold of 0.05 mm/day to define the moisture sources (NATL, NORWEGIAN, MED and EAST).	118

List of Acronyms

AGU Agulhas Current

AGU American Geophysical Union

ALPSP Association of Learned and Professional Society Publishers

ARAB Arabian Sea

BALTIC Baltic Sea

BLACK Black Sea

CAS Caspian Sea

CCR Continental Climatic Region

CFSR Climate Forecast System Reanalysis

CLLJ Caribbean Low Level Jet

CORALS Coral Sea

COSMO Consortium for Small-scale Modeling

CPC Climate Prediction Center

EAST Eastern Europe

ECMWF European Centre for Medium-Range Weather Forecast

ENSO El Niño-Southern Oscillation

LIST OF ACRONYMS

EOS The Newspaper of Earth and Space Sciences

GCM Global Circulation Model

GFS Global Forecast System

GNU GNU's Not Unix

GPCP Global Precipitation Climatology Project

GR Giorgi Region

GRIB Gridded Binary

HSSR Hot Spot Source Region

IND Indian Ocean

IPCC AR4 Intergovernmental Panel on Climate Change Fourth Assessment Report

ITCZ Inter Tropical Convergence Zone

LPDM Lagrangian Particle Dispersion Model

MED Mediterranean Sea

MERRA Modern Era Retrospective-Analysis for Research and Applications

MEXCAR Mexico-Caribbean Sea

MKR Malstein-Knutti Region

MM5 Fifth-Generation Mesoscale Model

NAM Northern Annular Mode

NAMI Northern Annular Mode Index

NATL North Atlantic Ocean

NCAR National Center for Atmospheric Research

NCEP National Centers for Environmental Prediction

LIST OF ACRONYMS

NEU Northern Europe

NMEU Northern-Middle Europe

NOAA National Oceanic and Atmospheric Administration

NORWEGIAN Norwegian Sea

NPAC North Pacific Ocean

ONI Oceanic Niño Index

PC Principal Components

PSU Pennsylvania State University

RCM Regional Climate Model

REDS Red Sea

SACZ South Atlantic Convergence Zone

SAM Southern Annular Mode

SAMI Southern Annular Mode Index

SATL South Atlantic Ocean

SLP Sea Level Pressure

SPAC South Pacific Ocean

VIMT Vertical Integrated Moisture Transport

WA Western Asia

WRF Weather Research and Forecasting

WVT Water Vapour Tracers

ZAN Zanzibar Current

*“Research is to see what everybody
else has seen, and to think what no-
body else has thought”*

Albert Szent-Györgyi (1893-1986)
Hungarian Physiologist

SECTION

1

Introduction

In view of the threat of global climate change, the proper understanding of the intensity of the hydrological cycle and its development over time is one of the most important challenges of the century, at least in the area of the geosciences.

The hydrological cycle can essentially be summarized to be the evaporation of moisture in one location, offset by precipitation elsewhere. The rate of evaporation exceeds the rate of precipitation over the oceans, which are therefore a net source of moisture; this moisture is then transported to the land masses, which are a net sink for moisture, and where precipitation thus exceeds evapotranspiration. In consequence, surface runoff enters rivers and other water courses, which discharge into the ocean, thereby completing the cycle.

The global hydrological cycle is supplied annually with circa 500000 km³ of water evaporated from the Earth's surface, with the bulk of this volume evaporating from the oceanic surface (86%) and only 14% from continents (Oki, 2005).

The vast majority of the water that evaporates from the oceans (90%) every year precipitates directly back to them, while the remaining 10% is transported to the continents where it precipitates. About two thirds of the latter 10% are recycled over the continents and one third runs off directly to the ocean; this mechanism is therefore essential in feeding the land branch of the hydrological cycle. Ultimately, despite the continental recycling component, all water used by or available to land ecosystems and human

1. INTRODUCTION

socio-economic activities has its origins in the oceans. Any future changes in meteorological conditions over the oceanic moisture source regions may therefore have an impact on water availability in many river basins. In this context, the relentless upward trend in temperature observed in recent decades may pose an additional burden on the reliability of future moisture sources.

Modelling studies suggest that the high sensitivity to temperature of saturation vapour pressure will result in increases in evaporation and precipitation leading to an intensification of the water cycle (Held and Soden, 2006). The volume of water that evaporates will depend largely on changes of sea and air temperature and wind over major moisture source regions, and these changes are bound to influence specific continental regions. The 3-D Lagrangian transport model FLEXPART uses meteorological analysis data as input, together with a moisture tracking scheme with a small temporal domain and a low precision approach. This scheme was successfully used by Gimeno et al. (2010a) to identify where continental regions are affected by precipitation originating from specific oceanic regions.

The aim of this study is to characterize the behaviour and interannual variability of the moisture sources, using a larger temporal domain and a high-precision approach to determine the distribution of continental precipitation from oceanic moisture source regions, in order to gain a better understanding of the role that these sources play in the contribution of moisture to continental precipitation.

1.1 Problem

The lack of any climatological studies or characterizations of global moisture transport using a Lagrangian Particle Dispersion Model (LPDM) is the main driver behind this research, given the impact on the scientific community of the first attempt to do this by Gimeno et al. (2010a) using a small temporal domain and a low-precision approach. In fact, the American Geophysical Union (AGU) highlighted it as one of the three most important geophysical articles published during the first half of 2010 in The Newspaper of Earth and Space Sciences (3rd August EOS issue). The response to the work suggested the importance of extending the temporal domain and exploring the high-precision approach further, in order to gain a more appropriate characterization and understanding of global moisture sources.

1.2 Proposal

Gimeno et al. (2010a) used five years of data 2000-2004 to show that the supply of oceanic moisture to the continents is highly asymmetrical, with the Northern Atlantic subtropical ocean source affecting the continents considerably more than the large Southern Indian and North Pacific sources. Also, the small Mediterranean Sea and Red Sea basins are important moisture sources for relatively large land areas. The Indian subcontinent receives moisture from six different major oceanic source regions. The temporal limitation of this study means that some aspects of the atmospheric branch of the hydrological cycle are still poorly understood, however; for this reason, in this thesis the analysis is extended to three decades (1980-2012) in order to answer the following four scientific questions: (i) have the moisture source regions remained stationary, or have they changed over the last three decades?, (ii) how have the changes in the intensity (i.e., more evaporation) and position of the sources affected the distribution of continental precipitation?, (iii) what is the role of the main modes of climate variability such as ENSO, NAM and SAM in the variability of the moisture regions? and (iv) what are the source-sink relationships in the atmospheric water cycle for regional climates?

To answer these questions a sophisticated Lagrangian diagnosis method was used to identify where continental regions are affected by precipitation originating from specific oceanic regions. The analysis was extended to three decades (1980-2012) using the ERA-40 and ERA-Interim reanalysis datasets in order to allow the study also of the interannual variability and trends in the moisture sources, both in position and intensity.

Some consideration was also given to the likely impacts of climate change. Using a set of Global Circulation Model (GCM) outputs, Seager et al. (2010) identified the oceanic regions with higher evaporation minus precipitation rates in a future climate change scenario; these were used to study their potential future influence in continental precipitation.

Additionally, a catalogue of moisture sources associated with continental climatic regions was created based on two different regionalization schemes, supplying a reliable and robust assessment of source-sink relationships in the atmospheric water cycle for regional climates, which is a requirement for understanding the major driving factors affecting extreme weather and climate events.

“Nothing in life is to be feared, it is only to be understood. Now is the time to understand more, so that we may fear less”

Marie Curie (1867-1934)
Polish Physicist

SECTION

2

Objectives

Motivated to answer the questions set out in the introductory section and related to the global sources of moisture and the key aspects of the atmospheric branch of the hydrological cycle, a climatological study is herein presented. The primary set of objectives is as follows:

- (1) To generate new forward trajectory datasets that allow the study of the major oceanic sources of moisture and its variability for a longer time period and with higher precision than the previous analysis of Gimeno et al. (2010a).
 - (a) Two time periods, 1980-2000 and 1980-2012, were used for the analysis due to the availability of ERA-40 and ERA-Interim reanalysis data, respectively, with a resolution of one degree; these data were used as input for the LPDM FLEXPART model in order to generate the forward trajectory datasets.
 - (b) Using a global domain, the forward trajectory datasets were generated with output every six hours (further details can be found in Section 3).
- (2) To generate the backward trajectory datasets that allow the study of the moisture sources for continental climatic regions and their variability, making possible the assessment of source-sink relationships in the atmospheric water cycle for regional climates.

2. OBJECTIVES

- (a) The 1980-2012 time period was used for the analysis due to availability of ERA-Interim data with a resolution of one degree; this was used as input for the LPDM FLEXPART model in order to generate the backward trajectory datasets.
 - (b) Using a global domain, the backward trajectory datasets were generated with output every six hours (further details can be found in Section 3).
- (3) To present a climatological study of the oceanic sources of moisture using the forward datasets.
- (a) Analysis of the sources of continental precipitation at a global scale: for this objective three scientific questions will be addressed:
 - To assess whether the source regions have remained stationary, or whether they have changed over the last three decades.
 - To investigate how the changes in intensity (more evaporation) and position of the sources affect the distribution of continental precipitation.
 - To investigate the role of the main modes of climate variability such as ENSO, NAM and SAM in the variability of the moisture source regions and the continental precipitation associated with each source.
 - (b) Analysis of the oceanic sources of continental precipitation linked to climate change.
 - To assess the potential influence on continental precipitation of the oceanic regions with higher evaporation minus precipitation rates in a future climate change scenario (Seager et al., 2010).
- (4) To identify and characterize using a catalogue all the major moisture sources associated with continental climatic regions based on two different regionalization schemes using the backward datasets:
- (a) based on a homogenous future change regionalization scheme that considers 35 regions with similar or homogenous projected changes in precipitation over the surface of the globe (Mahlstein and Knutti, 2010).

-
- (b) based on a homogenous current climate regionalization scheme that consider 21 regions representing different climatic regimes widely used in the IPCC reports (Giorgi and Francisco, 2000).

“There are no facts, only interpretations”

Friedrich Nietzsche (1844-1900)
German Philosopher

SECTION

3

Overall methodology

In order to undertake a detailed analysis of the global sources of moisture and their associated variability over the entire planet, the Lagrangian approach developed by Stohl and James (2004, 2005) was used. This method was applied with successful results as described by Gimeno et al. (2013), Castillo et al. (2014a, 2014b) and Nieto et al. (2014a, 2014b), and the main body of the thesis is based on this approach. Prior to its presentation in Section 4, the methodology used for each of the foregoing objectives is discussed.

3.1 Oceanic moisture source regions

3.1.1 Major oceanic sources of continental precipitation

The identification of the main oceanic moisture source regions is based on the maxima of the annual climatological vertically integrated moisture flux divergence using the available European Centre for Medium-Range Weather Forecast reanalysis ERA-Interim data (Dee et al., 2011) on a $1^\circ \times 1^\circ$ grid between January 1980 and December 2012. Ten oceanic moisture source regions were identified based on a threshold of 750 mm/yr for the integrated moisture flux divergence (Figure 3.1) following the criteria of Gimeno et al. (2010a). The method identified 10 oceanic moisture source regions,

3. OVERALL METHODOLOGY

namely NPAC, North Pacific; SPAC, South Pacific; NATL, North Atlantic; SATL, South Atlantic; MEXCAR, Mexico-Caribbean; ARAB, Arabian Sea; ZAN, Zanzibar Current; AGU, Agulhas Current; IND, Indian Ocean; and CORALS, Coral Sea. Two additional sources were included, defined using the physical boundaries of oceanic basins, namely MED, Mediterranean Sea and REDS, Red Sea. These regions were used as moisture sources in the forward integrations to accomplish objective 1a for each time period.

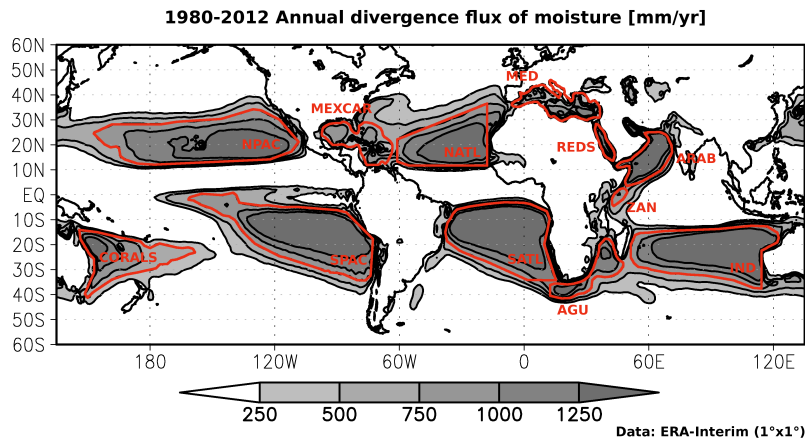


Figure 3.1: Major oceanic moisture sources: Climatological annual vertically integrated moisture flux divergence (mm/yr) for the period 1980-2012 using data from ERA-Interim. Values greater than 250 mm/yr are shown in gray scale, with intervals between isolines of 250 mm/yr. Areas inside the red contour lines indicate the regions considered as moisture sources in the forward integrations.

3.1.2 Oceanic sources of continental precipitation linked to climate change

The identification of oceanic regions with higher evaporation minus precipitation rates in a future climate change scenario was based on data generated by 15 of the GCMs included in the Coupled Model Intercomparison Project phase 3 used for IPCC AR4 (Meehl et al., 2007). Here moisture budget calculations were performed for a future period of climate change between 2046 and 2065 and a multimodel ensemble mean (Seager et al., 2010) was computed. The criteria for using only 15 out of 24 models and the corresponding list can be found in the work of Seager et al. (2010). To

3.1 Oceanic moisture source regions

identify regions of higher change, a comparison was made against the period 1961-2000 for the semiannual periods of October-March and April-September. Those regions that exceeded a threshold of 0.3 mm/day (indicated by the closed red line in Figures 3.2 and 3.3), hereinafter referred to as Hot Spot Source Regions (HSSRs), were used with the FLEXPART model in forward mode to achieve objective 3b for the time period 1980-2000 in order to identify which continental regions would be affected by changes in precipitation ($E - P < 0$) originating in these oceanic moisture sources.

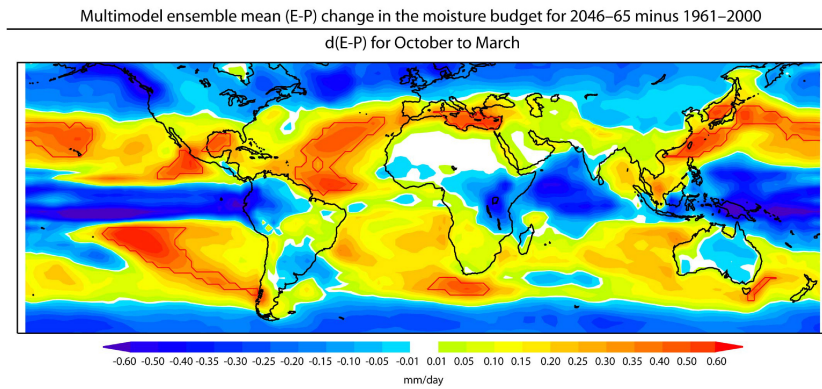


Figure 3.2: Multimodel ensemble mean ($E - P$) change in moisture budget for 2046-1965 minus 1961-2000 for October-March, based on the data generated using 15 GCMs run as part of the Coupled Model Intercomparison Project phase 3 (Meehl et al., 2007) and used for the Intergovernmental Panel on Climate Change Fourth Assessment Report (IPCC AR4). Data provided by Richard Seager (Seager et al., 2010).

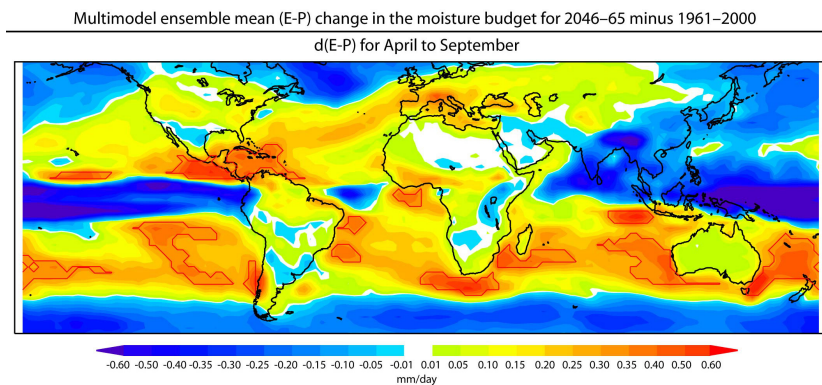


Figure 3.3: As Figure 3.2 for April-September.

3. OVERALL METHODOLOGY

3.2 Moisture sources for continental climatic regions

Two sets of continental climatic regions based on two different regionalization schemes. The first considers 35 regions with similar late-20th Century mean climates (1970-1999) and similar projected late-21st Century precipitation changes (2070-2099) over the surface of the globe [homogenous future change], which were defined by Mahlstein and Knutti (2010) and herein termed MKRs; the second contains the 21 so-called Giorgi regions (Giorgi and Francisco, 2000) widely used in the IPCC reports, which represent different climatic regimes [homogenous current climate], and hereafter referred to as GRs, were used to create a catalogue of moisture sources to assess the source-sink relationships in the atmospheric water cycle for regional climates.

These regions (Figures 3.4 and 3.5) were used with the FLEXPART model in backward mode to address objective 2a, for the identification and characterization of all major moisture sources associated with these continental climatic regions (CCRs). Tables 3.1 and 3.2 show the names of these regions with their respective acronyms.

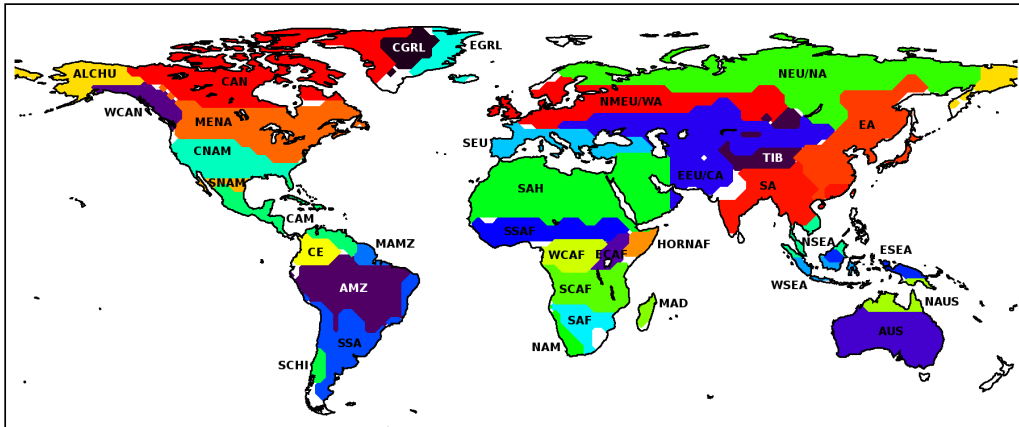


Figure 3.4: Set of 35 continental climatic regions with similarities not only in terms of mean climate (1970-1999) but also in terms of projected changes in precipitation (2070-2099) [homogenous future change] defined by Mahlstein and Knutti (2010), [MKRs].

3.2 Moisture sources for continental climatic regions

Table 3.1: List of MKR regions used in this study.

Name	Acronym	Name	Acronym
Alaska/Chukotka	ALCHU	Northern Europe/Northern Asia	NEU/NA
Amazon Basin	AMZ	Northern-Middle Europe/Western Asia	NMEU/WA
Canada	CAN	Northern Southeast Asia	NSEA
Central Greenland	CGRL	Sahara	SAH
Central America	CAM	Southern Africa	SAF
Central North America	CNAM	Southern Asia	SA
Colombia/Ecuador	CE	Southern Australia	SAUS
Eastern Asia	EA	Southern Central Africa	SCAF
Eastern Central Africa	ECAF	Southern Chile	SCHI
Eastern Europe/Central Asia	EEU/CA	Southern Europe	SEU
Eastern Greenland	EGRL	Southern North America	SNAM
Eastern Southeast Asia	ESEA	Southern Sahel Africa	SSAF
Horn of Africa	HORNAF	Southern South America	SSA
Madagascar	MAD	Tibet	TIB
Middle Eastern North America	MENA	Western Canada	WCAN
Mouth of the Amazon River	MAMZ	Western Central Africa	WCAF
Namib Desert	NAM	Western Southeast Asia	WSEA
Northern Australia	NAUS		

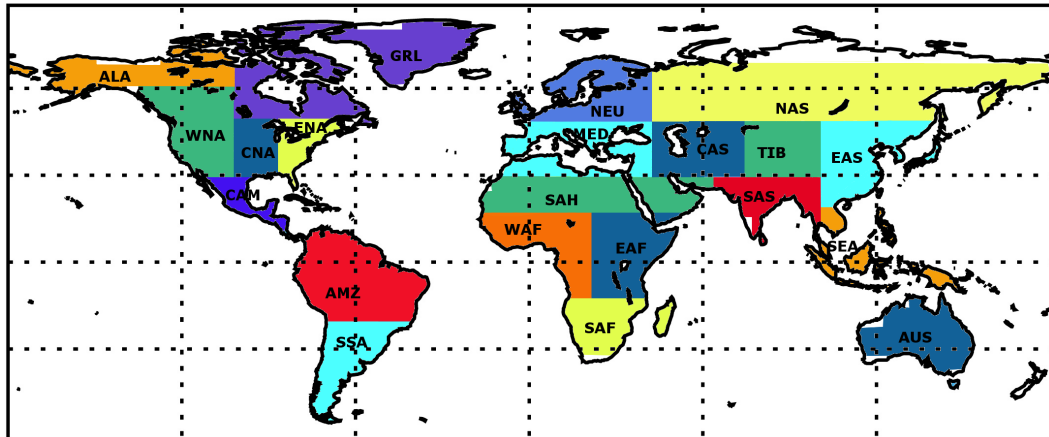


Figure 3.5: Set of 21 continental climatic regions widely used in IPCC reports representing different climatic regimes [homogenous current climate] defined by Giorgi and Francisco (2000), [GRs].

3. OVERALL METHODOLOGY

Table 3.2: As Table 3.1 for the GR regions.

Name	Acronym	Name	Acronym
Alaska	ALA	North Asia	NAS
Amazon Basin	AMZ	Northern Europe	NEU
Australia	AUS	Sahara	SAH
Central America	CAM	Southern Africa	SAF
Central Asia	CAS	South Asia	SAS
Central North America	CNA	Southeast Asia	SEA
Eastern Africa	EAF	Southern South America	SSA
East Asia	EAS	Tibet	TIB
Eastern North America	ENA	Western Africa	WAF
Greenland	GRL	Western North America	WNA
Mediterranean Basin	MED		

3.3 The choice of Lagrangian approach

Nowadays most workers agree that the most recently developed Lagrangian techniques are the most suitable for evaluating the origin of the water that precipitates over a continental area (Gimeno et al., 2012). The Lagrangian approach uniquely provides realistic traces of air parcels, enabling the trajectories to be followed and source-receptor relationships to be established. Using these models alone, it is possible to identify the geographical origin of the moisture that reaches a continental area. Of course, other methodologies provide other types of useful and interesting information that also aids the analysis. The Eulerian methodology, for example, is widely used due its simplicity but it is far from easy to extract the link between the precipitation over a region and the moisture source using this method. While the “box models” allow the identification of the moisture inflow and outflow given defined lateral boundaries, they provide no information about the physical processes that occur within the box itself. The use of isotopes depends on the sensitivity of the isotopic signal. A complete review of the limitations of this Lagrangian approach, its uncertainty and significance as well as the advantages and disadvantages with respect to other methods for estimating moisture sources can be found in the recent comprehensive review of the topic by Gimeno et al. (2012). Despite the range of methods available, the robustness of the Lagrangian trajectory method was demonstrated in a number of previous studies assessing global sources of moisture (e.g., Stohl and James, 2005; Dirmeyer and Brubaker, 2007; Gimeno et al., 2010a; Knippertz et al., 2013), and in the regional analyses using FLEXPART, including those for the great

3.3 The choice of Lagrangian approach

Mississippi River (Stohl and James, 2005), the Sahel (Nieto et al., 2006), the Norwegian west coast (Stohl et al., 2008), the South American Monsoon System (Drumond et al., 2008), the areas over ice-cores in the Antarctic (Nieto et al., 2010), Central America (Durán-Quesada et al., 2010), the Iberian Peninsula (Gimeno et al., 2010b), the Indian Peninsula (Ordóñez et al., 2012), the Ethiopian highlands (Viste and Sorteberg, 2013), and in semiarid grassland in China (Sun and Wang, 2014).

The Lagrangian technique is one of two types of method that make use of numerical water vapour tracers (WVT); the other type is Eulerian tagging. Table 3.3 shows a comparative summary of the advantages and disadvantages of each.

Table 3.3: Summary of the methods that make use of numerical water vapour tracers, taken from Gimeno et al. (2012).

Type	Advantages	Disadvantages	References
Eulerian	<ul style="list-style-type: none"> -Detailed atmospheric processes -Realistic moisture circulation 	<ul style="list-style-type: none"> -Dependent on the model bias -Global forcing is required -Poor representation of short time scale hydrological cycle parameters -Do not include the remote sources of water for a region 	<ul style="list-style-type: none"> Benton and Estoque (1954) Starr and Peixoto (1958) Peixoto and Oort (1992) Joussaume et al. (1984) Koster et al. (1986) Bosilovich and Schubert (2002)
Lagrangian	<ul style="list-style-type: none"> -High spatial resolution moisture sources diagnostics -Quantitative interpretation of moisture origin allowed -No limited by a specific RCM domain and spin-up -Source-receptor relationship establishment can be easily assessed as budgets can be traced along suitably defined trajectory ensembles -Net freshwater flux can be tracked from a region both forward and backward in time -Realistic trails of air parcel -Computationally efficient compared to performing multiyear GCM simulations -More information provided than a purely Eulerian description of velocity fields -Parallel use of information from Eulerian tagging methods allowed 	<ul style="list-style-type: none"> -Moisture fluxes computations sensitivity to data noise increases for shorter time periods or smaller regions -Simple method do not provide diagnostics of surface fluxes of moisture -Surface fluxes under (over) estimation if dry (cold) air masses tracking as the budget is not closed -Evaporation rates are based on calculations rather than observations in some methods -Evaporation and precipitation are not clearly separable (in some methods) -Movement and extraction of water do not depend on the physical tendencies included in the reanalysis data 	<ul style="list-style-type: none"> D'Abreton and Tyson (1995) Wernli (1997) Massacand et al. (1998) Dirmeyer and Brubaker (1999) Brubaker et al. (2001) Dirmeyer and Brubaker (2006) Stohl and James (2004,2005)

3. OVERALL METHODOLOGY

There are two other methods used to establish source-sink relationships for atmospheric water vapour, namely “analytical and box models” and “physical water vapour tracers” (isotopes). Table 3.4 summaries the advantages and disadvantages of these methods used for the analysis of the source-receptor relationship.

Table 3.4: Summary of the methods used to establish source-sink relationships for atmospheric water vapour, taken from Gimeno et al. (2012).

Type	Advantages	Disadvantages	References
Analytical Box Models	-Simple as few parameters are required and they consider grid based spatial variability	-Neglects in-boundary processes -Some are based on the well mixed assumption (the local source of water in the whole vertical column) -Requires knowledge on the ratios of recycled to total precipitation and precipitable water -Most are only valid for monthly or longer timescales	Budyko (1974) Brubaker et al. (1993) Eltahir and Bras (1994) Burde and Zangvil (2001a, 2001b) Dominguez et al. (2006)
Physical Water Vapour Tracers	-Simplicity -Global coverage -Include vertical processes -Reanalysis input data (high spatiotemporal resolution) -Enable the combination of GCMs and Lagrangian Rayleigh models	-Sensitivity of the isotopic signal -Calculation time -Availability of data for validation -Does not account for convection and rainwater evaporation/equilibrium	Gat and Carmi (1970) Salati et al. (1979) Rozanski et al. (1982) Coplen et al. (2008)

3.4 Input data and simulations

In order to characterize and study the variability of the global sources of moisture two different experiments were used, both based on the method developed by Stohl and James (2004, 2005). Both experiments use the FLEXPART Lagrangian particle dispersion model (Stohl et al., 1998) to track atmospheric moisture along trajectories over the entire depth of the atmosphere. At the outset of this research the 21-year period from 1980 to 2000 was used, making use of ECMWF reanalysis ERA-40 (Uppala et al., 2005); later a longer period of 33 years from 1980 to 2012 was used with the ERA-Interim reanalysis (Dee et al., 2011), when this dataset was completely available. It has

been shown that the performance of ERA-Interim in reproducing the hydrological cycle and in terms of water balance closure is much better than that of ERA-40 (Trenberth et al., 2011) and better even than that of the newest reanalysis products such as the Modern Era Retrospective-Analysis for Research and Applications (MERRA) and the Climate Forecast System Reanalysis (CFSR) (Lorenz and Kunstmann, 2012). Data from the years prior to 1980 were not used to run the FLEXPART model because the results of the reanalysis were of poor quality (especially over the oceans) before the inclusion of satellite data (Bengtsson et al., 2004). The usefulness of the data from before 1980 is somewhat limited for two reasons: (i) the FLEXPART model uses derived variables as input data such as zonal wind (u), meridional wind (v), and specific humidity (q), which were not reliable before 1980, and these are highly sensitive to errors, so the model outputs might be erroneous (Stohl et al., 2005), and (ii) it is impossible to work with data obtained before the incorporation of satellite imagery in the reanalysis from 1979 onwards. Prior to this date, there were insufficient observations over large oceanic areas and the datasets are considerably less reliable (Bengtsson et al., 2004; Uppala et al., 2005).

To analyze the transfer of the moisture content in the air between locations, the vertically integrated total flux of water vapour was used, which provides an approximation to the transport of moisture in the atmosphere and is defined as:

$$\Theta = \frac{1}{g} \int_0^{p_s} q \vec{V} dp \quad (3.1)$$

where g is the acceleration due to gravity, q is the specific humidity, p_s is the surface pressure, and \vec{V} is the horizontal wind vector. Making use the conservation of mass, the hydrological balance in the atmosphere may be described by the following relationship:

$$\frac{\partial W}{\partial t} + \nabla \cdot \Theta = E - P \quad (3.2)$$

where W is the precipitable water and is given by:

$$W = \frac{1}{g} \int_0^{p_s} q dp \quad (3.3)$$

When the time period of the averaging is large (i.e., several years), the precipitable water storage term becomes small and can be neglected so that the vertically integrated

3. OVERALL METHODOLOGY

moisture transport divergence is equivalent to the net evaporation (E) minus precipitation (P) (Trenberth and Guillemot, 1998).

$$\nabla \cdot \Theta = E - P \quad (3.4)$$

Equation 3.4 is very useful in the interpretation of the presence of sources and sinks of moisture, because it provides an estimate of the freshwater flux balance at the surface from the divergence of the moisture transport flux.

Lagrangian particle models compute trajectories of a large number of infinitesimally small air parcels (so-called “particles”) to model the transport and diffusion of atmospheric tracers (Stohl et al., 2005). At the start of the model run, the atmosphere was “filled” homogeneously with particles, each representing a fraction of the total atmospheric mass (Stohl and James, 2004). During the run, these particles were advected using the three-dimensional reanalysis wind, with superimposed stochastic turbulent and convective motions. The particle positions and specific humidity (q) were recorded every 6 hours. Increases (evaporation, e) and decreases (precipitation, p) in the parcel’s moisture along the trajectory were calculated from changes in specific humidity (q) with time (Equation 3.5)

$$e - p = m \frac{dq}{dt} \quad (3.5)$$

where m is the mass of each particle.

Adding the moisture changes ($e - p$) of all the particles in the atmospheric column over a specified area A gives the surface freshwater flux ($E - P$), where E is the evaporation rate per unit area, and P is the precipitation rate per unit area (Equation 3.6)

$$E - P \approx \frac{\sum_{k=1}^K (e - p)_k}{A} \quad (3.6)$$

where K is the total number of particles in the atmospheric column.

In the present work, the global atmosphere was divided into nearly 1.9 million particles using the ERA-40 dataset and into about 2.0 million using the ERA-Interim reanalysis. Each particle was tracked for a transport time of 10 days because this is the average residence time of water vapour in the atmosphere (Numaguti, 1999). The tracks were computed using ERA-40 and ERA-Interim reanalysis data available at intervals of

3.5 Technique and Significance of Composites

six hours (00, 06, 12 and 18 UTC) and at a spatial resolution of 1° latitude by 1° longitude. All 61 vertical levels of the reanalysis data were used, from 0.1 to 1000 hPa with approximatively 14 model levels below 1500 m, and 23 between 1500 m and 5000 m. These particles were tracked in time, forward for oceanic and backward for continental regions, and the $(E - P)$ field was calculated every 6 hours over the ten day periods. Daily $(E - P)$ values were calculated as the sum of the four daily outputs (at times 00, 06, 12, 18 h), and designated $(E - P)_{n\text{-day}}$ for the n^{th} day ($n=1\ldots 10$) of the forward or backward trajectory. For instance, the spatial pattern $(E - P)_{2\text{-day}}$ shows where moisture was acquired or lost during the second day of the trajectory. The total $(E - P)$ integrated over the whole forward or backward tracking period (10 days) was designed $(E - P)_{\text{integrated}}$. A detailed explanation of the estimation of $(E - P)$ can be found in Nieto et al. (2008).

3.5 Technique and Significance of Composites

Composite analysis is a convenient tool to be used in the construction of an estimate of the mean state of a given variable conditioned by the value of an external index. Herein, the composites were constructed for the positive and negative phases of the main variability modes (ENSO, NAM and SAM) and for the year set with the highest and lowest values of divergence intensity for the major oceanic moisture sources. To select the basis for compositing of the moisture sinks regions ($E - P < 0$), the climate indices for each mode were used and the highest and lowest values associated with the intensity of the sources were calculated.

Composites Technique

This technique is represented by the equation:

$$\hat{X}_{\Gamma} = \frac{1}{i} \sum_{j=1}^i x_{ti} \quad (3.7)$$

where Γ is the set (composite) of the field X conditioned by an index t for a number of observations i .

3. OVERALL METHODOLOGY

Statistical Bootstrap Test

In statistics, bootstrapping is a computer-based method for assigning measures of accuracy (defined in terms of bias, variance, confidence intervals, prediction error or some other such measure) to sample estimates according to Efron and Tibshirani (1994). This remarkable computational technique provides scope for the generation of an estimate of the sampling distribution of almost any statistic using very simple methods. Bootstrapping is the practice of estimating properties of an estimator (such as its variance) by measuring those properties when sampling from an approximating distribution. One standard choice for an approximating distribution is the empirical distribution of the observed data. In the case where a set of observations can be assumed to be taken from an independent and homogeneously distributed population, bootstrapping can be achieved by constructing a number of resamples of the observed dataset (and of equal size to the observed dataset), each of which is obtained by random sampling with replacement from the original dataset. Several books and articles explain the statistical theory behind this method, including Efron and Tibshirani (1994), which provides an excellent introduction, as well as Davison and Hinkley (1997) and Efron (2003).

3.5.1 Composites of the intensification for the major oceanic moisture sources

The composite differences between the average of the five highest intensity episodes and the average of the five lowest intensity events (representing the lower and upper quartile of the year set for the period 1980-2000) identified for each of the major oceanic moisture sources (High-Low) were obtained for both boreal summer (June, July, August [JJA]) and winter (December, January, February [DJF]), as shown in Tables 3.5 and 3.6, respectively. Then a bootstrap method (Wei et al., 2012) was used to test the statistical significance of the composite differences between the highest and the lowest intensity events at the 90% confidence level by selecting two 5-year periods at random (a total of 10 years) from the 21 year climatology, permuting the original time series 1000 times.

3.5 Technique and Significance of Composites

Table 3.5: Upper (red colour) and lower (blue colour) years of the divergence intensity of the vertically integrated flux of moisture per unit area $[10^{-8} \cdot \frac{\text{mm}}{\text{yr} \cdot \text{m}^2}]$ for boreal summer (JJA) during the period 1980-2000. Data: ERA-40.

Year	AGU	ARAB	CORALS	IND	MED	MEXCAR	NATL	NPAC	REDS	SATL	SPAC	ZAN
1980	12.86	10.24	16.81	16.25	5.38	5.45	11.70	9.71	3.80	13.12	12.76	13.73
1981	11.71	10.47	15.06	14.99	7.19	5.36	10.55	7.43	3.36	14.13	11.94	19.71
1982	10.31	11.39	17.64	16.62	6.20	6.87	12.40	8.34	2.76	14.91	12.47	14.33
1983	11.21	6.65	15.07	15.27	5.63	3.74	12.52	9.90	4.50	13.64	12.67	16.63
1984	10.56	11.14	12.79	14.66	7.25	5.69	12.68	6.98	5.22	14.05	12.45	18.27
1985	9.66	11.46	12.59	14.70	9.47	4.72	9.46	7.33	4.10	13.26	11.72	14.31
1986	8.88	10.28	14.03	15.01	6.17	5.32	12.49	5.35	4.93	14.24	9.54	12.92
1987	8.75	11.41	12.12	13.93	7.17	5.83	13.22	10.30	3.42	14.13	10.48	15.55
1988	10.21	11.20	10.07	15.70	6.68	-0.26	11.61	9.62	0.08	15.64	11.54	11.53
1989	9.15	10.26	8.89	15.48	7.24	5.64	8.97	8.03	7.05	15.31	11.45	15.52
1990	11.69	13.97	12.51	16.04	8.56	7.94	10.87	6.54	6.45	15.02	11.37	16.59
1991	12.04	14.09	14.77	16.31	8.22	7.18	11.54	7.26	8.25	15.95	11.36	15.32
1992	13.32	9.47	14.60	16.94	8.04	7.53	12.05	8.48	7.26	15.20	11.56	14.40
1993	11.54	14.01	15.30	15.77	9.46	8.67	12.38	9.36	8.23	13.89	11.20	13.90
1994	11.17	13.28	16.12	18.20	9.19	8.86	12.07	6.79	7.42	14.70	10.93	11.92
1995	10.69	13.34	16.82	17.82	8.47	2.82	9.04	10.31	7.40	15.40	11.62	10.35
1996	11.15	8.42	10.51	16.77	9.27	6.36	12.73	7.51	6.77	15.81	11.01	17.01
1997	7.82	9.71	16.26	16.74	7.30	6.95	13.03	7.92	2.69	13.71	11.30	7.21
1998	11.68	11.46	10.64	16.67	8.49	6.68	12.35	9.10	0.72	14.87	12.76	15.39
1999	9.59	12.06	13.87	16.48	5.66	4.06	9.49	9.86	0.34	13.78	11.49	14.15
2000	10.93	11.32	16.51	16.89	9.05	5.41	11.92	8.96	2.18	13.82	15.29	16.99

3. OVERALL METHODOLOGY

Table 3.6: As Table 3.5 for boreal winter (DJF).

Year	AGU	ARAB	CORALS	IND	MED	MEXCAR	NATL	NPAC	REDS	SATL	SPAC	ZAN
1980	8.45	13.00	3.35	6.10	2.35	12.56	12.61	9.72	11.30	11.52	9.79	7.57
1981	4.36	14.68	1.70	10.61	3.23	14.00	12.03	10.26	6.25	11.83	10.04	14.15
1982	7.60	15.15	3.57	10.00	0.82	12.01	14.50	11.33	3.82	13.42	11.97	11.44
1983	10.28	16.38	5.59	6.15	5.43	10.45	12.39	16.19	5.14	12.25	-0.76	10.59
1984	5.93	18.32	5.03	6.42	2.42	12.31	15.09	11.99	10.55	10.43	9.55	18.95
1985	8.82	15.09	2.15	6.45	3.20	15.93	15.00	11.19	10.83	11.49	10.43	12.30
1986	9.06	14.88	1.53	6.61	3.28	12.87	15.74	10.65	9.76	11.71	10.35	12.71
1987	8.35	14.72	10.30	7.81	4.31	10.67	13.88	14.59	9.43	13.01	9.17	12.14
1988	6.37	14.76	4.17	8.61	3.68	13.42	15.92	13.49	10.88	12.98	11.22	12.30
1989	6.92	15.71	-1.74	8.37	5.41	14.14	16.93	11.59	14.04	11.14	8.92	9.16
1990	7.43	13.85	1.33	5.47	5.11	13.30	15.21	11.81	10.69	12.12	8.97	6.99
1991	5.62	14.87	-1.72	9.60	4.36	14.15	15.12	12.30	12.07	12.89	10.53	7.99
1992	11.25	17.21	2.96	5.36	7.33	14.38	14.19	14.15	13.47	10.98	5.82	10.72
1993	5.82	14.21	7.27	12.62	6.98	14.01	14.46	12.73	11.67	13.16	9.17	1.95
1994	10.19	15.77	3.58	11.21	4.00	12.63	15.74	11.64	12.55	13.26	11.12	12.27
1995	7.98	18.05	7.49	9.67	5.85	12.73	14.68	13.00	13.69	12.62	10.65	4.52
1996	8.64	14.43	1.67	10.62	0.55	14.22	14.77	11.17	12.68	12.78	10.26	3.03
1997	4.55	14.54	3.13	8.61	3.80	13.69	14.73	11.77	14.73	14.41	10.33	14.01
1998	9.20	15.35	5.46	9.87	4.44	10.87	14.35	16.52	12.76	12.79	-0.33	-20.17
1999	1.20	14.20	-6.19	12.88	5.45	13.54	17.02	13.83	12.33	12.46	9.83	9.89
2000	6.54	15.51	1.15	8.86	7.06	14.61	17.15	10.91	14.90	11.68	10.34	11.45

3.5.2 El Nino-Southern Oscillation (ENSO) composites for the major oceanic moisture sources

To analyze the influence of the ENSO cycle on the transport of moisture from the major oceanic sources, the composite differences between the positive and negative phases of ENSO were computed. The ONI (Oceanic Niño Index) was used from the NOAA/CPC in the region Niño 3.4 (5°N-5°S, 120°W-170°W) (Smith et al., 2008). ONI is defined by overlapping seasons, so to select a whole year as El Niño or La Niña those years when the phase repeated itself a minimum of five times consecutively from June in year 0 to May in year 1 (for given ENSO cycle) were considered. For this analysis the period 1980-2012 was used, therefore, the quartile year set selected was represented by the eight highest intensity episodes for El Niño (1982-1983, 1986-1987, 1991-1992, 1994-1995, 1997-1998, 2002-2003, 2004-2005, and 2009-2010) and

3.5 Technique and Significance of Composites

for La Niña (1984-1985, 1988-1989, 1995-1996, 1998-1999, 1999-2000, 2007-2008, 2010-2011, and 2011-2012). It must be stressed that the boundaries of each oceanic source (Figure 3.1) were assumed to remain stationary throughout the years considered. A bootstrap method was used to test the statistical significance of the composite differences. The methodology that follows was proposed by Wei et al. (2012) as previously described. The significance of the difference between the El Niño and the La Niña composites was tested at a 90% confidence level by selecting two 8-year periods at random (a total of 16 years) from the 33-year climatology and calculating their difference 1000 times. To be considered significant, the absolute value of the composite of the differences must be larger than 90% of the 1000 differences. Monthly composite differences in the precipitation and in the divergence of the vertically integrated flux of moisture Θ between opposite phases of the ENSO were also obtained. Data were obtained from the Global Precipitation Climatology Project (GPCP; Adler et al., 2003; Huffman et al., 2009), and from ERA-Interim, respectively, and both datasets were estimated over the entire globe for the 33-year period.

3.5.3 Hemispheric annular modes composites for the major oceanic moisture sources

The influence of the two dominant modes of the extratropical winter climate, the Northern and Southern Annular Modes (NAM and SAM, respectively) on the transport of moisture from the oceanic sources was explored using the composite technique. Composite differences of moisture transport between the positive and negative phases of each mode of variability were obtained. The events were selected based on the monthly NAM and SAM Indices (NAMI and SAMI). NAM and SAM are more active during their respective hemispheric winters (from December to February for NAM and from June to August for SAM), and therefore the corresponding semiannual period was chosen, i.e., from November to April for NAM and from May to October for SAM. The most common methods used to identify extreme events of SAM and NAM are those that (i) formulate the first principal components (PC) of some meteorological variable over the extratropics (e.g., geopotential height, mean sea level pressure, wind, temperature) (Thompson and Wallace, 2000; Nan and Li, 2003), (ii) calculate the difference between

3. OVERALL METHODOLOGY

normalized zonal mean pressure between two latitudes using reanalysis data (Gong and Wang, 1999; Li and Wang, 2003) or between two selected points (Hurrell, 1995), (iii) are based on data obtained from observational stations (Marshall, 2003; Visbeck, 2009). The literature reveals some inconsistencies regarding the identification of the extreme episodes of both modes, particularly for SAM, and primarily arising due to the different methodologies and datasets applied in the definition of the indices (Ho et al., 2012). For the SAM Index, but also applying to NAM, Ho et al. (2012) showed that those indices calculated using reanalysis data are more effective where there is some attempt to understand the relationship with their impacts. However, prior to the assimilation of satellite data (pre-1979) the reanalysis-based indices are likely to be flawed, and it is better to choose those that are station-based. With this in mind, for each mode two indices were considered based on different methods using normalized monthly Sea Level Pressure (SLP) data: one station-based and the other reanalysis-based; the respective semianual averages are shown in Nieto et al. (2014a, Table 1) and form part of this thesis (page 66). The station-based NAMI obtained from SLP differences between Lisbon (Portugal) and Stykkisholmur/Reykjavik (Iceland) (Hurrell, 1995; Hurrell et al., 2013) was available at https://climatedataguide.ucar.edu/sites/default/files/climate_index_files/nao_station_monthly.ascii, while the SAMI was obtained from Marshall (2003) at <http://www.nerc-bas.ac.uk/icd/gjma/sam.html>, who produced a similar SAM Index based on 12 appropriately located station-based observations. Those that use reanalysis data (NCEP/NCAR; Kalnay et al., 1996) can be found at <http://ljp.lasg.ac.cn/dct/page/65544>. The NAMI is defined as the difference in the normalized monthly zonal-mean SLP between 35°N and 65°N, and the SAMI is taken to be the same difference between 40°S and 70°S (Li and Wang, 2003; Nan and Li, 2003, respectively). The composites consider the six highest intensity episodes for both phases of each mode for the period November 1979 to October 2012; where there are discrepancies between the two indices the year with the higher (or lower) value was selected using reanalysis data. Thus for the NAM Index the positive high values occurred in 1989, 1990, 1993, 2000, 2007, and 2012; and the negative high values occurred in 1981, 1986, 1996, 2006, 2010, and 2011 (the year shown here refers to the January of the interval). For the SAMI the positive high values occurred in 1989, 1993, 1998, 2008, 2010, and 2012, and the negative high values occurred in 1980, 1981, 1988, 1992, 1994, and 2002. To test the statistical significance of the composite, the bootstrap method was used to obtain the differences for

two 6-year random samples (a total of 12 years) 1000 times from the 33-year climatology. The absolute value of the composite difference was considered significant if it was greater than 90% of the 1000 iterations. The same method was applied to the case of the ENSO mode of variability; the monthly composite differences in the precipitation and in the divergence of the vertically integrated flux of moisture Θ between opposite phases of the annular modes were also calculated using the GPCP and ERA-Interim datasets, respectively.

3.5.4 Composites for the continental climatic regions

The evaluation of the role of the major teleconnection patterns in the catalogue of moisture sources for continental climatic regions was achieved using ENSO as the global mode of atmospheric circulation, and NAM and SAM as the hemispheric ones.

Modes of variability

To investigate the potential influence of the main teleconnection patterns (ENSO, NAM and SAM) in the moisture sources associated with the continental climatic regions, the composite differences between eight extreme phases of each mode (representing the lower and upper quartile of the year set) were evaluated for the period 1980-2012. For the ENSO, the eight highest intensity episodes from June to May were used. The selected years for El Niño were 1982-1983, 1986-1987, 1991-1992, 1994-1995, 1997-1998, 2002-2003, 2004-2005, and 2009-2010; for La Niña: 1984-1985, 1988-1989, 1995-1996, 1998-1999, 1999-2000, 2007-2008, 2010-2011, and 2011-2012. The ONI (Oceanic Niño Index) of Smith et al. (2008) was used as the ENSO Index to assess the semiannual periods from October to March (ONDJFM) and from April to September (AMJJAS). To check the NAM modulation for the moisture sources, the Hurrell wintertime (DJFM) SLP-based Northern Annular Mode Index, available at https://climatedataguide.ucar.edu/sites/default/files/climate_index_files/nam_pc_djfm.ascii (Hurrell, 1995; Hurrell et al., 2013), was used to calculate the composites for those years: higher values of the index were seen in 1989, 1990, 1992, 1993, 2000, 2002, 2007, and 2008, and lower values in 1985, 1986, 1987, 1996, 2001, 2006, 2010, and 2011. To examine the SAM modulation for the moisture sources, the Marshall wintertime (ASON)

3. OVERALL METHODOLOGY

Observation-based Southern Annular Mode Index (Marshall, 2003) was used to assess the composites for those years: higher values of the index were found in 1983, 1985, 1986, 1993, 1998, 1999, 2001, and 2010, and lower values in 1980, 1996, 1997, 2000, 2002, 2007, 2009, and 2011.

*“The most incomprehensible thing
about the world is that it is compre-
hensible”*

Albert Einstein (1879-1955)
German Physicist

SECTION

4

Collection of publications

This section presents the essential elements of this research, which were originally published in five separate articles. The articles were not published in the order presented here, so the range of years of data used in each do not match their sequence of publication. Part of this work involved the study of the distribution of continental precipitation from oceanic moisture source regions. To achieve this, a separate estimation of the net precipitation ($E - P < 0$) from the evaporative term ($E - P > 0$) in the balance of the freshwater flux ($E - P$) was made, which arose from the need to know the time scale at which this separation could be achieved without affecting the resulting precipitation term. The first article was entitled: ***(1) Estimating the temporal domain when the discount of the net evaporation term affects the resulting net precipitation pattern in the moisture budget using a 3-D lagrangian approach***, by R. Castillo, R. Nieto, A. Drumond and L. Gimeno (2014a) and was published in the PlosOne Journal. It addressed the issue of assessing the minimum temporal domain for which the climatological approach of the atmospheric branch of the hydrological cycle is valid in terms of precipitation, and it is referred to throughout this thesis.

The title of the second article was: ***(2) Influence of the intensification of the major oceanic moisture sources on continental precipitation***, by L. Gimeno, R. Nieto, A. Drumond, R. Castillo and R. Trigo (2013), published in Geophysical Research Letters.

4. COLLECTION OF PUBLICATIONS

This paper addressed two key issues in the hydrological cycle that have remained elusive: (i) the impact of climate change on the transport of moisture and, in particular, (ii) the effects of changes in source intensity (i.e., more evaporation) on the distribution of continental precipitation.

The impact of the modes of climate variability in terms of the precipitation from major oceanic moisture sources was analyzed in two articles: **(3) *The role of the ENSO cycle in the modulation of moisture transport from major oceanic moisture sources***, by R. Castillo, R. Nieto, A. Drumond and L. Gimeno (2014b) published in *Water Resources Research*, and: **(4) *The modulation of oceanic moisture transport by the hemispheric annular modes***, by R. Nieto, R. Castillo and A. Drumond (2014a) published in *Frontiers in Earth Science*. The effects of the global mode of atmospheric circulation (ENSO) and the two dominant modes of extratropical winter climate (NAM and SAM) were analyzed in order to assess their effects on the transport of moisture from the major oceanic moisture sources, which in turn affects precipitation over the continents.

Finally and in view of the fact that there are more source regions of moisture for continental sinks than those that have a maximum vertically integrated moisture flux divergence (Figure 3.1), a catalogue of moisture sources for continental climatic regions was compiled as completely as possible. Two sets of continental climatic regions were selected: one based on regions with similar late-20th Century mean climate and similar projected late-21st Century precipitation changes (Figure 3.4), and one using regions used in IPCC assessment reports (Figure 3.5). Because there were more than 50 continental regions to analyze, the outcomes were presented to the scientific community in an online catalogue. In order to illustrate the content of the catalogue, an example region was given in a technical note: **(5) *A catalog of moisture sources for continental climatic regions***, by R. Nieto, R. Castillo, A. Drumond and L. Gimeno (2014b), also published in *Water Resources Research*.

The supporting information related to articles (2) and (3) is contained in Appendices B.1 and B.2. The supplementary figures of article (5) appear in Appendix B.3 and the complete catalogue of moisture sources for all the continental climatic regions can be found at: <http://ephyslab.uvigo.es/tramo/ccrs/>.

A description of the impact and quality criteria of the journals of publication is given in Tables 4.1 and 4.2. However, due to the recent launch of *Frontiers in Earth Science*, some specific information is currently not available, and it does not appear in

the tables. Nevertheless, Frontiers won the ALPSP Award for Innovation in Publishing in recognition of its Open-Science platform that provides open-access academic publishing and networking for researchers. This prestigious award acknowledges the best innovators in the scholarly publishing industry and Frontiers received the top Gold prize at the awards ceremony in London, UK. Moreover, in February 2013, the Nature Publishing Group and Frontiers formed a strategic partnership, to advance the global Open Science movement. The Nature Publishing Group recognized Frontiers' transformative solutions to open-access publishing, peer review and impact metrics. Combining these strengths with Nature's world-renowned reputation for excellence and its long history of academic publishing offers many new opportunities to advance their combined mission to serve scholars better and to lead a change in the landscape of science communication.

Table 4.1: Summary of the journal rank in category.

Journal	Category Name	Total Journals in Category	Journal Rank in Category	Quartile in Category
PLOS ONE	Multidisciplinary Sciences	55	8	Q1
Geophysical Research Letters	Geosciences, Multidisciplinary	173	9	Q1
Water Resources Research	Water Resources	79	3	Q1
Frontiers in Earth Science	Earth Science	coming soon	coming soon	coming soon

4. COLLECTION OF PUBLICATIONS

Table 4.2: Summary of the impact and quality criteria of the journals of publication.

Journal	Description	Facts
PLOS ONE	PLOS ONE features reports of primary research from all disciplines within science and medicine. By not excluding papers on the basis of subject area, PLoS ONE facilitates the discovery of the connections between papers whether within or between disciplines.	Abbreviation: PLoS ONE Impact factor: 3.53 5-year impact: 4.24 Cited half-life: 2.40 Immediacy index: 0.41 Eigenfactor: 0.78 Article influence: 1.55 ISSN: 1932-6203 OCLC: 70662135
Geophysical Research Letters	Geophysical Research Letters publishes short, concise research letters that present scientific advances that are likely to have immediate influence on the research of other investigators. GRL letters can focus on a specific discipline or apply broadly to the geophysical science community.	Abbreviation: Geophys. Res. Lett. Impact factor: 3.98 5-year impact: 4.07 Cited half-life: 7.10 Immediacy index: 0.68 Eigenfactor: 0.23 Article influence: 2.13 ISSN: 0094-8276 OCLC: 1795290
Water Resources Research	WRR is an interdisciplinary journal integrating research in the social and natural sciences of water. Contains original contributions in hydrology; in the physical, chemical, and biological sciences; and in the social and policy sciences, including economics, systems analysis, sociology, and law. Printed on acid-free paper.	Abbreviation: Water Resour. Res. Impact factor: 3.15 5-year impact: 3.45 Cited half-life: 0.00 Immediacy index: 0.62 Eigenfactor: 0.05 Article influence: 1.19 ISSN: 0043-1397 OCLC: 1171541
Frontiers in Earth Science	Frontiers in Earth Science embraces and encourages the interdisciplinary nature of the field, and promotes cooperation between researchers from fields spanning physics to marine science to chemistry, and integrating methods from remote sensing to field work to microscopy.	Abbreviation: Front. Earth Sci. Impact factor: coming soon ISSN: 2296-6463 Indexed in: coming soon PMCID: NA



Estimating the Temporal Domain when the Discount of the Net Evaporation Term Affects the Resulting Net Precipitation Pattern in the Moisture Budget Using a 3-D Lagrangian Approach

Rodrigo Castillo*, Raquel Nieto, Anita Drumond, Luis Gimeno

EPhysLab, Departamento de Física Aplicada, Faculdade de Ciencias, Universidade de Vigo, Ourense, Spain

Abstract

The Lagrangian FLEXPART model has been used during the last decade to detect moisture sources that affect the climate in different regions of the world. While most of these studies provided a climatological perspective on the atmospheric branch of the hydrological cycle in terms of precipitation, none assessed the minimum temporal domain for which the climatological approach is valid. The methodology identifies the contribution of humidity to the moisture budget in a region by computing the changes in specific humidity along backward (or forward) trajectories of air masses over a period of ten days beforehand (afterwards), thereby allowing the calculation of monthly, seasonal and annual averages. The current study calculates as an example the climatological seasonal mean and variance of the net precipitation for regions in which precipitation exceeds evaporation ($E-P < 0$) for the North Atlantic moisture source region using different time periods, for winter and summer from 1980 to 2000. The results show that net evaporation ($E-P > 0$) can be discounted after when the integration of E-P is done without affecting the general net precipitation patterns when it is discounted in a monthly or longer time scale.

Citation: Castillo R, Nieto R, Drumond A, Gimeno L (2014) Estimating the Temporal Domain when the Discount of the Net Evaporation Term Affects the Resulting Net Precipitation Pattern in the Moisture Budget Using a 3-D Lagrangian Approach. PLoS ONE 9(6): e99046. doi:10.1371/journal.pone.0099046

Editor: Moncho Gomez-Gesteira, University of Vigo, Spain

Received: November 1, 2013; **Accepted:** May 11, 2014; **Published:** June 3, 2014

Copyright: © 2014 Castillo et al. This is an open-access article distributed under the terms of the Creative Commons Attribution License, which permits unrestricted use, distribution, and reproduction in any medium, provided the original author and source are credited.

Funding: The authors would like to thank the "Xunta de Galicia" for partially funding this research through the CHEGA project (INCITE09.383.278) and the Spanish Ministry responsible for Science for its contribution through the TRAMO project (CGL2012-35485), both of which were cofunded by FEDER. The funders had no role in study design, data collection and analysis, decision to publish, or preparation of the manuscript.

Competing Interests: The authors have declared that no competing interests exist.

* E-mail: rcastillo@uvigo.es

Introduction

The atmospheric transport of water vapour from regions of net evaporation to regions of net precipitation is an important part of the hydrological cycle [1]. A Lagrangian approach based on the dispersion model FLEXPART [2] has been used extensively for several years to estimate sources of moisture and precipitation at both global [3,4,5] and regional scales [6]. These studies integrate the difference between evaporation and precipitation ($E-P$) to obtain the surface fresh-water flux at a monthly, seasonal or annual scale. However, when an estimation of the net precipitation wants to become separately, the evaporative term ($E-P > 0$) in the balance of $E-P$ is eliminated, remaining only $E-P < 0$. The present study observes the impact of discounting the net evaporation $E-P > 0$ term at different temporal scales from the climatological estimate of the surface fresh-water flux, using a 3-D Lagrangian approach. Suitability tests were performed using the North Atlantic region (NATL) for winter and summer seasons, for the years 1980 to 2000. The NATL source region was chosen based on the results of Gimeno et al. [3], who found this area as the dominant oceanic source providing moisture for precipitation over continents. It influences vast geographical areas, such as Eastern North America, Central America and Northern South America during JJA, and it extends its contribution also towards Europe, Northern Africa and Central South America during DJF.

The influence of other large oceanic sources (e.g., Southern Indian and the North Pacific oceans) is confined towards much smaller continental areas when compared to the contribution from the NATL source. The importance of this source has been well documented in previous analysis for Central America [7], South America [8] and Europe [9]. Also the NATL source is an important oceanic contributor to the North and South American Monsoon Systems, as well as the Atlantic Inter Tropical Convergence Zone (ITCZ). It is affected by the El Niño-Southern Oscillation (ENSO) [5] and by the North Annular (NAM) modes [10]. Using the same methodology as Gimeno et al. [3], we determine the time scales for which $E-P > 0$ may be discounted after the integration of $E-P$ without affecting the resultant patterns of precipitation.

Method

The present study is based on the method developed by Stohl & James [11,12], which uses the FLEXPART Lagrangian particle dispersion model [2] and ERA-40 Reanalysis data [13] to track atmospheric moisture along trajectories through the entire depth of the atmosphere. Lagrangian particle models compute trajectories of a large number of infinitesimally small air parcels (so-called "particles") to model the transport and diffusion of atmospheric tracers [14]. At the start of each model run, the atmosphere was

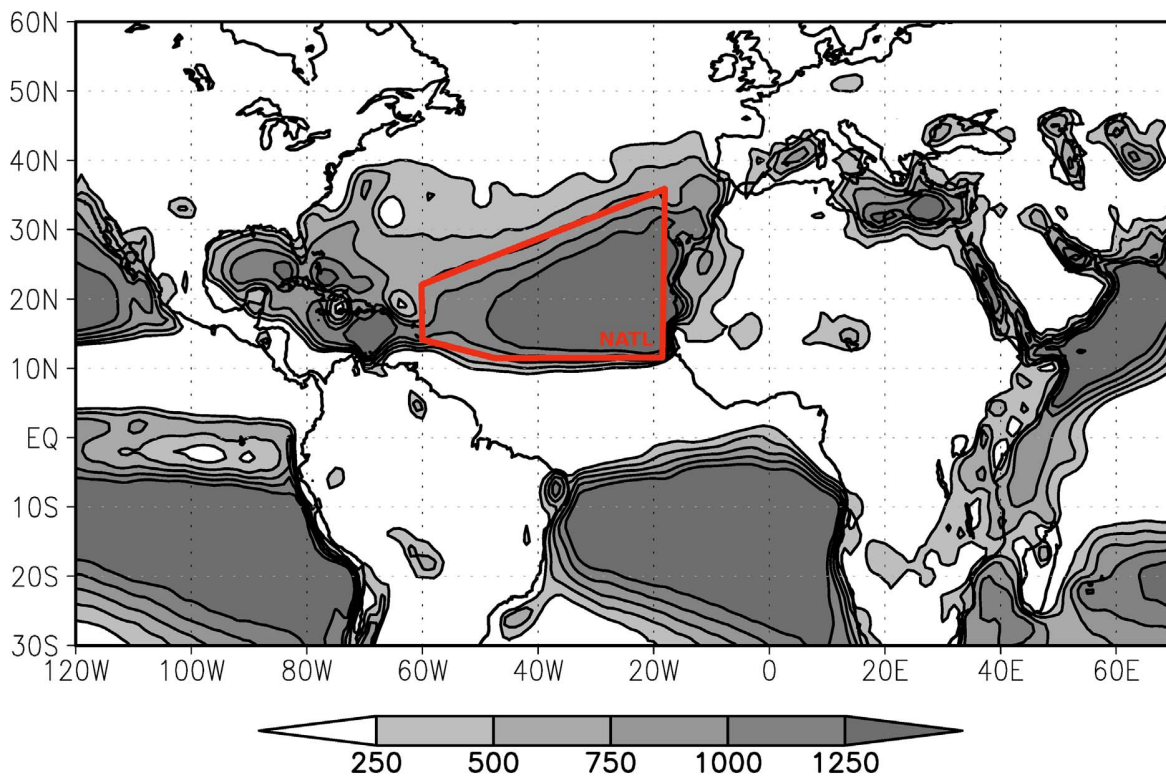


Figure 1. Annual vertically integrated divergence moisture flux (mm/year). Values higher than 250 mm/year are in grey, and the interval between isolines is 250 mm/year. The North Atlantic moisture source is outlined in red. Data: ERA-40 (1958–2001). doi:10.1371/journal.pone.0099046.g001

“filled” homogeneously with particles, each representing a fraction of the total atmospheric mass [11]. During the run, these particles were advected using the three-dimensional Reanalysis wind, with superimposed stochastic turbulent and convective motions. The particle positions and specific humidity (q) were recorded every 6 hours. Increases (evaporation, e) and decreases (precipitation, p) in the parcel’s moisture along the trajectory were calculated from changes in specific humidity (q) with time (Equation 1)

$$e - p = m \frac{dq}{dt} \quad (1)$$

where m is the mass of each particle.

Summing the moisture changes ($e-p$) of all of the particles in the atmospheric column over a specified area gives the surface freshwater flux ($E-P$), where E is the evaporation rate per unit area, P is the precipitation rate per unit area (Equation 2)

$$(E - P) \approx \frac{\sum_{k=1}^K (e - p)}{A} \quad (2)$$

where K is the total number of particles in the atmospheric column. In the present work, the global atmosphere was divided into 1.9 million particles.

Each particle is tracked for a transport time of 10 days because that is the average residence time of water vapour in the atmosphere [15]. The tracks were computed using ERA-40 Reanalysis data available at an interval of six hours (00, 06, 12 and 18 UTC), at a spatial resolution of 1° latitude by 1° longitude. All 60

vertical levels of Reanalysis data were used, from 0.1 to 1000 hPa, with approximately 14 model levels below 1500 m, and 23 between 1500 m and 5000 m.

The area of the NATL moisture source used for the forward integration of $E-P$ was defined using a threshold of 750 mm/year for the annual divergence of vertically integrated moisture flux [3]. The spatial extent of the NATL moisture source is shown in Figure 1.

For each time step, around 30000 particles were selected over the NATL source. These particles were tracked forward in time, and the $E-P$ field was calculated every 6 hours for ten days. Daily $E-P$ values were calculated as the sum of the four daily outputs (at times 00, 06, 12 and 18 h), and designated $(E-P)_{n\text{-day}}$ for the n th day ($n = 1 \dots 10$) of the forward trajectory. For instance, the spatial pattern $(E-P)_{2\text{-day}}$ shows where moisture was acquired or lost during the second day of the trajectory. The total $E-P$ integrated over the whole forward tracking period (10 days) is designated $(E-P)_{\text{integrated}}$.

Experiment

Discounting net evaporation ($E-P > 0$) at different time scales from the estimation of precipitation net ($E-P < 0$) through surface fresh-water flux

The focus of this study is climatological continental precipitation derived solely from moisture uptake from the NATL source area. Since the Lagrangian approach is unable to separate precipitation (p) and evaporation (e) during the computation, the contribution of net evaporation was discounted by considering only negative $E-P$ values ($E-P < 0$). The integrated $E-P$ values are available at

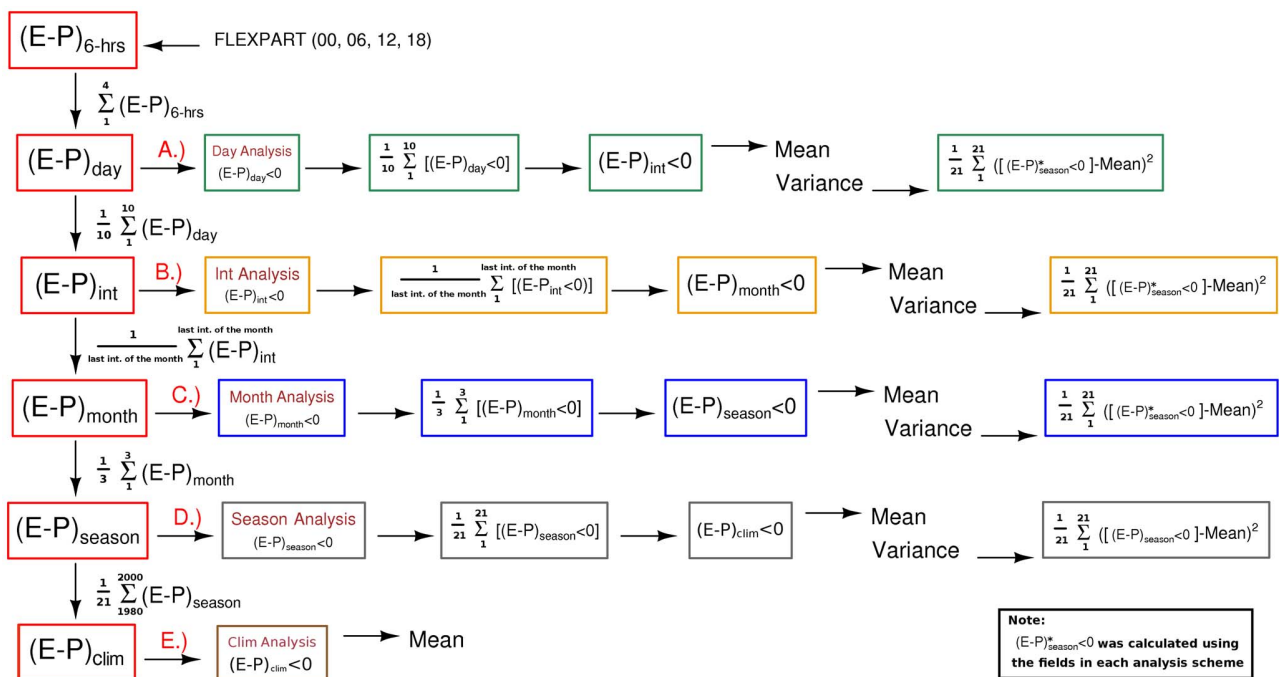


Figure 2. Approaches used to estimate the seasonal climatological mean and the seasonal-interannual variance of E-P<0 net through the E-P budget, by discounting the net evaporation E-P>0 from E-P at different time scales. Where the analysis abbreviations mean; hrs/hours, day/daily, int/integrated, month/monthly, season/seasonal and clim/climatological.
doi:10.1371/journal.pone.0099046.g002

different time scales, and our aim was to find time scales at which E-P>0 may be discounted without affecting the consequent climatological net precipitation patterns.

Ten-day E-P forward trajectories originating in the NATL source region were calculated for winter (December to February, DJF) and summer (June to August, JJA) for each year from 1980 to 2000. E-P>0 values were discounted at five different time scales before calculating climatological seasonal means of E-P<0. The quality of the process was assessed by evaluating differences in the mean, variance fields, correlations and using a Student-t test.

Figure 2 summarises the different approaches used, which were:

- 'Daily analysis'** – (E-P) >0 values were discounted on each individual forward day of the 10-day trajectories. So, the field contained only negative values (E-P<0, net precipitation) at the beginning of the calculation. The seasonal average and the interannual variance are then computed for the period of analysis;
- 'Integrated analysis'** – (E-P) >0 values were discounted after calculated the 10-day forward trajectories. What means that the E-P is averaged over the ten forward days, obtaining a day-integrated approximation, then the positive (E-P) values (net evaporation) are removed from the field in order to calculate the seasonal mean and the interannual variance;
- 'Monthly analysis'** – (E-P) >0 values were discounted after calculated the monthly (E-P) mean fields. What means that firstly we calculate the monthly means of the 10-day integrated (E-P) values, and after we remove positive (E-P) values (net evaporation) from the monthly fields. Then, the monthly means of the negative (E-P) values are used to calculate the seasonal mean and the interannual variance of the negative (E-P) fields;

- 'Seasonal analysis'** – (E-P) >0 values were discounted after calculated the seasonal (E-P) mean fields. Firstly, we calculate 'n' forward days, day-integrated, monthly means, and then seasonal-annual means. Then, we remove the positive (E-P) values (net evaporation) from the seasonal-annual mean fields in order to calculate the seasonal mean and the interannual variance of the negative (E-P) fields;
- 'Climatological analysis'** – We calculated the 21-year climatological seasonal (E-P) mean, and then the positive (E-P) values were removed from the field at the end of the procedure.

For each scheme (except for "Climatological analysis"), after E-P>0 was discounted, the seasonal-annual averages of E-P<0 were computed for the 21 years of the study, and they were used to calculate the seasonal-interannual variance.

Results

Comparison of patterns generated by discounting E-P>0 at different time scales

The results of the suitability test, for estimating the DJF and JJA seasonal mean and interannual variance of E-P<0 for the NATL source region, are shown in Figures 3 and 4, respectively. The 'Daily' and 'Integrated' analyses overestimated mean net precipitation (Figure 3a and 3b) by comparison with the 21-year average presented by Gimeno et al. [1], and also showed high variance values (Figure 4a and 4b). By comparison, when E-P>0 was discounted at longer time scales (the 'monthly', 'annual' and 'climatological' schemes), the resulting seasonal climatological net precipitation patterns are similar (Figure 3c, 3d and 3e), with smaller values of interannual variance (Figure 4c, 4d and 4e).

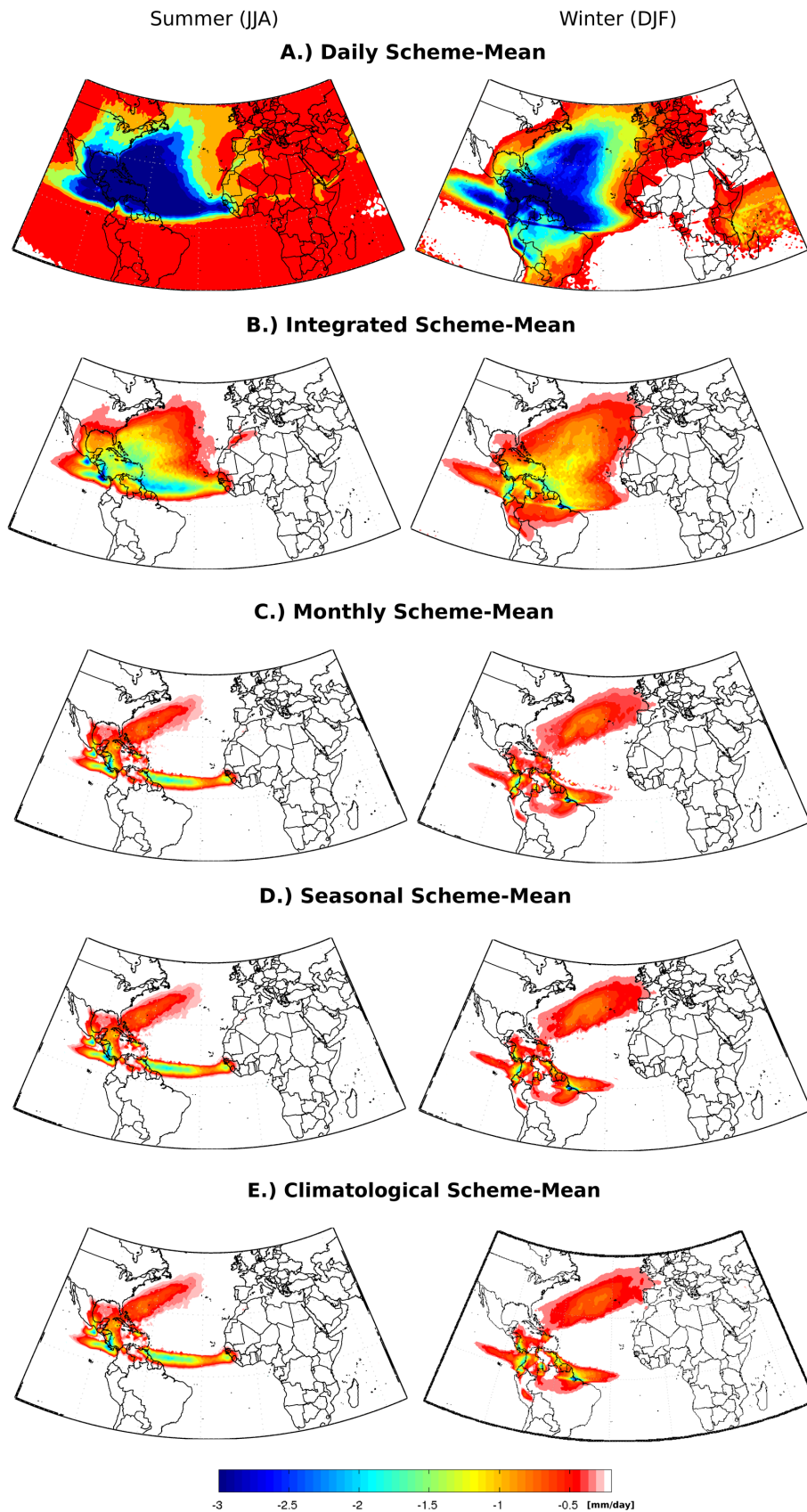


Figure 3. Summer (JJA) and winter (DJF) climatological seasonal net precipitation ($E-P < 0$), from 1980 to 2000, estimated by integrating E-P over 10-day forward trajectories from the North Atlantic moisture source region, using the numerical approaches shown in Figure 2.

doi:10.1371/journal.pone.0099046.g003

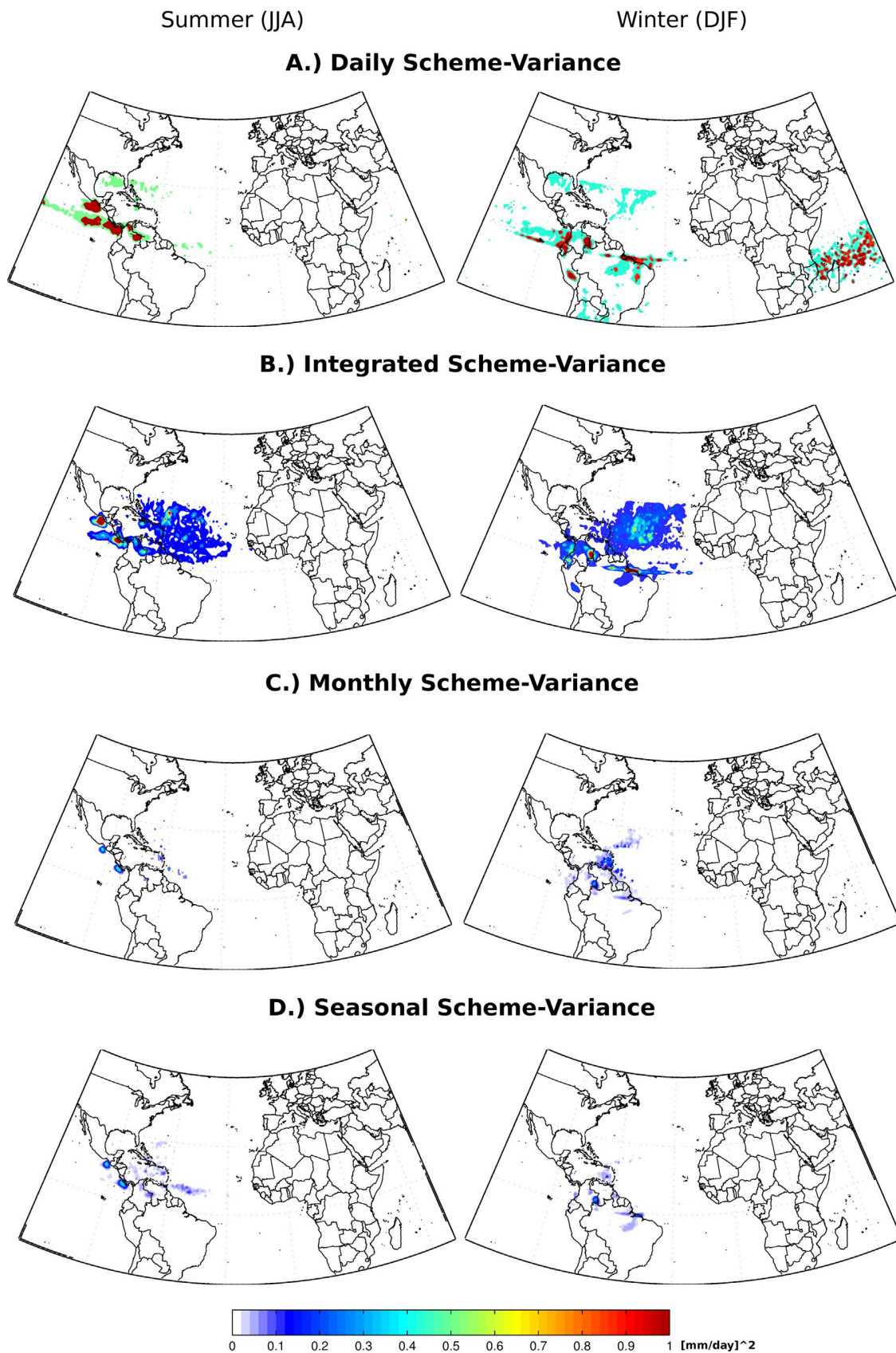


Figure 4. As for Figure 3, but for interannual variance of net precipitation ($E-P < 0$).
doi:10.1371/journal.pone.0099046.g004

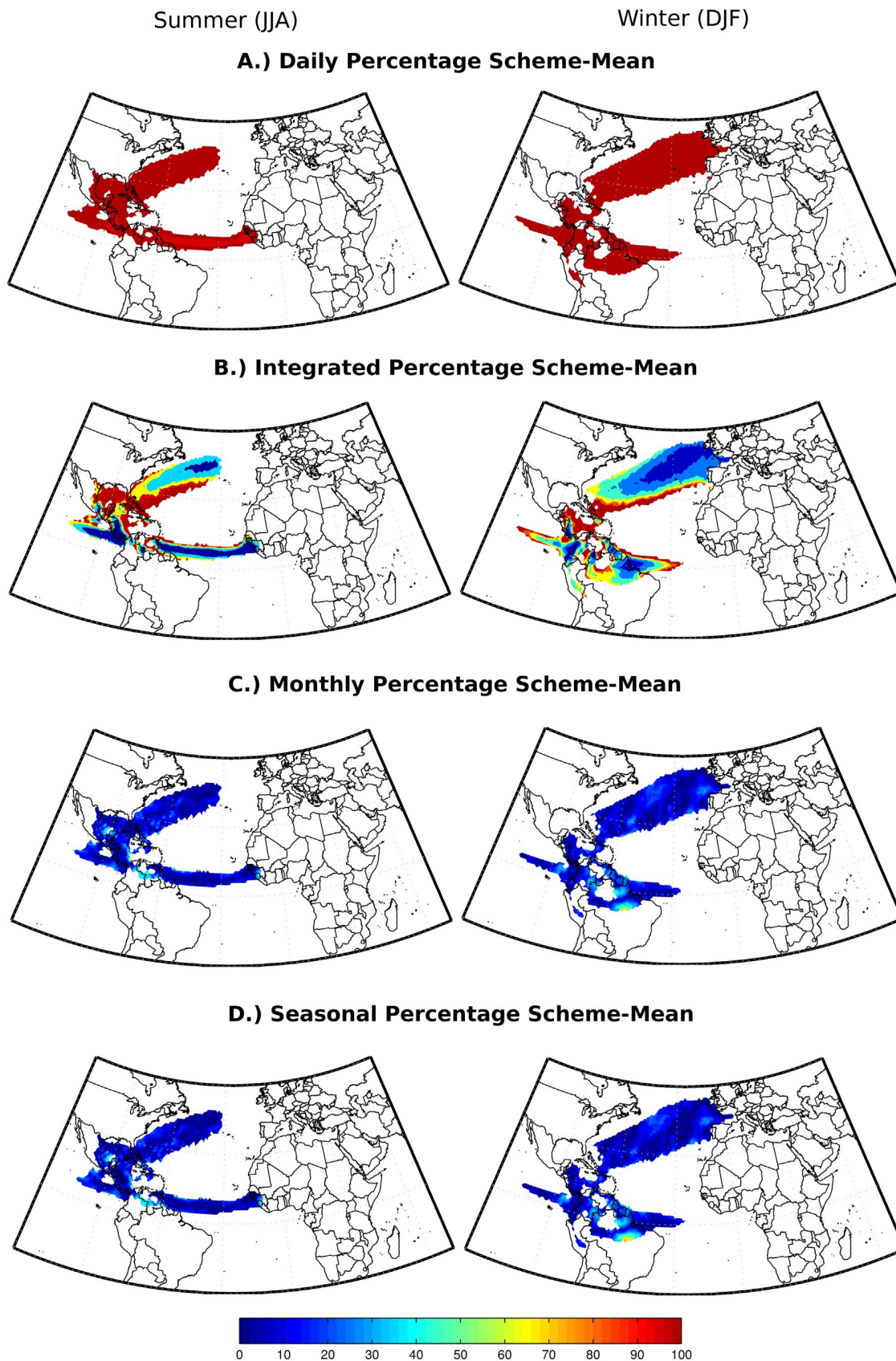


Figure 5. Percentage magnitude of the differences in mean net precipitation with respect to the 21-year average (climatological scheme-mean) for each one of the approaches.

doi:10.1371/journal.pone.0099046.g005

PLOS ONE | www.plosone.org

June 2014 | Volume 9 | Issue 6 | e99046

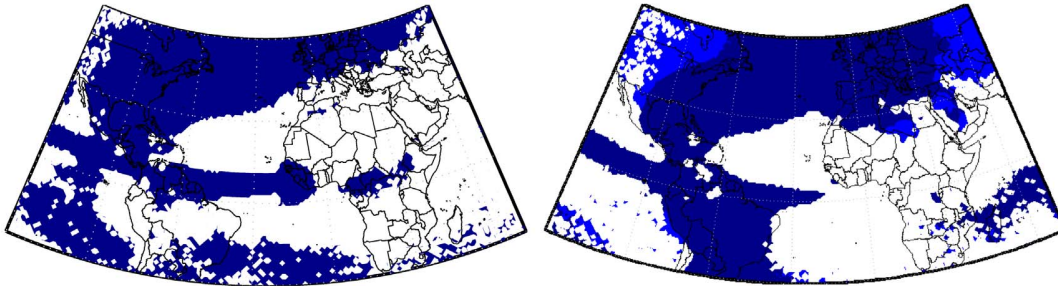
Statistical Significance Test of Composite Anomalies

95% two tail distribution

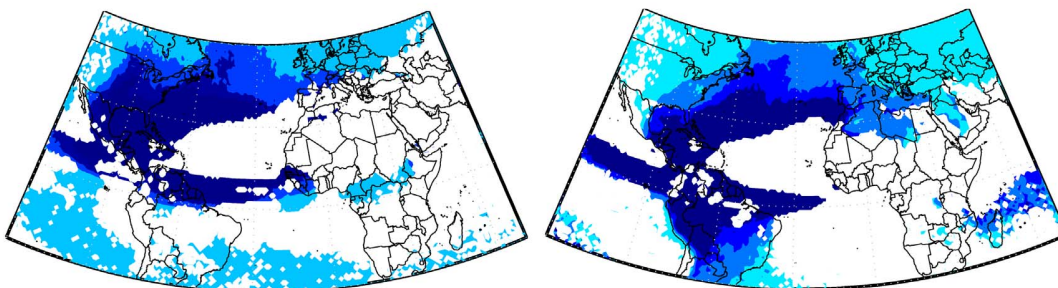
Summer (JJA)

Winter (DJF)

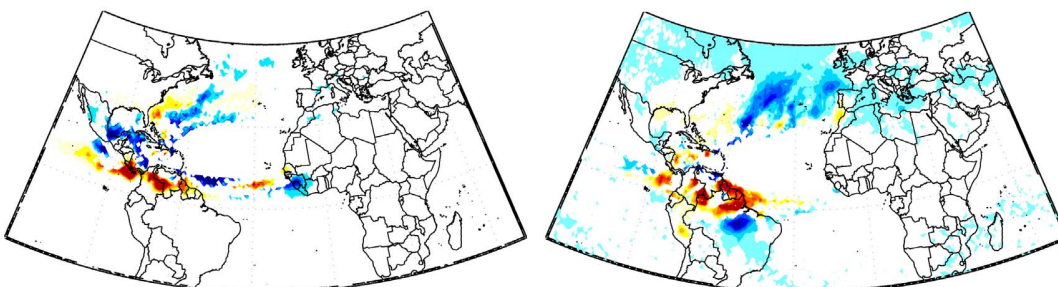
A.) Daily Scheme-Test



B.) Integrated Scheme-Test



C.) Monthly Scheme-Test



D.) Seasonal Scheme-Test

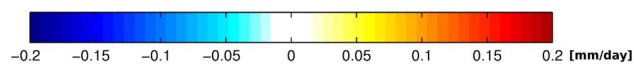
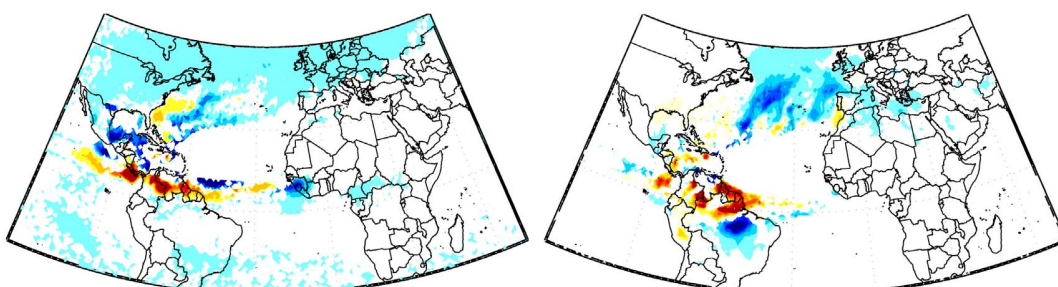


Figure 6. Differences between the climatological scheme-mean net precipitation and the shorter time scale scheme-means. Only significant differences through the T test using a two tail distribution and 95% of significance are shown.
doi:10.1371/journal.pone.0099046.g006

In order to quantify the magnitudes of the differences in DJF and JJA mean net precipitation, we calculated the percentage error between each one of the approaches with respect to the 21-year average (climatological scheme-mean). The values of the percentage errors reduce at 'Monthly' or longer time scales (Figure 5).

Two statistical tests were performed. The first one evaluates the significance of the differences between the climatological scheme-mean and the other shorter time scale scheme-means through the one sample T test using the two tail distribution with 95% of significance (Figure 6). This test revealed that the differences between the means reduce at 'Monthly' and the longer time scales. The second one is the calculation of the Pearson time correlation coefficients (and the respective T statistical test with the 95% level of significance) of the 21-year net precipitation values obtained

through the seasonal scheme-mean and the other ones estimated via the shorter time scale schemes. The main finding is that at 'Monthly' time scale the resulting correlation displays a very similar pattern with respect to the seasonal one, suggesting that both schemes reproduce quite similar patterns of the interannual variability (Figure 7).

Figures 5, 6 and 7 corroborate our conclusions that it is possible to discount $(E-P) > 0$ values after the integration of $(E-P)$ without affecting the general net precipitation patterns, if the positive $(E-P)$ values are discounted in monthly or longer time scales. It is likely that discounting $(E-P) > 0$ values at shorter time scales ('Daily' and 'Integrated' analyses) distorts the long-term atmospheric column moisture budget, leading to overestimated moisture losses and expanded sink regions, as shown in the climatological averages in Figures 3a and 3b.

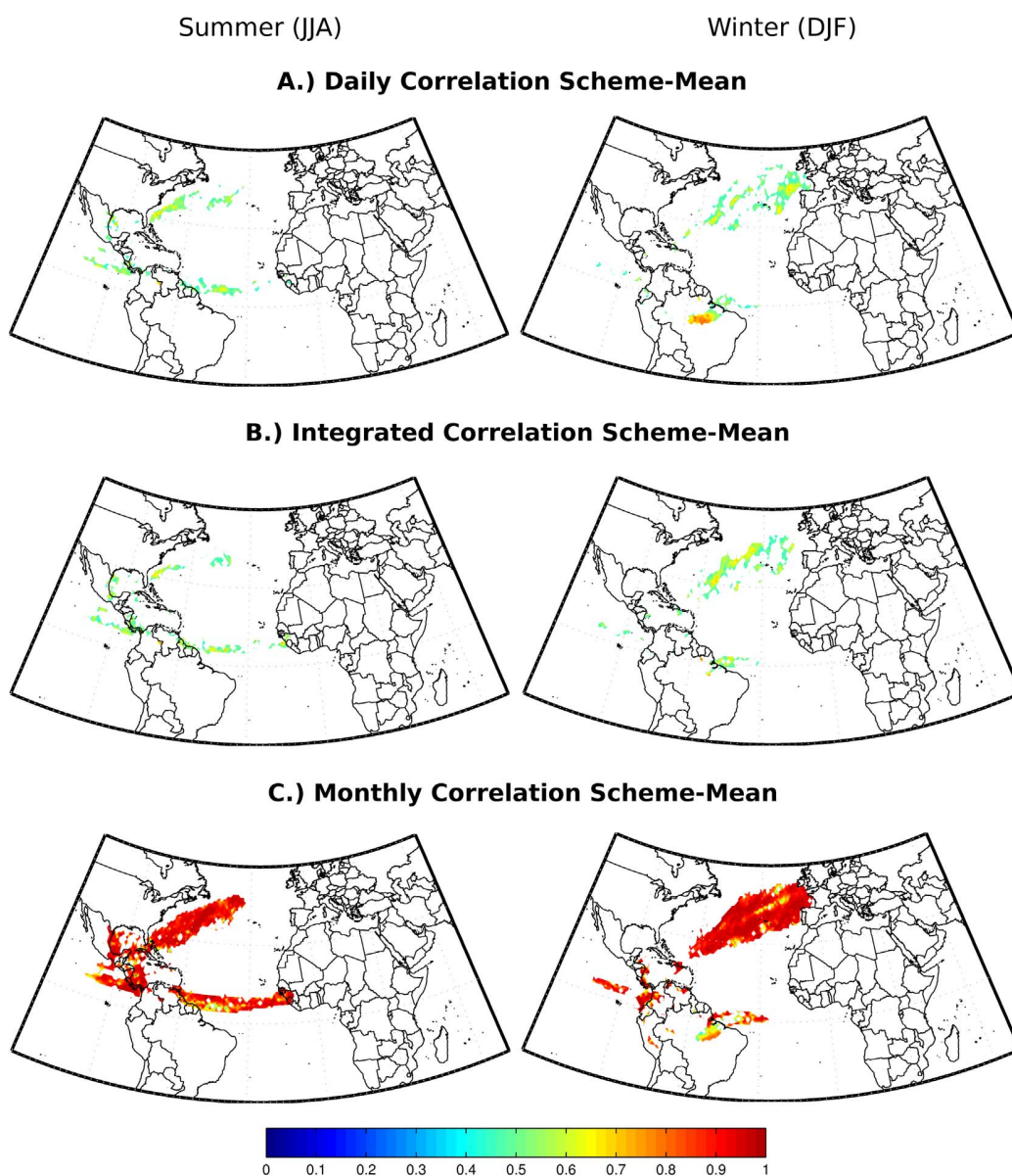


Figure 7. Pearson correlation of the 21-year of the net precipitation between the seasonal scheme-mean and the shorter time scale scheme-means (T test with 95% of significance).
doi:10.1371/journal.pone.0099046.g007

Conclusions

The aim of the present study was to evaluate the impact of discounting net evaporation at different temporal scales, when estimating the climatological seasonal precipitation using the atmospheric component of the E-P moisture budget. Suitability and quality tests were performed using 3-D Lagrangian approach data by forward tracking from the North Atlantic moisture source, during winter and summer seasons from 1980 to 2000. Discounting E-P>0 from the E-P budget was tested at five different time scales, and the corresponding climatological seasonal E-P<0 means and interannual E-P<0 variances were calculated.

The results show that E-P>0 can be discounted after E-P has been integrated without altering the general patterns of net

precipitation, if E-P>0 is discounted using a monthly or longer time scale.

Acknowledgments

The authors would like to thank Dr. Juan Carlos Antuña and an anonymous reviewer whose comments helped us to improve the manuscript.

Author Contributions

Conceived and designed the experiments: RC RN AD LG. Performed the experiments: RC AD. Analyzed the data: RC RN LG. Contributed reagents/materials/analysis tools: RN LG. Wrote the paper: RC LG RN.

References

1. Gimeno L, Stohl A, Trigo RM, Dominguez F, Yoshimura K, et al. (2012) Oceanic and Terrestrial Sources of Continental Precipitation. *Rev. Geophys.* 50: doi:10.1029/2012RG000389.
2. Stohl A, Hittenberger M, Wotawa G (1998) Validation of the Lagrangian particle dispersion model FLEXPART against large scale tracer experiment data. *Atmospheric Environment* 32: 4245–4264.
3. Gimeno L, Drumond A, Nieto R, Trigo RM, Stohl A (2010) On the origin of continental precipitation. *Geophysical Research Letters* 37: doi:10.1029/2010GL043712.
4. Gimeno L, Nieto R, Drumond A, Castillo R, Trigo RM (2013) Influence of the intensification of the major oceanic moisture sources on continental precipitation. *Geophysical Research Letters* doi:10.1002/grl.50338.
5. Castillo R, Nieto R, Drumond A, Gimeno L (2014) The role of the ENSO cycle in the modulation of moisture transport from major oceanic moisture sources. *Water Resour. Res.* 50:doi: 10.1002/2013WR013900.
6. Drumond A, Nieto R, Gimeno L (2011) On the contribution of the Tropical Western Hemisphere Warm Pool source of moisture to the Northern Hemisphere precipitation through a Lagrangian approach. *J. Geophys. Res.* 116: doi:10.1029/2010JD015397.
7. Durán-Quesada AM, Gimeno L, Amador JA, Nieto R (2010) Moisture sources for Central America: Identification of moisture sources using a Lagrangian analysis technique. *J. Geophys. Res.* 115: D05103 doi:10.1029/2009JD012455.
8. Drumond A, Nieto R, Gimeno L, Ambrizzi T (2008) A Lagrangian identification of major sources of moisture over central Brazil and La Plata Basin. *J. Geophys. Res.* 113: D14128 doi:10.1029/2007JD009547.
9. Gimeno L, Nieto R, Trigo RM, Vicente-Serrano SM, López-Moreno JI (2010b) Where does the Iberian Peninsula moisture come from? An answer based on a Lagrangian approach. *J. Hydrometeorol.* 11: 421–436 doi:10.1175/2009JHM1182.1.
10. Thompson DW, Wallace JM (2001) Regional climate impacts of the Northern Hemisphere annular mode. *Science* 293(5527):85–89.
11. Stohl A, James P (2004) A Lagrangian analysis of the atmospheric branch of the global water cycle: part 1: method description, validation, and demonstration for the August 2002 flooding in central Europe. *Journal of Hydrometeorology* 5: 656–678.
12. Stohl A, James P (2005) A Lagrangian analysis of the atmospheric branch of the global water cycle. Part II: moisture transports between earth's ocean basins and river catchments. *Journal of Hydrometeorology* 6: 961–984.
13. Uppala SM, Kållberg PW, Simmons AJ, Andrae U, Da Costa Bechtold V, et al. (2005) The ERA-40 re-analysis. *Quarterly Journal of the Royal Meteorological Society* 131: 2961–3012.
14. Stohl A, Forster C, Frank A, Seibert P, Wotawa G (2005) Technical Note: The Lagrangian particle dispersion model FLEXPART version 6.2. *Atmos Chem Phys* 5: 2461–2474.
15. Numaguti A (1999) Origin and recycling processes of precipitating water over the Eurasian continent: experiments using an atmospheric general circulation model. *Journal of Geophysical Research* 10: 1957–1972.

Influence of the intensification of the major oceanic moisture sources on continental precipitation

Luis Gimeno,¹ Raquel Nieto,¹ Anita Drumond,¹ Rodrigo Castillo,¹ and Ricardo Trigo^{2,3}

Received 28 January 2013; revised 7 March 2013; accepted 7 March 2013.

[1] In this study, we address two key issues in the hydrological cycle that have remained elusive: 1) to what extent can we expect climate change to affect the transport of moisture? and, in particular, 2) how will the changes in the sources' intensity (that is, more evaporation) affect the distribution of continental precipitation? This was achieved using a multimodel ensemble that allowed delimiting those oceanic areas where climate change will likely lead to an increase in evaporation (E) minus precipitation (P). Finally, a sophisticated Lagrangian model was used to identify which continental regions will be affected by changes in precipitation ($E - P < 0$) originating in each oceanic moisture source. We find that in boreal winter, wide sectors of Europe, Asia, Middle East, South America, and southern Africa are affected, but North America emerges as the most affected continental region. In austral winter, the largest changes are confined to northern and Central America. **Citation:** Gimeno, L., R. Nieto, A. Drumond, R. Castillo, and R. Trigo (2013), Influence of the intensification of the major oceanic moisture sources on continental precipitation, *Geophys. Res. Lett.*, 40, doi:10.1002/grl.50338.

1. Introduction

[2] One of the greatest threats posed by climate change stems from major changes in the hydrological cycle, including the location and strength of the most important oceanic moisture sources [Gimeno *et al.*, 2012]. Global warming driven by increasing concentrations of greenhouse gases is expected to cause increased global mean precipitation and evaporation [Wentz *et al.*, 2007; Intergovernmental Panel on Climate Change (IPCC), 2007]. Furthermore, according to the Clausius-Clapeyron equation, the high sensitivity of saturated vapor pressure to temperature will result in increased atmospheric water vapor and, hence, water vapor transport that amplifies the water cycle [Allen and Ingram, 2002; Held and Soden, 2006]. This effect will in turn

accentuate the pattern of evaporation minus precipitation ($E - P$); put simply, wet (dry) regions get wetter (drier).

[3] An indirect way of predicting trends in oceanic evaporation, and their relationship with precipitation, is through salinity time series. Various authors have consistently shown an increase in the salinity of the upper subtropical oceans in all oceanic basins in recent decades [e.g., Curry *et al.*, 2003], which indicates an increase in ($E - P$). Observational studies of atmospheric moisture content and precipitation are consistent with these expectations [Durack *et al.*, 2012]. According to the satellite-based Special Sensor Microwave Imager [Santer *et al.*, 2007], since 1988, there has been an increase of 0.041 kg/m²/yr in the total atmospheric moisture content over the oceans and an increase in global mean precipitation over land by about 2% over the period 1900–1998 [Dai *et al.*, 1997]. Regional changes in precipitation also illustrate how wet (dry) regions get wetter (drier): for example, an increase in precipitation in the extratropical latitudes (about 7%–12% in zonally averaged precipitation between 30°N and 85°N), more intense rainfall associated with the Asian and Indian summer monsoons, and substantially less precipitation in dry regions, including the Sahel, the Mediterranean, southern Africa, and parts of southern Asia [Folland *et al.*, 2001; IPCC, 2007].

[4] Climate models do indeed indicate a general increase of precipitation associated with several tropical monsoon systems (particularly the Asian and South American ones), and also at high latitudes (due to intensification of the global hydrological cycle), accompanied by a decrease in the subtropical latitudinal band [Curry *et al.*, 2003]. Models also predict that subtropical dry zones will expand poleward [Seager *et al.*, 2010].

[5] Moisture transport from oceanic sources to the continents links oceanic evaporation and continental precipitation, and analyzing this transport can provide a better understanding of observed changes and an improved physical understanding of future climate projections [Gimeno *et al.*, 2012]. Recent studies have considered the moisture transported both between latitudes [Knippertz and Wernli, 2010] and on a global scale [Gimeno *et al.*, 2010, hereafter G10]. We previously used a 3-D Lagrangian approach to identify the continental regions affected by precipitation that originated from specific oceanic source regions [Gimeno *et al.*, 2010]. We found that the supply of oceanic moisture to the continents is highly asymmetrical and specific to each oceanic basin and season. However, this analysis was restricted to 5 years of data, which does not allow the generation of a climatology of moisture transport from the oceanic sources to the continents, or the study of interannual variability or possible trends. Moreover, we used a lower precision approach where the total number of particles followed was relatively low. Here the analysis has been extended to

All Supporting Information may be found in the online version of this article.

¹Environmental Physics Laboratory (EPhysLab), Departamento de Física Aplicada, Facultad de Ciencias de Ourense, Universidad de Vigo, Ourense, Spain.

²CGUL, IDL, University of Lisbon, Lisbon, Portugal.

³Departamento de Engenharias, Universidade Lusófona, Lisbon, Portugal.

Corresponding author: L. Gimeno, Environmental Physics Laboratory, Departamento de Física Aplicada, Facultad de Ciencias de Ourense, Universidad de Vigo, Campus As Lagoas s/n, ES-32004 Ourense, Spain. (l.gimeno@uvigo.es)

©2013. American Geophysical Union. All Rights Reserved.
0094-8276/13/10.1002/grl.50338

two decades (1980–2000) of the ERA-40 reanalysis and using the Lagrangian model tuned to higher precision, allowing a reevaluation of the previous results. By considering composites of extreme years of high and low values of $E - P$, we performed an assessment of how increased evaporation in the source regions affects continental precipitation, as well as the identification of possible regions where precipitation is affected more by changes in moisture transport as the climate warms. This restriction of the analysis to data since 1979 reflects the impossibility to work meaningfully with high-resolution upper-level data prior to the incorporation of satellite data in the reanalysis.

2. Methods

[6] Identification of the main oceanic moisture source regions are based on the maxima of the annual climatological vertically integrated moisture flux divergence using the available European Centre for Medium-Range Weather Forecasts reanalysis ERA-40 data [Uppala *et al.*, 2005] on a $1^\circ \times 1^\circ$ grid between January 1980 and December 2000. Ten oceanic moisture source regions were identified based on a threshold of 750 mm/yr for the integrated moisture flux divergence (Figure 1, top). The work is based on the approach [Stohl and James, 2004] which uses the FLEXPART three-dimensional (3-D) Lagrangian particle dispersion model [Stohl *et al.*, 2005] to diagnose specific humidity changes along a large number of trajectories linking moisture source to moisture sink regions. The model was initialized in forward mode to track atmospheric moisture for the entire atmosphere using the ERA-40 reanalysis 24 data set, with a 1° horizontal resolution and a vertical resolution in 61 vertical levels. This was done for a 21 year period, from 1980 to 2000, and considering that the atmosphere is divided homogeneously into 1.9 million particles which are advected using the ERA-40 3-D wind input data. The FLEXPART model requires consistent high-quality data of wind and humidity at all these 61 vertical levels, thus hampering the application to older reanalysis data (~ 1979), i.e., prior to the significant decrease of the errors of these variables (namely, over the oceans) due to the inclusion of satellite data [Bengtsson *et al.*, 2004; Uppala *et al.*, 2005]. Records were made at 6 h intervals (00, 06, 12, and 18 UTC) of the position and specific humidity values q of every particle along its trajectory over a 10 day period, which is the average time that water vapor resides in the atmosphere [Numaguti, 1999]. A data base was constructed that identified all trajectories originating from oceanic moisture sources. The ($E - P < 0$) values, integrated over the 10 days of transport, indicate the most important sinks of moisture for precipitation originating in each oceanic moisture source. It should be noted that there are several differences between the methods and data sets used in G10 that preclude a completely objective comparison between results. Thus, in G10, the Lagrangian model was used in a low precision mode, with much less particles being considered in each box. Here the methodology is applied in a higher precision mode, allowing particles located between latitude degree lines to be selected. Integration of contribution of a much higher number of particles may provide a higher magnitude of $E - P$ values.

[7] The composite differences between the average of the five highest intensity episodes and the average of the five lowest intensity events identified for that source

(High – Low) were obtained for JJA and DJF. A bootstrap method [Wei *et al.*, 2012] was used to test the statistical significance of composite differences.

[8] The identification of oceanic regions with higher evaporation rate in a future climate change scenario was based on data generated by 15 of the GCM models included in the Coupled Model Intercomparison Project phase 3 [Meehl, *et al.*, 2007] used for IPCC AR4. Here we performed moisture budget calculations for a future period of climate change between 2046 and 2065 and computed a multimodel ensemble mean [Seager *et al.*, 2010]. The criteria for using only 15 of the 24 models and the corresponding list can be found in the work by Seager *et al.* [2010, Table 1]. To identify regions of higher changes, a comparison was made against the period 1961–2000 for the semiannual periods of October–March and April–September. These regions were defined based on the threshold of 0.3 mm/yr. These regions were used with the FLEXPART model in forward mode to identify which continental regions would be affected by changes in precipitation ($E - P < 0$) originating in each oceanic moisture source.

[9] Full methods and any associated references are available in Method section in the auxiliary material.

3. Results

[10] The first step in quantifying atmospheric water vapor transport is to locate moisture source regions where evaporation exceeds precipitation on average; these are sources in the sense that, in these regions, there is net moisture transport into the atmosphere. These regions can be identified through diagnosis of the divergence of the vertically integrated moisture flux [Trenberth and Guillemot, 1998] (see Method section in the auxiliary material). The main net moisture sources are shown in Figure 1 (top left) for both boreal summer (JJA) and winter (DJF). The highest values of $E - P$ are found in the subtropical oceans (Indian, North and South Pacific, and North and South Atlantic), in smaller semiencllosed seas such as the Caribbean, Mediterranean and Red Seas, and South Africa (Agulhas Current region). We acknowledge that not all the precipitation falling over the continents was originated within these major oceanic source areas, and a fraction may have its origins in negative $E - P$ regions observed over the extratropical Oceans and in local recycling [Gimeno *et al.*, 2012]. In order to evaluate the role played by the nonsource areas, we computed the moisture contribution evaporated from all the oceanic areas that were not considered in the analysis (white oceanic areas in Figure 1, top right) and concluded that their contribution is restricted to a narrow tropical strip and two large high latitudinal bands, being moderately relevant in boreal winter over northern Europe and the patches of the North American continents (see Figure S1 in the auxiliary material).

[11] The second step uses a Lagrangian approach [Stohl and James, 2004] to diagnose specific humidity changes along a large number of trajectories (see Methods section), hence linking moisture source to moisture sink regions. The main oceanic source areas and their associated continental sink regions are shown for both winter and summer: at the global scale in Figure 1 (top right) and for individual sources in Figure S2. Overall, the pattern is similar to that identified by the initial study based on the lower density of particles approach and the shorter 5 year (2000–2005) period [Gimeno *et al.*, 2010]. In terms of influence on

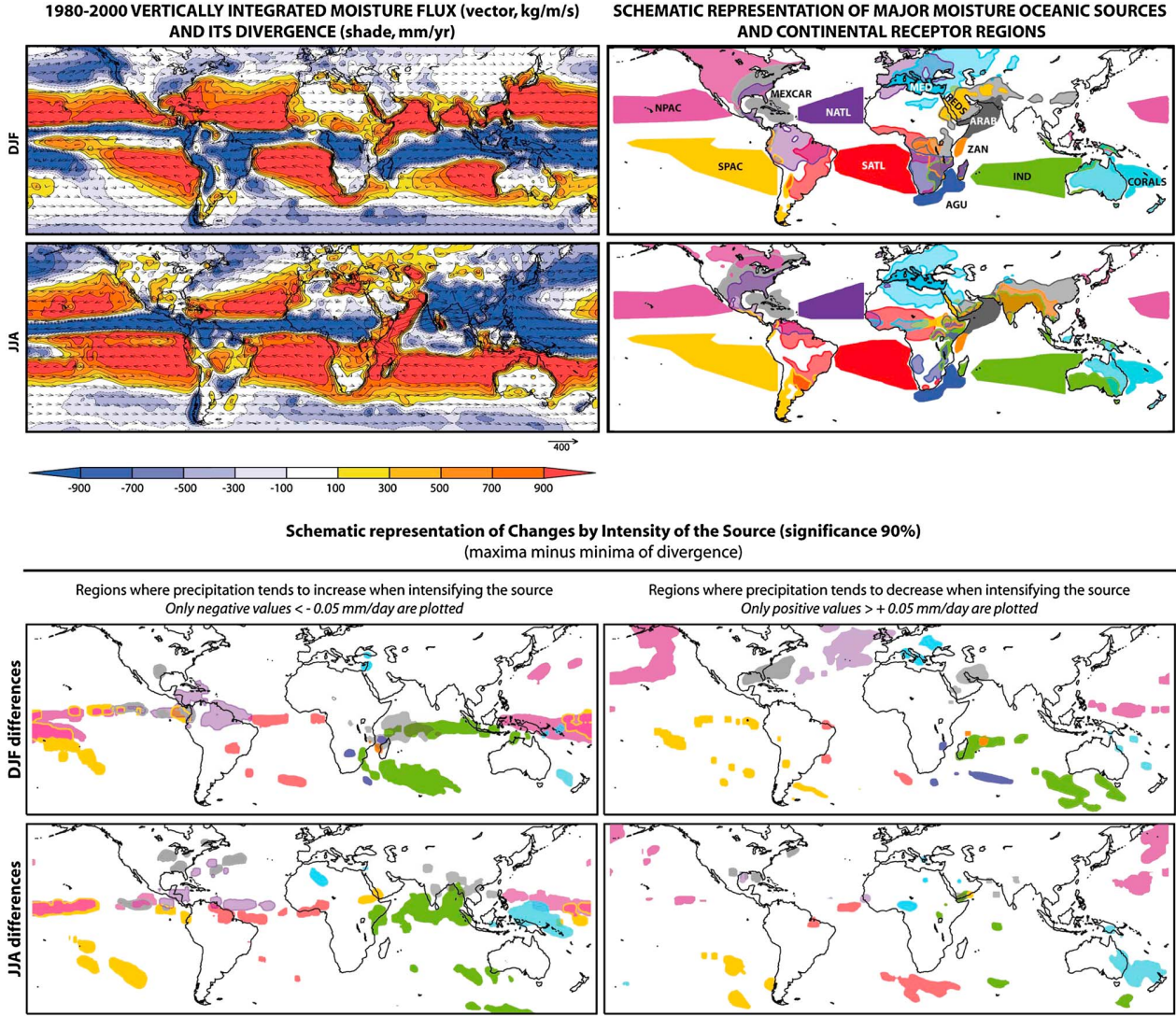


Figure 1. Main oceanic moisture sources associated with continental sink regions of the evaporated moisture and changes associated with the intensity of the source. (top left) Vertically integrated moisture flux for the period 1980–2000, shown as vectors (measured in kg/m/s), and its divergence, shown as warm and cool colors (measured in mm/yr) for summer (JJA) and winter (DJF). Data are from ERA-40. (top right) Schematic representation of oceanic moisture source regions and continental sink regions, for the period 1980–2000, for JJA and DJF. The sources of moisture are the same as in Gimeno *et al.* [2010, Figure 1]: NPAC, North Pacific; SPAC, South Pacific; NATL, North Atlantic; SATL, South Atlantic; MEXCAR, Mexico Caribbean; MED, Mediterranean Sea; REDS, Red Sea; ARAB, Arabian Sea; ZAN, Zanzibar Current; AGU, Agulhas Current; IND, Indian Ocean; CORALS, Coral Sea. Six of these source regions were defined based on the threshold of 750 mm/yr of the annual vertically integrated moisture flux calculated for the period 1980–2000 using data from ERA-40 for the oceanic sources. The Mediterranean and Red Seas were defined using their physical boundaries. $E - P$ fields are calculated by forward tracking from the defined moisture sources. Continental regions with an $E - P$ value less than -0.05 mm/d are shown using the same colors as the oceanic source region that contributes their moisture. Overlapping continental regions are plotted with a shaded mask comprising the relevant colors. (bottom) The composite differences in $E - P$ generated by each moisture source (identified using the same color scheme as the upper plot) between the average of the five highest intensity of source episodes and the average of the five lowest intensity seasons, during (left) December–February and (right) June–August. The black contour lines indicate areas where the absolute values of differences greater than 0.01 mm/d are significant at the 90% confidence level, according to a bootstrap test permuting the original time series 1000 times.

continental precipitation, the northern Atlantic subtropical ocean is the dominant source providing moisture for precipitation over vast areas, especially during DJF when its influence extends from Mexico to parts of Eurasia and from the Eurasian Arctic to the Amazon. This Atlantic influence on the Central and South American continent owes to the very

efficient low-level jet systems associated, namely, the Caribbean low-level jet [Amador, 2009], the South American low-level jet [Marengo *et al.*, 2004], and the Choco jet [Poveda and Mesa, 2000] that controls precipitation (mainly in DJF) over central America, tropical and Subtropical South America east of the Andes, and tropical Pacific coast of South

America, respectively. However, its influence on Europe during the summer vanishes. Major oceanic sources do not contribute directly to precipitation over vast continental areas (including most arid inland regions), though they can contribute through subsequent local moisture recycling. By contrast, a few small oceanic sources provide disproportionate amounts of moisture relative to their size. For instance, the Mediterranean is a dominant source for Europe and northern Africa during JJA, and the Red Sea provides large quantities of moisture that precipitate between the Gulf of Guinea and Indochina during JJA and between the African Great Lakes and Asia during DJF. There is also significant interhemispheric transport, with implications for continental precipitation, from the North Atlantic source during DJF and from western Indian sources during JJA. While vast areas, including Europe, South America, and Australia, receive moisture mainly from a single source, the monsoonal regimes in India, tropical Africa, and the quasi-monsoonal regime of North American Great Plains are fed by moisture from multiple source regions.

[12] Moisture source regions are not stationary, varying in intensity from year to year and expected to change in the future. The longer data set employed here allows us to perform a sensitivity analysis on the influence of source intensity (periods with enhanced or reduced $E - P$) on the transport of moisture from the net evaporating oceanic regions to the net precipitating continental ones (an analysis impossible to perform in G10). Differences in $E - P$ between the average of the five highest and lowest intensity episodes/seasons were obtained for each source during DJF (Figure 1, upper panels in the bottom plot) and JJA (Figure 1, lower panels in the bottom plot): see Method section and Figure S3 in the auxiliary material for further details. Using the same color scheme as employed previously for each source region, the figures indicate that precipitation tends to increase along the tropical band (and for both seasons) when the source is intensified. The subtropical oceanic sources contribute more to increases in precipitation in the central and western parts of the corresponding basin, while the intensification observed in the eastern tropical Pacific is due to moisture transported from the Caribbean source. The increase in precipitation associated with more intense monsoon circulations is evident during DJF for the South American monsoon (from the North Atlantic source), confirming the role of cross-equatorial moisture transport during intense monsoon events over the Amazon basin [Carvalho *et al.*, 2010]. The role of the enhanced transport of moisture from the Arabian Sea in the intensification of the rainfall associated with the Asian and Indian summer monsoons is apparent, confirming previous results [Meehl and Arblaster, 2003; Misra *et al.*, 2012]. Likewise, stronger than usual North America monsoon systems during JJA also rely on enhanced moisture availability from the Caribbean source [Hu and Feng, 2002]. According to our results, there is no significant displacement of the continental sink regions receiving precipitation from oceanic sources during periods of high intensity. Thus, the enhanced precipitation in tropical areas and monsoon regions projected by climate models might be related to enhanced moisture transport from the same moisture sources as before. Furthermore, there is no evidence of a general intensification of precipitation over the continents associated with strengthening of the moisture source in midlatitudes, being mostly restricted to the North Pacific and North Atlantic oceanic areas. Finally, most areas

affected by a decreasing trend during periods of high intensity tend to be also restricted to the oceanic areas with the few exceptions of southeastern U.S. and Mediterranean areas in DJF and eastern Australia in JJA (Figure 1, lower panels in the bottom plot). This insensitivity of precipitation at higher latitudinal bands (particularly over the continents) to changes in moisture source intensity suggests that the main process responsible for the expected intensification of precipitation at these latitudes is dynamical.

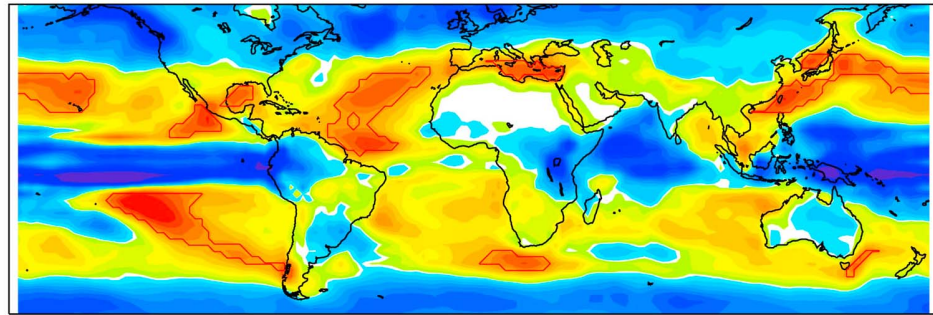
[13] A complementary approach to identifying continental regions most vulnerable to increased intensity of oceanic moisture sources focuses on sources that will experience the highest increase in $E - P$ in the next few decades according to a large ensemble of global climate models (GCMs), which are able to reproduce very consistently the current main moisture sources pattern [see Seager *et al.*, 2010, Figure 1]. It should then be possible to identify where moisture coming from these sources contributes to precipitation currently. We show as hot spot source regions (hssr's) those areas with modeled $E - P$ increases greater than 0.3 mm/d for the periods 2046–2065 compared with 1961–2000, as predicted by 15 GCMs used in the AR4 assessment, for boreal winter (Figure 2, top) and boreal summer (Figure 3, top) half years [Seager and Vecchi, 2010]. Ideally, we should use the same Lagrangian method directly to climate change scenario fields obtained with GCMs, in order to detect changes in the continental areas affected by these hssr's. However, the vast majority of GCMs available have neither the same spatial resolution as the ERA-40 data sets nor sufficient vertical levels of data to apply the FLEXPART model efficiently [Stohl *et al.*, 2005]. Instead, we applied the same Lagrangian approach as for current climate data (1980–2000) to identify those potentially vulnerable continental regions that receive moisture from these hssr areas in boreal winter (Figure 2, bottom) and boreal summer (Figure 3, bottom) (see also Method section in the auxiliary material).

[14] In boreal winter (Figure 2, top), large sectors of Europe, Asia, Middle East, North and South America, and southern Africa are affected. Two hssr's have the widest influence: one in the central North Atlantic that influences precipitation over Europe and South America, and the other in the subtropical western North Pacific that influences precipitation over North America and the Southeast Asian continent. It is worth mentioning the potential or an amplified role of the North Atlantic and North Pacific sources to increase the frequency of atmospheric river events (confined areas of lower troposphere that transport vast amounts of moisture from the subtropics). It has been widely reported in the last decade that a large fraction of intense precipitation and flood events in North American west coast and also over the UK and the Mediterranean are related with the occurrence of these extreme episodes [see Gimeno *et al.*, 2012].

[15] The small Mediterranean hssr has a strong influence on European precipitation; nevertheless, this influence can soften the expected combined impact of climate change in southern Europe, i.e., more frequent droughts and summer heat waves, which is so consistent among different GCMs [IPCC, 2007]. On the whole, North America is the most affected continental region, being directly influenced by four different hssr's: in the Caribbean, the tropical Mexican coastal Pacific, the subtropical western North Pacific, and the central North Atlantic.

[16] In austral winter (Figure 3, top), the two regions most likely to be influenced by future extreme changes in $E - P$

Multimodel ensemble mean ($E - P$) change in the moisture budget for 2046–65 minus 1961–2000
d($E - P$) for October to March



($E - P$) < -0.01 mm/day for October to March 1980–2000 for those region with d($E - P$) > 0.30 mm/day

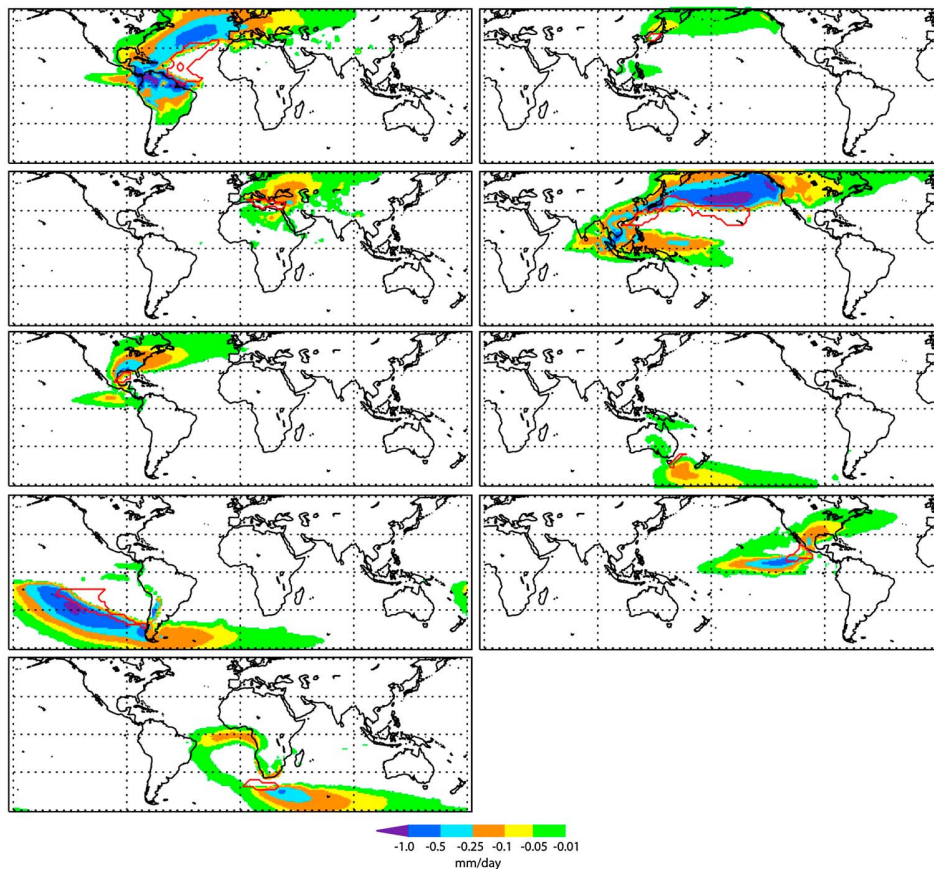


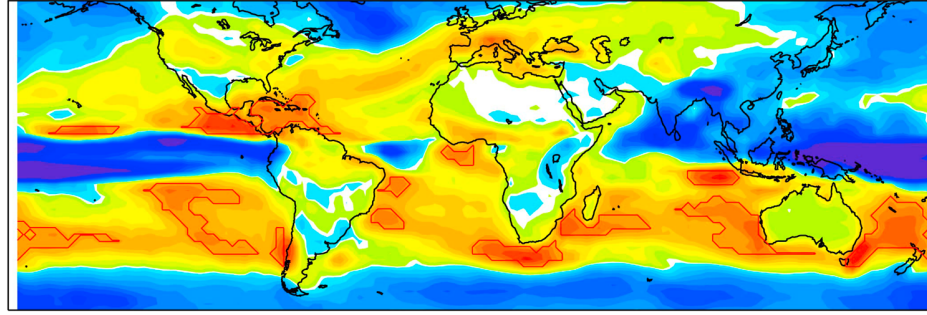
Figure 2. Oceanic moisture sources with the highest predicted change of intensity associated with continental sink regions of the evaporated moisture (for October–March). (top) Multimodel ensemble mean ($E - P$) change in moisture budget for 2046–1965 minus 1961–2000 for October–March, based on the data generated using 15 GCMs run as part of the Coupled Model Intercomparison Project phase 3 [Meehl *et al.*, 2007] and used for the Intergovernmental Panel on Climate Change’s Fourth Assessment Report (IPCC AR4). Data provided by Richard Seager [Seager *et al.*, 2010]. (bottom) Each of these plots is associated with a single moisture source. ($E - P$) values integrated over 10 days for October–March for the period 1980–2000, calculated by forward tracking the FLEXPART model from the moisture source (indicated by the closed red line) and identified according to the largest values of the multimodel ensemble mean change in ($E - P$) which exceeded a threshold of 0.3 mm/d. Only negative values less than -0.01 mm/d are plotted.

are in the northern and Central America, which receive moisture for precipitation from the Atlantic warm pool hssr [Drumond *et al.*, 2011], and the Sahel [Nieto *et al.*, 2006], which is affected by moisture from the nearby Gulf of Guinea hssr. These two areas are particularly prone to

prolonged drought events, and therefore, the possibility of having an intensified supply of precipitation from their main oceanic source corresponds to good news, particularly for Mexico and southwestern, where GCMs predict increase of evaporation and less precipitation and soil moisture [IPCC,

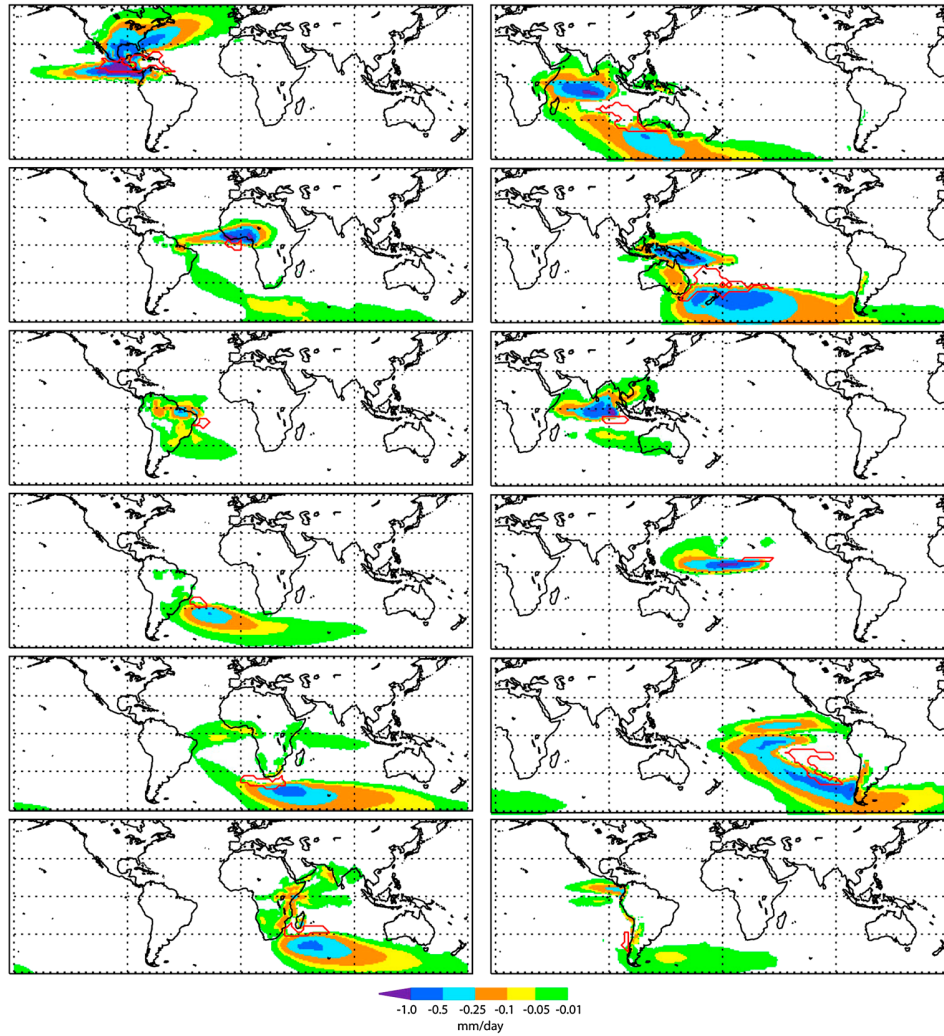
Multimodel ensemble mean (E-P) change in the moisture budget for 2046–65 minus 1961–2000

d(E-P) for April to September



-0.60 -0.50 -0.40 -0.35 -0.30 -0.25 -0.20 -0.15 -0.10 -0.05 -0.01 0.01 0.05 0.10 0.15 0.20 0.25 0.30 0.35 0.40 0.50 0.60
mm/day

(E-P) < -0.01 mm/day for April to September 1980–2000 for those region with d(E-P) > 0.30 mm/day



-1.0 -0.5 -0.25 -0.1 -0.05 -0.01
mm/day

Figure 3. Potential oceanic moisture sources with higher predicted change of intensity associated with continental sink regions of the evaporated moisture (for April–September). Same as Figure 2 but for the months April–September.

2007]. The two hssr's located in the Indian Ocean have a moderate effect on surrounding continental areas: the hssr to the south of the Bay of Bengal influences the Malaysian Peninsula, while the hssr close to the Agulhas Current provides moisture for the East African coast and the Indian sub-continent. This is consistent with the results obtained

showing that the increase in the monsoon rainfall in the future is mainly related with the intensification of the atmospheric moisture transport into the Indian region related to rather strong increases in evaporation over the Arabian Sea (May 2011). Finally, the Pacific hssr located to the east of Australia affects the eastern half of the continent.

4. Concluding remarks

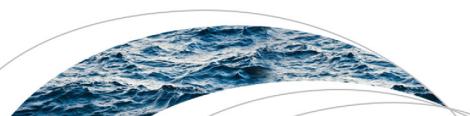
[17] Observational and modeling studies suggest that the strong dependence of saturated vapor pressure on temperature will result in increases of evaporation and, hence, precipitation, leading to an exacerbation of the water cycle. Robust identification of those regions particularly vulnerable to changes in the hydrological cycle requires the location of all major oceanic moisture sources and the tracking of the water that evaporates from those sources to where it precipitates over land [Gimeno *et al.*, 2010]. In this study, we first provide a more robust identification of all major oceanic moisture sources and assess their recent changes in amplitude. In particular, we address two key issues in the atmospheric branch of the hydrological cycle that have remained elusive: (1) to what extent can we expect climate change to affect the transport of moisture? and, in particular, 2) how will the changes in the sources' intensity (that is, more evaporation) affect the distribution of continental precipitation? We have confidence in the overall representativeness of these results, because the underlying assumptions are relatively robust: (i) the use of FLEXPART for climatological assessment of oceanic and continental moisture source areas has been shown to be consistent at the regional and global scales [Gimeno *et al.*, 2012]; (ii) the identification of areas prone to significant changes in $E - P$ was derived using a large ensemble of GCMs and agrees well for those regions receiving precipitation from the hssr's; and (iii) our results stand despite the moisture contribution evaporated from all the oceanic areas that were not considered in the analysis, as their overall contribution to the precipitation over midlatitude continents is only relevant in boreal winter over northern Europe and a few patches of the North American continents (Figure S1). Finally, we must stress that areas affected by these highly sensitive hssr regions are often spread over the oceans (Figures 2 and 3). However, we have identified those hssr's that do have an impact over specific continents, including highly populated areas (e.g., Central and North America, Europe, and Gulf of Guinea) that are under water stress [Vörösmarty *et al.*, 2010] and could become less prone to disruption of their water resources under climate change.

[18] **Acknowledgments.** This work was supported by the Spanish Government and FEDER through the projects MSM and TRAMO. The authors thank Richard Seager and two anonymous reviewers for their critical comments. Ricardo Trigo was partially supported by the FCT (Fundação para a Ciência e a Tecnologia, Portugal) through project STORMEx FCOMP-01-0124-FEDER-019524 (PTDC/AAC-CLI/121339/2010) cofunded by FEDER through COMPETE program.

References

- Allen, M. R., and W. J. Ingram (2002), Constraints on future changes in climate and the hydrologic cycle, *Nature*, **419**, 224–232, doi:10.1038/nature01092.
- Amador, J. A. (2009), The Intra-Americas Sea low-level jet: Overview and future research, *Ann. N. Y. Acad. Sci.*, **1146**, 153–188, doi:10.1196/annals.1446.012.
- Bengtsson, L., S. Hagemann, and K. I. Hodges (2004), Can climate trends be calculated from reanalysis data?, *J. Geophys. Res.*, **109**, doi:10.1029/2004JD004536.
- Carvalho, L. M. V., A. E. Silva, C. Jones, B. Liebmann, P. L. Silva Dias, and H. R. Rocha (2010), Moisture transport and intraseasonal variability in the South America monsoon system, *Clim. Dyn.*, **46**, 1865–1880, doi:10.1002/joc.2147.
- Curry, R. G., R. R. Dickson, and I. Yashayaev (2003), A change in the freshwater balance of the Atlantic Ocean over the past four decades, *Nature*, **426**, 826–829, doi:10.1038/nature02206.
- Dai, A., I. Y. Fung, and A. D. Del Genio (1997), Surface observed global and precipitation variations during 1900–1988, *J. Clim.*, **10**, 2943–2962.
- Drumond, A., L. Gimeno, and R. Nieto (2011), On the contribution of the tropical Western Hemisphere warm pool source of moisture to the Northern Hemisphere precipitation through a Lagrangian approach, *J. Geophys. Res.*, **116**, D00Q04, doi:10.1029/2010JD015397.
- Durack, P. J., S. E. Wijffels, and R. J. Matear (2012), Ocean salinities reveal strong global water cycle intensification during 1950 to 2000, *Science*, **336**, 455–458, doi:10.1126/science.1212222.
- Folland, C. K., et al. (2001), Observed climate variability and change, in *Climate Change 2001: The Scientific Basis. Contribution of Working Group I to the Third Assessment Report of the Intergovernmental Panel on Climate Change*, edited by J. T. Houghton et al., pp. 99–181, Cambridge Univ. Press, Cambridge, U. K.
- Gimeno, L., A. Drumond, R. Nieto, R. M. Trigo, and A. Stohl (2010), On the origin of continental precipitation, *Geophys. Res. Lett.*, **37**, L13804, doi:10.1029/2010GL043712.
- Gimeno, L., et al. (2012), Oceanic and Terrestrial Sources of Continental Precipitation, *Rev. Geophys.* doi:10.1029/2012RG000389.
- Held, I. M., and B. J. Soden (2006), Robust responses of the hydrological cycle to global warming, *J. Clim.*, **19**, 5686–5699, doi:10.1175/JCLI3990.1.
- Hu, Q., and S. Feng (2002), Interannual rainfall variations in the North American summer monsoon region: 1900–98, *J. Clim.*, **15**, 1189–1202, doi:10.1175/1520-0442(2002)015.
- Intergovernmental Panel on Climate Change (IPCC) (2007), *Climate Change 2007: The Physical Science Basis. Contribution of Working Group I to the Fourth Assessment Report of the Intergovernmental Panel on Climate Change*, edited by S. Solomon et al., Cambridge Univ. Press, Cambridge, U. K.
- Knippertz, P., and H. A. Wernli (2010), A Lagrangian climatology of tropical moisture exports to the Northern Hemisphere extratropics, *J. Clim.*, **23**, 987–1003, doi:10.1175/2009JCLI3333.1.
- Marengo, J. A., et al. (2004), Climatology of the low-level jet east of the Andes as derived from NCEP-NCAR reanalyses: Characteristics and temporal variability, *J. Clim.*, **17**, 2261–2280, doi:10.1175/1520-0442(2004)017.
- May, W. (2011), The sensitivity of the Indian summer monsoon to a global warming of 2 degrees C with respect to pre-industrial times, *Clim. Dyn.*, **37**, 1843–1868, doi:10.1007/s00382-010-0942-8.
- Meehl, G. A., and J. M. Arblaster (2003), Mechanisms for projected future changes in South Asian monsoon precipitation, *Clim. Dyn.*, **21**, 659–675, doi:10.1007/s00382-003-0343-3.
- Meehl, G., et al. (2007), The WCRP CMIP3 multimodel dataset: A new era in climate change research, *Bull. Am. Meteorol. Soc.*, **88**, 1383–1394, doi:10.1175/BAMS-88-9-1383.
- Misra, V., P. Pantina, S. C. Chan, and S. Di Napoli (2012), A comparative study of the Indian summer monsoon hydroclimate and its variations in three reanalyses, *Clim. Dyn.* doi:10.1007/s00382-012-1319-y.
- Nieto, R., L. Gimeno, and R. M. Trigo (2006), A Lagrangian identification of major sources of Sahel moisture, *Geophys. Res. Lett.*, **33**, L18707, doi:10.1029/2006GL027232.
- Numaguti, A. (1999), Origin and recycling processes of precipitating water over the Eurasian continent: Experiments using an atmospheric general circulation model, *J. Geophys. Res.*, **104**, 1957–1972.
- Poveda, G., and O. J. Mesa (2000), On the existence of Lloró (the rainiest locality on Earth): Enhanced ocean-atmosphere-land interaction by a low-level jet, *Geophys. Res. Lett.*, **27**(11), 1675–78.
- Santer, B. D., et al. (2007), Identification of human-induced changes in atmospheric moisture content, *Proc. Natl. Acad. Sci. U. S. A.*, **104**, 15248–15253, doi:10.1073/pnas.0702872104.
- Seager, R., and G. A. Vecchi (2010), Climate Change and Water in Southwestern North America Special Feature: Greenhouse warming and the 21st century hydroclimate of southwestern North America, *Proc. Natl. Acad. Sci. U. S. A.*, **107**, 21,277–21,282, doi:10.1073/pnas.0910856107.
- Seager, R., and G. A. Vecchi (2010), Thermodynamic and dynamic mechanisms for large-scale changes in the hydrologic cycle in response to global warming, *J. Clim.*, **23**, 4651–4668, doi:10.1175/2010JCLI3655.1.
- Seager, R., and G. A. Vecchi (2010), A. Climate change and water in southwestern North America Special Feature: Greenhouse warming and the 21st century hydroclimate of southwestern North America, *PNAS* **2010**, **107**, 21277–21282.
- Stohl, A., and P. A. James (2004), Lagrangian analysis of the atmospheric branch of the global water cycle. Part I: Method description, validation, and demonstration for the August 2002 flooding in central Europe, *J. Hydrometeorol.*, **5**, 656–678, doi:10.1175/1525-7541(2004)005.
- Stohl, A., C. Forster, A. Frank, P. Seibert, and G. Wotawa (2005), G. Technical Note: The Lagrangian particle dispersion model FLEXPART version 6.2, *Atmos. Chem. Phys.*, **5**, 2461–2474.
- Trenberth, K. E., and C. J. Guillemot (1998), Evaluation of the atmospheric moisture and hydrological cycle in the NCEP/NCAR reanalyses, *Clim. Dyn.*, **14**, 213–231.

- Uppala, S. M., et al. (2005), The ERA-40 re-analysis, *Q. J. R. Meteorol. Soc.*, *131*, 2961–3012, doi:10.1256/qj.04.176.
- Vörösmarty, C. J., et al. (2010), Global threats to human water security and river biodiversity, *Nature*, *467*, 555–561, doi:10.1038/nature09440.
- Wei, J., P. A. Dirmeyer, M. G. Bosilovich, and R. Wu (2012), Water vapor sources for Yangtze River Valley rainfall: Climatology, variability, and implications for rainfall forecasting, *J. Geophys. Res.*, *117*, D05126, doi:10.1029/2011JD016902.
- Wentz, F. J., L. Ricciardulli, K. Hilburn, and C. Mears (2007), How much more rain will global warming bring?, *Science*, *317*, 233–235.



Water Resources Research

RESEARCH ARTICLE

10.1002/2013WR013900

Special Section:

Oceanic Sources of
Continental Precipitation

Key Points:

- ENSO modulates the transport of moisture from the major oceanic sources
- Coherence with variations of the large-scale atmospheric and precipitation systems
- Most of moisture sources keep position and extension stationary along the ENSO cycle

Supporting Information:

- info_auxiliary_material
- Figures S1 and S2

Correspondence to:

L. Gimeno,
lgimeno@uvigo.es

Citation:

Castillo, R., R. Nieto, A. Drumond, and L. Gimeno (2014), The role of the ENSO cycle in the modulation of moisture transport from major oceanic moisture sources, *Water Resour. Res.*, 50, doi:10.1002/2013WR013900.

Received 2 APR 2013

Accepted 19 JAN 2014

Accepted article online 24 JAN 2014

The role of the ENSO cycle in the modulation of moisture transport from major oceanic moisture sources

Rodrigo Castillo¹, Raquel Nieto¹, Anita Drumond¹, and Luis Gimeno¹
¹EPhysLab (Environmental Physics Laboratory), Facultade de Ciencias, Universidade de Vigo, Ourense, Spain

Abstract The influence that the evolution of the ENSO cycle has on the moisture transport from the major oceanic moisture sources is investigated using a sophisticated Lagrangian approach informed by ERA-interim data, together with composites of ENSO phases. When maintaining the sources of moisture defined for the climatological period 1980–2012, the variations in the moisture sinks associated with each of these evaporative sources throughout the ENSO cycle reproduce the known patterns of variations of the large-scale atmospheric and precipitation systems over this cycle. Such variations include those observed in rainfall over the equatorial Pacific, in the major Summer monsoon systems, and in subtropical rainfall. When the areas of the sources were redefined according to the phase of ENSO, most of them remained stationary over the period of interest, nevertheless four of them showed notable differences in terms of their extents, namely the South Pacific and the Coral Sea (Pacific Ocean); the Mexican Caribbean (Atlantic), and the Arabian Sea (Indian).

1. Introduction

The atmospheric branch of the hydrological cycle plays a fundamental role in the climate system. Evaporation from the oceanic moisture sources to the continents and subsequent precipitation over terrestrial regions has for some years been of key interest at both local [e.g., Nieto *et al.*, 2006; Drumond *et al.*, 2008; Ordóñez *et al.*, 2012] and global scales [e.g., Gimeno *et al.* 2010a; Dirmeyer and Brubaker, 2007; Knippertz *et al.*, 2013]. In recent studies, sophisticated and robust Lagrangian approaches were used to link oceanic evaporation with continental precipitation in an attempt at least to detect the major oceanic moisture sources areas [Gimeno *et al.*, 2010a]. The resulting 12 evaporative sources obtained by analyzing a 5 year period of data (2000–2004) showed the supply of moisture to the continents to be highly asymmetrical with a strong seasonal variability. A subsequent study for a 21 year period (1980–2000) using a higher precision mode of calculation of E-P [Gimeno *et al.*, 2013] found similar patterns. The North and South Atlantic source regions are generally thought to be the most significant sources of moisture for precipitation over the continents, and it would appear that they also contribute to the seasonal structure of the Intertropical Convergence Zone (ITCZ). The subtropical Atlantic Ocean in the North Hemisphere has a larger impact over the continents than the Indian (Southern Hemisphere) and Pacific (Northern Hemisphere) sources of moisture. In terms of the influence on precipitation over continental regions, the subtropical Atlantic provides moisture for vast areas, particularly during DJF when its influence extends toward Mexico, Eurasia, and the Amazon; however, its influence on Europe diminishes greatly during JJA. The smaller moisture sources of the Mediterranean and Red Seas are important for relatively large continental areas such as Europe or Africa, and the Arabian Peninsula, respectively. The Indian subcontinent receives moisture from six different oceanic sources, while there are sizeable areas, such as Europe, South America, or Australia that receive moisture mainly from a single source. The American, African, and Asian-Australian monsoonal systems are fed by moisture provided from a larger number of source regions.

Previous studies have characterized the general pattern of moisture transport from a climatological perspective; however, no analysis of the variability of these major oceanic moisture sources due the main global teleconnection modes such as El Niño-Southern Oscillation (ENSO) has yet been undertaken. The ENSO has an effect on regional climate impacts throughout the world, including important aspects of interannual variability in patterns of global weather and precipitation. There is a vast literature on the influence of ENSO on the changes in precipitation patterns and the interested reader can approach the topic via the summaries of the IPCC [IPCC, 2013]. In this paper, we aim to evaluate the evolution of the

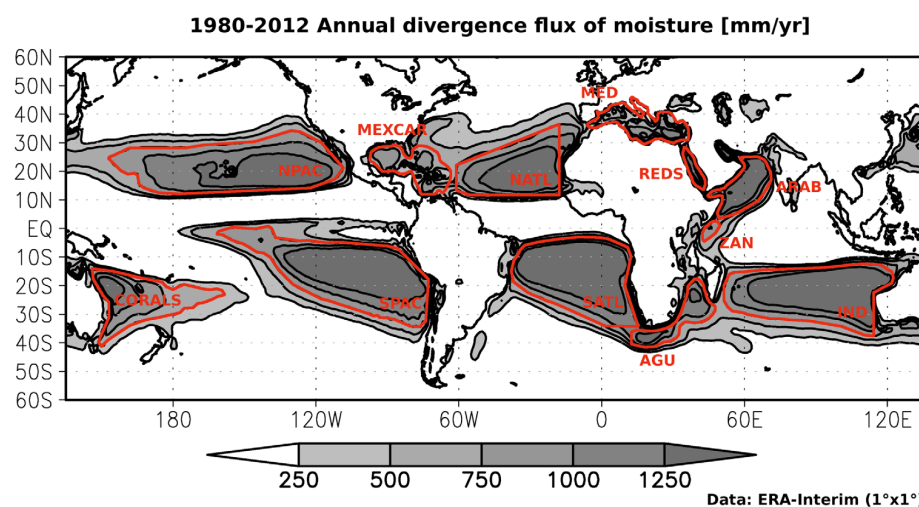


Figure 1. Major oceanic moisture sources: Climatological annual vertically integrated moisture flux divergence (mm/yr) for the period 1980–2012 using data from ERA-Interim. Values greater than 250 mm/yr are shown in gray scale, with intervals between isolines of 250 mm/yr. Areas inside the red contour lines indicate the regions considered as moisture sources in the forward integrations following the criteria of Gimeno *et al.* [2010]. Ten of these source regions were defined using the threshold of 750 mm/yr of the annual vertically integrated moisture flux calculated for the oceanic sources: NPAC, North Pacific; SPAC, South Pacific; NATL, North Atlantic; SATL, South Atlantic; MEXCAR, Mexico Caribbean; MED, Mediterranean Sea; REDS, Red Sea; ARAB, Arabian Sea; ZAN, Zanzibar Current; AGU, Agulhas Current; IND, Indian Ocean and CORALS, Coral Sea. The Mediterranean Sea (MED) and the Red Sea (REDS) were defined using their physical boundaries.

ENSO cycle with regard to the transport of moisture from the major oceanic moisture sources using the Lagrangian methodology of Gimeno *et al.* [2013].

2. Methods

The main moisture source regions were identified as the annual maxima of vertically integrated moisture flux divergence (threshold of 750 mm/yr). The vertically integrated moisture transport Θ is defined as: $\Theta = \frac{1}{g} \int_0^{p_s} qVdp$, where g is the acceleration due to gravity, q is the specific humidity, p_s is the surface pressure, and V is the horizontal wind vector. The divergence of this flux is equivalent to the net evaporation (E) minus precipitation (P) [Trenberth and Guillemot, 1998]; here we consider a 33 year period, making use of ECMWF reanalysis (ERA-interim) data on a $1^\circ \times 1^\circ$ grid and 60 vertical levels (from the surface to 0.1 hPa) from January 1980 to December 2012 (Figure 1) following the criteria of Gimeno *et al.* [2010a]. The method identified 10 oceanic moisture source regions, namely NPAC, North Pacific; SPAC, South Pacific; NATL, North Atlantic; SATL, South Atlantic; MEXCAR, Mexico Caribbean; ARAB, Arabian Sea; ZAN, Zanzibar Current; AGU, Agulhas Current; IND, Indian Ocean; and CORALS, Coral Sea. Two additional sources were included, defined using the physical boundaries of oceanic basins, namely MED, Mediterranean Sea and REDS, Red Sea. A schematic representation of the oceanic sources of moisture considered is included in the figures shown in this paper.

In order to identify the sinks for the moisture evaporated from the 12 oceanic sources, we based our analysis on the method developed by Stohl and James [2004], which uses the latest version of the freely available Lagrangian particle dispersion model FLEXPART v9.0 [Stohl *et al.*, 2005]. Lagrangian techniques are one of two types of method that make use of numerical water vapor tracers (WVT); the other type is Eulerian tagging. There are two other methods used to establish source-sink relationships for atmospheric water vapor, namely “analytical and box models” and “physical water vapor tracers” (isotopes); however, nowadays most workers agree that the most recently developed Lagrangian techniques are the most suitable for evaluating the origin of the water that precipitates over a continental area [Gimeno *et al.*, 2012]. The Lagrangian approach uniquely provides realistic traces of air parcels, enabling the trajectories to be followed and source-receptor relationships to be established. Using these models alone, it is possible to

identify the geographical origin of moisture that reaches a continental area. Of course, the other methodologies provide other types of useful and interesting information that also aids the analysis. The Eulerian methodology, for example, is widely used due its simplicity but it is far from easy to extract the link between the precipitation over a region and the moisture source using this method. While the “box models” allow the identification of the moisture inflow and outflow given defined lateral boundaries, they give no information about the physical processes that occur within the box itself. The use of isotopes depends on the sensitivity of the isotopic signal. An intercomparison of the source-receptor methods, including the advantages and disadvantages of each, is given in the recent comprehensive review of this topic by Gimeno *et al.* [2012]. Despite the range of methods available, the robustness of the Lagrangian trajectory method was demonstrated in a number of previous studies assessing global sources of moisture [e.g., Stohl and James, 2005; Dirmeyer and Brubaker, 2007; Gimeno *et al.*, 2010a; Knippertz *et al.*, 2013], and in regional analyses using FLEXPART, including for the great Mississippi River [Stohl and James, 2005], the Sahel [Nieto *et al.*, 2006], the Norwegian west coast [Stohl *et al.*, 2008], the South American Monsoon System [Drumond *et al.*, 2008], the areas over ice-cores in the Antarctic [Nieto *et al.*, 2010], Central America [Durán-Quesada *et al.*, 2010], the Iberian Peninsula [Gimeno *et al.*, 2010b], the Ethiopian highlands [Viste and Sorteberg, 2011], and the Indian Peninsula [Ordóñez *et al.*, 2012].

In the context of the studies described above, the ERA-interim reanalysis from January 1980 to December 2012 of the European Centre for Medium-Range Weather Forecasts [Dee *et al.*, 2011] was used to run the Lagrangian FLEXPART model. The ERA-interim data set represents the latest and best reanalysis for reproducing and interpreting the atmospheric branch of the hydrological cycle [Trenberth *et al.*, 2011; Lorenz and Kunstmann, 2012]. The usefulness of the data from before 1980 is somewhat limited for two reasons: (i) the FLEXPART model uses derived variables as input data such as U-wind, V-wind, and q (specific humidity), which were not reliable before 1980, and these are highly sensitive to errors, so the model outputs might be erroneous [Stohl *et al.*, 2005] and (ii) it is impossible to work with data obtained before the incorporation of satellite imagery in the reanalysis from 1979 onward. Prior to this date, there were insufficient observations over large oceanic areas and the data sets are considerably less reliable [Bengtsson *et al.*, 2004; Uppala *et al.*, 2005].

Based on the Lagrangian approach proposed by Stohl and James, we computed the increases (e) and decreases (p) in moisture by analyzing changes in specific humidity (q) along trajectories, i.e., $e - p = m \cdot (dq/dt)$, where m is the mass of each particle. We computed these changes for all the particles selected previously and the results were integrated in the atmospheric column over a given area, thereby obtaining $E - P$, the surface freshwater flux, where E and P are the rates of evaporation and precipitation per unit area, respectively. FLEXPART can calculate and track the trajectories of atmospheric moisture backward and forward in time to produce information on the spatial distribution of moisture sources. From a Lagrangian perspective, this estimation, made for a large number of trajectories, links the source regions to their respective sinks.

We initialized the model in forward mode to track around approximately 2.0 million “particles” (the highest limit allowed by the model) of equal mass distributed in the global atmosphere along 3-D trajectories. Each particle represents a fraction of the total atmospheric mass. The particles moved by the wind are considered as air parcels with internal negligible motion and unique thermodynamic properties. It is assumed that they do not interact or mix with neighboring particles and that they remain whole over time. Data were retrieved every 6 h (00, 06, 12, and 18 UTC). Changes in specific humidity (q), together with the positions of each particle, were recorded for each particle along its trajectory, limited to 10 days (the average residence time of water vapor in the atmosphere [Numaguti, 1999]). In order to derive the Lagrangian estimation of evaporation minus precipitation, the (E-P) values were integrated over each $1^\circ \times 1^\circ$ column over the gridded area. The analysis of (E-P) values can tell us where the air particles from a given source area either received (E-P > 0) or lost moisture (E-P < 0). (E-P) values integrated along 10 day forward trajectories were analyzed in order to investigate the main moisture sinks observed along trajectories starting in each of the 12 evaporative sources considered.

To analyze the influence of the ENSO cycle on the transport of moisture from the oceanic sources, we obtained composite differences between the positive and negative phases of ENSO, which were obtained from the NOAA/CPC Oceanic Niño Index (ONI) in the El Niño region 3.4 (5°N – 5°S , 120°W – 170°W), Smith *et al.* [2008]. ONI is defined by overlapping seasons, so to select a whole year as El Niño or La Niña we

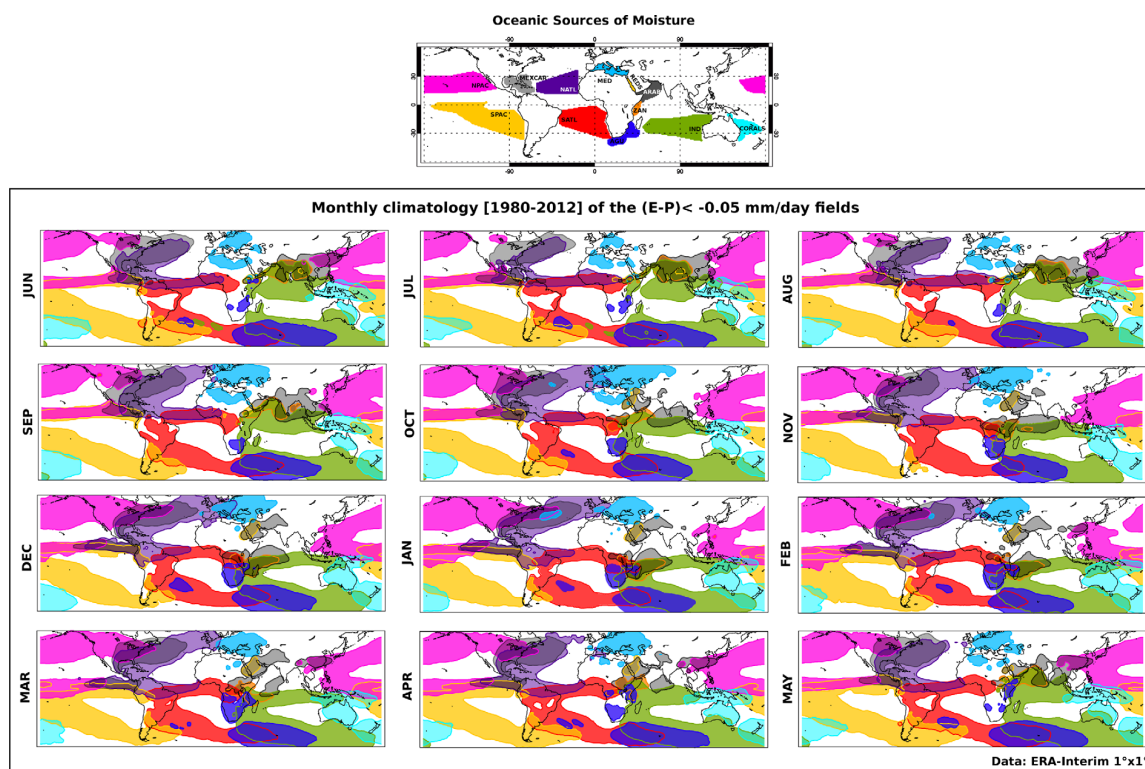


Figure 2. Monthly schematic representation of moisture sink regions for the period 1980–2012. The sources of moisture (bottom maps) are those detected in Figure 1. Only negative values of E-P larger than -0.05 mm d^{-1} are plotted and shown in the same colors as the corresponding oceanic source regions. Overlapping continental regions are plotted using the appropriate shading mask. E-P fields are calculated by forward tracking from the defined moisture sources.

considered those years when the phase repeated itself a minimum of five times consecutively from June in year 0 to May in year 1 (for a given ENSO cycle).

The eight highest intensity episodes for El Niño (1982–1983, 1986–1987, 1991–1992, 1994–1995, 1997–1998, 2002–2003, 2004–2005, and 2009–2010) and for La Niña (1984–1985, 1988–1989, 1995–1996, 1998–1999, 1999–2000, 2007–2008, 2010–2011, and 2011–2012) were selected. It must be stressed that we assumed that the boundaries of each oceanic source remained stationary throughout the years considered (Figure 1).

A bootstrap method was used to test the statistical significance of the composite differences. The methodology follows that proposed by Wei *et al.* [2012]. We tested the significance of the difference between the El Niño and the La Niña composites at a 90% confidence level by selecting two 8 year periods at random (a total of 16 years) from the 33 year climatology and calculating their difference 1000 times. To be considered significant, the absolute value of the composite of the differences must be larger than 90% of the 1000 differences.

3. Results

In order to gain a better understanding of the role of ENSO in moisture transport, it is useful to identify the climatologically favored sink regions associated with each oceanic source. Figure 2 summarizes the monthly variability of the favored sink regions associated with the sources studied, and allows the identification of the ways in which oceans contribute to the moisture budget of the major global precipitation systems throughout the year. As discussed in the Introduction section, a more detailed analysis of the climatological aspects of the moisture transport from the major oceanic sources toward the continents can be found in Gimeno *et al.* [2010a, 2013].

Concerning the Inter Tropical Convergence Zone (ITCZ), Figure 2 shows the contribution of different oceanic sources according to the subregion considered. While the Atlantic ITCZ receives moisture from the North and South Atlantic oceans, the Indian ITCZ may receive contributions from up to four different sources throughout the year (IND, ZAN, ARAB, and AGU). It must be remembered that the present discussion is limited only to the sources investigated and contributions from other regions may also be important. For instance, throughout the year NPAC and SPAC feed moisture to the Pacific ITCZ, which may also receive some moisture from MEXCAR and CORALS in its eastern and western domains, respectively.

Consideration of Figure 2 shows some aspects of the moisture contribution to the annual cycle of the continental summer monsoon systems. For example, there are important contributions from the ARAB, ZAN, REDS, and IND sources during the Indian summer, but there is no moisture transport from these sources to the region during the winter months. On the other hand, the NATL and SATL are the only of the investigated oceanic sources that contribute to the moisture observed in the region of the South America Monsoon System [Drumond *et al.*, 2008, and references therein]. The sources NATL, NPAC, and MEXCAR are important oceanic contributors to the region of the North American Monsoon System. As far as the precipitation in southern Africa is concerned [Cook, 2000; D'Abreton and Tyson, 1995; Todd *et al.*, 2004], while the AGU source contributes throughout the year, the additional sources SATL, ARAB, and ZAN are important during the austral Summer. The Indian-Pacific Warm Pool can receive moisture from different sources throughout the year, including NPAC, SPAC, IND, CORALS, and ARAB.

The rest of the oceanic areas that were not considered in Figure 2 (in white) also contribute for the precipitations around the world. Their influence is mainly restricted to a narrow tropical strip and two large high latitudinal bands (Figure S2).

Among the preferred climatological sink regions shown in Figure 2, it is also possible to identify the main transport moisture export (TME) paths discussed by Knippertz *et al.* [2013]. Differently from the approach applied here, they used another Lagrangian analysis tool (LAGRANTO) [Wernli and Davies, 1997] to construct a climatology of TMEs on the basis of 7 day forward trajectories, begun daily in the tropical lower troposphere, and required to reach a certain amount in terms of the water vapor flux somewhere outside the tropical latitudes. The authors identified four preferential activity centers in the Northern Hemisphere, these are: (i) The "pineapple express" (PE), which connects tropical moisture sources near Hawaii with precipitation near the North American west coast; (ii) The west Pacific maximum (WP), which contributes significantly to the global annual TME and is linked to the East Asian monsoon and the Meiyu-Baiu front; (iii) The narrow TME maximum over the Great Plains (GP) of North America, which originates over the Gulf of Mexico and the Caribbean Sea and has therefore been referred to as the "Maya express"; and (iv) TME over the western North Atlantic (the Gulf Stream maximum (GS)). These four paths each have a distinct seasonal cycle, ranging from warm-season maxima related to monsoon-type circulations over East Asia and central North America (WP and GP regions), to oceanic activity with a small annual cycle (GS), and winter maxima over the eastern North Pacific (PE).

In the Southern Hemisphere, Knippertz *et al.* [2013] also identified four major paths, these are: (i) the central and eastern South Pacific Ocean (170°W–90°W); (ii) eastern South America and the adjacent South Atlantic Ocean (60°W–0°W); (iii) the western South Indian Ocean south of Madagascar (30°E–80°E); and (iv) a rather weak maximum over western Australia and adjacent waters (110°E–140°E). The first three are located in the western parts of austral subtropical oceanic anticyclones. Analysis of Figure 2 reveals that the annual cycle of expansion of the sink areas over these export paths agrees with the findings of Knippertz *et al.* [2013], according to which maximum (minimum) transport moisture exports via these four paths occurs during the Austral Summer (Winter), when the sink domains expand (shrink).

Following this climatological analysis of the conditions of the moisture transport from the oceanic sources, we studied the fingerprint of ENSO in this process. To assess the potential influence of ENSO, as discussed we evaluated the composite of the 8 years characterized by the extreme phases of the mode (representing the lower and upper quartile of the year set). Supporting information Figure S1 shows the monthly composite analysis for El Niño and La Niña years. Simple visual inspection does not easily allow any great differences between the two ENSO phases patterns to be seen, and it is therefore necessary to study the differences between the composites of the two phases.

Figures 3–6 show the seasonal variations in the moisture sinks associated with each of the oceanic moisture sources studied throughout the ENSO cycle. The left-hand columns illustrate the differences in the

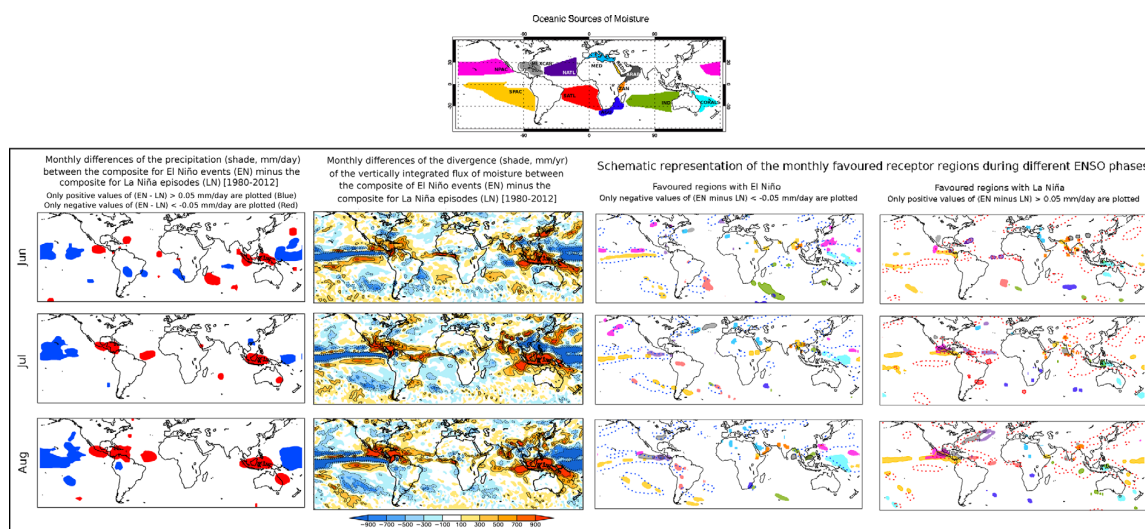


Figure 3. The monthly influence of the evolution of the ENSO cycle during its early stages (June, July, and August; JJA) over the moisture transport of the main oceanic sources of precipitation for 1980–2012. (top) Schematic representation of the main oceanic sources of moisture. (bottom, left-hand column) Monthly differences in precipitation (in mm per day) between the composites for El Niño events (EN) minus the composite for La Niña episodes (LN) [1980–2012]. Only positive values of (EN - LN) > 0.05 mm/day are plotted (Blue). Only negative values of (EN - LN) < -0.05 mm/day are plotted (Red). (bottom, second column) Monthly differences in divergence of the vertically integrated moisture flux (measured in mm per year) between the composites for El Niño and La Niña episodes, shown as cool and warm colors, respectively. Data obtained from ERA-Interim. (bottom, third and right-hand columns) The composite differences in E-P generated by each moisture source between El Niño and La Niña events. (third column) Schematic representation of the favored receptor regions of precipitation during the El Niño phase; (right-hand column) during La Niña phase. Only areas where the absolute value of differences greater than 0.05 mm/d are significant at the 90% confidence level are plotted, according to a bootstrap test permuting the original time series 1000 times.

precipitation and the second columns show the divergence of the vertically integrated moisture transport, both between the composites of the two ENSO phases, while the third and right-hand columns show the favored sink regions observed during El Niño and La Niña events, respectively. Following a bootstrap test for the precipitation figures and the favored sink region plots, we show only those areas where the absolute value of differences greater than 0.05 mm/d are significant at the 90% confidence level.

In general, the changes in the sink regions identified through the Lagrangian analysis agree with the main variations in vertically integrated moisture transport Θ observed with ENSO. During El Niño (La Niña)

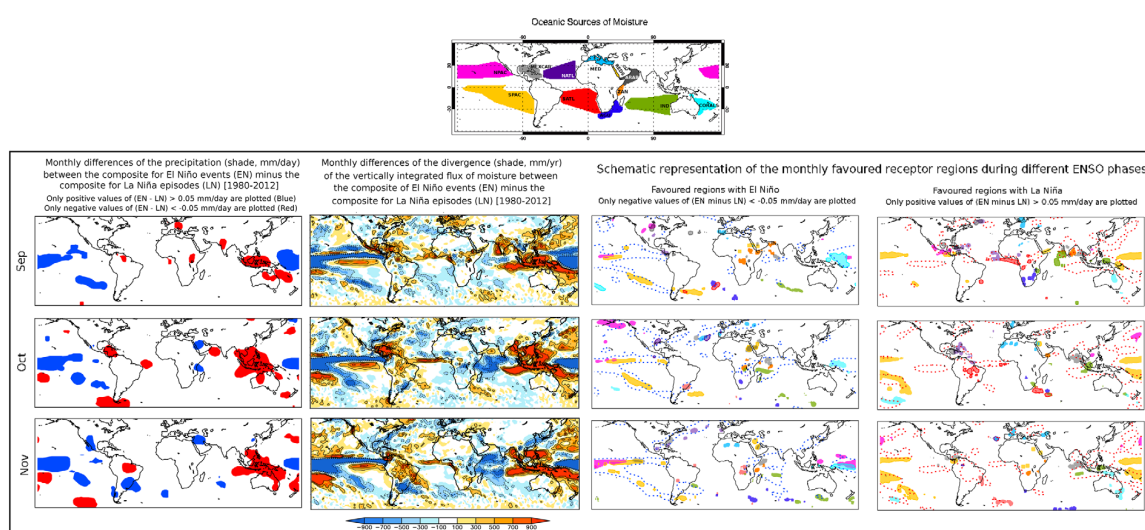


Figure 4. The monthly influence of the evolution of the ENSO cycle during boreal autumn (September, October, and November; SON) over the moisture transport of the main oceanic sources of precipitation. As Figure 3, for SON.

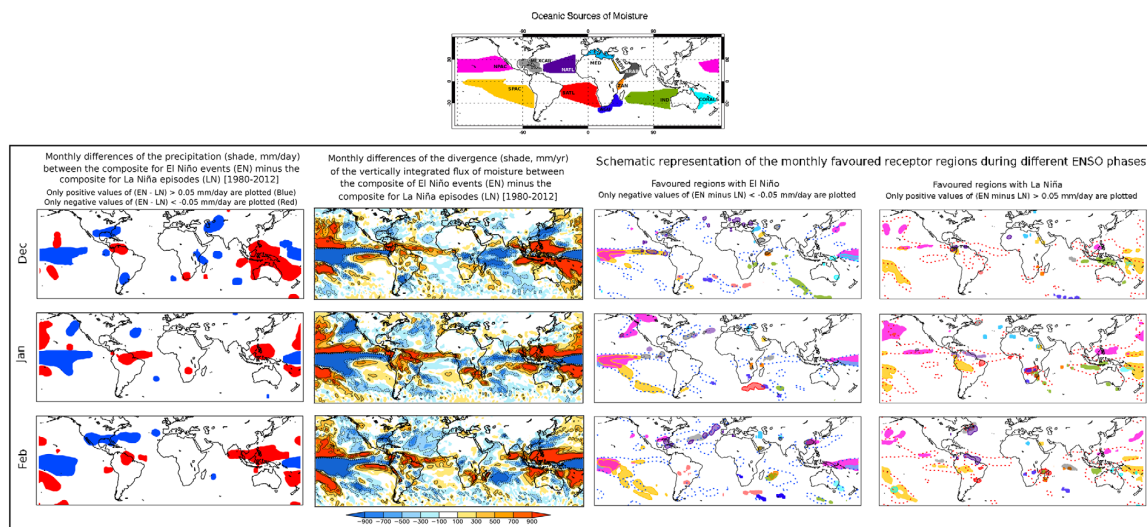


Figure 5. The monthly influence of the evolution of the ENSO cycle during its mature stage (December, January, and February; DJF) over the moisture transport of the main oceanic sources of precipitation. As Figure 3, for DJF.

episodes, the blue (red) areas where the convergence of Θ is higher (Figures 3–6, second columns) coincide with the favored sink areas indicated in the third columns (right-hand columns). Keeping in mind that increased convergence of Θ is associated with enhanced precipitation over a region (left-hand columns show the monthly differences in the composites of precipitation between the two ENSO phases), the results suggest that the variations in moisture sinks associated with these evaporative sources reproduce the major patterns of variation of large-scale atmospheric and precipitation systems under ENSO. Displacements of the Walker Cell system over the Equatorial Pacific and consequent alterations in the Hadley cell system during extreme ENSO phases are accompanied by changes in precipitation patterns. In general terms, such variations observed during El Niño episodes may include the displacement of equatorial Pacific rainfall toward the eastern basin, the weakening of the major Summer monsoon systems (e.g., Australia/Southeast Asia, South America, Central America, and tropical Africa), and enhanced

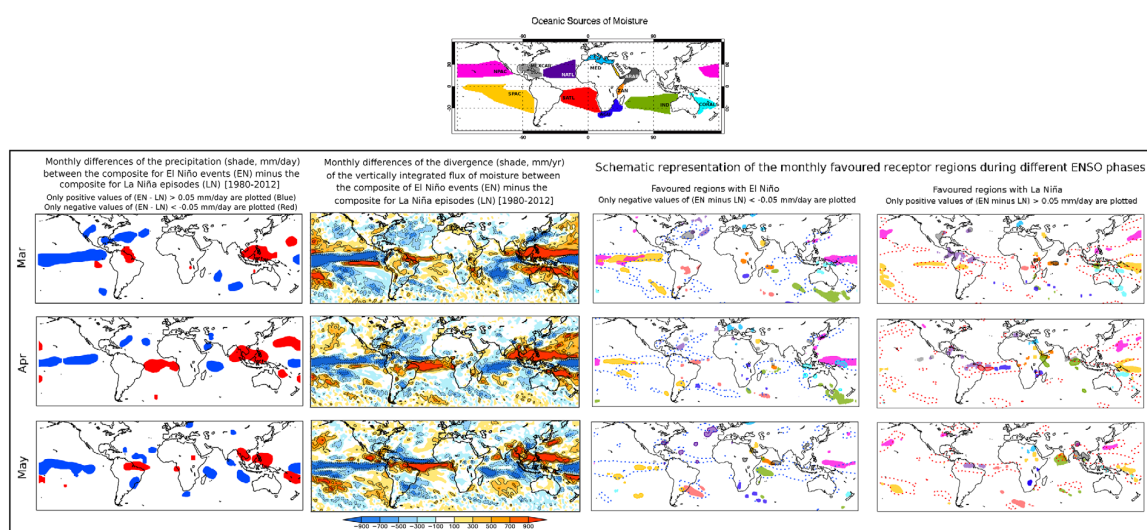


Figure 6. The monthly influence of the evolution of the ENSO cycle during boreal spring (March, April, and May; MAM) over the moisture transport of the main oceanic sources of precipitation. As Figure 3, for MAM.

subtropical rainfall. In contrast, during La Niña episodes equatorial Pacific rainfall is concentrated over the western basin, the major summer monsoon systems are enhanced, and precipitation over the subtropics weakens. In terms of moisture transport from the tropics toward the extratropics, Knippertz *et al.* [2013] confirmed that during warm events there is a reduction in activity over the South Pacific and eastern North Pacific, while activity increases further east over the South and North Atlantic. According to these authors, these variations are most likely to be connected to more zonally elongated jets over the Pacific during ENSO warm events, which act as a stronger waveguide and reduce tropical-extratropical and interhemispheric interactions.

More detailed analysis of Figures 3–6 (third and right-hand columns) may indicate the regions where the transport of moisture from the sources investigated is enhanced during an ENSO cycle. No increase in precipitation is implied, however, because this depends on the interaction of the moisture transported from a source with the other air particles present in the atmospheric column at a given time. Because we are considering the contribution of moisture from specific sources, precipitation may not occur at the surface if dry air predominates in the atmospheric column and dynamical conditions do not favor the generation of rain. In any case, a joint analysis of the preferred sinks (shaded) and the enhanced convergence of Θ (contours) may reveal where anomalous moisture transport is associated with enhanced precipitation (left-hand columns).

During JJA, the early stages of El Niño events (Figure 3, second column), enhanced convergence of Θ (blue contours) and increased precipitation (blue areas in left-hand columns) were observed over the central part of the Eastern Equatorial Pacific, the region receiving the enhanced moisture contribution from NPAC, SPAC, MEXCAR, and NATL. Increased moisture transport from MEXCAR was also verified over the region of enhanced convergence of Θ in the eastern USA. Concerning the development of the Indian Summer monsoon, although the moisture contribution from REDS and ZAN increases to the region, it is interesting to observe the inhibition of precipitation (left-hand columns) and the displacement of the convergence of Θ eastward. This finding suggests that there was no dynamical support for the occurrence of precipitation over India during the Monsoon Season. Nevertheless, the increased displacement of the convergence of Θ over southeastern Asia was associated with the enhanced contribution of moisture from REDS, ARAB, ZAN, and IND. Over the Southern Pacific and Atlantic Oceans, the results also suggest an increasing moisture contribution from SPAC and SATL to the enhanced convergence of Θ and to the regions of increased precipitation (left-hand columns).

In contrast, during the early stages (JJA) of La Niña events (Figure 3, right-hand column), enhanced convergence of Θ (red contours in the second columns) and increased precipitation (red areas in left-hand columns) were observed over India, associated with the enhanced moisture contribution from the REDS, ZAN, and ARAB sources. Convergence of Θ and precipitation were also enhanced over the India-Pacific Warm Pool, a region receiving a higher moisture contribution from the IND and CORALS sources. Other regions that showed an intensification of the convergence of Θ are Central America (with higher contributions from NATL, MEXCAR, NPAC, and SPAC) and the Atlantic ITCZ (with enhanced contributions from NATL and SATL and increased precipitation).

The development stages of El Niño events during SON (Figure 4, center column) may be characterized by a spatial expansion of the enhanced convergence of Θ , together with increased precipitation over the central part of the eastern Equatorial Pacific, a region that receives an enhanced moisture transport from NPAC, SPAC, and MEXCAR. The Western Indian Ocean was also characterized by an enhanced convergence of Θ , as well as an increasing supply of moisture from the ARAB, ZAN, and IND sources. In continental areas, the increased convergence of Θ and enhanced precipitation were observed over the subtropics of North and South America, regions receiving enhanced moisture contribution from MEXCAR and NATL, and SATL, SPAC, and IND, respectively.

Considering SON during La Niña events (Figure 4, right-hand column), the enhanced convergence of Θ and increased precipitation were still seen over India during September; these are associated with increased moisture transport from the IND, ARAB, and ZAN sources. The Indian-Pacific Warm Pool and the Western Pacific were both characterized by an intensification of the convergence of Θ and enhanced precipitation, and by an increased moisture transport from the ARAB, IND, CORALS, NPAC, and SPAC sources. An enhanced convergence of Θ occurred over Central America, with the intensification of moisture transport

from NATL and MEXCAR. The Atlantic ITCZ (NATL and SATL were intensified) and Tropical South America (contribution from SATL intensified) showed enhanced convergence of Θ and increased precipitation.

During the mature phases (DJF) of El Niño episodes (Figure 5, third column), there is an enhanced transport of moisture toward the central part of the eastern Equatorial Pacific, with increased contributions from the NPAC, SPAC, NATL, and CORALS sources. In the western Indian Ocean, there is also an intensification of the convergence of Θ and increased precipitation (particularly in December), associated with an increased moisture contribution from the IND, ZAN, and ARAB sources. An enhanced convergence of Θ and increased precipitation were seen over subtropical South America, a region that receives intensified moisture transport from the SATL and SPAC sources. The transport from the NPAC, NATL, and MEXCAR sources was intensified toward the southeastern part of North America, where enhanced convergence of Θ and increased precipitation can be seen. Enhanced exports of moisture to subtropical North and South America during El Niño events were similarly observed by Knippertz *et al.* [2013]. Their correlation analyses revealed enhanced TME over the subtropical South Atlantic during El Niño years, particularly during the austral summer. An inhibited convergence of Θ and precipitation can be seen over Tropical Southern Africa, even with the intensification of the moisture transport from IND, ZAN, and AGU to the region.

The mature stages (DJF) of La Niña events (Figure 5, right-hand column) are characterized by the enhanced convergence of Θ and precipitation over the regions of Tropical Summer Monsoon Systems, such as South America (accompanied by the intensification of moisture transport from NATL, SATL, and SPAC) and Southern Africa (with enhanced transport from ZAN, AGU, and IND). The Indian-Pacific Warm Pool also received intensified moisture transport from the NPAC, SPAC, IND, and CORALS sources, associated with enhanced convergence of Θ and precipitation.

There was a reduction in the extent of the enhanced convergence of Θ and precipitation over the central part of the Eastern Equatorial Pacific and the western Indian Ocean during the dismissal stages of El Niño events (MAM, Figure 6). However, these two regions still received enhanced moisture contribution from NPAC and SPAC, and ARAB, IND, and ZAN, respectively. Subtropical South America was characterized by the enhanced convergence of Θ , higher precipitation, and intensified moisture transport from the SPAC and SATL sources.

In MAM during La Niña episodes (Figure 6, right-hand column), the reduction in the tropical domains of the enhanced convergence of Θ and intensified precipitation were probably associated with the dismiss stage of the tropical Summer precipitation systems. Tropical South America still received enhanced moisture contributions from the NATL, SATL, and SPAC sources, as did tropical Southern Africa from ZAN, AGU, IND, and SATL.

To quantify the role of ENSO in the transport of moisture, we assume that the annual climatological oceanic moisture sources are defined according to Gimeno *et al.* [2010a] and as shown in Figure 1. It is well known that the moisture sources are not stationary, and that they follow an annual cycle as well as interannual variability. Table 1 shows the annual climatology of the vertically integrated moisture divergence for each oceanic source of moisture with values shown in bold, together with the values obtained from the composites of El Niño (blue) and La Niña (red). For example, over the NATL source the maximum is reached during January (1581 mm/yr) and the minimum during September (730.3 mm/yr). In addition, there exist sources of moisture that during some months show values of vertically integrated moisture divergence that are very low or even negative. This is the case for MEXCAR in August (31.7 mm/yr) and September (−236.5 mm/yr), for CORALS in February (−53.6 mm/yr), and for ZAN in April and May (−492 and −92.6 mm/yr, respectively). While not going negative, some other sources show reductions of up to 50%; for example, the SPAC source reaches a maximum in August (1347 mm/yr) and a minimum in March (618.2 mm/yr, a reduction of 54%). A brief comparison with the intensity of the sources during extreme ENSO phases (Table 1) highlights some interannual variability, particularly in those with a marked climatological annual cycle as described previously. While the ZAN and SPAC sources weakened during El Niño events (ZAN became negative during OND, reaching a value of −311.3 mm/yr in October), CORALS weakened during La Niña episodes (becoming negative during DJF while reaching more than three times its climatological value of 128.4 mm/yr in January of the El Niño cycle). It is interesting to note that the anomalies in the intensity of MEXCAR varied during the La Niña cycle: the source weakened with respect to the climatological mean from June to October and intensified from November to May.

Table 1. Monthly Vertically Integrated Moisture Flux Divergence (mm per year) for Each of the Stationary Sources of Moisture Defined in Figure 1^a

	AGU	ARAB	CORALS	IND	MED	MEXCAR	NATL	NPAC	REDS	SATL	SPAC	ZAN
Jun	1143	769.7	1278	1708	524.8	58.7	1238	1040	947.1	1562	1210	1115
	1068	821.4	1366	1802	485.9	56.1	1254	1040	878.3	1595	1185	894.6
	1082	722.2	1111	1681	520.9	3.3	1253	1061	1020	1538	1289	1020
Jul	1125	788.3	1555	1770	711.7	280.5	1230	817.4	875.8	1521	1324	1264
	1095	890.2	1686	1851	663.1	419.3	1276	751.3	832.4	1486	1256	1156
	1190	698.5	1510	1691	723.4	103.4	1210	832.9	772.5	1639	1285	1286
Aug	1035	686.6	1451	1753	781	31.7	908.5	646.6	1022	1454	1347	1160
	917.5	722.8	1617	1792	732.2	222.5	1004	524.7	988.2	1427	1307	1259
	1112	637.2	1178	1727	793.5	−209.7	850.8	780.8	1073	1492	1394	996.9
Sep	1047	621	1296	1620	763.4	−236.5	730.3	768.9	1041	1344	1347	963.9
	1023	648.9	1411	1586	672.8	−185.5	765.5	714.1	1007	1277	1294	881.8
	1140	591.8	1028	1595	800.6	−447.4	685.8	844.6	1085	1414	1348	996.5
Oct	1028	678.7	1102	1461	557.7	278.8	859.7	1034	824	1335	1285	349.2
	1112	658.6	1306	1398	494.7	484.3	774.7	1091	636.2	1311	1189	−135.1
	1037	663.5	842.5	1420	632.1	61.4	911.3	1050	902.8	1381	1306	540.9
Nov	924.5	959.1	902.2	1298	475.9	973.9	1123	1281	1061	1328	1223	82.4
	952.8	815.8	1181	1230	444.3	882.6	1191	1405	1110	1318	1039	−311.3
	983.8	1033	697	1299	514.8	1066	1041	1189	1178	1359	1277	247.8
Dec	835.1	1365	460.5	1118	388.1	1366	1438	1345	1205	1242	1139	345.7
	914.1	1424	783.9	1015	374.9	1273	1418	1524	1320	1189	836.7	−54.9
	802.3	1374	−173.8	1111	440.7	1462	1463	1244	1143	1237	1208	539.8
Jan	756.4	1429	128.4	834.3	387.5	1356	1581	1257	1237	1183	1030	1129
	876	1418	411.5	899.3	459.3	1367	1426	1435	1142	1150	647.7	966.9
	514.8	1407	−142.2	793.5	353	1485	1608	1145	1273	1173	1114	1238
Feb	832	1218	−53.6	618.2	358.7	1201	1487	1170	1203	1176	840.7	1293
	1013	1146	331	411.5	360	995.4	1282	1252	1215	1210	514	1297
	833	1306	−449.5	589.4	394.8	1321	1671	1081	1287	1111	900	1281
Mar	958.7	978.5	419	816.2	312.6	1081	1357	1258	952.2	1133	618.2	569.9
	965.6	1042	658	681	421.1	924.8	1151	1343	973.6	1198	439	635.1
	797.7	989.7	73.4	860.5	256.4	1113	1404	1138	969.7	1101	678.7	523.9
Apr	1145	817.4	1005	1083	240.1	887.4	1276	1272	543.2	1208	719.2	−492
	1219	832.6	1049	983.9	271.6	826.1	1193	1336	558.4	1325	544.1	−564.1
	1282	780	484.4	1059	235.8	899.4	1403	1133	555.3	1037	765.2	−313.8
May	1084	679.1	1233	1491	276.7	270.6	1201	1131	756.2	1456	1022	−92.6
	1045	634.6	1159	1518	261.8	319.7	1,118	1189	721.3	1491	901.5	−236
	993.3	637.7	1242	1482	280	388	1125	1073	819.7	1399	1045	−152.8

^aData from ERA-Interim. In black (bold) for the whole period 1980–2012. In blue for El Niño years, red for La Niña years.

In addition to the interannual variations in intensity [Gimeno *et al.*, 2013], we must also consider the variability in their areal extent. This points to another possible influence of ENSO, in that the sources of moisture change in size and position for the two phases. We therefore redefined the 12 oceanic sources of moisture using the composite of the highest and lowest years of the ENSO mode. Figure 7 shows the 750 mm/d threshold of the annual vertically integrated moisture flux for El Niño (blue contour) and La Niña (red contour) years. Most of the sources maintain their positions, with little change, but there are some that

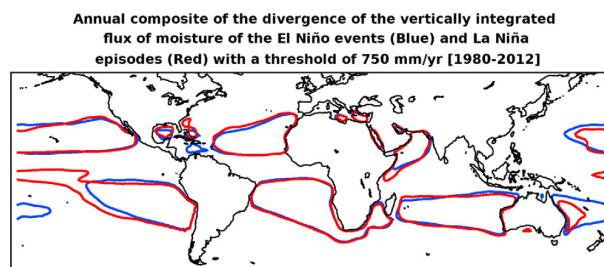


Figure 7. Oceanic moisture sources for El Niño and La Niña years: Climatological annual vertically integrated moisture flux divergence (mm per year) for the composite of the eight highest and lowest years of the ENSO mode for 1980–2012 using data from ERA-Interim and following the criteria of Gimeno *et al.* [2010]. Contours were defined using the threshold of 750 mm/yr, in blue for El Niño composite and in red for La Niña.

exhibit a notable modification in their extents. SPAC reduces in size toward the coast of South America during El Niño, MEXCAR shows a northward displacement during La Niña, ARAB expands toward the east coast of Africa during La Niña, and CORALS extends its influence eastward during El Niño. We do not consider MED and REDS because these sources are defined following their coastlines.

Figure 8 shows the monthly composites of the E-P fields (< -0.05 mm/d) for the El Niño and

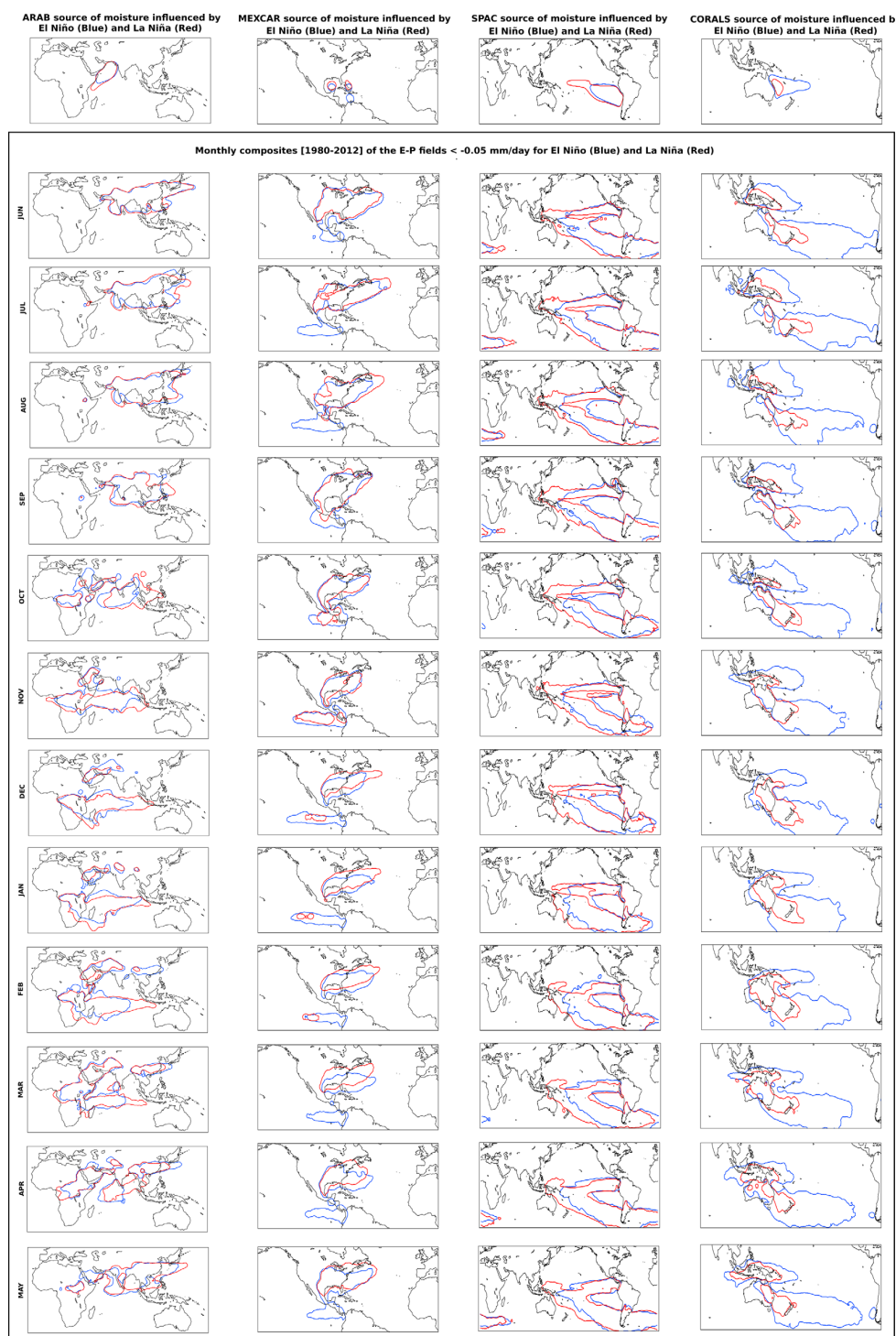


Figure 8. Monthly composites of the E-P fields (<-0.05 mm/d) for El Niño (blue contour) and La Niña (red contour) phases associated with changing sources of moisture defined in Figure 7. Arabian, ARAB; Mexican-Caribbean, MEXCAR; Southern Pacific, SPAC; and Coral Sea, CORALS.

La Niña phases associated with these changing sources of moisture. A brief comparison of these figures with Figure S1 suggests different transports of moisture when more realistic alterations to the spatial structure of the sources during extreme ENSO phases are considered. For example, the reduction in the size

of the SPAC source during El Niño events implies less moisture transport toward Indonesia (Figure 8, third column) compared to the moisture transport from the SPAC stationary source (Figure S1). The reduced moisture transport toward Indonesia agrees with the displacement of the tropical convection from the western Pacific toward the central part of the Eastern basin observed during these episodes (Figures 3–6, first and second columns). Therefore, the reduced precipitation over the western Pacific during El Niño may also be associated with the expansion of the CORALS source and the respective transport of moisture eastward (Figure S8, fourth column). At the same time, the increased precipitation over Indonesia during La Niña may be associated with a reduction in the CORALS source, and consequently with a confinement of its transport toward the western Pacific. This anomalous pattern of CORALS during La Niña is not captured if we only consider a stationary source (Figure S1) that expands its influence toward Indonesia and the central Pacific.

A further example of changes in moisture transport is seen in the northward displacement of MEXCAR during La Niña (Figure S8, second column). With this pattern, there is a reduction in the moisture transport toward the Pacific ITCZ that is not evident in the results obtained if a stationary source is considered (Figure S1). MEXCAR influence in Figure 8 accords more with the displacement of precipitation toward the western Pacific observed during La Niña episodes (Figures 3–6, first and second columns).

Finally, in the Indian Ocean the expansion of ARAB toward the eastern African coast during La Niña (Figure S8, first column) is associated with enhanced moisture transport toward the basin particularly during the months from December to March. The results obtained when only the stationary source is considered (Figure S1) do not reproduce these changes so clearly.

4. Concluding Remarks

We have herein investigated the influence of the evolution of the ENSO cycle on the moisture transport from the major oceanic moisture sources using the Lagrangian FLEXPART data set fed by ERA-interim Reanalysis data. We calculated differences between the composites of the vertically integrated moisture transport divergence, the precipitation, and of the favored sink regions observed during the two ENSO phases. Our results suggest that in maintaining the sources of moisture defined for the climatological period 1980–2012, there are significant differences between the two phases. In general terms, the variations in the moisture sinks associated with the evaporative sources coincide with the known patterns of variation of Θ associated with large-scale atmospheric systems throughout ENSO cycles. Such variations include those observed over equatorial Pacific rainfall, the major Summer monsoon systems, and subtropical rainfall. During the mature stage of ENSO (DJF) contributions from SPAC, NPAC, MEXCAR, and CORALS to the equatorial Pacific are enhanced for El Niño years, while IND, NPAC, and SPAC contribute more to the western equatorial Pacific during La Niña. This pattern reproduces the known “see-saw” characteristic associated with ENSO over this region. The subtropical areas receive more moisture from the nearest sources during El Niño, for example southern North America from NATL and MEXCAR, South America from SATL and SPAC, or southern Africa from IND, AGU, and ZAN. The Indian Monsoon regime exhibits an inhibition of convergence associated with a lack of moisture uptake from its typical (own) sources during El Niño episodes. However, from June to November the region is a preferred sink for moisture from IND, ZAN, and ARAB during La Niña, and the convergence is favored.

When the areas of the sources are redefined according to the phase of ENSO, most remain stationary, but four of the sources show notable differences in their extent. Two of them are more involved in the region of ENSO occurrence, i.e., SPAC and CORALS in the Pacific; the others are MEXCAR in the Atlantic and ARAB in Indian Ocean. A Lagrangian sensitivity analysis performed for these four sources considering the new areas defined according to the ENSO composites of the vertically integrated moisture transport divergence suggest some changes related to the results as far as the stationary sources are concerned. For example, the reduction in the SPAC source in size during El Niño events implies less moisture transport toward Indonesia compared with the moisture transport from the stationary SPAC source. The reduction in CORALS during La Niña and the confinement of its transport toward the western Pacific is not captured when we consider the stationary CORALS source, which extends its influence toward Indonesia and Central Pacific. The northward displacement of MEXCAR observed during La Niña and the associated reduction in the moisture transport toward the Pacific ITCZ during this phase is not evident in the results obtained when

only the stationary source is considered. The expansion of ARAB toward the eastern African coast during La Niña associated with enhanced moisture transport toward the Indian Ocean, particularly during DJFM, was not reproduced in the results for the stationary source. In any case, apart from these four specific sources, the small changes in the spatial structure of the remaining sources during different ENSO phases allowed the use of stationary sources in our analysis and the consequent evaluation and comparison of the impacts of both phases of ENSO over these prespecified regions.

Acknowledgments

The authors would like to thank the "Xunta de Galicia" for partially funding this research through the CHEGA project, and the Spanish Government through the TRAMO project. Both projects were cofunded by FEDER.

References

- Bengtsson, L., S. Hagemann, and K. I. Hodges (2004), Can climate trends be calculated from reanalysis data? *J. Geophys. Res.*, *109*, D11111, doi:10.1029/2004JD004536.
- Cook, K. H. (2000), The South Indian convergence zone and interannual rainfall variability over southern Africa, *J. Clim.*, *13*, 3789–3804.
- D'Abreton, P. C., and P. D. Tyson (1995), Divergent and nondivergent water vapour transport over southern Africa during wet and dry conditions, *Meteorol. Atmos. Phys.*, *55*, 47–59.
- Dee, D., et al. (2011), The ERA Interim reanalysis: Configuration and performance of the data assimilation system, *Q. J. R. Meteorol. Soc.*, *137*, 553–597, doi:10.1002/qj.828.
- Dirmeyer, P. A., and K. L. Brubaker (2007), Characterization of the global hydrologic cycle from a back-trajectory analysis of atmospheric water vapor, *J. Hydrometeorol.*, *8*(1), 20–37.
- Drumond, A., R. Nieto, L. Gimeno, and T. Ambrizzi (2008), A Lagrangian identification of major sources of moisture over Central Brazil and La Plata Basin, *J. Geophys. Res.*, *113*, D14128, doi:10.1029/2007JD009547.
- Durán-Quesada, A. M., L. Gimeno, J. A. Amador, and R. Nieto (2010), Moisture sources for Central America: Identification of moisture sources using a Lagrangian analysis technique, *J. Geophys. Res.*, *115*, D05103, doi:10.1029/2009JD012455.
- Gimeno, L., A. Drumond, R. Nieto, R. M. Trigo, and A. Stohl (2010a), On the origin of continental precipitation, *Geophys. Res. Lett.*, *37*, L13804, doi:10.1029/2010GL043712.
- Gimeno, L., R. Nieto, R. M. Trigo, S. M. Vicente-Serrano, and J. I. López-Moreno (2010b), Where does the Iberian Peninsula moisture come from? An answer based on a Lagrangian approach, *J. Hydrometeorol.*, *11*, 421–436, doi:10.1175/2009JHM1182.1.
- Gimeno, L., et al. (2012), Oceanic and terrestrial sources of continental precipitation, *Rev. Geophys.*, *50*, RG4003, doi:10.1029/2012RG000389.
- Gimeno, L., R. Nieto, A. Drumond, R. Castillo, and R. M. Trigo (2013), Influence of the intensification of the major oceanic moisture sources on continental precipitation, *Geophys. Res. Lett.*, *40*, 1443–1450, doi:10.1002/grl.50338.
- Intergovernmental Panel on Climate Change, Climate Change 2013 (2013), *The assessment report of the Intergovernmental Panel on Climate Change*, 5th Report, Cambridge Univ. Press, Cambridge, U. K.
- Knippertz, P., H. Wernli, and G. Gläser (2013), A global climatology of tropical moisture, *J. Clim.*, *26*, 3031–3045, doi:10.1175/JCLI-D-12-00401.1.
- Lorenz, C., and H. Kunstmann (2012), The hydrological cycle in three state-of-the-art reanalyses: Intercomparison and performance analysis, *J. Hydrometeorol.*, *13*, 1397–1420, doi:10.1175/jhm-d-11-088.1.
- Nieto, R., L. Gimeno, and R. M. Trigo (2006), A Lagrangian identification of major sources of Sahel moisture, *Geophys. Res. Lett.*, *33*, L18707, doi:10.1029/2006GL027232.
- Nieto, R., A. M. Durán-Quesada, and L. Gimeno (2010), Major sources of moisture over Antarctic ice-core sites identified through a Lagrangian approach, *Clim. Res.*, *41*, 45–49, doi:10.3354/cr00842.
- Numaguti, A. (1999), Origin and recycling processes of precipitating water over the Eurasian continent: Experiments using an atmospheric general circulation model, *J. Geophys. Res.*, *104*, 1957–1972.
- Ordóñez, P., P. Ribera, D. Gallego, and C. Peña-Ortiz (2012), Major moisture sources for Western and Southern India and their role on synoptic-scale rainfall events, *Hydrol. Processes*, *26*, 3886–3895, doi:10.1002/hyp.8455.
- Smith, T. M., et al. (2008), Improvements to NOAA's historical merged land-ocean surface temperature analysis (1880–2006), *J. Clim.*, *21*, 2283–2293.
- Stohl, A., and P. James (2004), A Lagrangian analysis of the atmospheric branch of the global water cycle: Part I: Method description, validation, and demonstration for the August 2002 flooding in central Europe, *J. Hydrometeorol.*, *5*, 656–678.
- Stohl, A., and P. James (2005), A Lagrangian analysis of the atmospheric branch of the global water cycle: Part II: Earth's river catchments, ocean basins, and moisture transports between them, *J. Hydrometeorol.*, *6*, 961–984, doi:10.1175/JHM470.1.
- Stohl, A., C. Forster, A. Frank, P. Seibert, and G. Wotawa (2005), Technical note: The Lagrangian particle dispersion model FLEXPART version 6.2, *Atmos. Chem. Phys.*, *5*, 2461–2474.
- Stohl, A., C. Forster, and H. Sodemann (2008), Remote sources of water vapor forming precipitation on the Norwegian west coast at 60°N: A tale of hurricanes and an atmospheric river, *J. Geophys. Res.*, *113*, D05102, doi:10.1029/2007JD009006.
- Todd, M. C., R. Washington, and P. Palmer (2004), Water vapour transport associated with tropical-temperate trough systems over southern Africa and the southwest Indian Ocean, *Int. J. Climatol.*, *24*, 555–568.
- Trenberth, K. E., and C. J. Guillemot (1998), Evaluation of the atmospheric moisture and hydrological cycle in the NCEP/NCAR reanalyses, *Clim. Dyn.*, *14*, 213–231.
- Trenberth, K. E., J. T. Fasullo, and J. Mackaro (2011), Atmospheric moisture transports from ocean to land and global energy flows in reanalyses, *J. Clim.*, *24*, 4907–4924, doi:10.1175/2011jcli4171.1.
- Uppala, S. M., et al. (2005), The ERA-40 re-analysis, *Q. J. R. Meteorol. Soc.*, *131*, 2961–3012.
- Viste, E., and A. Sorteberg (2011), Moisture transport into the Ethiopian highlands, *Int. J. Climatol.*, *33*, 249–263, doi:10.1002/joc.3409.
- Wei, J., P. A. Dirmeyer, M. G. Bosilovich, and R. Wu (2012), Water vapor sources for Yangtze River Valley rainfall: Climatology, variability, and implications for rainfall forecasting, *J. Geophys. Res.*, *117*, D05126, doi:10.1029/2011JD016902.
- Wernli, H., and H. C. Davies (1997), A Lagrangian-based analysis of extratropical cyclones: I: The method and some applications, *Q. J. R. Meteorol. Soc.*, *123*, 467–489.



The modulation of oceanic moisture transport by the hemispheric annular modes

Raquel Nieto*, Rodrigo Castillo and Anita Drumond

Environmental Physics Laboratory, Departamento de Física Aplicada, Faculdade de Ciencias, Universidade de Vigo, Ourense, Spain

Edited by:

Tercio Ambrizzi, University of Sao Paulo, Brazil

Reviewed by:

Moacyr Cunha De Araujo, Universidade Federal de Pernambuco, Brazil
Rosmeri Porfirio Da Rocha, University of Sao Paulo, Brazil
Juan José Taboada, MeteoGalicia, Spain

*Correspondence:

Raquel Nieto, Environmental Physics Laboratory, Departamento de Física Aplicada, Faculdade de Ciencias, Universidade de Vigo, Edif. Física, Campus As Lagoas S/N, 32004 Ourense, Spain
e-mail: rnieto@uvigo.es

Leaving aside the contribution made by recycling, it is the main oceanic moisture sources that are responsible for most of the precipitation that falls on the continents. The transport of moisture from these sources can be affected by large-scale variability according to the hemispheric annular modes. The influence of the two dominant modes of extratropical winter climate: the Northern and the Southern Annular Modes (NAM and SAM) are herein investigated to assess how they affect the transport of moisture from the major oceanic moisture sources. A Lagrangian model was used, together with ERA-Interim reanalysis data (1979–2012), and differences between the composites of the six strongest higher and lower events observed for both phases of the two modes for the period were analyzed. The method is able to reproduce the general pattern of known variations for both annular patterns. Lower values of the NAM Index are associated with the displacement of the storm track toward tropical latitudes. Thus, moisture transport is enhanced from the Northern Pacific toward the northeastern basin and from the Northern Atlantic and Mediterranean toward southern Europe. On the other hand, during higher values of NAM, moisture transport is favored from the Northern Pacific toward eastern Asia, and moisture transport is enhanced from the Northern Atlantic toward the Caribbean Sea. In the Southern Hemisphere, during higher values of SAM more moisture is transported from the Atlantic and Indian oceanic sources southwards and eastwards than during the opposite phase. In this SAM phase it is also noted by an enhancement of moisture transport from the Coral Sea and Southern Pacific sources toward the Indian Ocean/West Pacific Warm Pool. Southeastern South America received more moisture from the Pacific and Atlantic sources during years with a lower SAM, episodes which also favored the influx of moisture from the Southern Atlantic toward Africa, causing monsoon conditions to occur.

Keywords: annular modes, oceanic sources of moisture, moisture sinks, moisture transport, Lagrangian analysis, FLEXPART, Northern Annular Mode (NAM), Southern Annular Mode (SAM)

INTRODUCTION

The characterization of the hydrological cycle has become one of the main topics of debate for the climate community in recent years. Knowledge of transport of moisture may be considered one of the grand challenges of atmospheric science (Gimeno, 2013) given that this branch of the hydrological cycle is essential to the global climate. In recent years, many studies have characterized the sources of moisture for climatological areas of interest (e.g., the Sahel, Nieto et al., 2006), the Monsoon System in South America (Drumond et al., 2008), Central America (Durán-Quesada et al., 2010), the areas over Antarctic ice-cores (Sodemann and Stohl, 2009; Nieto et al., 2010), the Ethiopian highlands (Viste and Sorteberg, 2013), and the Indian Peninsula (Ordóñez et al., 2012); or else they have assessed sources of moisture at a global scale (e.g., Stohl and James, 2005; Dirmeyer and Brubaker, 2007; Gimeno et al., 2010; Knippertz et al., 2013). Many of these studies have used Lagrangian models to detect sources of moisture, and we use this approach here. This sophisticated method is highly powerful, having the remarkable ability to

evaluate net changes in specific humidity along defined trajectories in order to identify the points at which the atmosphere gains or loses moisture.

The general pattern of moisture transport from a climatological perspective was characterized by Gimeno et al. (2010) and updated by Castillo et al. (2014). These authors found 12 main oceanic evaporative sources, and showed that the supply of moisture to the continents is highly asymmetric, with strong seasonal variability. However, to date no studies have been undertaken of the variability of the contribution of the oceanic moisture sources due to the major teleconnection modes. On interannual to multidecadal timescales, atmospheric moisture transport must be strongly modulated by large-scale climate modes due to associated changes in atmospheric circulation, sea surface temperature, air temperature and precipitation (Rogers et al., 2001). The Northern Annular Mode (NAM) and the Southern Annular Mode (SAM) are the two dominant modes for the extratropical winter climate (Thompson and Wallace, 2000; Thompson et al., 2000), and their influence on the main oceanic moisture

sources and associated precipitation is therefore a key objective in our understanding of the present-day atmospheric water cycle. In literature, as far as we know, there are no works which analyse the moisture source-receptor relationship under the influence of the Annular Modes using a Lagrangian approach. We can find a few studies that estimate the source regions of evaporation supplying precipitation during the extreme phases of the North Atlantic Oscillation (NAO), being the NAO the Atlantic fingerprint of NAM. As an example, Sodemann et al. (2008) analyzed the sources for Greenland during winter, and Gómez-Hernández et al. (2013) studied the variability moisture sources for the surrounding Mediterranean areas.

Both annular modes are characterized by north-south shifts in atmospheric mass between the middle and polar latitudes. They describe oscillations in the wind pattern between the latitude bands centered on latitudes $\sim 55\text{--}60^\circ$ and $\sim 30\text{--}35^\circ$. By convention, when the Sea Level Pressure (SLP) shows anomalously lower (higher) values in the polar areas and the opposite anomalies

are detected over the middle latitudes, the mode is said to be in a higher or positive (lower or negative) phase (**Figure 1**). Thus, high indices correspond to lower than average pressures over the polar regions, to more intense polar vortices and to stronger westerlies along the band centered on $\sim 55\text{--}60^\circ$ in the troposphere. For lower values of the indices, the reverse conditions apply. As described above, the modes may modify the atmospheric dynamics, and may therefore affect the respective hemispheric climate. Under high values of NAM Index, surface temperatures increase over northern Eurasia and North America, and sea-surface temperatures (SSTs) increase over the North Atlantic (Thompson and Wallace, 2000). An increase in precipitation may be also detected over the same areas due to the northerly movement of the storm track (Hurrell, 1995). Large anomalies associated with the distribution and extension of Arctic sea-ice are linked with high values of NAM Index (Deser and Teng, 2008; Ogi and Yamazaki, 2010). The mode also affects the modulation of the spatial distribution of the ozone in the lower stratosphere (Thompson and

Composites of SLP (isolines, Pa) and 500hPa geopotential (shading, m^2/s^2) anomalies during winters of NAM and SAM extreme events

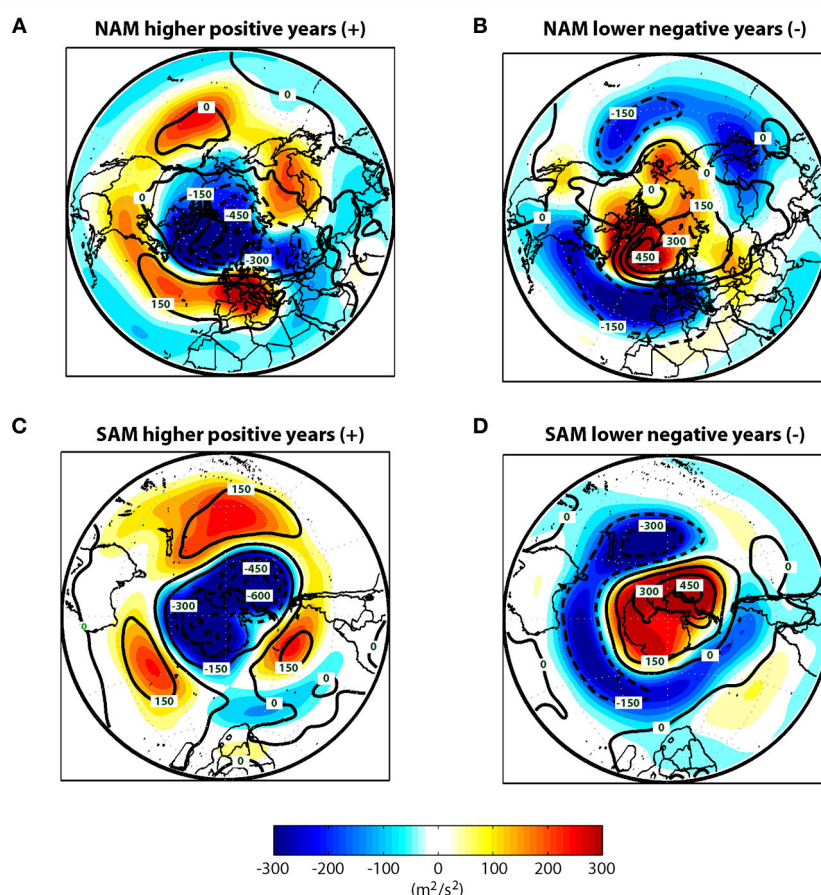


FIGURE 1 | Composites of SLP (isolines, units Pa) and 500 hPa geopotential (shading, units $\text{m}^2 \text{s}^{-2}$) anomalies during the winters of the Northern and Southern Annular Modes events (see Table 1 for the years included in the composites). Top: NAM winters

(November–April) of (A) high-index and (B) low-index values. Bottom: SAM winters (May–October) of (C) high-index and (D) low-index values. Positive or zero (negative) anomalies are shown in continuous (dotted) lines.

Wallace, 2001). In a similar way, the SAM modulates the climate in the southern hemisphere through modulations in Antarctic temperatures (Marshall et al., 2011) and the distribution of the sea-ice surrounding that continent (Parkinson and Cavalieri, 2012). Southern Ocean SSTs exhibit positive anomalies for high SAM indices (Thompson et al., 2000). Both modes can occur throughout the year, but the indices are generally highest during colder months (Baldwin and Dunkerton, 1999).

In light of the foregoing, we herein attempt to explain the modulation of moisture transport from the major oceanic moisture sources under the influence of the main hemispheric modes of climate variability using a Lagrangian methodology.

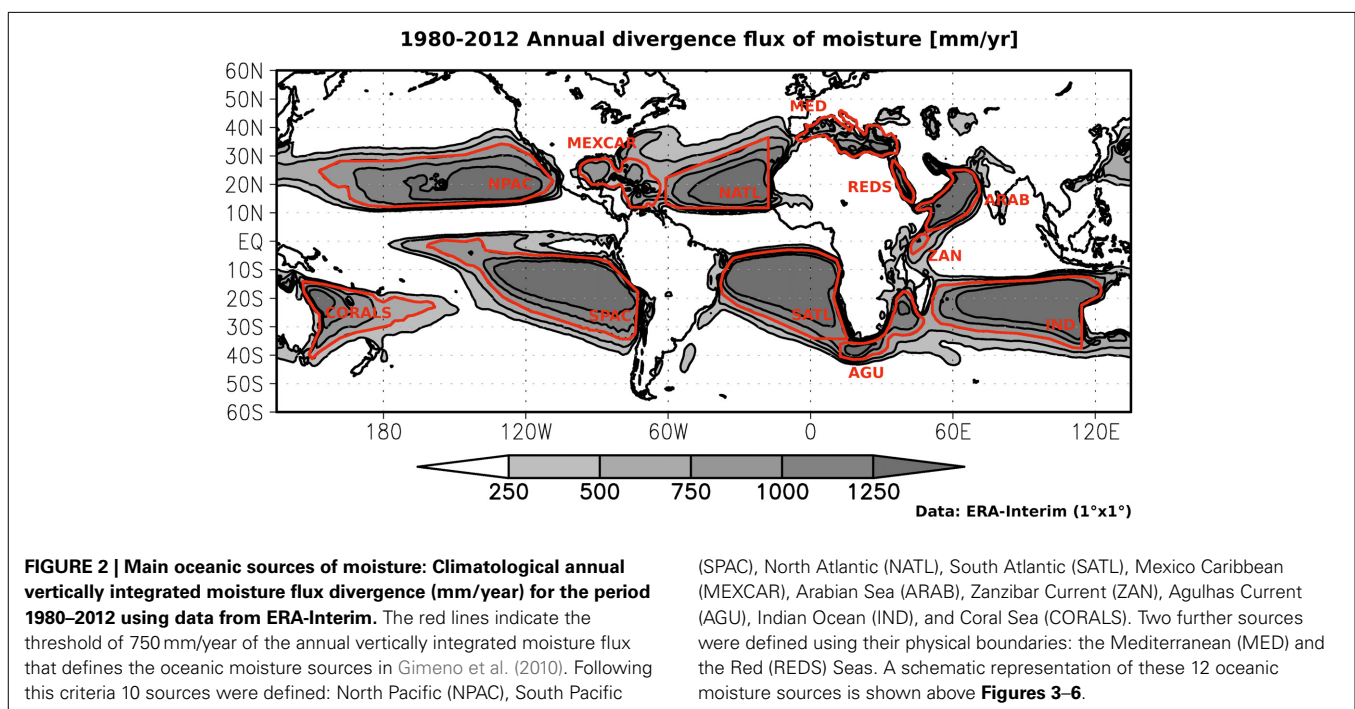
DATA AND METHODS

In the present study, we applied a Lagrangian moisture source diagnostic scheme to examine the influence of NAM and SAM on the variability of the uptake and transport of moisture from the major oceanic sources. **Figure 2** shows the moisture source regions identified following the criteria of Gimeno et al. (2010) but now considering a longer period of 33 years (from November 1979 to October 2012) and the ERA-Interim Reanalysis data set (Dee et al., 2011) on a regular $1 \times 1^\circ$ horizontal grid and with 61 vertical levels (from the surface to 0.1 hPa). ERA-Interim reproduces the hydrological cycle in a more realistic way than previous ERA reanalysis versions (Trenberth et al., 2011). We do not use data from the years prior to 1979 because the results of the reanalysis are of insufficient quality (especially over the oceans) to run the FLEXPART model before the inclusion of satellite data (Bengtsson et al., 2004). Ten oceanic moisture source regions were directly identified by the method, namely: NATL, North Atlantic; SATL, South Atlantic; MEXCAR, Mexico Caribbean; NPAC, North Pacific; SPAC, South Pacific; IND, Indian Ocean;

ARAB, Arabian Sea; ZAN, Zanzibar Current; AGU, Agulhas Current; and CORALS, Coral Sea. The Mediterranean Sea (MED) and Red Sea (REDS) sources were defined using the physical boundaries of their oceanic basins.

The Lagrangian method is today considered the most suitable method for the evaluation of the origin of the water that precipitates over a continental area (Gimeno et al., 2012). The advantages, disadvantages, uncertainties, limitations and significance of the methodology were discussed in a complete review by Gimeno et al. (2012). In addition, these authors provided a detailed comparison of all approaches establishing source-sink relationships for atmospheric water vapor available to the scientific community, such as the Eulerian technique using numerical water vapor tracers, “analytical and box models,” and “physical water vapor tracers” (isotopes).

Our Lagrangian approach makes use of the FLEXPART V9.0 particle dispersion model (Stohl and James, 2004, 2005) forced by ERA-Interim data. The methodology permits a description of air movement (in space and time) by individual trajectories of “air parcels” or “particles.” These “particles” are three-dimensional finite elements created via the homogeneous discretization of the atmosphere, and their trajectories are tracked following advection by three-dimensional wind fields in a regular $1 \times 1^\circ$ grid. Values of latitude, longitude and specific humidity are stored along each trajectory at 6-h intervals. Variations in moisture along each trajectory are obtained via changes in specific humidity (q) with time, which is proportional to the difference between the increase of the evaporation (e) and decrease of the precipitation (p) in moisture for the particle concerned, i.e., $e-p = m \, dq/dt$, where (m) is the mass of the particle. Considering an atmospheric column over a given area, the net difference between evaporation (E) and precipitation (P) is the result of adding together ($e-p$) for



all particles. To derive this, we integrated the (E-P) column values over each $1 \times 1^\circ$ global grid considering only those particles that leave the moisture source of interest. From the analysis of (E-P) we can identify whether the atmosphere in a region received ($E-P > 0$) or lost ($E-P < 0$) moisture.

In order to simulate the transport of the air masses, a global data set of approximately 2.0 million “particles” was created using FLEXPART. These particles were moved by wind for a time period limited to 10 days, which represents the average residence time of water vapor in the atmosphere (Numaguti, 1999). (E-P) values integrated along these 10-day forward trajectories were analyzed in order to investigate the main moisture sinks observed along trajectories starting in each of the 12 evaporative sources considered. The positions and the changes in (q) were recorded at intervals of 6 h (00, 06, 12, and 18 UTC).

The influence of NAM and SAM on the transport of moisture from the oceanic sources was explored using composites. We obtained composite differences of moisture transport between the positive and negative phases of each mode of variability. The events were selected based on the monthly NAM and SAM Indices (NAMI and SAMI). NAM and SAM are more active during their respective hemispheric winters (from December to February for NAM and from June to August for SAM), and we therefore chose the corresponding semi-annual period, i.e., from November to April for NAM and from May to October for SAM. The most common methods used to identify extreme events of SAM and NAM are those that (1) formulate the first principal components (PC) of some meteorological variable over the extratropics (e.g., geopotential height, mean SLP, wind, temperature) (Thompson and Wallace, 2000; Nan and Li, 2003), (2) calculate the difference between normalized zonal mean pressure between two latitudes using reanalysis data (Gong and Wang, 1999; Li and Wang, 2003) or between two selected points (Hurrell, 1995), (3) are based on data obtained from observational stations (Marshall, 2003; Visbeck, 2009). The literature reveals that there are some inconsistencies regarding the identification of the extreme episodes of both modes, particularly for SAM, and primarily arising due to the different methodologies and data sets applied in the definition of the indices (Ho et al., 2012). For the SAM index, but also applying to NAM, Ho et al. (2012) showed that those indices calculated using reanalysis data are more effective where there is some attempt to understand the relationship with their impacts. However, prior to the assimilation of satellite data (pre-1979) the reanalysis-based indices are likely to be flawed, and it is better to choose those that are station-based. With this in mind, for each mode we considered two indices based on different methods using normalized monthly SLP data: one station-based and other reanalysis-based; the respective semi-annual averages are shown in **Table 1** (in red for lower values of the indices and in blue for the higher ones). The station-based NAMI was the available on https://climatedataguide.ucar.edu/sites/default/files/climate_index_files/nao_station_monthly.txt obtained from SLP differences between Lisbon (Portugal) and Stykkisholmur/Reykjavik (Iceland) (Hurrell, 1995; Hurrell and National Center for Atmospheric Research Staff, 2013), while the SAMI was obtained from Marshall (2003) on <http://www.nerc-bas.ac.uk/icd/gjma/sam.html>, who produced a similar SAM index based on 12 appropriately located station-based observations. Those that use reanalysis data (NCEP/NCAR; Kalnay et al., 1996) can be found at <http://ljp.lasg.ac.cn/dct/page/65544>. The NAMI is defined as the difference in the normalized monthly zonal-mean SLP between 35 and 65°N, and the SAMI is taken to be the same difference between 40 and 70°S (Li and Wang, 2003; Nan and Li, 2003, respectively). Our composites consider the six highest intensity episodes for both phases of each mode for the period 1979–2012; where there are discrepancies between the two indices we select the year with the higher (or lower) value using reanalysis data. Thus for the NAM Index the positive high values occurred in 1989, 1990, 1993, 2000, 2007, and 2012; and the negative high values occurred in 1981, 1986, 1996, 2006, 2010, and 2011 (the year shown here

Table 1 | Semiannual periods considered for the composites of both phases of NAM and SAM from 1979 to 2012; in red for lower values of the indices and in blue for the higher values.

	NAM index		SAM index		
	Station-based	Reanalysis	Station-based	Reanalysis	
1980	0.20	−0.08	−0.47	−0.76	1980
1981	−0.22	−0.14	−0.67	−0.96	1981
1982	−0.02	0.68	0.36	0.55	1982
1983	1.18	1.00	0.46	1.41	1983
1984	−0.20	−0.30	−0.15	0.80	1984
1985	−0.27	0.03	0.57	1.47	1985
1986	0.00	−0.38	0.14	−0.26	1986
1987	0.25	0.75	0.24	0.32	1987
1988	−0.38	1.03	−2.53	−0.46	1988
1989	1.32	2.95	0.99	2.31	1989
1990	1.13	2.69	−0.55	0.62	1990
1991	0.37	1.02	−0.22	0.04	1991
1992	1.10	1.70	−0.79	−0.77	1992
1993	1.42	2.32	1.73	2.58	1993
1994	2.03	1.56	−0.69	0.17	1994
1995	0.90	1.11	−0.09	0.59	1995
1996	−1.88	−1.97	−0.41	0.22	1996
1997	−0.32	0.68	0.60	1.45	1997
1998	0.13	0.78	1.28	2.73	1998
1999	1.03	1.21	1.06	1.72	1999
2000	0.60	1.98	−0.18	0.67	2000
2001	−0.48	0.19	0.18	2.07	2001
2002	0.43	1.62	−1.60	−1.40	2002
2003	−0.15	0.12	0.20	1.33	2003
2004	0.38	0.72	0.87	1.89	2004
2005	0.00	0.00	−0.10	0.77	2005
2006	−0.08	−0.73	0.81	1.66	2006
2007	1.20	1.96	−1.23	0.26	2007
2008	0.05	1.75	0.97	2.33	2008
2009	1.28	0.61	−0.25	0.65	2009
2010	−2.00	−1.99	2.02	4.15	2010
2011	−0.67	−0.48	−0.23	1.01	2011
2012	1.50	1.84	1.23	2.37	2012

refers to the January of the interval). For the SAMI the positive high values occurred in 1989, 1993, 1998, 2008, 2010, and 2012, and the negative high values occurred in 1980, 1981, 1988, 1992, 1994, and 2002. To test the statistical significance of the composite, we used the bootstrap method proposed by Wei et al. (2012). We obtained the differences for two 6-year period random samples (a total of 12 years) 1000 times from the 33-yr climatology. The absolute value of the difference composite was considered significant if it was greater than 90% of the 1000 iterations.

Monthly composite differences in the precipitation and in the divergence of the vertically integrated flux of moisture (Θ) between opposite phases of the modes were also obtained. We used data obtained from the Global Precipitation Climatology Project (GPCP; Adler et al., 2003; Huffman et al., 2009), and from ERA-Interim, respectively; both datasets were estimated over the entire globe for the 33-year period.

RESULTS

We studied the fingerprint of NAM and SAM in the moisture transport from the main oceanic sources of moisture in order to assess their impact. It must be remembered that the boundaries of each oceanic source were defined as stationary throughout the 33-year period considered (Figure 2). The composites of the 6 years associated with the extreme phases of each mode were evaluated month by month during the corresponding winter season. The resulting maps are shown in Figures 3, 4, for NAM and SAM respectively, where the monthly variability of the favored sink regions is summarized. Figure 3 shows the contribution of those oceanic sources of moisture located in the Northern hemisphere (NPAC, MEXCAR, NATL, MED, REDS, and ARAB), and Figure 4 shows the same for the Southern hemisphere (SPAC, SATL, ZAN, AGU, IND, and CORALS). The two figures only show contours with average values of (E-P) integrated over the 10 days of transport larger than of -0.05 mm/day. It must be stressed that we included in these figures only those sources of moisture in the same hemisphere as the variability mode concerned. From a simple visual inspection, and focusing on one source of moisture as an example, the NATL (Figure 3) provides moisture over larger areas of Eurasia during lower values of NAM Index (Hurrell et al., 2013), and the method is able to detect the known absence of precipitation during higher NAM over the Iberian Peninsula during early spring (Paredes et al., 2006), although in general it is not possible to extract detailed information on the differences between the two phases of the modes from these patterns. The differences between the composites of the two phases for both modes may help explain the significant changes in moisture transport, however.

The monthly differences in the influence of the oceanic moisture sources on the sink areas throughout the NAM and SAM cycles are summarized in Figures 5, 6, respectively. These two figures show the differences between the composites of the two mode phases in terms of the precipitation (left-hand column) and the divergence of the vertically integrated moisture transport (2nd column). The favored sink areas observed during the higher and lower phases of the mode are shown in the 3rd and right-hand columns, respectively. In the panels showing precipitation and the favored sink regions, we show only those areas where

the differences are significant at the 90% confidence level using a bootstrap test.

The blueish (reddish) areas in the variations of vertically integrated moisture transport observed for NAM or SAM (2nd column of Figures 5, 6) show where the transport is favored during higher (lower) values of the mode. In general, the favored regions of moisture transport coincide with the favored sink areas indicated in the 3rd (right-hand) column, and with enhanced precipitation (the left-hand columns show the monthly differences in the composites of precipitation).

A detailed analysis of Figures 5, 6 could point to the areas where the transport of moisture from the sources investigated is enhanced during the different phases of the modes. An increase in moisture does not imply in a direct response in terms of precipitation, because it also depends on the existence of other dynamical precursors (e.g., instability, local convergence, etc.), but the method does allow us to analyse the preferred sinks.

In the case of the NAM (Figure 5), for lower values of NAMI (right-hand column), enhanced convergence of Θ (red contours) and increased precipitation (red areas in the left-hand column) were observed over the northeastern Atlantic Ocean, the Mediterranean Sea areas, and over western and southern Europe. The pattern suffers a northward displacement during April, the last winter month analyzed. As a whole this area receives an enhanced moisture contribution from the NATL and MED sources. Increased moisture transport from NPAC was verified over the western North American region together with enhanced transport of Θ in the eastern Northern Pacific Ocean, especially during the first months.

During periods of higher values of NAMI (Figure 5, 3rd column) enhanced transport of Θ (blue contours in the 2nd column) was observed over the western North Pacific Ocean, associated with an enhanced moisture contribution from the NPAC source over the Asian coast, preferentially during early winter. Transport of Θ was also enhanced over the inland parts of the North American continent, a region receiving a higher moisture contribution from the NPAC, MEXCAR, and NATL sources. The MEXCAR shows a greater influence over the mid-east part of North America during December. Other regions that showed an intensification of the transport of Θ are Central America with higher contributions from NATL and MEXCAR, and northern South America, with an enhanced contribution from NATL during March.

The REDS and ARAB sources of moisture show no discernible pattern of behavior between the two phases of NAM.

For lower values of SAMI (Figure 6, right-hand column), the transport of moisture was enhanced toward central Africa, with increased contributions mainly from the SATL. Over the same continent, albeit to a lesser extent, the east coast receives intensified moisture transport from AGU and IND during some months. The higher transport of moisture from AGU to southern Africa during August is remarkable. Southeastern South America and the adjacent extratropical Atlantic region receive more moisture from the SATL, AGU and SPAC sources, and southern Australia and the neighboring oceans receive moisture from the IND source.

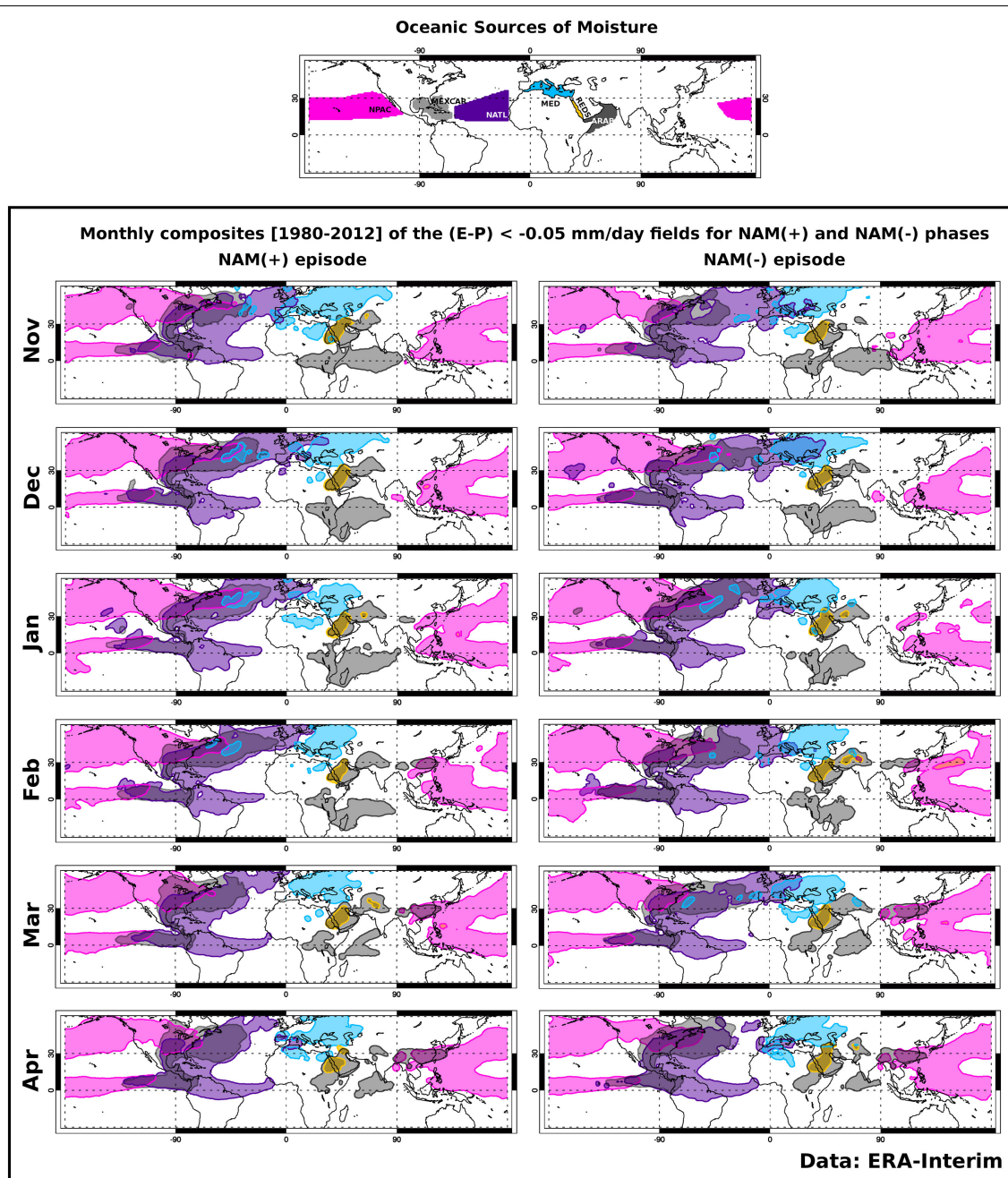


FIGURE 3 | Monthly composites of moisture sink areas detected for the NAM for the semi-annual winter period 1980–2012. The sink areas are shown in the same color as the corresponding oceanic source regions (top panel, schematic representation of

Figure 2). Only negative values of $E-P$, calculated by forward tracking from the defined moisture sources, larger than -0.05 mm d^{-1} , are plotted for (left) higher values of NAM Index and (right) lower values of NAM Index.

In respect of the higher values of the SAM Index (Figure 6, 3rd column), an enhanced transport of Θ was detected from the Indian Ocean/West Pacific Warm Pool toward northern Australia (blue contours in the 2nd column). This region received a higher moisture contribution from the IND, CORALS, and SPAC sources. The CORALS source has its major influence during September over Eastern Australia and the adjacent ocean, when

the other sources show no significant contribution. During the early austral winter, the northern part of South America and the Atlantic ITCZ receive enhanced transport of Θ with a contribution from the SATL source. Around the middle to the end of the austral winter, an enhancement of moisture transport from the SATL and AGU sources reaches the southwestern tropical Atlantic Ocean, while increased transport from the AGU and

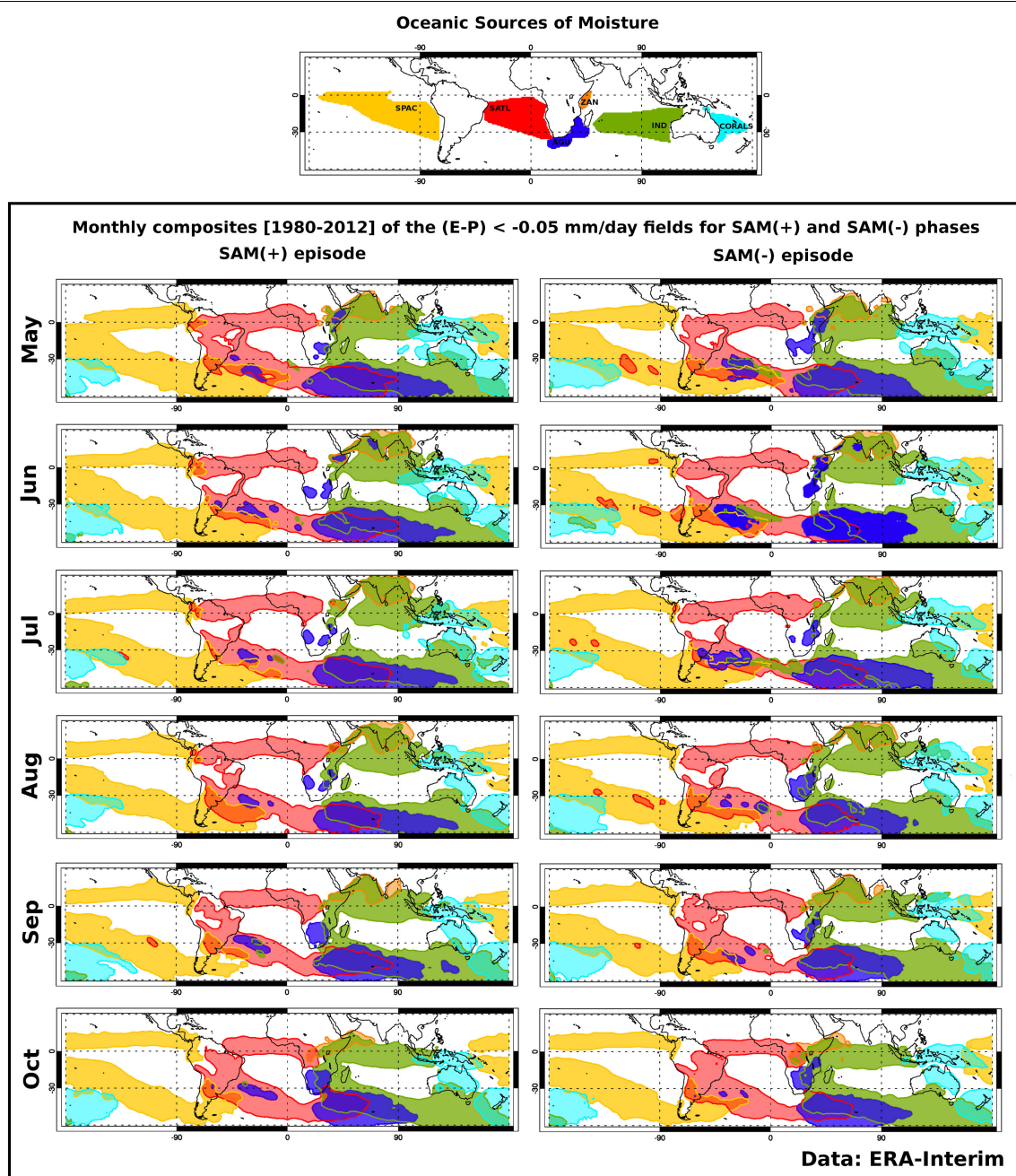


FIGURE 4 | As Figure 3, for SAM.

IND sources reaches southern Africa and the southwestern Indian Ocean.

The ZAN source of moisture contributes to the Indian region either during higher or lower values of SAM Index (Figure 6, 3rd and right-hand columns), showing that the transport is due to other reasons not attributable to this mode.

It must be stressed that the oceanic moisture sources used to characterize the role played by the annular modes in the transport of moisture were defined as stationary (Figure 2) following

the definition of Gimeno et al. (2010), based on their annual mean values. As previously discussed, the attributes of the sources may vary in intensity and/or size along the year, besides probably having some interannual variability. The areal mean divergence of the vertically integrated moisture flux over each oceanic source considered could therefore be an alternative means of comparing the possible impact of the two phases of NAM and SAM on the intensity of the sources. We calculated the monthly climatological values for each source defined as their annual mean value

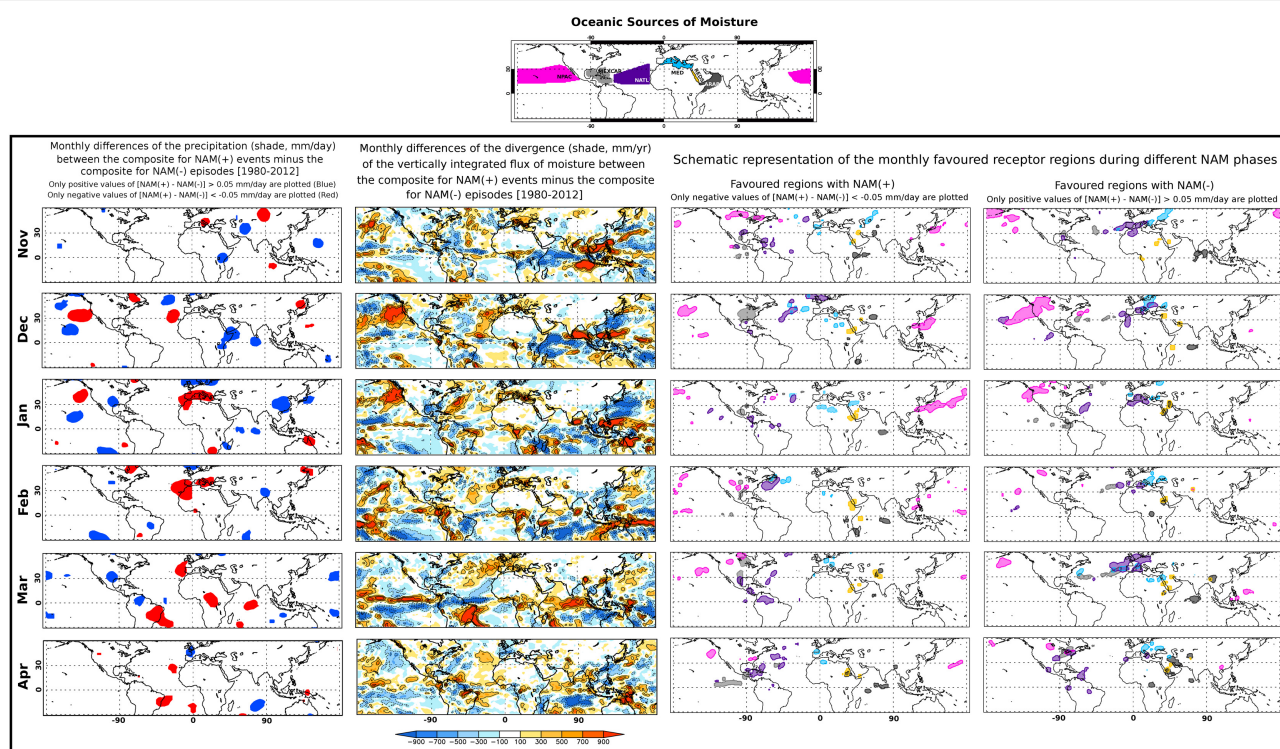


FIGURE 5 | Monthly influence of the evolution of the NAM during November to April (boreal winter) over the moisture transport of the main oceanic sources of precipitation for 1980–2012. Top: Schematic representation of the main oceanic sources of moisture. **Bottom, left-hand column:** Monthly differences in precipitation (in mm/day, data from GPCP) between the composites for years with higher and lower values of NAMI. **Bottom, 2nd column:** Monthly differences in divergence of the vertically integrated moisture flux (in mm/year, data from ERA-Interim) between the

composites for the years with higher (bluish colors) and lower (reddish colors) values of NAMI. **Bottom, 3rd and right-hand columns:** The composite differences in E-P generated by each moisture source between higher and lower NAMI values. 3rd column: Schematic representation of the favored receptor regions of precipitation during the higher NAMI; Right-hand column: during lower NAMI. Following a bootstrap test, only those areas where the absolute value of differences greater than 0.05 mm/day significant at the 90% confidence level are plotted.

and we also composited the divergence of the vertically integrated moisture flux of both phases of each annular mode. In attempting to find some linear variability in the results it would appear that there is an intensification (weakening) of the MED and NATL sources during the higher (lower) NAM episodes considered as compared with annual climatology. For the MED source the values of the higher NAM episodes from November to March exceed the average annual ones by between 116 and 157%, and for the lower NAM episodes the equivalent figure is between 31 and 93% lower than for average annual values for the winter, reaching the lowest during February. The other source that shows any appreciable difference is the NATL, but the signal is weaker: around 104% for higher NAM episodes and between 70 and 98% for lower values of the index (the minimum occurs in December). For the SAM the results do not indicate any linear joint variability of the index and the divergence of the moisture transport for the sources considered.

Another means of finding possible differences between the two phases of the modes would be to try to identify modifications in the areal extents or positions of the sources. We therefore redefined all the oceanic sources of moisture using the composites of the highest and lowest years of both modes of variability. It is important to stress that in this case the composites were only

evaluated for the winter months. Comparing these values with those for the whole semiannual period (1979–2012) showed that the sources maintained their positions and sizes (plot not shown).

CONCLUDING REMARKS AND DISCUSSION

We have herein investigated the impact of the Northern and Southern hemisphere annular modes on the moisture transport from the major oceanic moisture sources during winter using the Lagrangian FLEXPART dataset fed by ERA-Interim Reanalysis data. We calculated differences between the composites of the divergence of vertically integrated moisture transport, of the precipitation, and of the favored sink regions characterizing the six strongest events selected for both phases of the two modes during the period 1979–2012.

As a summary of the detailed analysis of income in the previous paragraphs, for the NAM mode it must be expected that the impacts of the extreme episodes in moisture transport mainly occur over the sources placed over the Atlantic and Pacific oceanic regions, due that the main centers of action of the mode in the middle latitudes are located over the Atlantic and Pacific subtropical high pressure systems. Although we have considered the sources to be stationary throughout the experiment, we must also consider possible changes in location and/or intensity of the

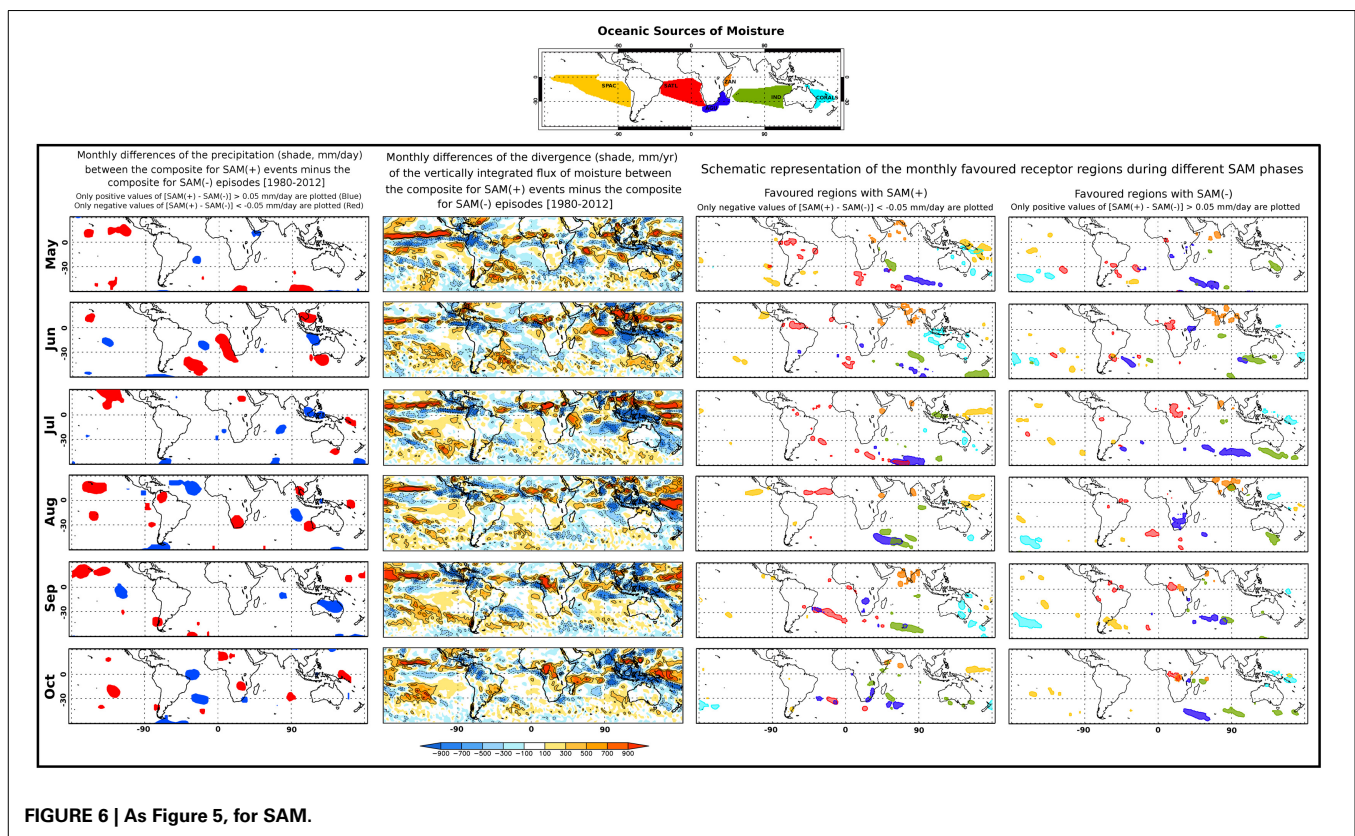


FIGURE 6 | As Figure 5, for SAM.

areas of divergence of Θ . In respect of the NPAC source in the northern Pacific Ocean, it is interesting to note the enhanced moisture transport toward the northeastern basin for the lower values of NAM Index associated with the weakening of the Pacific high pressure center and weak westerlies over the polar latitudes. Under these conditions, the storm tracks tends toward tropical latitudes affecting the northwestern part of North America (Wang et al., 2006). On the other hand, for higher values of the NAM Index the Pacific high pressure center is expected to intensify, and moisture transport from NPAC is favored toward eastern Asia. The East Asian Monsoon characterizes the major moisture pattern for the region, but although the East Asian Monsoon is not favored during winter there nevertheless exists a significant interaction with the Siberian High, which is modulated in its intensity by the NAM. So, the NAM plays an important role in the changes of the Siberian High, via a positive correlation in which a lower NAMI is related to a lower intensity of the Siberian High. This fact favors the influx of moisture from the ocean (Gong et al., 2001).

Over the North Atlantic Ocean the years with lower values of NAMI are characterized by lower than normal atmospheric pressures and weak westerlies over northern Europe. Enhanced moisture transport from the NATL, MEXCAR, and MED sources toward southern Europe and the Mediterranean basin therefore occurs; while the reverse applies for a high NAM index, when the transport is northwards over Europe (Dickson et al., 2000) and when droughts can occur over the southern part of the continent (Vicente-Serrano et al., 2011). Nevertheless, the intensification of the Atlantic high pressure center during higher NAM

years, and the associated easterly trade winds at its southern flank, occur with enhanced moisture transport from the NATL and MEXCAR sources toward the Caribbean Sea. The flow is thus intensified forming the Caribbean Low Level Jet (CLLJ) that splits into two branches, one following its way westwards across Central America, and the other turning northwards to North America crossing the Gulf of Mexico. This result accords with the variability of the CLLJ (Wang, 2007; Amador, 2008) and the characteristics of the moisture transport patterns over the area (Durán-Quesada et al., 2010). A higher (lower) NAM is therefore associated with a reinforcing (weakening) of transport from NATL and MEXCAR to Central and North America throughout the CLLJ. The intensification or weakening of the Atlantic High pressure system could be also related to the interannual variability found for the MED and NATL sources when the vertically integrated moisture divergence was analyzed.

In the Southern Hemisphere, the position and intensity of the semipermanent high pressures also define the circulation, and the influence of both phases of SAM over them defines the advection of moisture from the sources to the sinks. In this context, during higher values of SAM (Marshall et al., 2012), with high-pressure systems stronger than the normal, the belt of westerlies and the trade winds intensify, and the ITCZ is positioned to the north, the pattern found for the transport of moisture is, in general, as described. The moisture was transported southwards and eastwards from the AGU, IND, and SATL sources more than during the positive phase of SAM. Thus, in the Indian Ocean a horizontal band of precipitation over the southern basin appears with

moisture that originates from the AGU source, and little areas from IND behave in the same way.

This ties in with the poleward shifts in synoptic weather systems (Thompson and Wallace, 2000), which affects southwest Australia (Cai et al., 2011) and the southwestern coast of South Africa (Reason and Rouault, 2005), bringing negative anomalies in precipitation to these areas. It is well known that over Australia the positive phases of SAM bring anomalously wet conditions in spring and summer (Gillett et al., 2006). The pattern shown here represents quite well the wet conditions of the early austral spring (Min et al., 2013), when an enhanced uptake of moisture occurs from CORALS. The higher values for the SAM mode were also characterized by an enhanced transport of Θ over the Indian Ocean/West Pacific Warm Pool, with the area receiving a higher moisture contribution from the CORALS and SPAC sources. The higher pressures configured around Australia move the moisture northwards from CORALS, and then the trade winds advect it westwards, with more intensity during higher SAM events (intense values of divergence of the vertically integrated flux of moisture, blue colors in the 2nd column of **Figure 5**). The intensified trade winds bring moisture toward the region from the SPAC, which disappears for lower values of SAM Index when the trade winds are less intense.

Over the South Atlantic Ocean the intensified high pressure maintains the flow of moisture both to the Southern Atlantic Convergence Zone (SACZ) and to the ITCZ from the SATL source. It can be seen that during the early months the intensified trade winds introduce moisture to the inland parts of the continent (this signal is also recognizable in the Pacific, but only over the islands) and the SACZ receives more moisture during the later months. The results indicate that southeastern South America received more moisture from the SATL, AGU, and SPAC sources during the lower SAM Index years. These results agree with the finding that for lower values of SAMI the cyclone trajectories move northwards and South America suffers from intense frontogenetic activity associated with positive anomalies of precipitation over the southeastern part of the continent (Reboita et al., 2009). The weakness of the westerlies and trade winds for lower values of SAM Index favors the influx of moisture from SATL during the monsoon in Africa. The enhanced transport of moisture over southern Africa from AGU during August accords with the anomalous flux detected by Reason and Rouault (2005), in their analysis of the wettest winters for negative SAM phases.

Because the centers of activity of NAM lie principally over the larger basin oceans and around mid- and higher latitudes in the northern hemisphere, the REDS and ARAB sources seem relatively unaffected by the different phases of the mode. The variation of ZAN with SAM does not seem relevant, perhaps due the fact that it is positioned on the equator. These regions are more influenced by the evolution of the El Niño-Southern Oscillation as described by Castillo et al. (2014), who found that during winter El Niño events, the ZAN and ARAB sources increase their moisture contribution in the western Indian Ocean. Additionally, these sources are crossed by the Somali Jet, which is the main supply of moisture during the Indian Summer Monsoon, and is strongly modulated by the Madden-Julian Oscillation (Ordóñez et al., 2013).

An understanding of variability such as that described here provides scientists with information on the general configuration of climate around the globe. In light of our results we note that the modulation of both hemispheric annular modes is in good accordance with the expected circulation patterns and with findings made in previous studies. Analyzing the relationship between the major hemispheric modes of variability and the transport of moisture from their main oceanic sources will help to produce a map showing how precipitation could change under future climate change scenarios. The Annular Modes have shown a steady positive trend over recent decades (Miller et al., 2006), and if this trend continues the results presented here could help to identify those geographical areas most affected by climate change, and help politicians and economists plan future water resource strategies.

ACKNOWLEDGMENT

The authors gratefully acknowledge the support of the Spanish Government through their funding of the TRAMO (“TRANsport of MOisture”) project, which is also cofunded by FEDER (in spanish European regional development fund- ERDF).

REFERENCES

- Adler, R. F., Huffman, G. J., Chang, A., Ferraro, R., Xie, P., Janowiak, J. et al. (2003). The Version 2 Global Precipitation Climatology Project (GPCP) monthly precipitation analysis (1979–Present). *J. Hydrometeorol.* 4, 1147–1167. doi: 10.1175/1525-7541(2003)004%3C1147:TVGPCP%3E2.0.CO;2
- Amador, J. A. (2008). The intra-americas sea low-level jet. *Ann. N.Y. Acad. Sci.* 1146, 153–188. doi: 10.1196/annals.1446.012
- Baldwin, M. P., and Dunkerton, T. J. (1999). Propagation of the arctic oscillation from the stratosphere to the troposphere. *J. Geophys. Res.* 104, 30937–30946. doi: 10.1029/1999JD900445
- Bengtsson, L., Hagemann, S., and Hodges, K. I. (2004). Can climate trends be calculated from reanalysis data? *J. Geophys. Res.* 109, D11111. doi: 10.1029/2004JD004536
- Cai, W., van Rensch, P., Borlace, S., and Cowan, T. (2011). Does the Southern Annular Mode contribute to the persistence of the multidecade-long drought over southwest Western Australia? *Geophys. Res. Lett.* 38:L14712. doi: 10.1029/2011GL047943
- Castillo, R., Nieto, R., Drumond, A., and Gimeno, L. (2014). The role of the ENSO cycle in the modulation of moisture transport from major oceanic moisture sources. *Water Resour. Res.* 50, 1046–1058. doi: 10.1002/2013WR013900
- Dee, D. P., Uppala, S. M., Simmons, A. J., Berrisford, P., Poli, P., Kobayashi, S., et al. (2011). The ERA-Interim reanalysis: configuration and performance of the data assimilation system. *Q. J. R. Meteorol. Soc.* 137, 553–597. doi: 10.1002/qj.828
- Deser, C., and Teng, H. (2008). Evolution of Arctic sea ice concentration trends and the role of atmospheric circulation forcing, 1979–2007. *Geophys. Res. Lett.* 35, L02504. doi: 10.1029/2007GL032023
- Dickson, R. R., Osborn, T. J., Hurrell, J. W., Meincke, J., Blindheim, J., Adlandsvik, B., et al. (2000). The Arctic Ocean response to the North Atlantic Oscillation. *J. Clim.* 13, 2671–2696. doi: 10.1175/1520-0442(2000)013<2671:TAORTT>2.0.CO;2
- Dirmeyer, P. A., and Brubaker, K. L. (2007). Characterization of the global hydrologic cycle from a back-trajectory analysis of atmospheric water vapor. *J. Hydrometeorol.* 8, 20–37. doi: 10.1175/JHM557.1
- Drumond, A., Nieto, R., Gimeno, L., and Ambrizzi, T. (2008). A Lagrangian identification of major sources of moisture over Central Brazil and La Plata Basin. *J. Geophys. Res.* 113, D14128. doi: 10.1029/2007JD009547
- Durán-Quesada, A. M., Gimeno, L., Amador, J. A., and Nieto, R. (2010). Moisture sources for Central America: identification of moisture sources using a Lagrangian analysis technique. *J. Geophys. Res.* 115, D05103. doi: 10.1029/2009JD012455

- Gillett, N. P., Kell, T. D., and Jones, P. D. (2006). Regional climate impacts of the Southern Annular Mode. *Geophys. Res. Lett.* 33, L23704. doi: 10.1029/2006GL027721
- Gimeno, L. (2013). Grand challenges in atmospheric science. *Front. Earth Sci.* 1:1. doi: 10.3389/feart.2013.00001
- Gimeno, L., Drumond, A., Nieto, R., Trigo, R. M., and Stohl, A. (2010). On the origin of continental precipitation. *Geophys. Res. Lett.* 37, L13804. doi: 10.1029/2010GL043712
- Gimeno, L., Stohl, A., Trigo, R. M., Dominguez, F., Yoshimura, K., Yu, L., et al. (2012). Oceanic and terrestrial sources of continental precipitation. *Rev. Geophys.* 50, RG4003. doi: 10.1029/2012RG000389
- Gómez-Hernández, M., Drumond, A., Gimeno, L., and García-Herrera, R. (2013). Variability of moisture sources in the Mediterranean region during the period 1980–2000. *Water Resour. Res.* 49, 6781–6794. doi: 10.1002/wrcr.20538
- Gong, D., and Wang, S. (1999). Definition of Antarctic oscillation index. *Geophys. Res. Lett.* 26, 459–462. doi: 10.1029/1999GL000003
- Gong, D., Wang, S., and Zhu, J. H. (2001). East Asian winter monsoon and Arctic Oscillation. *Geophys. Res. Lett.* 28, 2073–2076. doi: 10.1029/2000GL012311
- Ho, M., Kiem, A. S., and Verdon-Kidd, D. C. (2012). The Southern Annular Mode: a comparison of indices. *Hydrol. Earth Syst. Sci.* 16, 967–982. doi: 10.5194/hess-16-967-2012
- Huffman, G. J., Adler, R. F., Bolvin, D. T., and Gu, G. (2009). Improving the global precipitation record: GPCP version 2.1. *Geophys. Res. Lett.* 36, L17808. doi: 10.1029/2009GL040000
- Hurrell, J. W. (1995). Decadal trends in the North Atlantic oscillation: regional temperatures and precipitation. *Science* 269, 676–679. doi: 10.1126/science.269.5224.676
- Hurrell, J. W., and National Center for Atmospheric Research Staff. (eds.). (2013). *The Climate Data Guide: Hurrell North Atlantic Oscillation (NAO) Index (Station-Based)*. Available online at: <https://climatedataguide.ucar.edu/climate-data/hurrell-north-atlantic-oscillation-nao-index-station-based>
- Hurrell, J. W., Kushnir, Y., Ottersen, G., and Visbeck, M. (2013). *The North Atlantic Oscillation: Climatic Significance and Environmental Impact*. Vol. 134. Washington, DC: American Geophysical Union.
- Kalnay, E., Kanamitsu, M., Kistler, R., Collins, W., Deaven, D., Gandin, L., et al. (1996). The NCEP/NCAR 40-year reanalysis project. *Bull. Am. Meteorol. Soc.* 77, 437–470. doi: 10.1175/1520-0477(1996)077<0437:TNYRP>2.0.CO;2
- Knippertz, P., Wernli, H., and Gläser, G. (2013). A global climatology of tropical moisture. *J. Clim.* 26, 3031–3045. doi: 10.1175/JCLI-D-12-00401.1
- Li, J. P., and Wang, J. X. L. (2003). A modified zonal index and its physical sense. *Geophys. Res. Lett.* 30, 1632. doi: 10.1029/2003GL017441
- Marshall, A. G., Hudson, D., Wheeler, M. C., Hendon, H. H., and Alves, O. (2012). Simulation and prediction of the Southern Annular Mode and its influence on Australian intra-seasonal climate in POAMA. *Clim. Dyn.* 38, 2483–2502. doi: 10.1007/s00382-011-1140-z
- Marshall, G. J. (2003). Trends in the Southern Annular Mode from observations and reanalyses. *J. Climate* 16, 4134–4143. doi: 10.1175/1520-0442(2003)016<4134:TITSAM>2.0.CO;2
- Marshall, G. J., Di Battista, S., Naik, S. S., and Thamban, M. (2011). Analysis of a regional change in the sign of the SAM-temperature relationship in Antarctica. *Clim. Dyn.* 36, 277–287. doi: 10.1007/s00382-009-0682-9
- Miller, R. L., Schmidt, G. A., and Shindell, D. T. (2006). Forced annular variations in the 20th century IPCC AR4 simulations. *J. Geophys. Res.* 111, D18101. doi: 10.1029/2005JD00
- Min, S. K., Cai, W., and Whetton, P. (2013). Influence of climate variability on seasonal extremes over Australia. *J. Geophys. Res. Atmos.* 118, 643–654. doi: 10.1002/jgrd.50164
- Nan, S., and Li, J. (2003). The relationship between the summer precipitation in the Yangtze River valley and the boreal spring Southern Hemisphere annular mode. *Geophys. Res. Lett.* 30, 2266. doi: 10.1029/2003GL018381
- Nieto, R., Durán-Quesada, A. M., and Gimeno, L. (2010). Major sources of moisture over Antarctic ice-core sites identified through a Lagrangian approach. *Clim. Res.* 41, 45–49. doi: 10.3354/cr00842
- Nieto, R., Gimeno, L., and Trigo, R. M. (2006). A Lagrangian identification of major sources of Sahel moisture. *Geophys. Res. Lett.* 33, L18707. doi: 10.1029/2006GL027232
- Numaguti, A. (1999). Origin and recycling processes of precipitating water over the Eurasian continent: experiments using an atmospheric general circulation model. *J. Geophys. Res.* 104, 1957–1972. doi: 10.1029/1998JD200026
- Ogi, M., and Yamazaki, K. (2010). Trends in the summer Northern Annular Mode and Arctic sea ice. *SOLA* 6, 41–44. doi: 10.2151/sola.2010-011
- Ordóñez, P., Ribera, P., Gallego, D., and Peña-Ortiz, C. (2012). Major moisture sources for Western and Southern India and their role on synoptic-scale rainfall events. *Hydrol. Process.* 26, 3886–3895. doi: 10.1002/hyp.8455
- Ordóñez, P., Ribera, P., Gallego, D., and Peña-Ortiz, C. (2013). Influence of Madden-Julian Oscillation on water budget transported by the Somali low-level jet and the associated Indian summer monsoon rainfall. *Water Resour. Res.* 49, 6474–6485. doi: 10.1002/wrcr.20515
- Paredes, D., Trigo, R. M., García-Herrera, R., and Trigo, I. F. (2006). Understanding precipitation changes in Iberia in early Spring: weather typing and storm-tracking approaches. *J. Hydrometeorol.* 7, 101–113. doi: 10.1175/JHM472.1
- Parkinson, C. L., and Cavalieri, D. J. (2012). Antarctic sea ice variability and trends, 1979–2010. *Cryosphere* 6, 871–880. doi: 10.5194/tc-6-871-2012
- Reason, C. J. C., and Rouault, M. (2005). Links between the Antarctic Oscillation and winter rainfall over western South Africa. *Geophys. Res. Lett.* 32, L07705. doi: 10.1029/2005GL022419
- Reboita, M., Ambrizzi, T., and da Rocha, R. (2009). Relationship between the southern annular mode and southern hemisphere atmospheric systems. *RBMET* 24, 48–55. doi: 10.1590/S0102-77862009000100005
- Rogers, A. N., Bromwich, D. H., Sinclair, E. N., and Cullather, R. I. (2001). The atmospheric hydrologic cycle over the Arctic basin from reanalyses. Part II: Interannual variability. *J. Clim.* 14, 2414–2429. doi: 10.1175/1520-0442(2001)014<2414:TAHCOT>2.0.CO;2
- Sodemann, H., Schwieler, C., and Wernli, H. (2008). Interannual variability of Greenland winter precipitation sources: lagrangian moisture diagnostic and North Atlantic Oscillation influence. *J. Geophys. Res.* 113, D03107. doi: 10.1029/2007JD008503
- Sodemann, H., and Stohl, A. (2009). Asymmetries in the moisture origin of Antarctic precipitation. *Geophys. Res. Lett.* 36, L22803. doi: 10.1029/2009GL040242
- Stohl, A., and James, P. (2005). A Lagrangian analysis of the atmospheric branch of the global water cycle. Part II: Earth's river catchments, ocean basins, and moisture transports between them. *J. Hydrometeorol.* 6, 961–984. doi: 10.1175/JHM470.1
- Stohl, A., and James, P. A. (2004). Lagrangian analysis of the atmospheric branch of the global water cycle. Part I: method description, validation, and demonstration for the August 2002 flooding in Central Europe. *J. Hydrometeorol.* 5, 656–678. doi: 10.1175/1525-7541(2004)005<0656:ALAOA>2.0.CO;2
- Thompson, D. W., and Wallace, J. M. (2000). Annular modes in the extratropical circulation, Part I: month-to-month variability. *J. Clim.* 13, 1000–1016. doi: 10.1175/1520-0442(2000)013<1000:AMITEC>2.0.CO;2
- Thompson, D. W., and Wallace, J. M. (2001). Regional climate impacts of the Northern Hemisphere annular mode. *Science* 293, 85–89. doi: 10.1126/science.1058958
- Thompson, D. W., Wallace, J. M., and Hegerl, G. C. (2000). Annular modes in the extratropical circulation, Part II: trends. *J. Clim.* 13, 1018–1036. doi: 10.1175/1520-0442(2000)013<1018:AMITEC>2.0.CO;2
- Trenberth, K. E., Fasullo, J. T., and Mackaro, J. (2011). Atmospheric moisture transports from ocean to land and global energy flows in reanalyses. *J. Clim.* 24, 4907–4924. doi: 10.1175/2011JCLI4171.1
- Vicente-Serrano, S. M., López-Moreno, J. I., Lorenzo-Lacruz, J., El Kenawy, A., Azorin-Molina, C., Morán-Tejeda, E., et al. (2011). The NAO impact on droughts in the mediterranean region. Hydrological, socioeconomic and ecological impacts of the North Atlantic Oscillation in the mediterranean region. *Adv. Glob. Change Res.* 46, 23–40. doi: 10.1007/978-94-007-1372-7_3
- Visbeck, M. (2009). A station-based southern annular mode index from 1884 to 2005. *J. Clim.* 22, 940–950. doi: 10.1175/2008JCLI2260.1
- Viste, E., and Sorteberg, A. (2013). Moisture transport into the Ethiopian highlands. *Int. J. Climatol.* 33, 249–263. doi: 10.1002/joc.3409

- Wang, C. (2007). Variability of the Caribbean low-level jet and its relations to climate. *Clim. Dyn.* 29, 411–422. doi: 10.1007/s00382-007-0243-z
- Wang, X. L., Wan, H., and Swail, V. R. (2006). Observed changes in cyclone activity in Canada and their relationships to major circulation regimes. *J. Clim.* 19, 896–915. doi: 10.1175/JCLI3664.1
- Wei, J., Dirmeyer, P. A., Bosilovich, M. G., and Wu, R. (2012). Water vapor sources for Yangtze River Valley rainfall: climatology, variability, and implications for rainfall forecasting. *J. Geophys. Res.* 117, D05126. doi: 10.1029/2011JD016902

Conflict of Interest Statement: The authors declare that the research was conducted in the absence of any commercial or financial relationships that could be construed as a potential conflict of interest.

Received: 13 March 2014; accepted: 06 June 2014; published online: 02 July 2014.

Citation: Nieto R, Castillo R and Drumond A (2014) The modulation of oceanic moisture transport by the hemispheric annular modes. *Front. Earth Sci.* 2:11. doi: 10.3389/feart.2014.00011

This article was submitted to *Atmospheric Science*, a section of the journal *Frontiers in Earth Science*.

Copyright © 2014 Nieto, Castillo and Drumond. This is an open-access article distributed under the terms of the Creative Commons Attribution License (CC BY). The use, distribution or reproduction in other forums is permitted, provided the original author(s) or licensor are credited and that the original publication in this journal is cited, in accordance with accepted academic practice. No use, distribution or reproduction is permitted which does not comply with these terms.

TECHNICAL NOTE

10.1002/2013WR013901

Special Section:

Oceanic Sources of
Continental Precipitation

Key Points:

- Moisture sources for two continental climate regionalization schemes
- Role of major teleconnections on moisture transport
- Influence of the hot spot source regions over climatic regions

Supporting Information:

- Readme
- Supporting figure S1
- Supporting figure S2
- Supporting figure S3
- Supporting figure S4
- Supporting figure S5
- Supporting figure S6
- Supporting figure S7
- Supporting figure S8
- Supporting figure S9
- Supporting table S1

Correspondence to:

R. Nieto,
rnieto@uvigo.es

Citation:

Nieto, R., R. Castillo, A. Drumond, and L. Gimeno (2014), A catalog of moisture sources for continental climatic regions, *Water Resour. Res.*, 50, doi:10.1002/2013WR013901.

Received 3 APR 2013

Accepted 1 JUN 2014

Accepted article online 6 JUN 2014

A catalog of moisture sources for continental climatic regions

Raquel Nieto¹, Rodrigo Castillo¹, Anita Drumond¹, and Luis Gimeno¹
¹EPhysLab, Departamento de Física Aplicada, Facultad de Ciencias de Ourense, Universidad de Vigo, Ourense, Spain

Abstract This technical note describes a catalog of moisture sources for two sets of continental climatic regions: one based on regions with similar late 20th century mean climate and similar projected late 21st century precipitation changes, and the other widely used in IPCC assessment reports. By illustrating with one region by classification, the European one was selected and we identify and characterize all the major sources of moisture, and analyze their interannual variability and the role of the three dominant modes of global climate variability, including the El Niño-Southern Oscillation (ENSO) and the Northern and Southern Annular Modes (NAM, SAM). We also estimate the influence of those oceanic regions that will see the greatest increases in evaporation rate in future years.

1. Introduction

Changes in the hydrological cycle are expected to be one of the greatest threats with regard to global climate change because the impact of changes in the regional precipitation patterns may exceeds the tolerance of the natural world and human civilization; of particular concern, are changes in the location and strength of the most important moisture sources [Gimeno *et al.*, 2012]. The results of observational and modeling studies suggest that climate change will lead to an intensification of the water cycle, due to the strong dependence of saturated vapor pressure on temperature [Held and Soden, 2006; Wentz *et al.*, 2007]. As described in many studies and summarized by the *Intergovernmental Panel on Climate Change* [2007], under future climate change, the regional precipitation will increase due to the intensification of the global hydrological cycle in the high latitudes and over tropical Asia and America due monsoon regimes. At the same time, precipitation will decrease in the subtropical band, accompanied by a general expansion of dry areas to the Poles. In a recent study, Mahlstein *et al.* [2012] detected significant changes in the precipitation over many continental regions during the wet seasons at the end of the 20th century. To interpret these results, and to explain current and future changes in the precipitation patterns, the physical mechanisms from evaporation to precipitation must be understood. A good knowledge of the transport of moisture from the sources over the different oceans to the continents is therefore of great importance, and a robust identification of those regions particularly vulnerable to changes in the hydrological cycle is required. This entails the description of both the location of regions with similar projected changes in terms of precipitation and the identification of their moisture sources. Sophisticated Lagrangian models have been used over the last few decades to detect the sources of moisture for different climatological continental regions of interest. The Lagrangian approach used herein is a powerful and highly reliable tool for evaluating changes in specific humidity along a large number of trajectories, in order to analyze and identify links between moisture sources and respective sink regions. These relationships can be tested in a backward or forward mode. It is worth noting that the methodology used herein has already been successfully applied in climatological studies of moisture sources at global [e.g., Gimeno *et al.*, 2010] and regional scales, including the Sahel [Nieto *et al.*, 2006], China [Drumond *et al.*, 2011], and river basins such as the Mississippi [Stohl and James, 2005] and the Orinoco [Nieto *et al.*, 2008].

The aims of the present study are (a) to identify and characterize all the major moisture sources associated with continental climatic regions (CCRs) based on two different regionalization schemes, one that considers 35 regions with similar or homogenous projected changes over the surface of the globe [Malstein and Knutti, 2010], herein MK regions, and the other the so-called 21 Giorgi regions [Giorgi and Francisco, 2000] widely used in the IPCC reports, which represents different climatic regimes, (b) to analyze the interannual variability of the moisture sources and the role of the main modes of climate variability including the El Niño-Southern Oscillation (ENSO), the Northern Annular Mode (NAM)/Southern Annular Mode (SAM), and

(c) to assess the influence of those oceanic regions that will see the greatest increase in evaporation rate [Seager *et al.*, 2010] on the precipitation over a given target region. We analyzed with more detail one CCR in particular as one example of the full catalog of all 35 MK regions and the similar one in the Giorgi division, which will be freely available (www.ephyslab.uvigo.es/tramo/ccrs) in due course.

This paper could provide a tool to interpret current and future changes in the regional precipitation patterns by means of a robust identification of the moisture sources for those “homogenous current climate” regions where regional climate change is being analyzed [Giorgi and Francisco, 2000] and those “homogenous future change” regions where probably will be analyzed [Malstein and Knutti, 2010].

The methodology and data used to calculate the E-P field are described in Section 2, and in Section 3 we provide a description of the catalog itself.

2. Data and Methods

The approach described here is based on the Lagrangian particle dispersion model FLEXPART (v9.0) developed by Stohl and James [2004, 2005]. FLEXPART is optimized to drive with input data from the European Centre for Medium-Range Weather Forecasts (ECMWF) and from the Global Forecast System (GFS), and recently from Weather Research and Forecasting (WRF) regional models data [Brioude *et al.*, 2013]. The analysis was carried out using data from 1980 to 2012 obtained from the ERA-Interim reanalysis of the ECMWF [Dee *et al.*, 2011], the state-of-the-art reanalysis in terms of hydrological cycle. It has been shown that the performance of ERA-Interim in reproducing the hydrological cycle and in terms of water balance closure is much better than ERA-40 [Trenberth *et al.*, 2011] and even than the newest reanalysis products Modern Era Retrospective-Analysis for Research and Applications and Climate Forecast System Reanalysis [Lorenz and Kunstmann, 2012]. The variables that needs FLEXPART to run are essentially the wind (u and v) and the specific humidity (q), and those, or a combination of them linked to moisture transport (the integrated moisture flux) are used by Lorenz and Kunstmann [2012] to compare the different reanalysis data set available for the scientific community. They also conclude that the ERA-Interim is the best data to analyze the closure of the terrestrial and atmospheric water balance and in the agreement with the observation datasets. The restriction of the analysis to data since 1979 is the result of both the high sensitivity of FLEXPART model to be fed with erroneous data [Stohl *et al.*, 2005] and the impossibility to work with data prior to the incorporation of satellite data in the reanalysis. In fact, it is a well-know fact that prior to 1979 there is simply no sufficient observations over large oceanic areas and datasets are considerably less reliable [Bengtsson *et al.*, 2004]. We used a horizontal resolution of 1° and a vertical resolution of 61 vertical levels, used to track atmospheric moisture along trajectories. The atmosphere was divided homogeneously into a large number of particles (air parcels) that are then moved by the 3-D wind field. The specific humidity (q) and the position (latitude, longitude, and altitude) of all the particles are recorded at 6 h intervals. Therefore, at each time step, the model calculates increases (e) and decreases (p) in moisture along each trajectory via variations in (q) with respect to time i.e., $e-p = m \, dq/dt$. By summing ($e-p$) for all particles crossing a 1° grid column of the atmosphere, we obtain ($E-P$) for the area of interest, where E and P are the rates of evaporation and precipitation, respectively. The particles were tracked and a database was made with values of $E-P$ averaged and integrated over 10 days of transport ($(E-P)_{1-10}$) (water vapor resides in the atmosphere for about this length of time [Numaguti, 1999]). It is the analysis of the $(E-P)_{1-10}$ field that shows the main sources of moisture for the target area (when and where the air masses that reach the target area acquired or lost moisture). A complete review of the limitations of this Lagrangian approach, its uncertainty and significance as well as the advantages and disadvantages respect other methods to estimate moisture sources can be found in the recent comprehensive review about the topic published by Gimeno *et al.* [2012].

To assess the potential influence of the main teleconnection patterns (ENSO and NAM), we evaluated the composite differences between eight extreme phases of each mode (representing the lower and upper quartile of the year set). For the ENSO, we selected the eight highest intensity episodes from June to May. The selected years for El Niño were 1982–1983, 1986–1987, 1991–1992, 1994–1995, 1997–1998, 2002–2003, 2004–2005, and 2009–2010; for La Niña: 1984–1985, 1988–1989, 1995–1996, 1998–1999, 1999–2000, 2007–2008, 2010–2011, and 2011–2012. The ONI (Oceanic Niño Index) of Smith *et al.* [2008] was used as the ENSO index. To check the NAM modulation for the moisture sources, we used the Hurrell wintertime SLP-based Northern Annular Mode Index to calculate the composites for those years; higher values of the index were

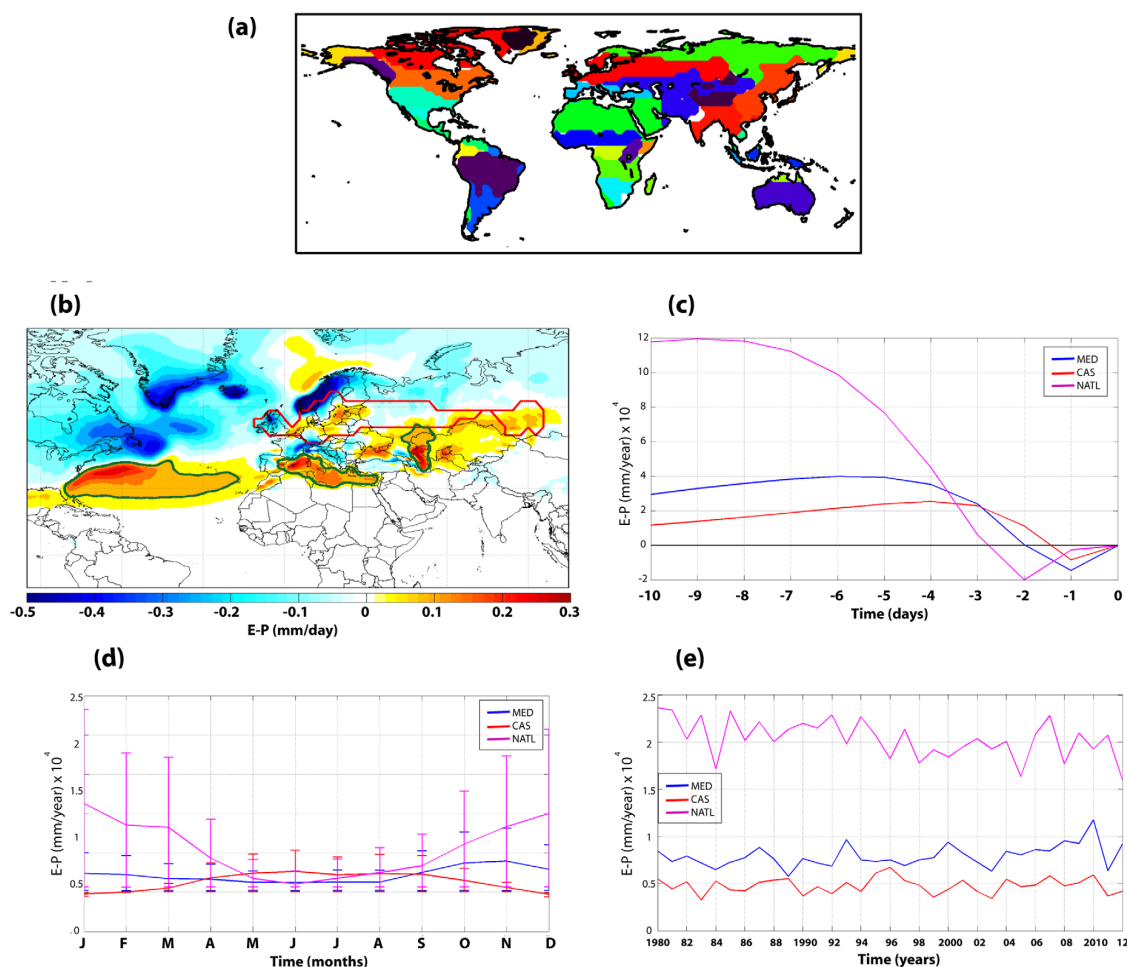


Figure 1. (a) Selected target continental climatic regions (CCRs) with homogenous future change in precipitation (MK regions). These regions were selected for having similar mean climate in terms of precipitation and similar projected changes. The 35 regions used in this study are an extension of the regions defined by Malstein and Knutti [2010] obtained by separating distant regions that belonged to the same original climatic region. (b) Annual average integrated values of $(E-P)_{1-10}$ for the first 10 days for 1980–2012. Units in mm/day. The red contour line indicates the Northern-Middle Europe/Western Asia (NMEU/WA) region of analysis, and the green lines show the main moisture sources for the target region defined by a threshold of 0.1 mm/day. (c) Annual time series of $(E-P)_n$ calculated backwards for moisture over the NMEU/WA region integrated over the moisture sources indicated in the left panel: North Atlantic (magenta line), Mediterranean (blue line), and the Caspian source (red line). (d) Averaged annual values of $(E-P)_{1-10}$ and bars of standard deviation ($\pm \sigma$) for the NMEU/WA CCR associated with its moisture sources: North Atlantic (magenta line), Mediterranean (blue line), and the Caspian source (red line). (e) Averaged annual values of $(E-P)_{1-10}$ values for the NMEU/WA CCR associated with its moisture sources: North Atlantic (magenta line), Mediterranean (blue line), and the Caspian source (red line).

seen in 1989, 1990, 1992, 1993, 2000, 2002, 2007, and 2008, and lower values in 1985, 1986, 1987, 1996, 2001, 2006, 2010, and 2011. The statistical significance of composite differences was tested by using a bootstrap method [Wei *et al.*, 2012] for the main mode of variability that affects the analyzed region, NAM in this case. Finally, we identified those oceanic regions with higher evaporation rates under a future climate change scenario [Seager *et al.*, 2010] that affect the region, following the results of Gimeno *et al.* [2013].

3. Description of the Catalog

The catalog contains an evaluation of sources of moisture for the 35 regions with similar projected changes in terms of precipitation over the surface of the globe [Malstein and Knutti, 2010], and the so-called 21 Giorgi regions [Giorgi and Francisco, 2000] widely used in the IPCC reports (Figure 1a and supporting information Figure S1a). The Northern-Middle Europe/Western Asia region (NMEU/WA) from the 35 MK regions classification and the Northern European region (NEU) from the 21 regions classification (marked in red in Figure 1b and supporting information Figure S1b) serves as an example to illustrate the catalog and its use. The catalog contains six items as summarized in Table 1.

Table 1. Summary of the Patterns Analyzed in the Catalog

Item	Concept	Approach	Temporal Scale	Patterns
Item 1	Identification of the moisture sources	Backward tracking for the target region	Annual and seasonal	$(E-P)_n$ and $(E-P)_{1-10}$
Item 2	Evaluation of the importance of the source throughout the 10 days of moisture transport	Backward tracking for the target region and integrated over the moisture sources areas.	Annual and seasonal	$(E-P)_n$ for each back-day over the limits defined for the moisture sources.
Item 3	Annual cycle of the contribution of the moisture sources to the precipitation on the target region	Backward tracking from target region	Annual	$(E-P)_n$ and $(E-P)_{1-10}$ budget over the limits defined for the moisture sources.
Item 4	Interannual/seasonal variability of the contribution of the moisture sources to the precipitation on the target region	Backward tracking from the target region	Annual and Annual Seasonal (DJF, MAM, JJA, and SON)	$(E-P)_n$ and $(E-P)_{1-10}$ budget over the limits defined for the moisture sources.
Item 5	Evaluation of the role of main teleconnection patterns	Backward tracking from the target region	ENSO: semiannual (ONDJFM and AMJJAS) NAM: boreal winter (DJFM) SAM: austral winter (ASON)	Modifications of the moisture source for the composites of eight extreme years of each mode
Item 6	Identification of hot areas in the region more influenced by future climate changes in evaporation	Forward tracking from hot spot source regions	Semiannual (ONDJFM and AMJJAS)	Areas with $(E-P)_{1-10} < -0.1$ mm/day over target region

3.1. Item 1: Identification of Moisture Sources on an Annual and Seasonal Basis

We calculated the annual/seasonal values of $(E-P)$ for all the days of transport. $(E-P)$ fields were calculated for each day, and labeled $(E-P)_n$, so e.g., $(E-P)_5$ shows where the air masses gained or lost moisture on the fifth day of transport; and averaged values of $(E-P)_{1-10}$ were obtained for the first 10 days of each trajectory. Figure 1b shows the annual averaged values of $(E-P)_{1-10}$ for the Northern-Middle Europe/Western Asia region (NMEU/WA CCR). The results could be interpreted thus: there are three main moisture source regions (reddish colors, $(E-P)_{1-10} > 0$) for the target area, namely the North Atlantic basin, the Mediterranean Sea, and the Caspian Sea. These main sources appeared also on a wet (from October to March, ONDJFM) and dry (from April to September, AMJJAS) seasonal basis (not shown here, but included in the catalog). Results for NEU region shown in supporting information Figure S1b.

3.2. Item 2: Evaluation of the Importance of the Source throughout the 10 Days of Moisture Transport

The method allows us to quantify the $(E-P)$ series for each day of the trajectory $(E-P)_n$, where n is the day of the back trajectory; e.g., $(E-P)_1$ is the $E-P$ field for the first day backwards in time, $(E-P)_2$ is for the second day, and so on). We can therefore calculate the $(E-P)_n$ annual, seasonal, and monthly series backward for the target region, integrated over the moisture source areas. The moisture source areas were limited by an objective threshold, here we used the 0.1 mm/day contour (green contours in Figure 1b). Figure 1c shows the annual values of $(E-P)_n$ for each back-day. The results indicate that the North Atlantic source dominates the uptake of moisture and is effective from 3 days back, although the Mediterranean and Caspian sources bring moisture from the second to the third day back. The same analysis for NEU region appears in supporting information Figures S1b and S1c. To check the sensitivity to other thresholds, we also used the 0.05, 0.15, and 0.2 mm/day contours for NMEU/WA region and the thresholds of 0.05 mm/day for NEU Giorgi region. Those results are shown in supporting information Figures S2, S3, and S4 for the NMEU/WA region and supporting information Figure S5 for NEU. It is highlighted that when a lower thresholds is used new sources of moisture appear (e.g. Norwegian Sea using 0.05 mm/day), and with higher (0.2 mm/day) values, the Mediterranean source disappear.

3.3. Item 3: Annual Cycle of the Contribution of the Moisture Sources to Precipitation in the Target Regions

The 33 years of data allow us to evaluate with some confidence the average monthly contribution of each moisture source to the precipitation for the NMEU/WA and NEU regions. The monthly mean values of the $(E-P)_n$ and $(E-P)_{1-10}$ terms for the detected moisture sources can be computed. Figure 1d shows the $(E-P)_{1-10}$ field for the three sources associated with the NMEU/WA CCR (supporting information Figure S1d for NEU

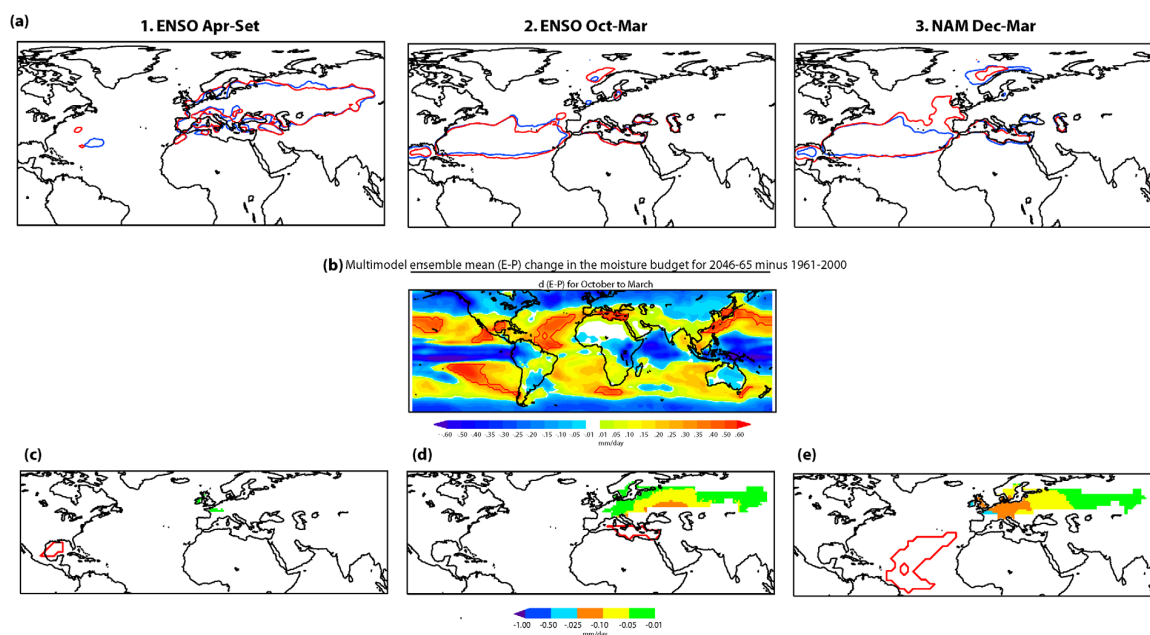


Figure 2. (a) Smoothed contour of 0.1 mm/day for $(E-P)_{1-10}$ for the Northern-Middle Europe/Western Asia (NMEU/WA) CCR for (1) April to September for El Niño composite (red) and La Niña composite (blue), (2) October to March for El Niño composite (red), and La Niña composite (blue), (3) December to March for high NAM year composite (red) and low NAM year composite (blue). (b) Multimodel ensemble mean $(E-P)$ change in moisture budget for 2046–65 minus that for 1961–2000 for October to March. Data provided by Richard Seager [Seager et al., 2010]. (c–e) $(E-P)$ values integrated over 10 days for October–March for the period 1980–2012 for the NMEU/WA region, calculated by forward tracking the FLEXPART model from the hot spot moisture source (indicated by the closed red line). Only those negative values less than -0.01 mm/day are plotted.

region). For example for the NMEU/WA, the North Atlantic source contribution peaks during the winter months, from October to March, while the Mediterranean source has its highest contribution only in October–November, and the Caspian source during the late spring to mid Autumn. The highest monthly variability is shown by the North Atlantic source during winter months, with some years deviating by as much as 25% of the long-term mean. In supporting information, we show the figures using all thresholds defined in Item 2.

3.4. Item 4: Interannual Variability of the Contribution of the Moisture Sources to the E-P in the Target Regions

The uptake of moisture from the evaporative sources changes in intensity over time. The method allows us to calculate the budget of $(E-P)_n$ and $(E-P)_{1-10}$ over the limits defined for the moisture sources for each year. The seasonal interannual variability can also be inferred. Figure 1e (supporting information Figure S1e) shows the results for the averaged integrated $(E-P)_{1-10}$ values over the sources of moisture for the NMEU/WA CCR (NEU region). It is possible to see strong interannual variability for all sources. To test the quantification of the variability, the standard deviation of $(E-P)_{1-10}$ values for each source was calculated (tables included in supporting information Tables S1 and S2). Figures and tables using all thresholds defined in Item 2 are shown in supporting information Tables S3–S6.

3.5. Item 5: Evaluation of the Role of Major Teleconnection Patterns

It is possible to estimate the modulation of the moisture transport from moisture sources to sink regions associated with the major teleconnection patterns. The catalog provides an analysis of the role of the ENSO, the NAM, and the SAM. For the example of the Northern-Middle Europe/Western Asia CCR, we analyzed the role of the ENSO as a global mode of atmospheric circulation, and of the NAM as a hemispheric one.

The first step in assessing whether the sources are affected by either of these modes is the computation of composites for the eight extreme years for each mode; after this, the different extents and contributions of the moisture sources can be evaluated. Because ENSO has a marked seasonality, we studied the semiannual period for El Niño and La Niña of October–March (boreal winter, Figure 2a.1) and April–September (boreal

summer, Figure 2a.2). The influence of the NAM was calculated for the boreal winter, defined from December to March (Figure 2a.3). Figure 2a shows the 0.1 mm/day contour for $(E-P)_{1-10}$ (the same value used to defined the moisture sources in Figure 1b) for their respective composites of variability modes and seasons. In Figures 2a.1 and 2a.2 (Figure 2a.3), the red lines correspond to El Niño (high NAM years) and the blue lines to La Niña (low NAM years). A latitudinal extension in winter during lower NAM years is observed; however, the sources of moisture are the same as in the climatology. ENSO appears to have no influence on the NMEU/WA moisture sources. The shift from ocean to land observed is due the seasonal behavior between boreal winter and summer in the transport of precipitable moisture. It is important to notice that we show here only results for one example region to illustrate the full catalog display. So, it is possible that much more different results occur for other climatic regions in which modes such as ENSO influences more. For the NEU region, see supporting information Figure S6.

Figures using other thresholds defined in Item 2 (supporting information Figures S7 and S8 for NMEU/WA CCR and NEU region, respectively) and the test that show the statistical significance of composite differences for NAM (supporting information Figure S9) are also shown in supporting information.

3.6. Item 6: Identification of Hot Areas in the Region That Will be Influenced More by Future Climate Changes in Evaporation

According to the climate models, some oceanic areas will in future show greater E-P. Those regions with an increase greater than 0.3 mm/day were defined by *Seager and Vecchi* [2010] as hot spot source regions (HSSRs). Its characterization was made by comparing the periods 2046–2065 and 1961–2000 for boreal winter and boreal summer as predicted by the 15 GCMs used in the AR4 assessment (red contours in Figure 2b). In a recent study, *Gimeno et al.* [2013] detected the potentially vulnerable continental areas that receive moisture from these HSSRs using the same Lagrangian method as that described herein and consequently could increment precipitation in the future due to an increment in the moisture transport from the HSSRs. Here, we select only those HSSRs that affect the Northern-Middle Europe/Western Asia target region during boreal Winter in terms of precipitation ($E-P < 0$, which would mean increased precipitation), following *Gimeno et al.* [2013] results. Three HSSRs affect precipitation in our example region, one in the middle of the Atlantic that affects the whole region (Figure 2d), another over the Caribbean that affects only a little area on the western part of the CCR (Figure 2c), and the Mediterranean HSSR, which affects the central and eastern part (Figure 2e). The same analysis was made for NEU region (supporting information Figure S6).

4. Future Directions and Use of the Catalog

The identification and characterization of moisture sources and its variability will be in the next years an important point for regional and global climatic assessments, including paleoclimatic reconstructions and future climate change scenarios. By performing a detailed analysis for a comprehensive number of climatic regions, this catalog will serve as a solid background for these studies. Additionally, this catalog provides a reliable and robust assessment of source-sink relationships in the atmospheric water cycle for regional climates which is a requirement for understanding the major driving factor for extreme weather and climate events.

Acknowledgments

The authors would like to thank the Spanish Government and FEDER, who contributed to this study via the TRAMO project.

References

- Bengtsson, L., S. Hagemann, and K. I. Hodges (2004), Can climate trends be calculated from reanalysis data?, *J. Geophys. Res. Atmos.*, *109*, D11111, doi:10.1029/2004JD004536.
- Brioude, J., et al. (2013), The Lagrangian particle dispersion model FLEXPART-WRF version 3.1, *Geosci. Model Dev.*, *6*, 1889–1904, doi:10.5194/gmd-6-1889-2013, 2013.
- Dee, D., et al. (2011), The ERA Interim reanalysis: Configuration and performance of the data assimilation system, *Q. J. R. Meteorol. Soc.*, *137*, 553–597, doi:10.1002/qj.828.
- Drumond, A., R. Nieto, and L. Gimeno (2011), Sources of moisture for China and their variations during drier and wetter conditions in 2000–2004: A Lagrangian approach, *Clim. Res.*, *50*, 215–225 doi:10.3354/cr01043.
- Gimeno, L., A. Drumond, R. Nieto, R. M. Trigo, and A. Stohl (2010), On the origin of continental precipitation, *Geophys. Res. Lett.*, *37*, L13804, doi:10.1029/2010GL043712.
- Gimeno, L., A. Stohl, R. M. Trigo, F. Dominguez, K. Yoshimura, L. Yu, A. Drumond, A. M. Durán-Quesada, and R. Nieto (2012), Oceanic and terrestrial sources of continental precipitation, *Rev. Geophys.*, *50*, RG4003, doi:10.1029/2012RG000389.
- Gimeno, L., R. Nieto, A. Drumond, R. Castillo, and R. M. Trigo (2013), Influence of the intensification of the major oceanic moisture sources on continental precipitation, *Geophys. Res. Lett.*, *40*, 1443–1450, doi:10.1002/grl.50338.

- Giorgi, F., and R. Francisco (2000), Uncertainties in regional climate change prediction: A regional analysis of ensemble simulations with the HADCM2 coupled AOGCM, *Clim. Dyn.*, **16**, 169–182.
- Held, I. M., and B. J. Soden (2006), Robust responses of the hydrological cycle to global warming, *J. Clim.*, **19**(21), 5686–5699, doi:10.1175/JCLI3990.1.
- Intergovernmental Panel on Climate Change (2007), Summary for policymakers, in *Climate Change 2007: The Physical Science Basis—Contribution of Working Group I to the Fourth Assessment Report of the Intergovernmental Panel on Climate Change*, edited by S. Solomon et al., pp. 1–18, Cambridge Univ. Press, Cambridge, U. K.
- Lorenz, C., and H. Kunstmann (2012), The hydrological cycle in three state-of-the-art reanalyses: Intercomparison and performance analysis, *J. Hydrometeorol.*, **13**, 1397–1420, doi:10.1175/jhm-d-11-088.1.
- Malstein, I., and R. Knutti (2010), Regional climate change patterns identified by cluster analysis, *Clim. Dyn.*, **35**, 587–600, doi:10.1007/s00382-009-0654-0.
- Mahlstein, I., R. W. Portmann, J. S. Daniel, S. Solomon, and R. Knutti (2012), Perceptible changes in regional precipitation in a future climate, *Geophys. Res. Lett.*, **39**, L05701, doi:10.1029/2011GL050738.
- National Center for Atmospheric Research Staff (Eds.), The Climate Data Guide: Hurrell wintertime SLP-based Northern Annular Mode (NAM) Index. [Available at: <https://climatedataguide.ucar.edu/es/guidance/hurrell-wintertime-slp-based-northern-annular-mode-nam-index>, last accessed 25 September 2012.]
- Nieto, R., L. Gimeno, and R. M. Trigo (2006), A Lagrangian identification of major sources of Sahel moisture, *Geophys. Res. Lett.*, **33**, L18707, doi:10.1029/2006GL027232.
- Nieto, R., D. Gallego, R. M. Trigo, P. Ribera, and L. Gimeno (2008), Dynamic identification of moisture sources in the Orinoco basin in equatorial South America, *Hydrol. Sci. J.*, **53**(3), 602–617.
- Numaguti, A. (1999), Origin and recycling processes of precipitating water over the Eurasian continent: Experiments using an atmospheric general circulation model, *J. Geophys. Res.*, **104**, 1957–1972, doi:10.1029/1998JD200026.
- Seager, R., and G. A. Vecchi, (2010), A. Climate change and water in southwestern North America special feature: Greenhouse warming and the 21st century hydroclimate of southwestern North America, *Proc. Natl. Acad. Sci., USA*, **107**, 21277–21282.
- Seager R., N. Naik, and G. A. Vecchi (2010), Thermodynamic and dynamic mechanisms for large-scale changes in the hydrological cycle in response to global warming, *J. Clim.*, **23**, 4651–4668.
- Smith, T. M., R. W. Reynolds, T. C. Peterson, and J. Lawrimore (2008), Improvements to NOAA's historical merged land-ocean surface temperature analysis (1880–2006), *J. Clim.*, **21**, 2283–2293.
- Stohl, A., and P. James (2004), A Lagrangian analysis of the atmospheric branch of the global water cycle: Part I. Method description, validation, and demonstration for the August 2002 flooding in central Europe, *J. Hydrometeorol.*, **5**(4), 656–678, doi:10.1175/1525-7541(2004)005<0656:ALAOTA>2.0.CO;2.
- Stohl, A., and P. James (2005), A Lagrangian analysis of the atmospheric branch of the global water cycle. II. Moisture transports between Earth's ocean basins and river catchments, *J. Hydrometeorol.*, **6**, 961–984.
- Stohl, A., C. Forster, A. Frank, P. Seibert, and G. Wotawa (2005), Technical Note: The Lagrangian particle dispersion model FLEXPART version 6.2. *Atmos. Chem. Phys.*, **5**, 2461–2474.
- Trenberth, K. E., J. T. Fasullo, and J. Mackaro (2011), Atmospheric moisture transports from ocean to land and global energy flows in reanalyses, *J. Clim.*, **24**(18), 4907–4924, doi:10.1175/2011jcli4171.1.
- Wei, J., P. A. Dirmeyer, M. G. Bosilovich, and R. Wu (2012), Water vapor sources for Yangtze River Valley rainfall: Climatology, variability, and implications for rainfall forecasting, *J. Geophys. Res.*, **117**, D05126, doi:10.1029/2011JD016902.
- Wentz, F. J., L. Ricciardulli, K. Hilburn, and C. Mears (2007), How much more rain will global warming bring?, *Science*, **317**, 233–235.

“Life is the art of drawing sufficient conclusions from insufficient premises”

Samuel Butler (1835-1902)
British Novelist

SECTION

5

Summary and Conclusions

Throughout this thesis, crucial aspects of the atmospheric branch of the hydrological cycle such as the characterization of the global sources of moisture, the interannual variability of the moisture transport, the distribution of continental precipitation from oceanic moisture source regions, and the role of the main teleconnection patterns (ENSO, NAM and SAM) in the variability of the moisture regions have been addressed. The study was based on a Lagrangian technique, which is the most suitable for evaluating the origin of the water that precipitates over continental area, and is a good alternative to the traditional Eulerian approach to studying processes within the water cycle. Moreover, this approach allowed the identification of the main moisture sources associated with continental climatic regions, providing a reliable and robust assessment of source-sink relationships in the atmospheric water cycle for regional climates, which is a requirement for understanding the major driving factors in extreme weather and climate events.

5. SUMMARY AND CONCLUSIONS

Following the sequence of publications presented in Section 4, the most important conclusions of these works are as follows:

(1) *The minimum temporal domain of the atmospheric moisture budget to account for the precipitation*

The search for answers to the scientific questions related to the distribution of continental precipitation arising from oceanic moisture source regions and related to the variability of the moisture sinks results in the need to separate net precipitation ($E - P < 0$) from net evaporation ($E - P > 0$) in the balance of the freshwater flux ($E - P$). For this reason, the behaviour of the averages and variances of the field ($E - P < 0$) (where precipitation is favoured) in the North Atlantic region were investigated under different schemes of analysis for winter and summer for the period 1980-2000. Five different schemes were used to eliminate the contributions ($E - P > 0$) before proceeding with the calculations of mean and variance of the complete period of analysis, accounting only for the precipitation term. An attempt was made to identify where the effect of the approach on the final results and the variance noise was minimal. In this thesis the results were assessed using a daily climate scale, to reveal the consistency of the results at monthly, seasonal and climatological scales.

The most important finding, as outlined below, was a confirmation of the consistency of the dataset, allowing the intraseasonal and interannual variability to be studied, because below these scales the signal was found to be rather noisy.

- The net evaporation term ($E - P > 0$) can be discounted after ($E - P$) has been integrated without altering the general patterns of net precipitation ($E - P < 0$), when the term ($E - P > 0$) is discounted month by month or where annual or climatological means are used, i.e., using a monthly or longer time scale.

This finding is essential to this thesis because throughout the characterization and study of the variability of the global sources of moisture it was vital to use data output at a time scale appropriate to the consistency of the results. At present, it is clear that if the contributions ($E - P > 0$) are eliminated at the end of the climatological calculation procedure, the same pattern is obtained as that obtained at a monthly or seasonal time scale (see Castillo et al., [2014a], Figures 3 and 4, pages 34-35 of this thesis). This outcome allowed the analysis to be made month by month, at seasonal or climatological

scales, as in the studies referred to in this thesis: Gimeno et al. (2013) used a seasonal scale, Castillo et al. (2014b) carried out an analysis of the annual cycle month by month and then used a climatological scale, Nieto et al. (2014a) undertook a semiannual cycle analysis month by month, and Nieto et al. (2014b) used climatological and seasonal scales within this type of estimation.

(2) Quantification of the contribution of the major oceanic moisture source regions to continental precipitation

First, the analysis was extended to 21 years of data (1980-2000), using the FLEXPART model tuned to a higher precision approach in forward trajectory mode to detect the continental sink regions for the 12 major oceanic moisture sources (Figure 3.1) for both boreal summer (JJA) and winter (DJF). The use of FLEXPART for the climatological assessment of oceanic and continental moisture source areas has been shown to be consistent at the regional and global scales (Gimeno et al., 2012). This assessment allows the re-evaluation of the results obtained by Gimeno et al. (2010a) and provides a more robust identification of all the major oceanic moisture sources.

The results show that the supply of oceanic moisture to the continents is highly asymmetrical and specific to each oceanic basin and season. The most important outcomes related to the contribution of the major oceanic moisture source regions to continental precipitation are listed below.

- In terms of influence on continental precipitation, the northern Atlantic subtropical ocean is the dominant source, providing moisture for precipitation over vast areas, especially during DJF when its influence extends from Mexico to parts of Eurasia and from the Eurasian Arctic to the Amazon.
- The influence of the Atlantic on the Central and South American continent is related to the very efficient low-level jet systems associated with the Caribbean low-level jet, the South American low-level jet, and the Choco jet that controls precipitation (mainly in DJF) over central America, tropical and Subtropical South America east of the Andes, and the tropical Pacific coast of South America, respectively. However, its influence on Europe vanishes during the summer.

5. SUMMARY AND CONCLUSIONS

- The major oceanic sources do not contribute directly to precipitation over vast continental areas (including most arid inland regions), although they can contribute through subsequent local moisture recycling.
- A few small oceanic sources provide disproportionate amounts of moisture relative to their size. For instance, the Mediterranean is a dominant source of moisture for Europe and northern Africa during JJA, and the Red Sea provides large quantities of moisture that precipitate between the Gulf of Guinea and Indochina during JJA and between the African Great Lakes and Asia during DJF.
- There is significant interhemispheric transport, with implications for continental precipitation, from the North Atlantic source during DJF and from western Indian sources during JJA.
- Vast areas, including Europe, South America, and Australia, mainly receive moisture from a single source; the monsoonal regimes in India, tropical Africa, and the quasi-monsoonal regime of North American Great Plains are fed by moisture from multiple source regions.

It is acknowledged that not all the precipitation falling over the continents originates from within these major oceanic source areas, and a fraction may have its origins in negative ($E - P$) regions observed over the extratropical Oceans and in local recycling (Gimeno et al., 2012). For this reason the role played by the nonsource areas was evaluated, by computing the moisture contribution that evaporates from all the oceanic areas that were not considered in the analysis (the white oceanic areas in Figure 3.1), and it was concluded that their contribution is restricted to a narrow tropical strip and two large high latitudinal bands, being moderately relevant in boreal winter over northern Europe and in patches over the North American continent (Figure B.1).

(3) Intensification of the major oceanic source regions and its contributions to continental precipitation

One of the major aims of this study was to evaluate the effect of changes in intensity of the sources in the distribution of continental precipitation linked to each source. Moisture source regions are nonstationary, varying in intensity from year to year and expected to change in the future. The longer dataset (1980-2000) employed here made it possible to perform a sensitivity analysis on the influence of source intensity (periods with enhanced or reduced $E - P$) on the transport of moisture from the net evaporating oceanic regions to the net precipitating continental ones, an analysis that was not possible in Gimeno et al. (2010a). Differences in $(E - P)$ between the average of the five highest and lowest intensity episodes were obtained for each source during winter DJF and summer JJA (Figure 1 of Gimeno et al. [2013], page 43 of this thesis). The most important results of the assessment of the recent changes in amplitude of the sources are summarized below.

- In both seasons precipitation tends to increase along the tropical band when the source intensifies.
- The subtropical oceanic sources contribute more to increases in precipitation in the central and western parts of the corresponding basin, while the intensification observed in the eastern tropical Pacific is due to moisture transported from the Caribbean source.
- The increase in precipitation associated with more intense monsoon circulations is evident during DJF for the South American monsoon (from the North Atlantic source), confirming the role of cross-equatorial moisture transport during intense monsoon events over the Amazon basin.
- The role of the enhanced transport of moisture from the Arabian Sea in the intensification of the rainfall associated with the Asian and Indian summer monsoons is apparent.
- Stronger than usual North American monsoon systems during JJA also rely on enhanced moisture availability from the Caribbean source.

5. SUMMARY AND CONCLUSIONS

- This insensitivity of precipitation at higher latitudinal bands (particularly over the continents) to changes in moisture source intensity suggests that the main process responsible for the expected intensification of precipitation at these latitudes is dynamic.

(4) *The oceanic moisture source regions of continental precipitation linked to climate change*

Climate change is likely to have effects far beyond changes in evaporation minus precipitation. It is clear that changes in atmospheric circulation in a warming climate will result in changes in circulation between source and sink, which will redirect moisture in a number of different ways. The identification of areas prone to significant changes in $(E - P)$ over the next few decades was derived using a multimodel ensemble of GCMs that allowed delimiting those oceanic areas where climate change will probably lead to an increase in the freshwater flux. Those areas with modelled increases in $(E - P)$ of greater than 0.3 mm/day for the periods 2046–2065 compared with 1961–2000 are shown as hot spot source regions (HSSRs), as predicted by 15 GCMs used in the AR4 assessment, for boreal winter and boreal summer half-years (Seager et al., 2010). The same Lagrangian approach was applied as for the present climate data (1980–2000) to identify those potentially vulnerable continental regions that receive moisture from the HSSRs for both boreal-season half-years.

The areas affected by these highly sensitive HSSRs are often spread over the oceans (Figures 2 and 3 of Gimeno et al. [2013] and pages 45-46 of this thesis). However, those HSSRs that do have an impact over specific continents have also been identified, including highly populated areas such as Central and North America, Europe, and Gulf of Guinea that are currently under water stress and could become less prone to disruption of their water resources under climate change. The most relevant findings associated with these oceanic areas linked to climate change are described below.

- Two HSSRs have the widest influence: one in the central North Atlantic that influences precipitation over Europe and South America, and the other in the subtropical western North Pacific that influences precipitation over North America and the Southeast Asian continent.

-
- The small Mediterranean HSSR has a strong influence on European precipitation; nevertheless, this influence can soften the expected combined impact of climate change in southern Europe.
 - North America is the most affected continental region, being directly influenced by four different HSSRs: the Caribbean, the tropical Mexican coastal Pacific, the subtropical western North Pacific, and the central North Atlantic.
 - The two HSSRs located in the Indian Ocean have a moderate effect on the surrounding continental areas: the HSSR to the south of the Bay of Bengal influences the Malaysian Peninsula, while the HSSR close to the Agulhas Current provides moisture for the East African coast and the Indian subcontinent.
 - The Pacific HSSR located to the east of Australia affects the eastern half of the continent.

(5) The role of the main global teleconnection patterns in the transport of moisture

The strongest natural fluctuation of climate that occurs on interannual timescales is the El Niño-Southern Oscillation (ENSO). It is an inherently coupled atmosphere-ocean mode with its core activity in the tropical Pacific, but with important regional climate impacts throughout the world. The annular modes are hemispheric-scale patterns of climate variability and owe their existence to internal atmospheric dynamics in the middle latitudes. There are two annular modes in the atmosphere: the Northern Annular Mode (NAM) and the Southern Annular Mode (SAM), and these are the most important patterns of climate variability in the Northern and Southern Hemisphere middle and high latitudes.

There is an increasing realization that natural circulation patterns, such as ENSO, NAM and SAM, play a fundamental role in global climate and its interannual and longer-term variability. Also the changing patterns of circulation will lead to significant regional changes in the moisture budget.

Previous studies have characterized the general pattern of moisture transport from a climatological perspective; however, no analysis of the variability of the major oceanic moisture sources (Figure 3.1) due the main global teleconnection modes (ENSO, NAM and SAM) has yet been undertaken. In consequence, the indices of these main modes

5. SUMMARY AND CONCLUSIONS

of climate variability were used in a monthly composite analysis to determine the principal influences of these modes in the global transport of moisture and the associated precipitation.

To understand the moisture transport rather better, the major oceanic sources of moisture were recalculated using the vertically integrated moisture flux divergence for a new extended period of 33 years (1980-2012) using the available ERA-Interim reanalysis data and the results were compared with the sources defined in Gimeno et al. (2010a), showing small differences that were not significant. The sink regions associated with the major oceanic sources were then summarized for first time in a monthly schematic representation for the newly available climatological period (Figure 2 of Castillo et al. [2014b] and page 52 of this thesis) using the FLEXPART model on a forwards-in-time basis. This allowed the identification of the ways in which oceans contribute to the moisture budget of the major global precipitation systems throughout the year. The remainder of the oceanic areas not considered in Figure 3.1 (in white) were also re-evaluated using this climatological dataset, revealing their influence on precipitation to be mainly restricted to a narrow tropical strip and two large high-latitude bands (Figure B.5).

In view of the monthly variability of the favoured sink regions associated with each oceanic source, the role of the main global teleconnection patterns in the moisture transport were then analyzed. The most relevant findings linked to each mode of variability are as follows:

El Niño-Southern Oscillation (ENSO)

The influence of the evolution of the ENSO cycle on the moisture transport from the major oceanic moisture sources is investigated using monthly composite differences between the eight highest intensity episodes for El Niño (positive phase) and for La Niña (negative phase) from June to May. The composites of the 8 years were computed using the FLEXPART model fed by the ERA-Interim dataset for the period 1980-2012. The results suggest that when the sources of moisture defined for the climatological period are remained stationary (Figure 3.1), there are significant differences between the two phases as outlined below.

- In general terms, the variations in the moisture sinks associated with the evaporative sources coincide with the known patterns of variation of the vertically inte-

grated moisture transport associated with large-scale atmospheric systems throughout ENSO cycles. Such variations include those observed over equatorial Pacific rainfall, the major summer monsoon systems, and subtropical rainfall.

- During the mature stage of ENSO (DJF) contributions from SPAC, NPAC, MEXCAR, and CORALS to the equatorial Pacific are enhanced for El Niño years, while IND, NPAC, and SPAC contribute more to the western equatorial Pacific during La Niña. This pattern reproduces the known “see-saw” characteristic associated with ENSO over this region.
- The subtropical areas receive more moisture from nearby sources during El Niño, for example southern North America from NATL and MEXCAR, South America from SATL and SPAC, or southern Africa from IND, AGU, and ZAN.
- The Indian Monsoon regime exhibits an inhibition of convergence associated with a lack of moisture uptake from its typical (own) sources during El Niño episodes. However, from June to November the region is a preferred sink for moisture from IND, ZAN, and ARAB during La Niña, and convergence is favoured.

When the source areas are redefined according to the ENSO phase, most remain stationary, but four of them show notable differences in their extent. Two are more involved in the region of ENSO occurrence: SPAC and CORALS in the Pacific Ocean, and the others are MEXCAR in the Atlantic Ocean and ARAB in Indian Ocean. A Lagrangian sensitivity analysis performed for these four sources considering the new areas defined according to the ENSO composites of the vertically integrated moisture transport divergence suggest some changes related to the results as far as the stationary sources are concerned. These findings are as follows.

- The reduction in the SPAC source in size during El Niño events implies less moisture transport toward Indonesia compared with the moisture transport from the stationary SPAC source.
- The reduction in CORALS during La Niña and the confinement of its transport towards the western Pacific is not captured when the stationary CORALS source is considered; this extends its influence toward Indonesia and the Central Pacific.

5. SUMMARY AND CONCLUSIONS

- The northward displacement of MEXCAR observed during La Niña and the associated reduction in the moisture transport towards the Pacific ITCZ during this phase is not evident in the results obtained when only the stationary source is considered.
- The expansion of ARAB toward the eastern African coast during La Niña associated with enhanced moisture transport towards the Indian Ocean, particularly during DJFM, was not reproduced in the results for the stationary source.

Northern Annular Mode (NAM)

The fingerprint of the NAM in the moisture transport from the main oceanic sources of moisture was considered in order to assess their impact using monthly composite differences for the corresponding semiannual cycle from November to April between the six highest intensity episodes for both NAM phases. The composites of 6 years were estimated using the FLEXPART model informed by the ERA-Interim dataset for the period from November 1979 to April 2012. It must be stressed that in the outcomes outlined below it is assumed that the boundaries of each oceanic source (Figure 3.1) remained stationary throughout the years considered.

- In respect of the NPAC source in the northern Pacific Ocean, it is interesting to note the enhanced moisture transport towards the northeastern basin for lower values of NAM Index associated with the weakening of the Pacific high pressure centre and weak westerlies over the polar latitudes. Under these conditions, the storm tracks tend towards tropical latitudes, affecting the northwestern part of North America.
- For higher values of the NAM Index, the Pacific high pressure centre is expected to intensify, and moisture transport from NPAC is favoured towards eastern Asia. The East Asian Monsoon characterizes the major moisture pattern for the region, but although the East Asian Monsoon is not favoured during winter there nevertheless exists a significant interaction with the Siberian High, which is modulated in its intensity by the NAM. So, the NAM plays an important role in the changes of the Siberian High, via a positive correlation in which a lower NAMI is related to a lower intensity of the Siberian High. This in turn favours the influx of moisture from the ocean.

-
- Over the North Atlantic Ocean the years with lower values of NAMI are characterized by lower than normal atmospheric pressures and weak westerlies over northern Europe. Enhanced moisture transport from the NATL, MEXCAR, and MED sources towards southern Europe and the Mediterranean basin therefore occurs; the reverse applies for a high NAM Index, when the transport is northwards over Europe and when droughts can occur over the southern part of the continent.
 - The intensification of the Atlantic high pressure centre during higher NAM years, and the associated easterly trade winds at its southern flank, occur with enhanced moisture transport from the NATL and MEXCAR sources towards the Caribbean Sea. The flow is thus intensified, forming the Caribbean Low Level Jet (CLLJ) that splits into two branches, one proceeding westwards across Central America, and the other turning northwards to North America crossing the Gulf of Mexico. This result accords with the variability of the CLLJ and the characteristics of the moisture transport patterns over the area. A higher (lower) NAM is therefore associated with a reinforcing (weakening) of transport from NATL and MEXCAR to Central and North America throughout the CLLJ.
 - The intensification or weakening of the Atlantic High pressure system could be also related to the interannual variability found for the MED and NATL sources when the vertically integrated moisture divergence was analyzed.
 - Because the centres of activity of the NAM lie principally over the larger basin oceans and around mid and higher latitudes in the northern hemisphere, the REDS and ARAB sources seem relatively unaffected by the different phases of the mode.

Southern Annular Mode (SAM)

The impact of the Southern hemisphere annular mode on the moisture transport from the major oceanic moisture sources was also investigated using the Lagragian FLEX-PART model fed by the ERA-Interim reanalysis data for the period from May 1980 to October 2012. Monthly composite differences were calculated for the corresponding semiannual cycle from May to October between the six highest intensity episodes for both SAM phases. In the same way as for the Northern Annular Mode, in the findings listed below it was assumed that the boundaries of each oceanic source (Figure 3.1) were stationary throughout the 33-year period considered.

5. SUMMARY AND CONCLUSIONS

- During higher values of SAM Index, when high-pressure systems are stronger than normal, the belt of westerlies and the trade winds intensify, the ITCZ is positioned to the north, and the pattern for the transport of moisture is, in general, as described.
- Moisture is transported southwards and eastwards from the AGU, IND, and SATL sources more during the positive phase of SAM. Thus, in the Indian Ocean a horizontal band of precipitation over the southern basin appears with moisture that originates from the AGU source, and small sections of IND behave in the same way.
- The pattern shown here represents the wet conditions of the early austral spring quite well, when an enhanced uptake of moisture occurs from CORALS.
- The higher values for the SAM mode were also characterized by an enhanced transport over the Indian Ocean/West Pacific Warm Pool, with the area receiving a higher moisture contribution from the CORALS and SPAC sources.
- The higher pressures configured around Australia move the moisture northwards from CORALS, and then the trade winds advect it westwards, with more intensity during higher SAM events.
- The intensified trade winds bring moisture toward the region from the SPAC, which disappears for lower values of SAM Index when the trade winds are less intense.
- Over the South Atlantic Ocean the intensified high pressure maintains the flow of moisture both to the Southern Atlantic Convergence Zone (SACZ) and to the ITCZ from the SATL source. It can be seen that during the early months the intensified trade winds introduce moisture to the inland parts of the continent (this signal is also recognizable in the Pacific, but only over the islands) and the SACZ receives more moisture during the later months.
- The results indicate that southeastern South America receives more moisture from the SATL, AGU, and SPAC sources during years with a lower SAM Index. There is some support for the finding that for lower values of SAMI the cyclone trajectories move northwards, and South America suffers from intense frontogenetic

activity associated with positive anomalies of precipitation over the southeastern part of the continent.

- The weakness of the westerlies and trade winds for lower values of SAM Index favours the influx of moisture from SATL during the monsoon in Africa.
- The variation of ZAN with SAM does not seem relevant, perhaps due the fact that it is positioned on the equator.

(6) Moisture sources for continental climatic regions

It can be seen that a good knowledge of the transport of moisture from the sources in the different oceans to the continents is of great importance, and a robust identification of those regions particularly vulnerable to any changes in the hydrological cycle is therefore essential. This entails the description of both the locations of regions with similar projected changes in terms of precipitation and the identification of their moisture sources. To this end, a catalogue of moisture sources was created to evaluate two sets of continental climatic regions, the MKRs (Figure 3.4) based on homogenous future change defined by Mahlstein and Knutti (2010) and the GRs (Figure 3.5) based on homogenous current climate and established by Giorgi and Francisco (2000).

The catalogue is freely available at <http://ephyslab.uvigo.es/tramo/ccrs/> and contains six items that may be used to interpret current and future climate changes in regional precipitation patterns. These are:

- (i) Identification of moisture sources on an annual and seasonal basis using backward tracking for the target region. The annual/seasonal values of $(E - P)$ for each day $(E - P)_n$ and for 10 days $(E - P)_{1-10}$ of transport were calculated.
- (ii) Evaluation of the importance of each source throughout the 10 days of moisture transport. The $(E - P)$ series for each day (n) of the trajectory were quantified as $(E - P)_n$, using a backward tracking for the target region integrated over the moisture source areas.
- (iii) Annual cycle of the contributions of the moisture sources to precipitation in the target regions. The $(E - P)$ series for the average monthly contribution of each moisture source were quantified.

5. SUMMARY AND CONCLUSIONS

- (iv) Interannual variability of the contributions of the moisture sources to $(E - P)$ in the target regions. The method allows the calculation of the budget of $(E - P)$ over the limits defined for the moisture sources for each year.
- (v) Evaluation of the role of the major teleconnection patterns. The catalogue provides an analysis of the role of the three dominant modes of global climate variability, including the El Niño-Southern Oscillation (ENSO) and the Northern and Southern Annular Modes (NAM, SAM). This enables the assessment of the modifications of the moisture sources for the composites of eight extreme years for each mode.
- (vi) Identification of any hot areas in the region that will be influenced more by future climate change in terms of evaporation minus precipitation. Only those HSSRs that affect each target region were selected in order to detect the potentially vulnerable continental areas that receive moisture from these HSSRs using a Lagrangian method following Gimeno et al. (2013), which forms part of this thesis.

Finally, the identification and characterization of moisture sources and their variability will in the next years form an important starting point for regional and global climatic assessments, including paleoclimatic reconstructions and future climate change scenarios. By performing a detailed analysis for a comprehensive number of climatic regions, this catalogue will serve as a solid source of information for these studies.



Further details of FLEXPART

A.1 Brief Review

FLEXPART (“FLEXible PARTicle dispersion model”) is a Lagrangian transport and dispersion model suitable for the simulation of a large range of atmospheric transport processes. Applications range from the dispersion of radionuclides or air pollutants, to the establishment of flow climatologies, and to the analysis of Earth’s water cycle. FLEXPART also produces output suitable for the inverse determination of emission sources, e.g., of greenhouse gases or volcanic ash.

FLEXPART is a more advanced version of its predecessor FLEXTRA (“FLEXible TRAjectory model”). Both FLEXTRA and FLEXPART have been ‘open source’ since their inception, and over time have attracted a large international user community. In addition to the reference version of FLEXPART, which uses as input meteorological reanalysis data from European Centre for Medium-Range Weather Forecast (ECMWF), the Global Forecast System (GFS) or the National Centers for Environmental Prediction (NCEP), several branches of FLEXPART have been developed, which can be run with meteorological data from mesoscale models, such as the Consortium for Small-scale Modeling (COSMO), the Weather Research and Forecasting (WRF) and the PSU/N-CAR numerical model (known as MM5).

A. FURTHER DETAILS OF FLEXPART

FLEXPART is a widely used Lagrangian Particle Dispersion Model (LPDM) developed by Andreas Stohl and co-workers. Dr Stohl now works in the Department of Atmospheric and Climate Research at the Norwegian Institute for Air Research. FLEXPART was originally (about 17 years ago) designed for calculating the long-range and mesoscale dispersion of air pollutants from point sources, such as after an accident in a nuclear power plant. In the mean time FLEXPART has evolved into a comprehensive tool for atmospheric transport modelling and analysis. Its fields of application have extended from air pollution studies to other areas where atmospheric transport plays a role (e.g., exchange between the stratosphere and troposphere, or the global water cycle).

The management of input data was largely taken from FLEXTRA, a kinematic trajectory model (Stohl et al., 1995). The original version of FLEXPART was developed at the nuclear-biological-chemical school of the Austrian Forces, and the deposition code was added later (version 2); this version was validated using data from three large tracer experiments (Stohl et al., 1998). Version 3 saw performance optimizations and the development of a density correction (Stohl and Thomson, 1999). Further updates included the addition of a convection scheme (Seibert, 2001) (version 4), better backward calculation capabilities (Seibert and Frank, 2004), and improvements in input/output handling (version 5). Version 5 also incorporated the special development of FLEXPART in order to extend its forecasting capabilities (Stohl et al., 2004).

Further information can be found in the model technical note of version 6.2 (Stohl et al., 2005) and all the details of the upgrades to versions 8.0 and 9.0 used in this research are available on the FLEXPART homepage (<http://flexpart.eu>).

A.2 Model Computing Aspects

FLEXPART is coded following the Fortran 77 standard and tested with several compilers (GNU, Absoft, Portland Group) under a number of operating systems (Linux, Solaris, etc). The code has been carefully documented and optimized for run-time performance. No attempts have been made to parallelize the code because the model is strictly linear, and it is therefore more effective for partitioned problems, and as such it is better run on a single processor. Results can subsequently be combined if needed.

Other users have developed FLEXPART versions using input data from a suite of different global (e.g., from NCEP) and mesoscale (e.g. MM5 and WRF) models.

FLEXPART is an off-line model that uses meteorological fields (analyses or forecasts) in Gridded Binary (GRIB) format from the European Centre for Medium-Range Weather Forecast numerical weather prediction model (Persson and Grazzini, 2007) on a latitude/longitude grid and using native ECMWF model levels as input.

The main general advantage of Lagrangian models is that, unlike in Eulerian models, there is no numerical diffusion. Furthermore, in Eulerian models a tracer released from a point source is instantaneously mixed within a grid box, whereas Lagrangian models are independent of any computational grids and have, in principle, an infinitesimally fine resolution.

A.3 Model Physical Aspects

FLEXPART needs five three-dimensional fields: horizontal and vertical wind components, temperature and specific humidity. Input data must be on ECMWF model (i.e., η) levels, which are defined by a hybrid coordinate system.

FLEXPART also needs the two-dimensional fields: surface pressure, total cloud cover, 10 m horizontal wind components, 2 m temperature and dew point temperature, large scale and convective precipitation, sensible heat flux, east/west and north/south surface stress, topography, land-sea-mask, and subgrid standard deviation of topography.

FLEXPART also contains large amounts of parameterization such as for the boundary layer, turbulent motions, wind fluctuations, mesoscale velocity fluctuations, moist convection, and others.

FLEXPART stores several variables at every output time step (see Table A.1).

A.3.1 Forward and backward modeling

Normally, when FLEXPART is run forwards in time, particles are released from one or a number of sources, and concentrations are determined downwind on a grid. However, FLEXPART can also be run backwards in time, which is more efficient than forward modelling for calculating source-receptor relationships if the number of receptors is smaller than the number of (potential) sources. In the backward mode, particles are released from a receptor location (e.g., a measurement site) and a four-dimensional

A. FURTHER DETAILS OF FLEXPART

(3 space dimensions plus time) response function (sensitivity) to emission input is calculated. A fuller description of this aspect may be found in Seibert and Frank (2004).

Table A.1: Output variables of the LPDM FLEXPART.

Variable	Symbol	Units
Latitude	lat	°
Longitude	lon	°
Height	H	m
Topography Height	TH	m
Potential Vorticity	PV	$10^{-6}(\text{m}^2\text{K/sKg})$
Specific Humidity	q	g/Kg
Air Density	ρ_{air}	Kg/m ³
Mixing Height	H_{mixi}	m
Temperature	T	K

Supporting Results

B.1 Influence of the intensification of the major oceanic moisture sources on continental precipitation

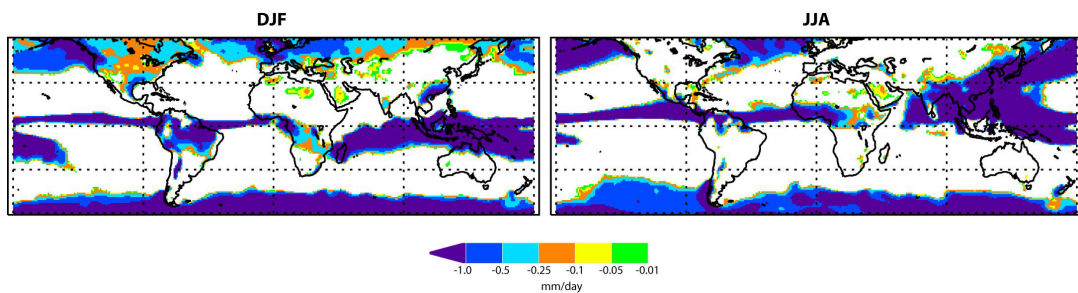


Figure B.1: Values of $(E - P)$ integrated over 10 days for the period 1980-2000, calculated by forward tracking from the oceanic regions but excluding the moisture sources indicated in Figure 3.1. Only negative values less than -0.01 mm/day are plotted ($E - P < -0.01$ mm/day). The left and right columns are for the periods DJF and JJA, respectively.

B. SUPPORTING RESULTS

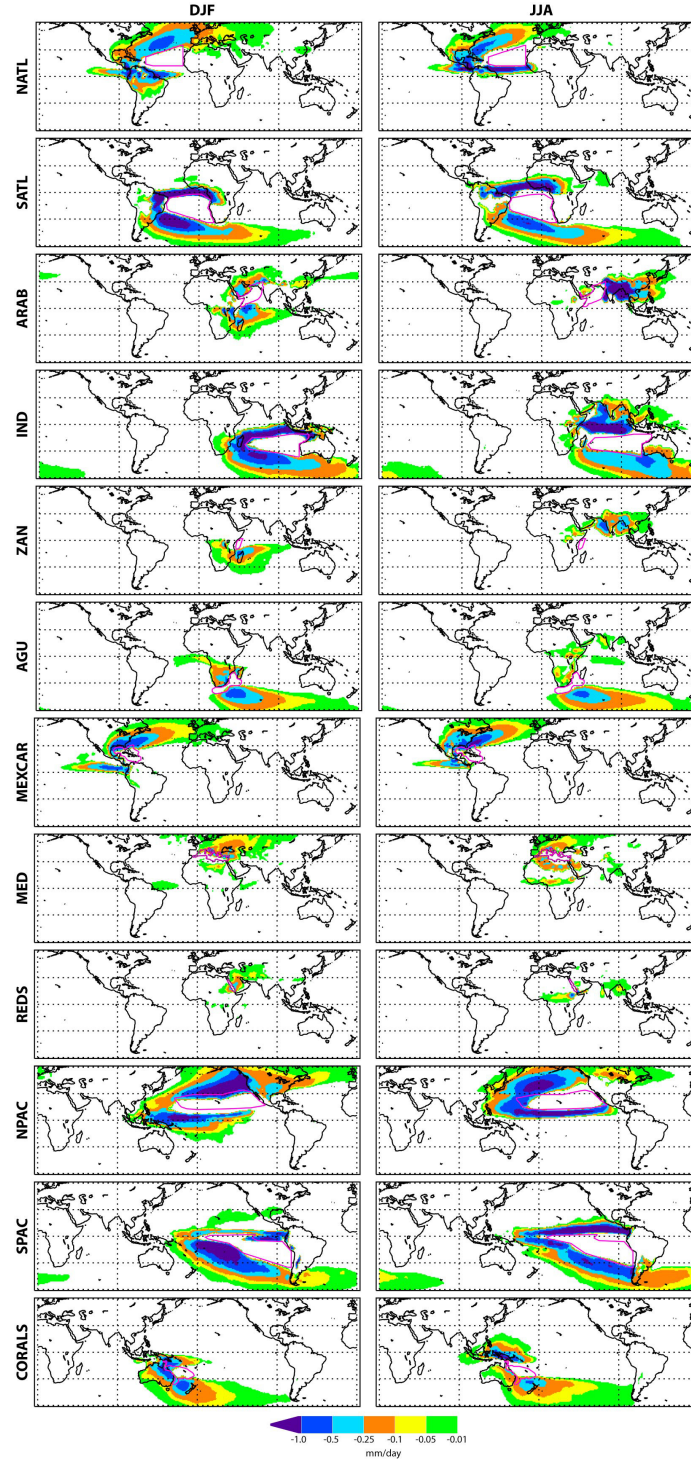


Figure B.2: Values of $(E - P)$ integrated over 10 days for the period 1980-2000, calculated by forward tracking from the oceanic moisture sources indicated by the closed pink lines and identified by their acronym. Only negative values less than -0.01 mm/day are plotted ($E - P < -0.01$ mm/day). The left and right columns are for DJF and JJA, respectively.

B.1 Influence of the intensification of the major oceanic moisture sources on continental precipitation

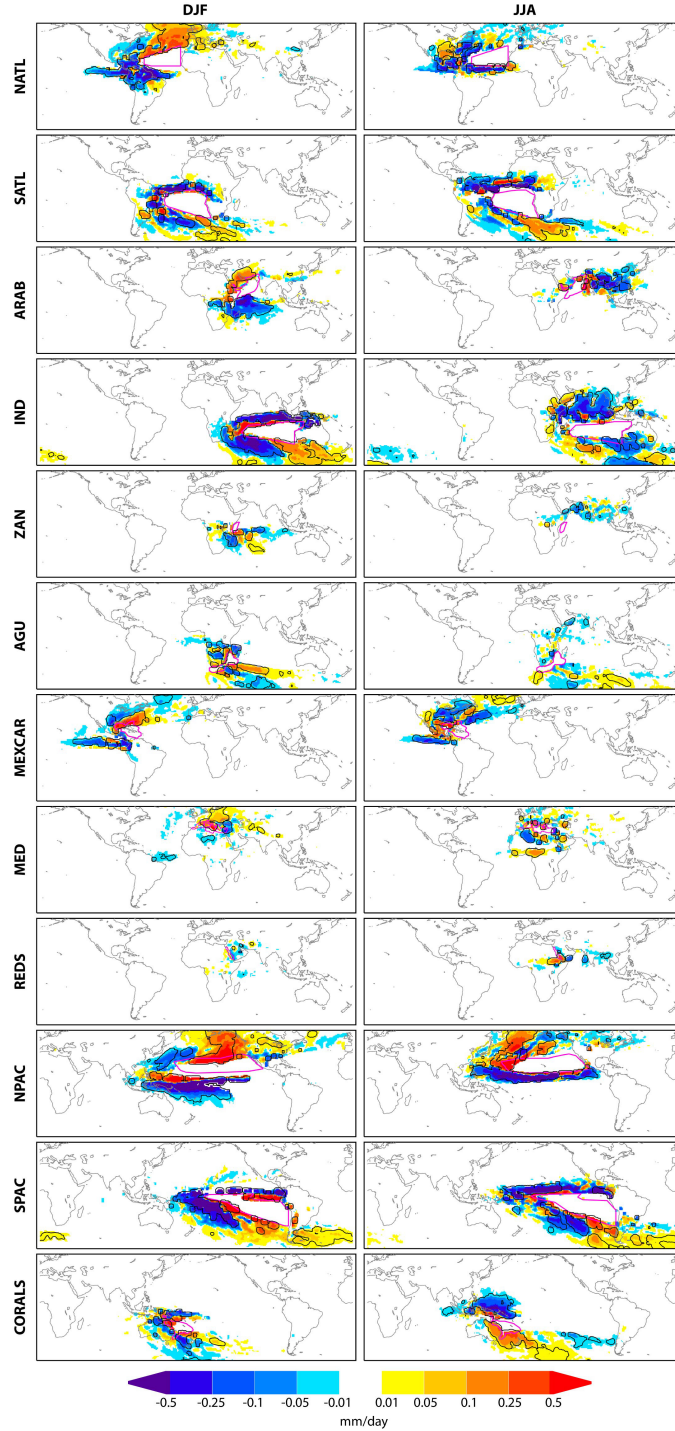


Figure B.3: The composite differences in $(E - P)$ between the average of the five highest source intensity periods and the average of the five lowest intensity periods for DJF (left panels) and JJA (right panels). Each moisture source is shown on a separate pair of panels. The black contour lines indicate areas where absolute values of the differences greater than 0.01 mm/day are significant at the 90% confidence level, according to a bootstrap test that permutes the original time series 1000 times.

B. SUPPORTING RESULTS

B.2 The role of the ENSO cycle in the modulation of moisture transport from major oceanic moisture sources

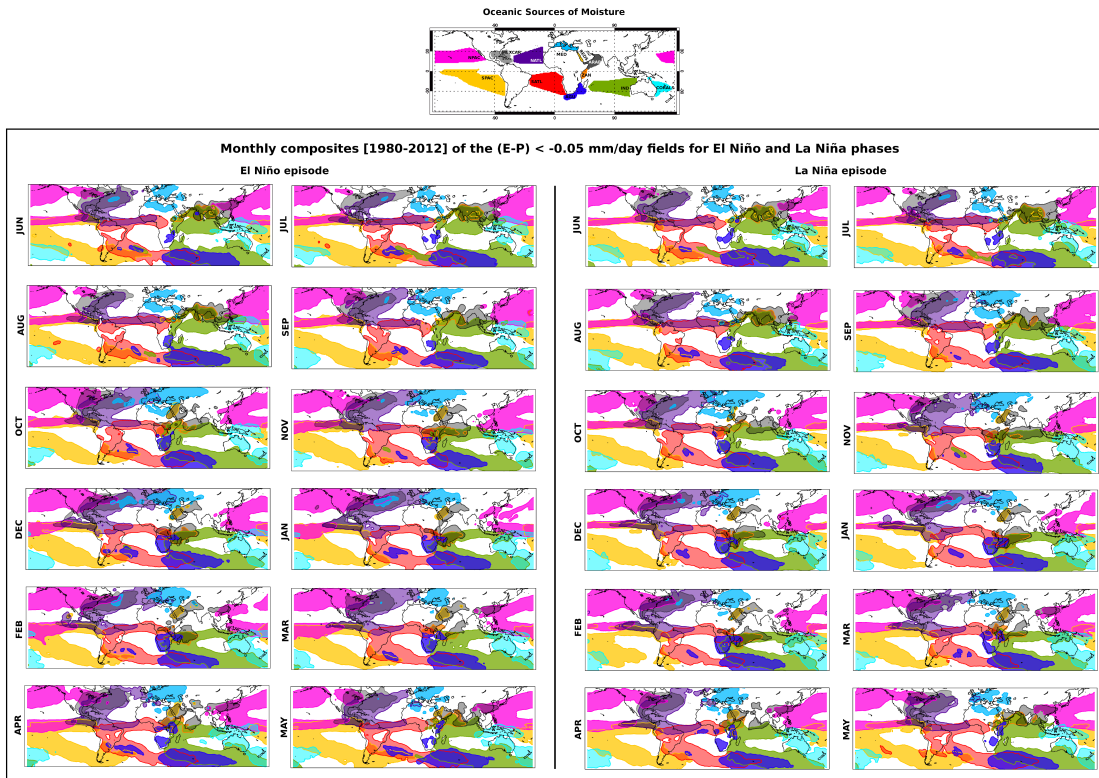


Figure B.4: Monthly composites of moisture sink areas detected for the ENSO phases for 1980-2012. The sources of moisture (bottom maps) are those detected in Figure 3.1. Only negative values of $(E - P)$ calculated by forward tracking from defined moisture sources greater than -0.05 mm/day are plotted for (left) El Niño episode and (right) La Niña phase.

B.2 The role of the ENSO cycle in the modulation of moisture transport from major oceanic moisture sources

E-P for Non-Principal oceanic sources of moisture [1980-2012]

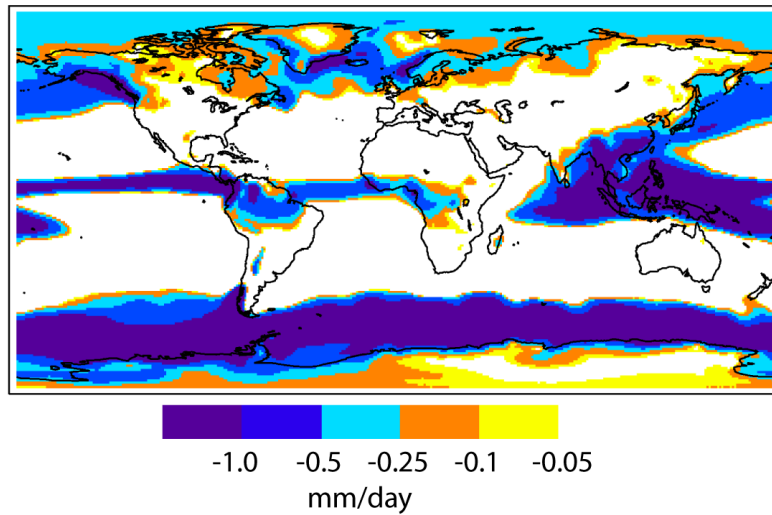


Figure B.5: Climatology values of $(E - P)$ integrated over 10 days for the period 1980-2012, calculated by forward tracking from the oceanic regions but excluding the moisture sources indicated in Figure 3.1. Only negative values less than -0.05 mm/day are plotted ($E - P < -0.05$ mm/day).

B. SUPPORTING RESULTS

B.3 A catalog of moisture sources for continental climatic regions

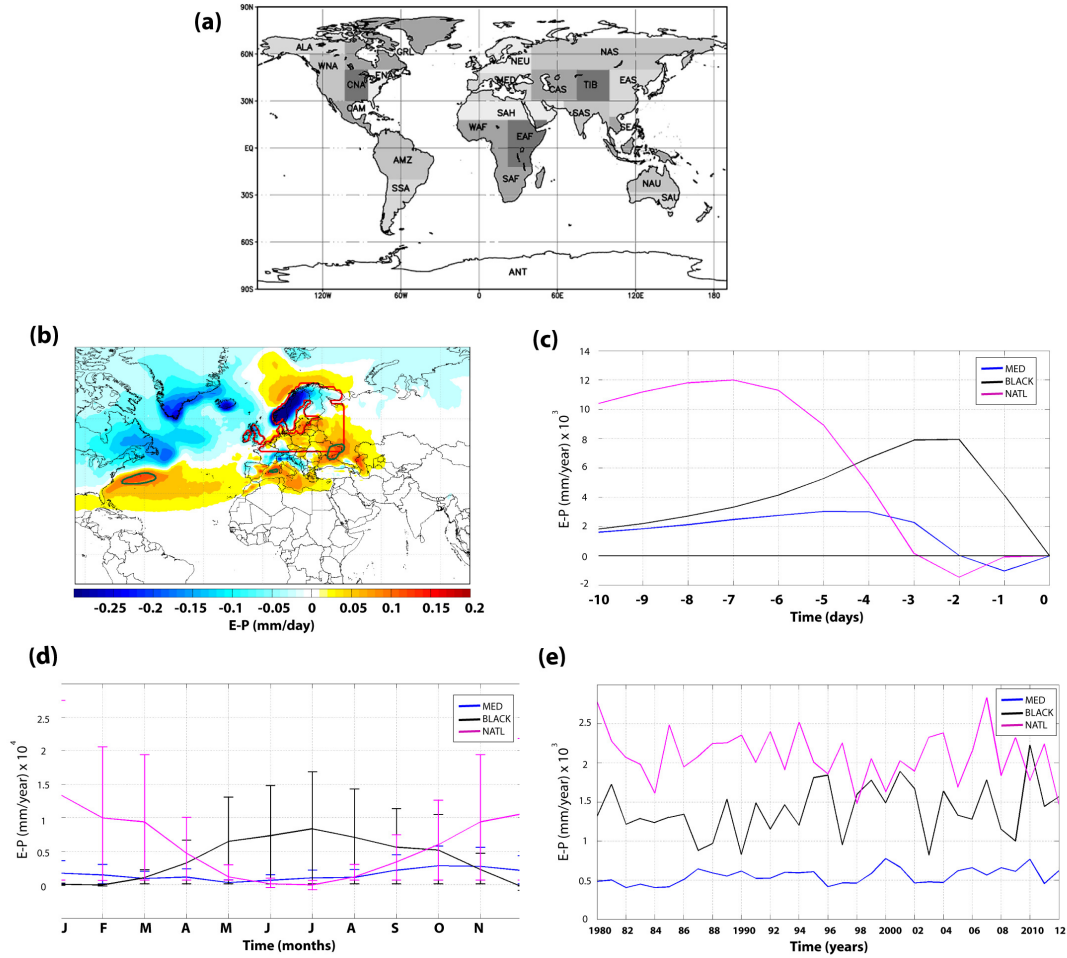


Figure B.6: (a) Selected target continental climatic regions (CCRs) with homogenous current climate (Giorgi regions). These regions are widely used in the IPCC reports and were identified by Giorgi and Francisco (2000). Items (b,c,d, and e) follow the same methodology of Figure 1 (Nieto et al. [2014b] and page 77 of this thesis) for the Northern Europe (NEU) region of analysis using a threshold of 0.1 mm/day.

B.3 A catalog of moisture sources for continental climatic regions

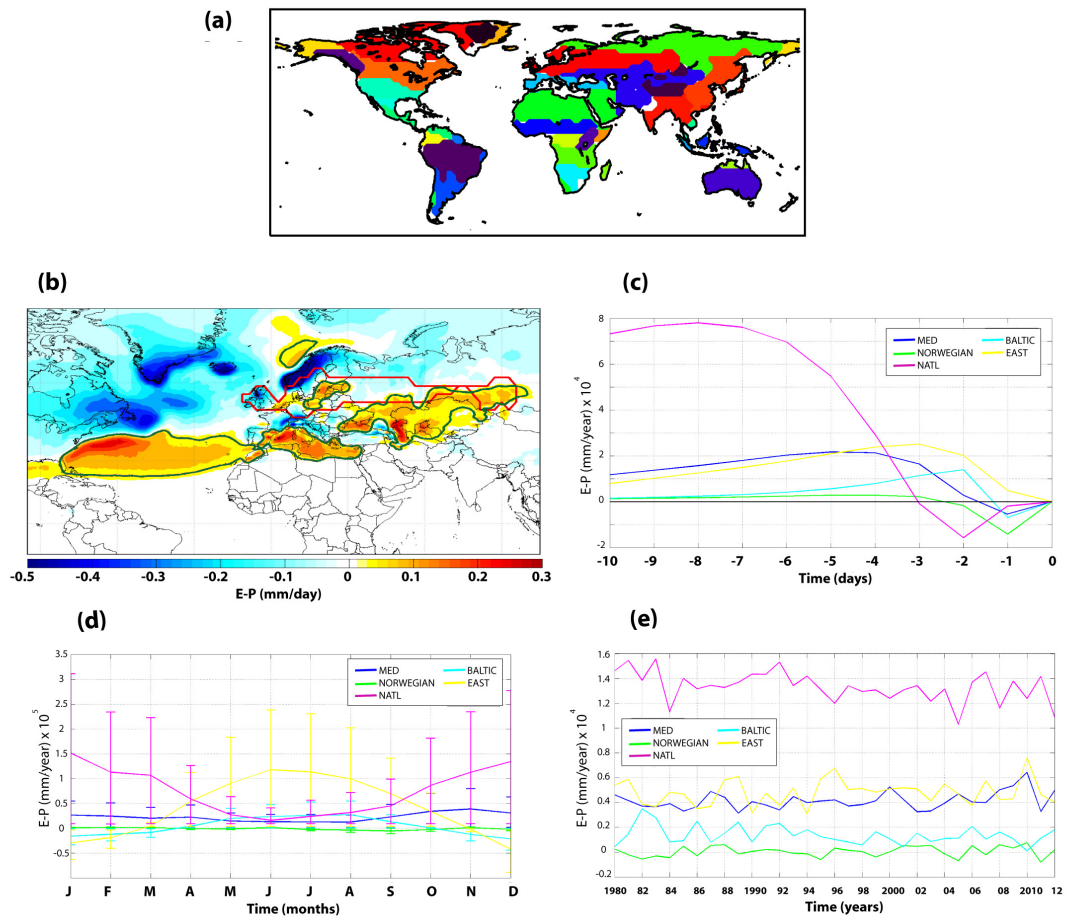


Figure B.7: Sensitivity test. As Figure 1 (Nieto et al. [2014b] and page 77 of this thesis) using a threshold of 0.05 mm/day.

B. SUPPORTING RESULTS

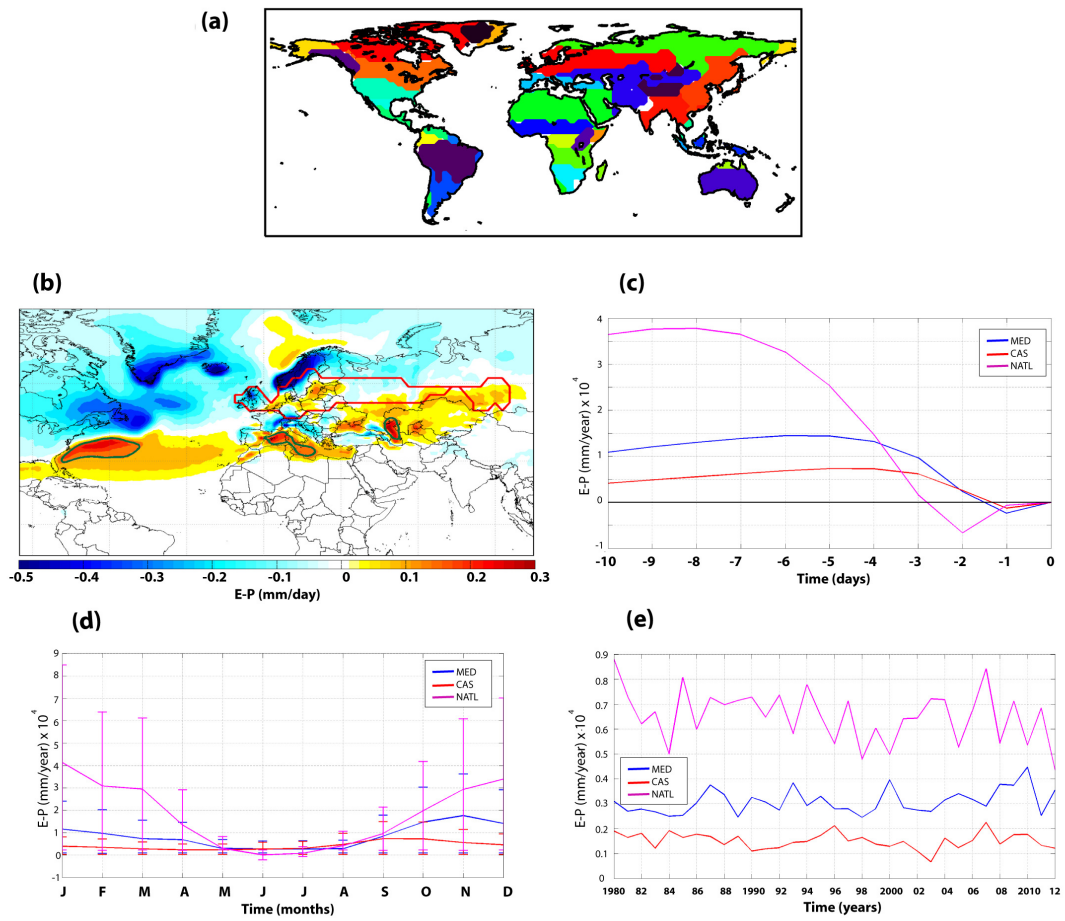


Figure B.8: Sensitivity test. As Figure 1 (Nieto et al. [2014b] and page 77 of this thesis) using a threshold of 0.15 mm/day.

B.3 A catalog of moisture sources for continental climatic regions

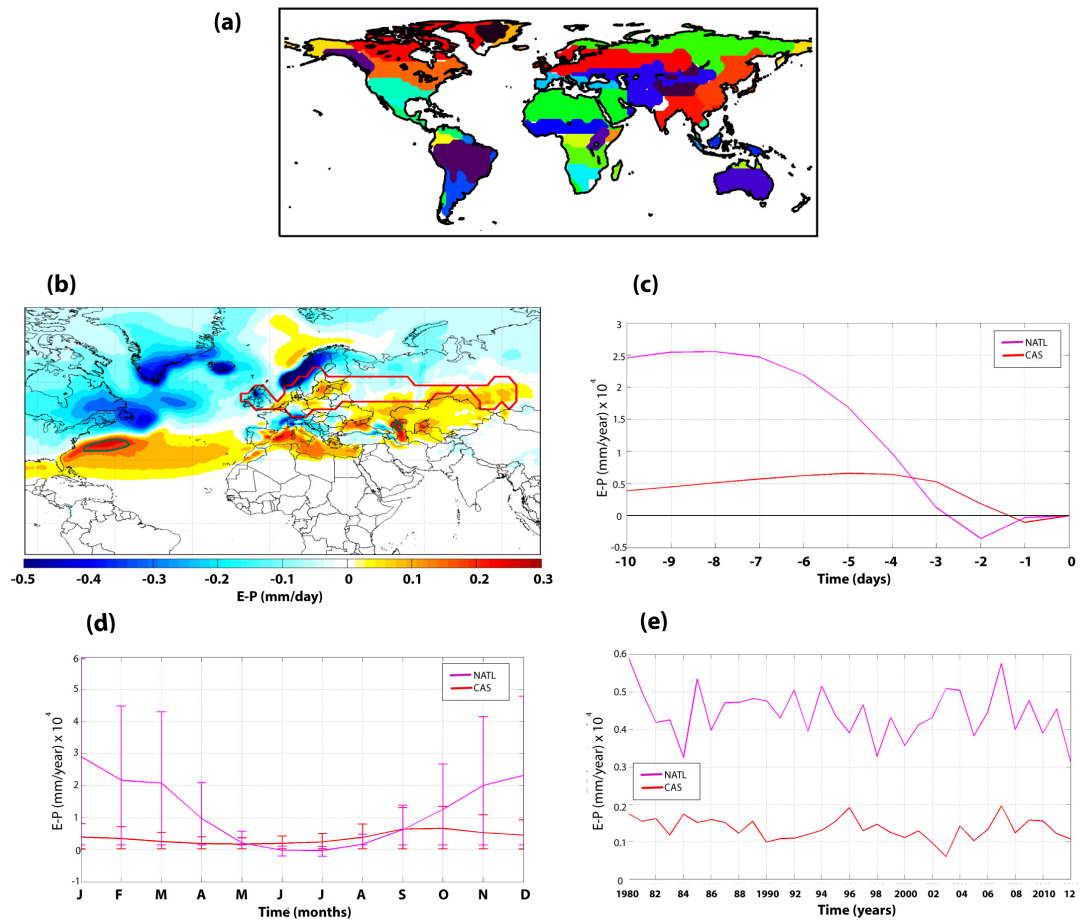


Figure B.9: Sensitivity test. As Figure 1 (Nieto et al. [2014b] and page 77 of this thesis) using a threshold of 0.2 mm/day.

B. SUPPORTING RESULTS

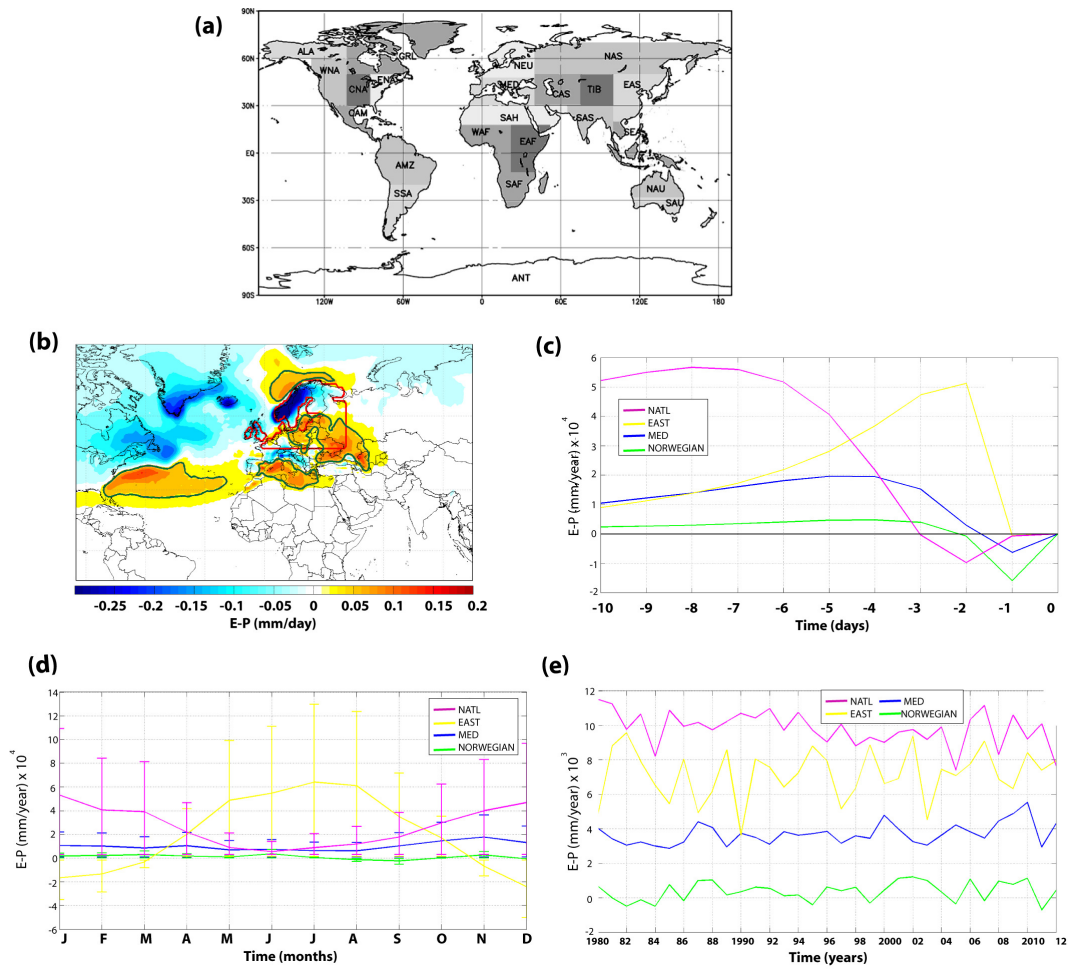


Figure B.10: Sensitivity test. As Figure B.6 using a threshold of 0.05 mm/day.

B.3 A catalog of moisture sources for continental climatic regions

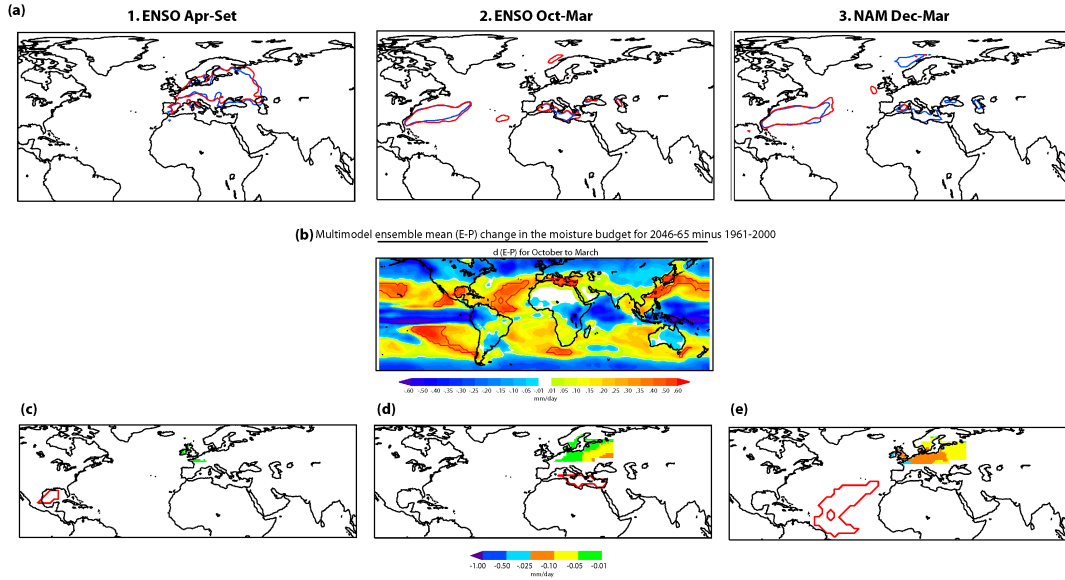


Figure B.11: Items (a,b,c,d, and e) follow the same methodology of Figure 2 (Nieto et al. [2014b] and page 79 of this thesis) for the Northern Europe (NEU) region of analysis using a threshold of 0.1 mm/day.

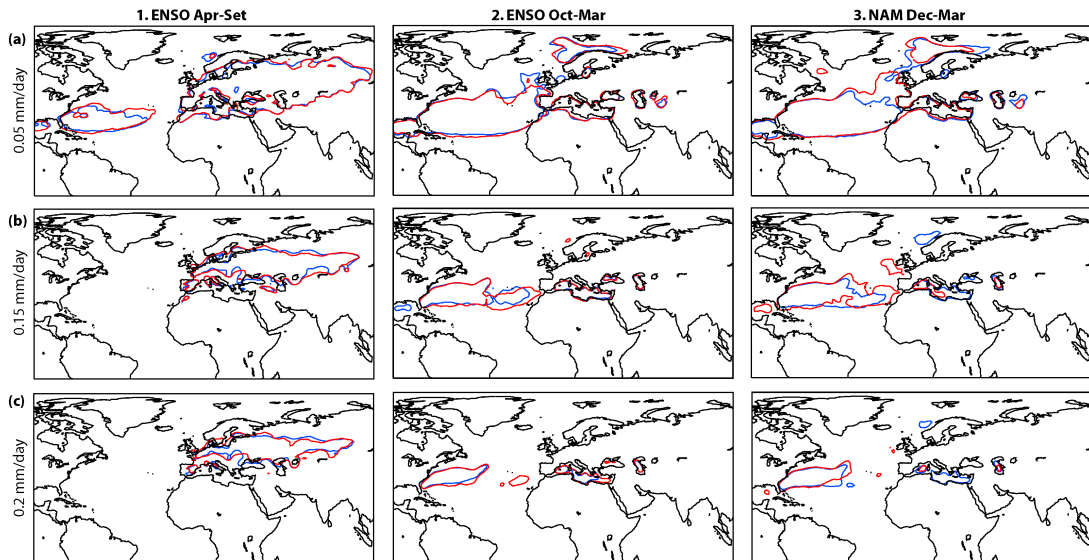


Figure B.12: Sensitivity test. As Figure 2.a (Nieto et al. [2014b] and page 79 of this thesis) using different thresholds: (a) 0.05 mm/day, (b) 0.15 mm/day and (c) 0.2 mm/day.

B. SUPPORTING RESULTS

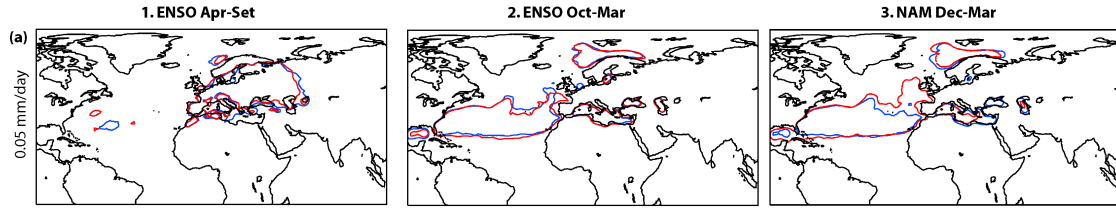


Figure B.13: Sensitivity test. As Figure B.11.a using a threshold of 0.05 mm/day.

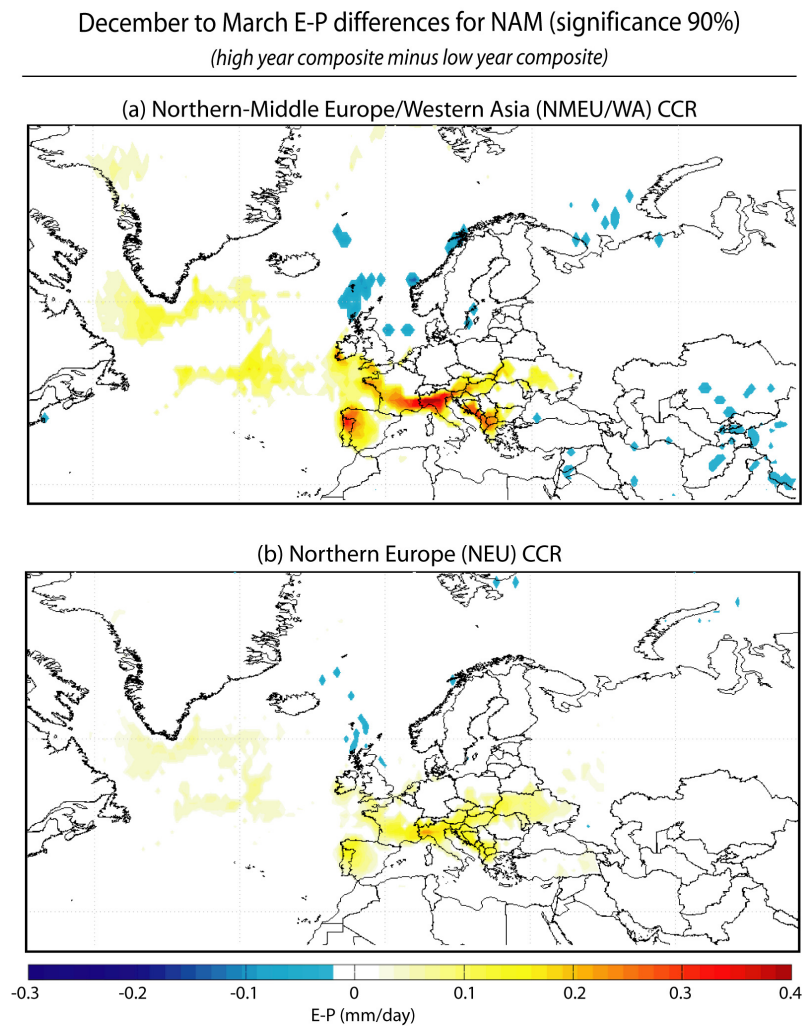


Figure B.14: The composite differences in $(E - P)$ between the average of the eight years with higher NAMI and the average of the eight years with lower NAMI for December-March. Only significant differences at the 90% confidence level are shown according to a bootstrap test that permutes the original time series 1000 times.

B.3 A catalog of moisture sources for continental climatic regions

Table B.1: Annual values of $(E - P)_{1-10}$ (in mm/day) for the North Atlantic (NATL), Caspian (CAS) and Mediterranean (MED) sources of moisture for the NMEU/WA CCR and the $(\pm\sigma)$ standard deviation, using a threshold of 0.1 mm/day.

	NATL			CAS			MED		
<i>Year</i>	$E - P$	$+\sigma$	$-\sigma$	$E - P$	$+\sigma$	$-\sigma$	$E - P$	$+\sigma$	$-\sigma$
1980	23650	24303	22996	5510	5654	5365	8474	8858	8089
1981	23379	24032	22726	4424	4569	4280	7334	7719	6950
1982	20313	20967	19658	5205	5349	5061	7905	8290	7521
1983	22879	23533	22226	3265	3410	3120	7181	7565	6797
1984	17157	17813	16502	5281	5425	5137	6476	6861	6091
1985	23312	23965	22659	4334	4478	4189	7273	7657	6889
1986	20150	20804	19495	4247	4391	4103	7753	8137	7369
1987	22125	22779	21472	5149	5293	5004	8861	9244	8477
1988	20014	20669	19359	5370	5515	5226	7618	8003	7234
1989	21354	22008	20700	5535	5680	5391	5784	6168	5399
1990	21977	22630	21323	3692	3837	3548	7665	8049	7282
1991	21485	22139	20831	4672	4816	4527	7196	7580	6812
1992	22880	23534	22225	3935	4079	3790	6875	7260	6490
1993	19788	20442	19133	5142	5287	4998	9673	10056	9289
1994	22663	23316	22009	4171	4315	4027	7522	7906	7138
1995	20702	21356	20048	6102	6246	5958	7349	7733	6965
1996	18290	18945	17635	6716	6860	6572	7523	7907	7138
1997	21343	21996	20689	5339	5484	5195	6917	7301	6532
1998	17799	18454	17144	4853	4997	4709	7521	7905	7136
1999	19188	19842	18533	3554	3698	3409	7757	8141	7373
2000	18441	19097	17786	4387	4532	4243	9400	9784	9016
2001	19479	20133	18825	5369	5513	5225	8267	8651	7884
2002	20359	21013	19705	4172	4317	4028	7292	7677	6908
2003	19292	19946	18638	3419	3564	3275	6343	6728	5959
2004	20060	20715	19405	5454	5598	5310	8441	8825	8056
2005	16357	17013	15702	4687	4831	4543	8050	8434	7666
2006	20796	21450	20142	4848	4992	4703	8595	8979	8211
2007	22821	23474	22168	5825	5969	5681	8491	8875	8107
2008	17715	18370	17059	4770	4915	4626	9554	9938	9170
2009	20956	21610	20302	5098	5242	4954	9269	9653	8886
2010	19275	19929	18620	5914	6058	5770	11781	12165	11398
2011	20738	21392	20084	3706	3851	3562	6374	6758	5990
2012	16020	16677	15364	4204	4349	4059	9172	9556	8788

B. SUPPORTING RESULTS

Table B.2: Annual values of $(E - P)_{1-10}$ (in mm/day) for the North Atlantic (NATL), Black Sea (BLACK) and Mediterranean (MED) sources of moisture for the NEU CCR and the $(\pm\sigma)$ standard deviation, using a threshold of 0.1 mm/day.

	NATL			BLACK			MED		
<i>Year</i>	$E - P$	$+\sigma$	$-\sigma$	$E - P$	$+\sigma$	$-\sigma$	$E - P$	$+\sigma$	$-\sigma$
1980	2777	2796	2758	1311	1333	1289	484	495	474
1981	2276	2295	2258	1722	1744	1700	503	513	492
1982	2066	2085	2047	1212	1234	1190	404	415	394
1983	1978	1997	1959	1287	1309	1265	449	459	438
1984	1613	1632	1594	1236	1258	1214	405	416	394
1985	2486	2505	2467	1304	1326	1283	415	425	404
1986	1947	1966	1928	1343	1365	1321	506	516	495
1987	2079	2098	2060	878	900	856	646	656	635
1988	2247	2266	2228	966	988	944	592	602	581
1989	2256	2275	2237	1535	1557	1513	551	562	540
1990	2355	2374	2336	827	849	805	616	627	606
1991	2004	2023	1985	1487	1509	1466	521	531	510
1992	2397	2416	2378	1153	1175	1131	524	534	513
1993	1910	1929	1891	1463	1485	1441	600	610	589
1994	2517	2536	2499	1201	1222	1179	593	603	582
1995	2009	2028	1990	1809	1831	1788	607	617	596
1996	1857	1876	1838	1843	1865	1821	417	428	406
1997	2256	2275	2237	950	972	929	466	477	455
1998	1480	1499	1461	1593	1615	1571	463	473	452
1999	2056	2075	2037	1778	1800	1757	583	593	572
2000	1627	1646	1608	1488	1510	1466	774	785	763
2001	2026	2045	2007	1890	1912	1868	665	676	655
2002	1892	1911	1873	1668	1690	1647	463	474	453
2003	2329	2348	2310	821	843	799	477	488	466
2004	2382	2401	2363	1639	1661	1617	470	481	459
2005	1688	1707	1669	1329	1351	1307	621	631	610
2006	2145	2164	2126	1279	1301	1257	659	669	648
2007	2835	2854	2816	1783	1805	1762	564	574	553
2008	1835	1854	1816	1150	1172	1128	658	669	648
2009	2320	2339	2301	999	1021	977	613	623	602
2010	1770	1789	1751	2228	2250	2206	767	778	756
2011	2243	2262	2224	1443	1465	1421	455	466	444
2012	1469	1488	1450	1568	1589	1546	620	630	609

B.3 A catalog of moisture sources for continental climatic regions

Table B.3: As Table B.1 but using the threshold of 0.05 mm/day to define the moisture sources (NATL, NORWEGIAN, MED, BALTIC and EAST).

	NATL			NORWEGIAN			MED			BALTIC			EAST		
<i>Year</i>	$E - P$	$+\sigma$	$-\sigma$	$E - P$	$+\sigma$	$-\sigma$	$E - P$	$+\sigma$	$-\sigma$	$E - P$	$+\sigma$	$-\sigma$	$E - P$	$+\sigma$	$-\sigma$
1980	14609	15063	14154	239	258	221	4607	4899	4314	422	448	397	5391	5647	5135
1981	15448	15901	14994	-213	-195	-231	4150	4442	3858	1463	1489	1438	5845	6100	5590
1982	13855	14309	13400	-545	-527	-563	3706	3998	3414	3491	3516	3465	3862	4117	3607
1983	15563	16017	15109	-307	-289	-325	3661	3953	3369	2766	2792	2741	3658	3913	3402
1984	11287	11743	10832	-452	-434	-470	3909	4202	3616	829	855	803	4826	5082	4570
1985	14002	14456	13548	467	485	449	3312	3604	3020	916	941	890	4682	4937	4426
1986	13156	13610	12701	-296	-278	-314	3672	3964	3380	2503	2528	2477	3501	3756	3245
1987	13445	13899	12991	541	559	523	4882	5173	4590	797	823	772	3692	3947	3437
1988	13271	13726	12815	596	614	578	4418	4710	4125	1517	1543	1491	5824	6080	5569
1989	13683	14138	13229	-157	-138	-175	3145	3438	2853	2412	2437	2386	6091	6346	5836
1990	14348	14802	13894	53	71	35	4062	4353	3770	823	849	798	3147	3403	2891
1991	14335	14789	13881	204	223	186	3794	4086	3503	2126	2152	2101	4742	4997	4487
1992	15307	15762	14853	151	169	132	3391	3684	3098	2310	2335	2284	3769	4025	3513
1993	13420	13874	12966	-87	-69	-105	4466	4757	4174	1304	1330	1279	5156	5411	4901
1994	14190	14644	13736	-141	-123	-159	3989	4281	3697	1794	1820	1769	3061	3317	2805
1995	13092	13547	12638	-609	-591	-628	4124	4416	3832	1243	1268	1217	5908	6163	5653
1996	11986	12442	11530	313	331	294	4203	4496	3911	1025	1051	999	6760	7015	6505
1997	13404	13858	12950	153	171	135	3714	4006	3422	822	848	797	5048	5303	4793
1998	12945	13399	12490	42	61	24	3830	4122	3538	577	602	551	5122	5377	4867
1999	13075	13529	12621	-395	-377	-413	4143	4435	3851	1637	1663	1612	4838	5093	4583
2000	12398	12854	11943	17	36	-1	5251	5543	4959	1076	1101	1050	5091	5347	4835
2001	13076	13530	12622	516	534	498	4254	4545	3962	416	442	390	5175	5430	4920
2002	13422	13876	12967	470	489	452	3255	3547	2963	1542	1568	1516	5100	5355	4845
2003	12154	12608	11699	539	558	521	3311	3603	3019	855	881	829	4133	4388	3877
2004	13131	13586	12675	-138	-120	-156	3952	4245	3659	1109	1134	1083	5492	5748	5236
2005	10298	10753	9843	-704	-685	-722	4681	4972	4389	1115	1140	1089	4671	4926	4416
2006	13688	14142	13234	521	539	502	4040	4332	3748	2065	2091	2039	3746	4001	3491
2007	14520	14974	14067	-226	-208	-244	3995	4287	3704	1043	1069	1018	5758	6012	5503
2008	11606	12062	11151	590	608	572	5033	5325	4741	1613	1639	1588	4232	4488	3976
2009	13783	14237	13329	323	341	305	5361	5652	5070	1060	1086	1035	4302	4557	4047
2010	12380	12834	11926	751	769	733	6429	6720	6138	87	113	62	7603	7858	7349
2011	14161	14615	13707	-806	-788	-825	3264	3556	2971	1123	1149	1098	4628	4883	4373
2012	10882	11338	10427	194	212	176	4987	5279	4695	1783	1809	1758	4016	4272	3761

B. SUPPORTING RESULTS

Table B.4: As Table B.1 but using the threshold of 0.15 mm/day to define the moisture sources (NATL, CAS and MED).

	NATL			CAS			MED		
<i>Year</i>	$E - P$	$+\sigma$	$-\sigma$	$E - P$	$+\sigma$	$-\sigma$	$E - P$	$+\sigma$	$-\sigma$
1980	8801	8972	8630	1902	1946	1858	3102	3240	2965
1981	7305	7477	7134	1647	1691	1603	2694	2832	2557
1982	6204	6376	6033	1811	1855	1767	2785	2923	2648
1983	6695	6867	6523	1215	1259	1170	2671	2809	2534
1984	4991	5163	4819	1915	1959	1871	2498	2636	2360
1985	8078	8249	7907	1647	1691	1603	2528	2665	2390
1986	5988	6160	5816	1775	1819	1731	3034	3171	2897
1987	7264	7435	7092	1684	1728	1640	3752	3889	3615
1988	6974	7145	6802	1361	1405	1317	3365	3503	3228
1989	7149	7320	6978	1695	1740	1651	2460	2597	2322
1990	7287	7458	7115	1099	1143	1055	3253	3390	3115
1991	6475	6647	6304	1191	1235	1146	3067	3204	2930
1992	7365	7537	7193	1231	1275	1187	2740	2878	2603
1993	5806	5978	5634	1442	1486	1398	3840	3977	3703
1994	7783	7955	7612	1483	1527	1439	2924	3061	2786
1995	6518	6690	6347	1728	1772	1684	3296	3433	3159
1996	5408	5580	5236	2116	2160	2072	2790	2927	2652
1997	7130	7302	6959	1500	1544	1456	2795	2932	2657
1998	4779	4951	4607	1641	1685	1597	2453	2590	2315
1999	6031	6202	5859	1373	1417	1329	2799	2936	2661
2000	4984	5157	4812	1287	1331	1243	3966	4103	3829
2001	6409	6581	6238	1484	1528	1440	2838	2975	2700
2002	6437	6609	6265	1099	1143	1055	2744	2882	2607
2003	7212	7383	7041	665	709	620	2689	2827	2552
2004	7176	7348	7005	1620	1664	1576	3146	3283	3008
2005	5260	5432	5088	1230	1274	1186	3397	3534	3260
2006	6718	6889	6546	1516	1560	1472	3171	3308	3033
2007	8425	8596	8254	2246	2290	2202	2901	3038	2764
2008	5433	5605	5261	1379	1423	1335	3777	3914	3640
2009	7126	7297	6955	1755	1799	1711	3745	3882	3608
2010	5350	5522	5179	1771	1815	1727	4466	4603	4329
2011	6849	7020	6677	1328	1373	1284	2527	2665	2390
2012	4345	4518	4173	1212	1256	1168	3541	3678	3404

B.3 A catalog of moisture sources for continental climatic regions

Table B.5: As Table B.1 but using the threshold of 0.2 mm/day to define the moisture sources (NATL and CAS).

	NATL			CAS		
<i>Year</i>	$E - P$	$+\sigma$	$-\sigma$	$E - P$	$+\sigma$	$-\sigma$
1980	5939	6062	5816	1751	1790	1712
1981	4993	5116	4869	1544	1583	1505
1982	4182	4306	4059	1619	1658	1579
1983	4249	4373	4126	1176	1216	1137
1984	3248	3371	3124	1733	1773	1694
1985	5349	5472	5226	1511	1550	1471
1986	3972	4095	3848	1593	1632	1554
1987	4712	4836	4589	1511	1551	1472
1988	4722	4845	4598	1227	1266	1187
1989	4820	4943	4697	1543	1583	1504
1990	4764	4888	4641	986	1026	947
1991	4297	4420	4174	1084	1123	1045
1992	5040	5163	4916	1090	1130	1051
1993	3945	4068	3821	1192	1231	1153
1994	5144	5267	5021	1301	1340	1262
1995	4362	4485	4239	1544	1583	1504
1996	3913	4036	3789	1907	1947	1868
1997	4663	4786	4540	1292	1332	1253
1998	3269	3392	3145	1461	1501	1422
1999	4309	4432	4185	1237	1277	1198
2000	3568	3692	3444	1109	1149	1070
2001	4117	4240	3994	1286	1325	1247
2002	4313	4437	4190	964	1004	925
2003	5094	5217	4971	596	636	557
2004	5042	5165	4919	1418	1457	1379
2005	3826	3949	3702	1024	1063	984
2006	4457	4581	4334	1319	1358	1279
2007	5766	5889	5643	1956	1995	1917
2008	3994	4118	3870	1232	1271	1192
2009	4763	4886	4640	1575	1614	1536
2010	3893	4016	3769	1553	1592	1514
2011	4545	4668	4421	1210	1250	1171
2012	3135	3259	3011	1072	1112	1033

B. SUPPORTING RESULTS

Table B.6: As Table B.2 but using the threshold of 0.05 mm/day to define the moisture sources (NATL, NORWEGIAN, MED and EAST).

	NATL			NORWEGIAN			MED			EAST		
<i>Year</i>	$E - P$	$+\sigma$	$-\sigma$	$E - P$	$+\sigma$	$-\sigma$	$E - P$	$+\sigma$	$-\sigma$	$E - P$	$+\sigma$	$-\sigma$
1980	11503	11584	11421	673	685	661	4033	4106	3960	4783	4877	4689
1981	11240	11321	11158	-3	9	-15	3415	3488	3342	8805	8898	8711
1982	9760	9842	9679	-497	-484	-509	3050	3123	2978	9566	9659	9473
1983	10644	10726	10563	-118	-105	-130	3232	3304	3159	7905	7999	7812
1984	8207	8289	8125	-494	-481	-506	3002	3075	2929	6523	6617	6430
1985	10868	10950	10787	763	776	751	2868	2940	2795	5455	5549	5361
1986	9939	10021	9858	-171	-158	-183	3227	3300	3155	8041	8134	7948
1987	10165	10247	10083	1006	1019	994	4404	4476	4331	4926	5020	4833
1988	9728	9809	9646	1027	1039	1014	4073	4145	4000	6182	6277	6088
1989	10225	10307	10144	172	185	160	2949	3021	2876	8580	8673	8486
1990	10695	10777	10614	359	372	347	3744	3816	3671	3628	3722	3534
1991	10418	10499	10336	622	635	610	3502	3574	3429	8045	8138	7952
1992	10976	11058	10894	547	559	535	3107	3180	3035	7576	7670	7483
1993	9713	9794	9631	117	130	105	3828	3900	3755	6423	6517	6330
1994	10752	10833	10670	163	176	151	3630	3702	3557	7238	7331	7144
1995	9707	9788	9625	-402	-390	-415	3716	3789	3644	8792	8886	8699
1996	9023	9105	8941	626	638	613	3848	3921	3775	7938	8032	7845
1997	10059	10141	9978	412	424	399	3154	3227	3081	5155	5249	5061
1998	8801	8883	8720	616	628	603	3590	3663	3518	6357	6451	6263
1999	9302	9383	9220	-310	-298	-323	3452	3524	3379	8863	8956	8769
2000	9008	9090	8926	445	458	433	4788	4860	4715	6616	6710	6522
2001	9602	9684	9521	1128	1140	1115	3985	4057	3912	6915	7009	6822
2002	9750	9832	9669	1219	1231	1207	3261	3333	3188	9369	9463	9276
2003	9172	9253	9090	1004	1016	991	3058	3130	2985	4528	4622	4434
2004	9898	9980	9816	338	350	325	3629	3702	3556	7448	7542	7354
2005	7400	7482	7318	-348	-336	-360	4225	4297	4152	7085	7179	6991
2006	10320	10401	10238	1087	1100	1075	3832	3904	3759	7754	7847	7660
2007	11148	11229	11067	-170	-158	-182	3449	3522	3376	9081	9174	8987
2008	8303	8385	8221	963	976	951	4451	4524	4379	6868	6962	6774
2009	10589	10670	10508	777	789	764	4869	4942	4797	6326	6420	6232
2010	9206	9287	9124	1137	1149	1124	5534	5606	5462	8412	8505	8318
2011	10077	10159	9995	-712	-699	-724	2938	3011	2865	7401	7495	7308
2012	7651	7733	7569	428	440	416	4306	4378	4233	7944	8038	7851

Resumen General

C.1 Introducción

En vista de la amenaza del cambio climático a nivel global, la comprensión adecuada de la intensidad del ciclo hidrológico y su evolución en el tiempo es uno de los retos más importantes de este siglo, al menos en el área de las Ciencias de la Tierra.

El ciclo hidrológico se puede resumir esencialmente como la evaporación del agua en un lugar determinado compensada por la precipitación en otro. Sobre los océanos la velocidad de evaporación supera la tasa de precipitación, siendo éstos, por lo tanto, una fuente neta de humedad, la cual es transportada a los continentes que son un sumidero neto, donde la precipitación supera la evapotranspiración. Esto se traduce en escorrentía superficial que se recoge en ríos y otros cursos de agua, los cuales descargan en el océano completando de esta forma el ciclo del agua.

El ciclo hidrológico global es abastecido cada año con cerca de 500000 km^3 de agua que se evaporan de la superficie de la Tierra. La mayor parte de este volumen evaporado procede de la superficie oceánica (86%) y sólo el 14% procede de la superficie continental (Oki, 2005).

La gran mayoría del agua que se evapora de los océanos (90%) precipita directamente de nuevo en ellos, mientras que el 10% restante se transporta a los continentes

C. RESUMEN GENERAL

donde precipita. Alrededor de dos tercios de este último 10% es reciclado en los continentes, mientras que el tercio restante vuelve directamente a los océanos, siendo este mecanismo esencial en la alimentación de la rama terrestre del ciclo hidrológico. En definitiva, a pesar de la componente de reciclaje continental, toda el agua utilizada o a disposición de los ecosistemas terrestres y actividades socio-económicas humanas tiene su origen en los océanos. Por lo tanto, cualquier cambio futuro en las condiciones meteorológicas de las fuentes de humedad oceánicas puede tener un impacto en la disponibilidad de agua en muchas cuencas fluviales. En este contexto, la tendencia al alza incesante de la temperatura observada en las últimas décadas puede suponer una carga adicional sobre la fiabilidad de las fuentes de humedad en el futuro.

Los estudios de modelización sugieren que la alta sensibilidad de la presión de vapor de saturación con la temperatura se traducirá en un aumento en la evaporación y la precipitación y que conducirá a una intensificación del ciclo hidrológico (Held y Soden, 2006). El volumen de agua que se evapora dependerá en gran medida de los cambios que ocurran en el mar, la temperatura del aire y el viento sobre las principales fuentes de humedad oceánica, y estos cambios estarán destinados a influir en regiones continentales específicas. Por esta razón, Gimeno et al. (2010a) con el uso del modelo lagrangiano de transporte FLEXPART, que utiliza datos de análisis meteorológico como entrada junto con un esquema de seguimiento de humedad, identificó con éxito aquellas regiones continentales que se ven afectadas por la precipitación asociada a masas de aire húmedo procedentes de regiones oceánicas específicas previamente identificadas como fuentes de humedad. No obstante este estudio tenía un dominio temporal bajo, sólo 5 años.

El **objetivo** de este estudio es caracterizar la distribución de la precipitación continental debida a las principales fuentes de humedad oceánica haciendo uso de una aproximación lagrangiana de alta precisión para un periodo temporal mayor que el usado hasta el momento, 33 años. Así se podrá analizar el comportamiento y la variabilidad inter-anual de las fuentes de humedad, con el fin de obtener una mejor comprensión del papel que éstas juegan en el aporte de humedad a la precipitación continental.

El **interés principal** de esta tesis se fundamenta en la falta de un estudio y una caracterización climática detallada y de dominio temporal amplio del transporte global de humedad utilizando un modelo lagrangiano de dispersión de partículas. La motivación inicial de este trabajo proviene del gran impacto en la comunidad científica del primer

intento de realizar un estudio de este tipo por Gimeno et al. (2010a), que como se dijo anteriormente, utilizó un dominio temporal pequeño de tan sólo cinco años de datos, de 2000 a 2004. Este trabajo fue destacado por la Unión Geofísica Americana (AGU, por sus siglas en inglés) en su revista EOS como uno de los tres artículos en geofísica más importantes publicados durante el primer semestre de 2010 (3^{ra} edición de agosto de EOS). Ya en esa publicación se sugería la importancia de extender el dominio temporal de estudio con el fin de obtener una caracterización y comprensión más adecuada de las fuentes globales de humedad.

La limitación temporal del estudio de Gimeno et al. (2010a) supone que algunos aspectos de la rama atmosférica del ciclo hidrológico fueron poco conocidos y detallados. Como una propuesta (respuesta) a este problema en esta tesis el análisis se amplía a las tres últimas décadas, 1980-2012, con el fin de responder, entre otras, a las siguientes preguntas científicas:

- (i) ¿han sido las regiones fuentes de humedad estacionarias o han cambiado a lo largo de las últimas tres décadas?
- (ii) ¿cómo los cambios en la intensidad, es decir, más evaporación sobre las regiones fuente de humedad oceánica, afectan a la distribución de la precipitación continental?
- (iii) ¿afecta también a la distribución de la precipitación continental los cambios de posición de las fuentes de humedad?
- (iv) ¿cuál es el papel de los principales modos de variabilidad climática como ENSO, NAM y SAM en la variabilidad de las fuentes de humedad?

También se ha intentado abordar en este trabajo los posibles impactos del cambio climático en el transporte de humedad desde los océanos hacia los continentes. Seager et al. (2010), mediante un conjunto de salidas de los Modelos de Circulación Global (GCM, por sus siglas en inglés), identificaron aquellas regiones oceánicas con altas tasas de evaporación menos precipitación en un futuro bajo los efectos del cambio climático. Estas regiones fueron definidas como fuentes de humedad para determinar las áreas de tierra afectadas por la precipitación asociada a ellas y así señalar donde, ante los cambios venideros en el clima, es esperable modificaciones en la precipitación continental.

C. RESUMEN GENERAL

Además, se analizan las fuentes de humedad asociadas con regiones climáticas continentales de interés del planeta, proporcionando una evaluación fiable y robusta de las relaciones fuente-sumidero en el ciclo atmosférico del agua para los climas regionales. Este estudio se realizó para dos conjuntos diferentes de regionalización climática, y se presenta en forma de un catálogo disponible libremente en la red a toda la comunidad científica. Conocer la procedencia de la humedad que genera precipitación para cualquier región del globo es un requisito imprescindible para comprender los factores que afectan a los fenómenos meteorológicos y climáticos extremos.

Para dar respuesta a estas cuestiones científicas se utiliza un sofisticado método de diagnóstico lagrangiano de identificación de fuentes o sumideros de humedad, que está basado en el modelo FLEXPART en su última versión. FLEXPART es un modelo de dispersión lagrangiano de partículas en 3D que permite seguir la trayectoria (hacia adelante o hacia atrás en el tiempo) de partículas en la atmósfera, en este caso pequeños volúmenes de masa de aire húmeda. Computando los cambios en la humedad específica puede realizarse un balance de ganancias y pérdidas de humedad, señalando así aquellas regiones que actúan como fuentes o sumideros, y pudiéndose hacer una relación entre ambas. Los diferentes cálculos en el modelo se realizan para las tres décadas comprendidas entre 1980 a 2012 utilizando datos del reanálisis ERA-40 y ERA-Interim del ECMWF. Se trabajaron diferentes técnicas estadísticas para dar valor significativo a las señales y resultados obtenidos.

C.2 Objetivos

Con la motivación de responder a las preguntas que se apuntaron en la sección introductoria relacionadas con las fuentes globales de humedad y los aspectos clave de la rama atmosférica del ciclo hidrológico, se propusieron los siguientes objetivos que se listan a continuación:

- (1) Generar un nuevo conjunto de datos de trayectorias hacia adelante en el tiempo usando un periodo temporal más largo que en el análisis previo de Gimeno et al. (2010a) que permita el estudio de las principales fuentes oceánicas de humedad y su variabilidad. Para ello se corre el modelo lagrangiano FLEXPART en una primera fase para 1980-2000 con datos del reanálisis ERA-40 y posteriormente para 1980-2012 con datos reanalizados de ERA-Interim, ambos generados por el

- ECMWF. Los datos de entrada del modelo tienen una resolución temporal de 6 horas y una resolución espacial en dominio global de $1^\circ \times 1^\circ$ en latitud y longitud, con 61 niveles en la vertical. Se generan por tanto, así, trayectorias de partículas que se pueden posicionar espacialmente en tres dimensiones cada seis horas (más detalles se pueden encontrar en la Sección C.3).
- (2) Generar un nuevo conjunto de datos de trayectorias hacia atrás en el tiempo que permita el estudio de las fuentes de humedad para las regiones climáticas continentales y su variabilidad, haciendo posible la evaluación de las relaciones fuente-sumidero en el ciclo atmosférico del agua para los climas regionales. El período utilizado es de 1980 a 2012 usando datos del reanálisis ERA-Interim.
 - (3) Presentar un estudio climatológico de las fuentes oceánicas de humedad utilizando los conjuntos de datos de trayectorias hacia adelante. Este objetivo se articula en los siguientes objetivos específicos:
 - (a) Analizar las fuentes de precipitación continental a escala global,
 - Evaluando si las regiones fuente se han mantenido estacionarias, o si han cambiado en las últimas tres décadas.
 - Investigando cómo los cambios en la intensidad (mayor evaporación) y la posición de las fuentes afectan a la distribución de la precipitación continental.
 - Investigando el papel de los principales modos de variabilidad climática, como ENSO, NAM y SAM, en la variabilidad de las regiones fuente de humedad y la precipitación continental asociada a cada una de ellas.
 - (b) Analizar las fuentes oceánicas de precipitación continental vinculadas al cambio climático evaluando la influencia potencial en la precipitación continental de las regiones oceánicas con altas tasas de evaporación menos precipitación detectadas en un futuro escenario de cambio climático.
 - (4) Identificar y caracterizar las principales fuentes de humedad asociadas a diferentes regiones climáticas continentales utilizando el conjunto de datos de las trayectorias calculadas hacia atrás en el tiempo. Las regiones continentales se eligieron basándose en dos sistemas de regionalización diferentes:

C. RESUMEN GENERAL

- (a) uno basado en una regionalización en función de los cambios en la precipitación detectados en las últimas décadas y proyectados para el futuro, según los resultados de Mahlstein y Knutti (2010). Se obtuvieron así 35 regiones en todo el globo que serán analizadas de manera independiente.
- (b) y otro basado en la regionalización climática realizada por Giorgi y Francisco (2000) que considera 21 regiones que representan los diferentes regímenes climáticos. Esta regionalización es y ha sido ampliamente utilizada en los diferentes informes del IPCC.

C.3 Metodología

Para llevar a cabo un análisis detallado de las fuentes globales de humedad y su variabilidad asociada para todo el planeta, se utilizó la aproximación lagrangiana desarrollada por Stohl y James (2004, 2005) usando el modelo FLEXPART. Este método se aplicó con un resultado exitoso, como lo demuestran los cinco artículos que componen el cuerpo principal de esta tesis: Gimeno et al. (2013), Castillo et al. (2014a, 2014b) y Nieto et al. (2014a, 2014b). En esta sección, y antes de presentar los resultados de los trabajos realizados en la Sección C.4, se hace una descripción muy breve de la metodología utilizada para cada uno de los objetivos planteados, ya que al ser esta tesis presentada como compendio de artículos los métodos de cada trabajo están descritos exhaustivamente en cada uno de ellos.

Para abordar el estudio de la precipitación continental asociada a las **principales fuentes oceánicas de humedad** han de volver a calcularse éstas (ya habían sido definidas Gimeno et al. 2010a) usando un periodo de tiempo más largo. Las regiones fuentes de humedad se definen como los valores máximos del campo climatológico anual de la divergencia de flujo de humedad integrado en la vertical (VIMT, siglas del término en inglés “*vertical integrated moisture transport*”). Para el cálculo del VIMT y su divergencia se usaron las variables necesarias disponibles en el reanálisis ERA-Interim del ECMWF (Dee et al., 2011) con una resolución de $1^\circ \times 1^\circ$ en latitud y longitud, 61 niveles en la vertical y datos cada 6 horas. Se identificaron diez regiones fuentes de humedad oceánica sobre la base de un umbral de 750 mm/año para la divergencia del flujo de humedad integrado en la vertical (Figura 3.1) siguiendo los criterios de Gimeno et al. (2010a). Estas diez regiones fuentes de humedad oceánica son: NPAC, Pacífico

Norte; SPAC, Pacífico Sur; NATL, Atlántico Norte; SATL, Atlántico Sur; MEXCAR, Golfo de México y Mar Caribe; ARAB, Mar de Arabia; ZAN, Corriente de Zanzíbar; AGU, Corriente de Agulhas; IND, Océano Índico; y CORALS, Mar de Coral. Además, dos fuentes adicionales fueron incluidas, y se definieron utilizando los límites físicos de sus cuencas oceánicas, éstas se denominan, MED, Mar Mediterráneo y REDS, Mar Rojo. Estas 12 regiones se utilizaron como fuentes de humedad en las integraciones hacia adelante para lograr el objetivo 1 para cada período de tiempo.

Para analizar la posible **influencia de un cambio climático en la precipitación continental debido a modificaciones en las fuentes evaporativas oceánicas** se identifican aquellas áreas en el océano que muestran un mayor cambio en evaporación menos precipitación ante un escenario de cambio climático futuro. Estas regiones fueron definidas por Seager et al. (2010) comparando las medidas de humedad para el período 1961-2000 en intervalos semestrales de octubre-marzo y abril-septiembre con aquellas estimadas para el período 2046-2065 usando datos generados por 15 modelos de circulación global incluidos en la fase 3 del proyecto del modelo de intercomparación acoplado utilizado por el IPCC AR4 (Meehl et al., 2007). El “*ensemble*” de estos 15 modelos sirve para definir regiones fuentes de humedad vinculadas a cambio climático a aquellas áreas que exceden el umbral de 0.3 mm/día (indicadas por las líneas rojas cerradas en las Figuras 3.2 y 3.3), de aquí en adelante referidas como regiones fuentes “*Hot Spot*” (HSSRs, por sus siglas en inglés). Las HSSRs fueron utilizadas como regiones fuente y analizadas las trayectorias que de ellas partían mediante el modelo FLEXPART para lograr el objetivo 3b para el período de tiempo 1980-2000, con el fin de identificar qué regiones continentales se verían afectadas en su patrón de precipitación debido a cambios en la evaporación oceánica.

Para el análisis de las **fuentes de humedad para las regiones climáticas continentales** se utilizaron dos conjuntos de regiones basados en dos esquemas de regionalización diferentes. El primero (Figura 3.4), definido por Mahlstein y Knutti (2010), considera las 35 regiones geográficas sobre toda la superficie del globo que presentan promedios climáticos similares a finales del siglo XX (1970-1999) y cambios similares u homogéneos en las proyecciones de precipitación para finales del siglo XXI (2070-2099). Se denominarán en esta tesis como MKRs. El segundo conjunto de regiones (Figura 3.5) contiene las 21 regiones llamadas “regiones de Giorgi” (Giorgi y Francisco, 2000) y que son ampliamente utilizadas en los informes del IPCC (de aquí en

C. RESUMEN GENERAL

adelante referidas como GRs). Las GRs representan diferentes regímenes climáticos homogéneos en la actualidad. Las Tablas 3.1 y 3.2 muestran los nombres de estas regiones con sus respectivas siglas. Ambos conjuntos de regiones continentales, MKRs y GRs, fueron utilizados para crear un catálogo de fuentes de humedad para cada una de ellas y poder así evaluar la relación fuente-sumidero en el ciclo atmosférico del agua para los diferentes climas regionales.

Con el fin de **caracterizar y estudiar la variabilidad de las fuentes globales de humedad** se realizaron dos experimentos diferentes basados en el método desarrollado por Stohl y James (2004, 2005). Estos experimentos utilizan el modelo lagrangiano de dispersión de partículas FLEXPART (Stohl et al., 1998) para realizar un seguimiento de la humedad atmosférica a lo largo de trayectorias en toda la columna de la atmósfera. Al comienzo de esta investigación se utilizó un período de 21 años comprendido entre 1980 a 2000, haciendo uso del reanálisis ERA-40 del ECMWF (Uppala et al., 2005), y más tarde se utilizó un período más largo de 33 años, comprendido entre 1980 y 2012, utilizando datos del reanálisis ERA-Interim (Dee et al., 2011), cuando este último conjunto de datos estaba completamente disponible. Se ha demostrado que el rendimiento de ERA-Interim en la reproducción del ciclo hidrológico y en términos de cierre del balance hídrico es mucho mejor que ERA-40 (Trenberth et al., 2011), y también mejor que el de los productos más recientes de reanálisis tales como el MERRA y el CFSR (Lorenz y Kunstmann, 2012). Los datos de años anteriores a 1980 no se utilizaron para ejecutar el modelo FLEXPART debido a que los resultados del reanálisis se consideran de insuficiente calidad (especialmente sobre los océanos) antes de la inclusión de los datos de satélite (Bengtsson et al., 2004). La utilidad de los datos antes de 1980 es un poco limitada por dos razones: (i) el modelo FLEXPART utiliza variables derivadas como datos de entrada, tales como viento zonal (u), viento meridional (v) y humedad específica (q), que no son fiables antes de esta fecha ya que son altamente sensibles a errores, y por lo tanto los resultados del modelo pueden ser erróneos (Stohl et al., 2005), y (ii) es imposible trabajar con datos obtenidos antes de la incorporación de imágenes de satélite en el reanálisis a partir de 1979. Antes de esta fecha, no había suficientes observaciones sobre las grandes áreas oceánicas y los conjuntos de datos son mucho menos fiables (Bengtsson et al., 2004; Uppala et al., 2005).

Los **modelos lagrangianos de partículas** calculan las trayectorias de un gran número de pequeñas parcelas de aire infinitesimales (denominadas “partículas”) para modelar el

transporte y difusión de trazadores atmosféricos (Stohl et al., 2005). Al inicio de la **ejecución del modelo**, la atmósfera fue “rellenada” de manera homogénea con partículas, cada una representando una fracción de la masa atmosférica total (Stohl y James, 2004). Durante la ejecución, estas partículas son advectadas usando el campo de velocidad tridimensional del reanálisis, con movimientos turbulentos estocásticos y convectivos superpuestos. Las posiciones de las partículas y la humedad específica (q) se registran cada 6 horas. Así, los aumentos (evaporación, e) y disminuciones (precipitación, p) en la humedad de la partícula a lo largo de la trayectoria se calculan a partir de cambios en la humedad específica (q) con respecto al tiempo, como lo muestra la Ecuación C.1

$$e - p = m \frac{dq}{dt} \quad (\text{C.1})$$

donde m es la masa de cada partícula.

La suma de los cambios de humedad ($e - p$) de todas las partículas en la columna atmosférica sobre un área específica A genera el **flujo de agua dulce superficial** ($E - P$), donde E es la tasa de evaporación por unidad de área, y P es la tasa de precipitación por unidad de área (Ecuación C.2)

$$E - P \approx \frac{\sum_{k=1}^K (e - p)_k}{A} \quad (\text{C.2})$$

donde K es el número total de partículas en la columna atmosférica.

En el presente trabajo, la atmósfera global se dividió en casi 1.9 millones de partículas en el experimento que usa el conjunto de datos ERA-40 y en alrededor de 2.0 millones en el del reanálisis ERA-Interim. Cada partícula fue rastreada durante 10 días ya que este es el tiempo medio de residencia del vapor de agua en la atmósfera (Numaguti, 1999). Las trayectorias se calcularon utilizando los datos disponibles de ambos reanálisis con intervalos de seis horas (00, 06, 12 y 18 UTC) y con una resolución espacial de 1° de latitud por 1° de longitud. Se utilizaron los 61 niveles verticales de los datos del reanálisis, de 0.1 a 1000 hPa, con aproximadamente 14 niveles por debajo de 1500 m y 23 entre 1500 m y 5000 m. Estas partículas fueron rastreadas hacia adelante en el tiempo para las regiones oceánicas y hacia atrás para las regiones continentales, calculando de esta forma el campo ($E - P$) cada seis horas durante los diez días de transporte.

C. RESUMEN GENERAL

Con el fin de analizar si los cambios en las fuentes de humedad oceánicas afectan a la precipitación continental o ver el papel que juegan los patrones de teleconexión climática en la variabilidad de estas fuentes se hace uso de la **técnica de “composites”**. Esta técnica es una herramienta muy conveniente para ser utilizada en la construcción de una estimación del estado promedio de una variable condicionada por el valor de un índice externo. En este trabajo los “composites” se realizaron para los campos de precipitación ($E - P < 0$) resultantes de las salidas de FLEXPART considerando los años de las distintas fases (positivas y negativas) de los principales modos de variabilidad climática (ENSO, NAM y SAM) y para el conjunto de años con los valores más altos y más bajos de intensidad de la divergencia de flujo de humedad integrado en la vertical de las principales fuentes oceánicas. Una vez realizados los “composites” se substrajeron ambas muestras con el fin de buscar las diferencias entre sí. Se aplicó la prueba conocida como “bootstrap” (Wei et al., 2012) para dotar de significatividad estadística a las señales obtenidas, buscando siempre un nivel de confianza del 90% mediante la selección de dos periodos de una muestra al azar del cuartil inferior y superior del conjunto de años, permutando la serie de tiempo original 1000 veces. (En la Sección 3.5 de esta tesis y en los artículos que la constituyen se hace una descripción más detallada del método).

Como se comenta en el párrafo anterior, con el propósito de evaluar los **cambios en intensidad de las principales fuentes oceánicas de humedad** se analizaron las diferencias entre los “composites” de los cinco episodios con mayor intensidad y aquellos de menor intensidad. Cinco años para el cálculo de cada uno de los “composites” representa el cuartil superior e inferior del conjunto de 21 años total para el período de 1980 a 2000. El estudio se realizó para cada una de las doce fuentes de humedad oceánica para el verano (junio-julio-agosto, JJA) e invierno boreal (diciembre-enero-febrero, DEF). Los valores de la divergencia de flujo de humedad integrado en la vertical para cada fuente y cada año se muestran en la Tabla 3.5 para JJA y en la Tabla 3.6 para DEF.

De igual manera con el objetivo de analizar la **influencia del ciclo ENSO en el transporte de humedad de las principales fuentes oceánicas**, se calcularon las diferencias entre los “composites” de los años de las fases positivas y negativas de ENSO. El índice utilizado para definir ENSO fue ONI de la NOAA/CPC en la región del Niño 3.4 (5°N-5°S, 120°W-170°W) (Smith et al., 2008). Para este análisis se tomó el período

comprendido entre 1980-2012, por lo tanto, el cuartil del conjunto de años seleccionados estuvo representado por los ocho episodios de más alta intensidad para El Niño y los ocho de menor intensidad para La Niña. Hay que destacar que se asumieron los límites de cada fuente oceánica (Figura 3.1) de forma estacionaria durante los años considerados. Además para comparar los resultados obtenidos se calcularon las diferencias entre los “*composites*” mensuales para la precipitación y la divergencia de flujo de humedad integrado en la vertical entre las fases opuestas de ENSO.

La **influencia de los modos de variabilidad anulares hemisféricos**, como son NAM y SAM (por sus siglas en inglés), **en el transporte de humedad de las principales fuentes oceánicas** se exploró, siguiendo la misma técnica de diferencia de “*composites*” que para ENSO. Los eventos positivos y negativos fueron seleccionados en base a los índices mensuales de NAM y SAM (NAMI y SAMI). Los modos NAM y SAM son más activos durante los inviernos de sus hemisferios respectivos (de diciembre a febrero para NAM y de junio a agosto para SAM), por lo tanto se eligió el período semestral correspondiente para realizar el análisis, es decir, de noviembre a abril para NAM y de mayo a octubre para SAM. El NAMI está definido como la diferencia del promedio mensual normalizado de la presión a nivel del mar entre 35° N y 65° N, y SAMI entre 40° S y 70° S (Li y Wang, 2003; Nan y Li, 2003, respectivamente). Los “*composites*” consideran los seis episodios de intensidad más altos para las dos fases de cada modo para el período de noviembre 1979 a octubre 2012. También se calcularon las diferencias entre los “*composites*” mensuales para la precipitación y la divergencia de flujo de humedad integrado en la vertical entre las fases positiva y negativa para los dos modos hemisféricos.

La **influencia de los principales modos de variabilidad global (ENSO) y hemisféricos (NAM y SAM)** también se analizó para las **fuentes de humedad asociadas a las regiones climáticas continentales**. Se evaluaron las diferencias entre los “*composites*” de las ocho fases extremas de cada modo (que representan el cuartil inferior y superior del conjunto de años) para el período 1980-2012. Para ENSO y utilizando el índice ONI de Smith et al. (2008) se usaron los periodos semestrales de octubre a marzo (ONDEFM) y de abril a septiembre (AMJJAS). Para comprobar la modulación de NAM en las fuentes de humedad se utilizó el índice NAMI calculado para el invierno boreal de diciembre a marzo (DEFM; Hurrell, 1995; Hurrell et al., 2013). Para examinar la modulación de SAM en las fuentes de humedad se utilizó el índice SAMI para el

C. RESUMEN GENERAL

invierno austral desde agosto a noviembre (ASON; Marshall, 2003).

C.4 Colección de Publicaciones

Las cuestiones científicas anteriores se respondieron en cinco artículos que forman la parte esencial de esta tesis.

Para analizar la precipitación continental que se genera a partir de la evaporación en el océano se ha de separar el campo de precipitación del de evaporación en las salidas del modelo FLEXPART, es decir, han de separarse los valores de $(E - P < 0)$, que llamaremos “precipitación”, de los de $(E - P > 0)$, que llamaremos “evaporación”, en el campo final del balance del flujo de agua dulce $(E - P)$. Hasta el comienzo de esta investigación los análisis que se habían realizado habían abordado siempre el problema eliminando el término evaporativo al final del cómputo, representando el campo de la precipitación siempre como mínimo en base anual. Dado que parte de los trabajos realizados aquí se necesitaba hacer estudios desde la escala temporal mensual, surgió la cuestión de si la eliminación mes a mes podía influir en los resultados finales cuando se hicieran estudios estacionales o anuales. La búsqueda del momento en el cual se pueden eliminar los valores de evaporación en la integración del campo de $(E - P)$ llevó a la publicación del primer artículo presentado en esta tesis *(1) Estimating the temporal domain when the discount of the net evaporation term affects the resulting net precipitation pattern in the moisture budget using a 3-D lagrangian approach*, por R. Castillo, R. Nieto, A. Drumond y L. Gimeno (2014a) y que se publicó en la revista PlosOne.

El título del segundo artículo que se presenta es *(2) Influence of the intensification of the major oceanic moisture sources on continental precipitation*, por L. Gimeno, R. Nieto, A. Drumond, R. Castillo y R. Trigo (2013), publicado en Geophysical Research Letters. Este trabajo aborda dos cuestiones clave del ciclo hidrológico: (i) el impacto del cambio climático en el transporte de la humedad y, en particular, (ii) los efectos de los cambios en la intensidad de la fuente (es decir, más evaporación) en la distribución de la precipitación continental.

El impacto de los modos de variabilidad climática en la precipitación continental generada a partir de la evaporación procedente de las principales fuentes oceánicas de humedad se analiza en dos artículos: *(3) The role of the ENSO cycle in the modulation*

of moisture transport from major oceanic moisture sources, por R. Castillo, R. Nieto, A. Drumond y L. Gimeno (2014b) publicado en Water Resources Research, y en **(4) *The modulation of oceanic moisture transport by the hemispheric annular modes***, por R. Nieto, R. Castillo y A. Drumond (2014a) publicado en Frontiers in Earth Science.

Por último, y en vista del hecho de que existen otras regiones fuentes de humedad para las regiones continentales diferentes de las regiones oceánicas que presentan los máximos de divergencia de flujo de humedad integrado en la vertical (Figura 3.1), se realizó el análisis de las fuentes de humedad para las regiones climáticas continentales de la manera más completa posible. Se seleccionaron dos grupos de regiones climáticas continentales: uno basado en regiones con un promedio climático similar para finales del siglo XX y proyecciones de cambios similares en la precipitación a finales del siglo XXI (Figura 3.4), y el otro con las regiones utilizadas en los informes de evaluación del IPCC (Figura 3.5). Debido a que suman más de 50 regiones continentales a analizar, los resultados se presentan a la comunidad científica en forma de un catálogo publicado de modo libre “*on-line*”. Con el fin de mostrar el contenido del catálogo, este se ilustró con una región ejemplo en la nota técnica **(5) *A catalog of moisture sources for continental climatic regions***, por R. Nieto, R. Castillo, A. Drumond y L. Gimeno (2014b), publicado en Water Resources Research.

La información suplementaria de los artículos **(2)** y **(3)** se puede encontrar en los Apéndices B.1 y B.2. Las figuras complementarias del artículo **(5)** se presentan en el Apéndice B.3. El catálogo completo de las fuentes de humedad para todas las regiones climáticas continentales se puede ver en <http://ephyslab.uvigo.es/tramo/ccrs/>.

C.5 Sumario y Conclusiones

A lo largo de esta tesis se abordan aspectos cruciales de la rama atmosférica del ciclo hidrológico, como la caracterización de las fuentes globales de humedad, la variabilidad interanual del transporte de la humedad, la distribución de la precipitación continental asociada a las principales fuentes oceánicas de humedad y el papel de los principales patrones de teleconexión (ENSO, NAM y SAM) en la variabilidad de las regiones de humedad. Este estudio se basa en una técnica lagrangiana, considerada como la más adecuada para evaluar el origen del agua que precipita en las áreas continentales y que es la mejor alternativa al tratamiento euleriano tradicional para el estudio de los procesos

C. RESUMEN GENERAL

dentro del ciclo del agua. Por otra parte, este trabajo ha permitido la identificación de las principales fuentes de humedad de regiones climáticas continentales, proporcionando una evaluación fiable y robusta de las relaciones fuente-sumidero en el ciclo atmosférico del agua para los climas regionales, que es un requisito para la comprensión de los principales factores que impulsan los fenómenos meteorológicos y climáticos extremos.

Siguiendo la secuencia de las publicaciones presentadas en la Sección 4, las conclusiones más importantes se presentan a continuación:

(1) Dominio temporal mínimo para la estimación de la precipitación asociada a una fuente oceánica

La estimación de la precipitación asociada a una fuente evaporativa necesita descartar el término de evaporación ($E - P > 0$), y esto se puede hacer después de que $(E - P)$ ha sido integrado, sin alterar los patrones generales de precipitación, cuando es descontado mes a mes o cuando se utilizan promedios anuales o climatológicos, es decir, utilizando una escala de tiempo mensual o mayor.

Este resultado es muy importante para esta tesis porque permite la caracterización y el estudio de la variabilidad de las principales fuentes globales de humedad desde escalas mensuales.

(2) Cuantificación de la contribución de las principales fuentes oceánicas de humedad a la precipitación continental

Utilizando el modelo FLEXPART para el cálculo de trayectorias hacia adelante en el tiempo se detectaron los sumideros continentales para la precipitación procedente de 12 fuentes principales de humedad oceánica. El análisis se amplió a 21 años de datos (1980-2000) en comparación con trabajos anteriores (Figura 3.1) para las estaciones de verano (JJA) e invierno (DEF). El uso de FLEXPART para la evaluación climatológica de las regiones fuentes de humedad oceánica y continentales ha demostrado ser consistente en las escalas regionales y globales (Gimeno et al., 2012). Los resultados obtenidos para un dominio temporal tan amplio permite la reevaluación de aquellos obtenidos por Gimeno et al. (2010a) que cubrían tan sólo 5 años, proporcionando resultados más sólidos.

Los resultados muestran que el suministro de la humedad oceánica hacia los continentes es muy asimétrico y específico para cada fuente oceánica y estación del año. Los

resultados más importantes relacionados con la contribución de las principales fuentes oceánicas de humedad a la precipitación continental se enumeran a continuación:

- En términos de influencia sobre la precipitación continental global, la fuente situada sobre el océano Atlántico Norte subtropical es la fuente dominante. Proporciona humedad para la precipitación sobre áreas muy extensas, especialmente durante el invierno boreal (DEF) cuando su influencia en longitud se extiende desde México hasta el este de Eurasia y en latitud desde las zonas del Ártico de Eurasia hasta el Amazonas, ya en el hemisferio Sur. La influencia del Atlántico Norte en Centroamérica y Suramérica se debe a la eficiencia en el transporte de humedad ligado a los sistemas de chorros en niveles bajos sobre la región. Entre ellos se encuentran el chorro del Caribe, de América del Sur y el chorro del Chocó que controlan la precipitación (principalmente durante el invierno boreal) sobre el centro de América, la zona tropical y subtropical de Suramérica al este de los Andes, y la costa Suramericana tropical del Pacífico, respectivamente. Sin embargo, su influencia sobre Eurasia se desvanece durante el verano.
- Las principales fuentes oceánicas no contribuyen directamente a la precipitación sobre grandes áreas continentales, incluyendo la mayoría de las regiones áridas del interior, aunque pueden hacerlo posteriormente a través del “*recycling*” local de humedad.
- Existen pequeñas fuentes oceánicas que proporcionan cantidades desproporcionadas de humedad en relación a su tamaño. Por ejemplo, el Mediterráneo es una fuente dominante de la humedad para Europa y el norte de África durante JJA, y el Mar Rojo ofrece una gran cantidad de humedad que precipita entre el Golfo de Guinea e Indochina durante JJA y entre los Grandes Lagos de África y Asia durante DEF.
- Hay un transporte significativo interhemisférico, con implicaciones para la precipitación continental desde la fuente del Atlántico Norte durante DEF y desde las fuentes de humedad más occidentales del océano Índico durante JJA.
- Es destacable también que la existencia de grandes regiones, entre las que se incluye Europa, América del Sur o Australia, que reciben humedad mayoritariamente desde una sola fuente; mientras que hay otras que son alimentadas de

C. RESUMEN GENERAL

humedad procedente de varias fuentes, como aquellas regidas por sistemas monzónicos en la India, el África tropical y por el régimen cuasi-monzónico de las Grandes Llanuras de América del Norte.

Es evidente que no toda la precipitación que cae sobre los continentes se origina en las doce fuentes principales de humedad oceánica y que existe una fracción de ésta que tiene su origen en las regiones oceánicas no incluidas en la definición de fuentes principales de humedad (áreas oceánicas blancas en la Figura 3.1), como asimismo no está incluido el “*recycling*” local continental (Gimeno et al., 2012). De la inspección del papel desempeñado por el resto de las áreas oceánicas (Figura B.1) se observa que su contribución se limita a una estrecha franja tropical y a dos grandes bandas en latitudes altas, siendo moderadamente relevantes durante el invierno boreal sobre el norte de Europa y América del Norte.

(3) Intensificación de las principales fuentes oceánicas de humedad y su contribución a la precipitación continental

Uno de los principales objetivos de este estudio fue evaluar el efecto de los cambios en la intensidad de las fuentes de humedad en la distribución de la precipitación continental vinculada a cada una de ellas. Es conocido que las fuentes de humedad no son estacionarias en intensidad, variando de un año para otro y también que se espera que sufran importantes cambios en el futuro. El periodo más amplio que se emplea en este estudio (1980-2000) permite realizar un análisis de sensibilidad sobre la influencia del cambio en intensidad de las fuentes (períodos con mayor o menor valor del campo de $E - P$) sobre el transporte de humedad desde las regiones de evaporación oceánica hasta las regiones continentales donde se produce la precipitación (análisis que no era posible realizar en el trabajo previo de Gimeno et al. [2010a]). Las diferencias en $(E - P)$ entre el promedio de los cinco episodios de mayor y menor intensidad fueron calculados para cada fuente durante el invierno (DEF) y verano (JJA) (Figura 1 en Gimeno et al. [2013], página 43 de esta tesis). Los resultados más destacables se resumen a continuación:

- En ambas estaciones del año la precipitación tiende a aumentar a lo largo de la banda tropical cuando las fuentes se intensifican.
- Las fuentes oceánicas subtropicales contribuyen más al aumento de las precipitaciones en la parte central y occidental de las cuencas oceánicas correspondientes,

mientras que la intensificación observada en el Pacífico tropical oriental se debe a la humedad transportada desde la fuente de humedad del Golfo de México-Mar Caribe.

- El aumento de las precipitaciones asociadas con circulaciones monzónicas más intensas es evidente durante DEF para el monzón de América del Sur (desde la fuente del Atlántico Norte), lo que confirma el papel del transporte de humedad que cruza la banda ecuatorial durante eventos monzónicos intensos sobre la cuenca del Amazonas.
- Se evidencia el papel del incremento del transporte de humedad desde el Mar de Arabia en la intensificación de la precipitación asociada con los monzones de verano de Asia y de la India.
- La mayor disponibilidad de humedad sobre la fuente del Caribe durante el verano boreal (JJA) influye en la precipitación sobre Norteamérica a través del sistema monzónico que regula la circulación local.
- No se han encontrado modificaciones importantes en la precipitación en latitudes altas debido a cambios en intensidad de las fuentes principales de humedad que las afectan. Esto sugiere que el principal proceso responsable del esperado aumento de precipitación en estas latitudes puede responder más a cuestiones dinámicas.

(4) Fuentes oceánicas de precipitación continental vinculadas al cambio climático

Las modificaciones en la circulación atmosférica debidas al calentamiento global dará lugar a cambios en la circulación entre las fuentes y sumideros de humedad, redirigiendo la humedad de diferente manera. La identificación de aquellas zonas más propensas a cambios significativos de $(E - P)$ en las próximas décadas se obtuvo utilizando un “ensemble” de 15 modelos de circulación global utilizados por el IPCC AR4. Esto permite delimitar las regiones oceánicas donde es más probable que el cambio climático conduzca a un aumento en el flujo de agua dulce. Serán estas “hot spot sources regions” o HSSRs, por sus siglas en inglés, las fuentes oceánicas de análisis y se definen como aquellas áreas donde $(E - P)$ se ve incrementado, como mínimo, en 0.3 mm/día para el período 2046-2065 en comparación con el de 1961-2000, según lo predicho por el “ensemble” de los 15 modelos de circulación global. La definición de las HSSRs se

C. RESUMEN GENERAL

hace para el invierno y el verano boreal (Seager et al., 2010). Se toman estas HSSRs como fuentes de humedad y se identifican, usando el modelo lagrangiano FLEXPART hacia adelante en el tiempo, las regiones sumidero continentales para el periodo reciente de 1980-2000. Así se localizan aquellas áreas continentales que son potencialmente más vulnerables en términos de precipitación a los cambios en las fuentes evaporativas.

En general las zonas más afectadas por la precipitación procedente de la humedad de las HSSRs se dan en los océanos, pero existen regiones continentales afectadas altamente pobladas como América Central y del Norte, Europa y el Golfo de Guinea, que se encuentran actualmente bajo un estrés hídrico y que podrían en un futuro verlo reducido.

Los hallazgos más relevantes asociados a estas áreas oceánicas vinculados al cambio climático se describen con más detalle a continuación.

- En el hemisferio norte durante el invierno, dos de las HSSRs tienen una influencia más amplia que las demás. Se trata de la situada en el centro del Atlántico Norte que influye en la precipitación en Europa y América del Sur, y la otra en el oeste subtropical del Pacífico Norte que influye en la precipitación de América del Norte y del sudeste del continente Asiático. La HSSR situada en el Mediterráneo, de pequeño tamaño en relación a las demás, tiene una fuerte influencia sobre la precipitación en Europa. En esta estación, América del Norte es la región continental más afectada, siendo directamente influida por cuatro HSSRs diferentes: la del Caribe, la de la costa del Pacífico mexicano tropical, la del oeste subtropical del Pacífico Norte y la del centro del Atlántico Norte.
- En el hemisferio sur durante el invierno las dos regiones más afectadas por los cambios en $(E - P)$ se sitúan en Centro y Norteamérica, que reciben humedad para la precipitación desde el HSSR situado sobre el “*warm pool*” del Atlántico, y la otra es el Sahel, afectada por la fuente de humedad cercana al Golfo de Guinea. Las dos HSSRs situadas en el Océano Índico tienen un efecto moderado en las áreas continentales circundantes: la HSSR al sur de la Bahía de Bengala influye en la Península de Malasia, mientras que la HSSR cerca de la Corriente de Agulhas proporciona humedad para la costa este de África y el subcontinente Indio. Finalmente, la HSSR del Pacífico situada al este de Australia afecta a la mitad oriental del continente.

(5) El papel de los principales modos de variabilidad en el transporte de humedad

La fluctuación natural más fuerte del clima global a escala interanual es el fenómeno de El Niño-Oscilación del Sur (ENSO). Este es un modo acoplado océano-atmósfera con su núcleo de actividad principal en el Pacífico tropical, pero con importantes impactos climáticos regionales en todo el mundo. A escala hemisférica y en extratropicos son los modos anulares los principales modos de variabilidad climática interanual y deben su existencia a la dinámica interna de la atmósfera en latitudes medias. Por estos motivos en este apartado se analizan aquí los efectos de ENSO y de los Modos Anulares del Norte (NAM) y del Sur (SAM).

Son conocidos los cambios en la circulación atmosférica asociados a ENSO, NAM y SAM, por lo que cabe esperar cambios significativos en el transporte de humedad, y por lo tanto, en la cantidad de humedad precipitable en regiones continentales asociada a estos modos.

El Niño-Oscilación del Sur (ENSO)

La influencia de la evolución del ciclo ENSO (desde junio a mayo) en el transporte de humedad desde las principales fuentes oceánicas se investigó utilizando las diferencias de los “*composites*” mensuales entre los ocho episodios de mayor intensidad de El Niño (fase positiva) y de La Niña (fase negativa).

En primer lugar se hizo el análisis definiendo como fuentes oceánicas de humedad las mismas doce que habían sido identificadas en Gimeno et al. (2013), es decir, no se supone que ENSO produzca cambios en la extensión de las fuentes (Figura 3.1). Al analizar las diferencias entre los “*composites*” de ambas fases se encuentra que:

- En términos generales, los cambios en los sumideros de humedad coinciden con los patrones conocidos de variación del transporte vertical de humedad integrado en la vertical observados con ENSO. Tales variaciones incluyen las observadas durante las lluvias ecuatoriales del Pacífico, los principales sistemas monzónicos de verano y las lluvias subtropicales.
- Durante la etapa de madurez de ENSO (DEF) con los años de El Niño se incrementan las contribuciones de humedad desde las fuentes del SPAC, NPAC, MEXCAR y CORALS hacia el Pacífico ecuatorial. Mientras, durante la Niña son

C. RESUMEN GENERAL

las fuentes del IND, NPAC y SPAC las que contribuyen más a la región occidental del Pacífico ecuatorial. Este patrón reproduce la característica conocida como “*see-saw*” asociada con ENSO sobre esta región.

- Las zonas subtropicales reciben más humedad de las fuentes más cercanas durante El Niño, por ejemplo, el sur de América del Norte desde las fuentes del NATL y MEXCAR, América del Sur desde SATL y SPAC, o el África meridional desde IND, AGU y ZAN.
- El régimen monzónico de la India muestra una inhibición en la convergencia de humedad y, por tanto, en la precipitación asociada con la falta de evaporación desde sus típicas fuentes de humedad durante los episodios de El Niño. Sin embargo, de junio a noviembre, la región actúa como sumidero para la humedad procedente de las fuentes del IND, ZAN y ARAB durante La Niña, y la convergencia se ve favorecida.

Cuando las áreas de las fuentes se redefinen de acuerdo con la fase de ENSO, la mayoría de ellas permanecen estacionarias, pero cuatro de ellas muestran diferencias notables en su extensión. Dos de ellas están más involucradas en la región de ocurrencia de ENSO: la del Pacífico Sur (SPAC) y la del Mar de Coral (CORALS) en el oeste del Océano Pacífico. Las otras dos son la fuente del Golfo de México-Mar del Caribe (MEXCAR) en el Océano Atlántico y la fuente sobre el Mar de Arabia (ARAB) en el Océano Índico. Para estas cuatro regiones se volvieron a calcular los sumideros de humedad asociados a ellas con las nuevas áreas de ocurrencia para ambas fases de ENSO. Los resultados de la comparativa con los resultados de cuando las fuentes se consideraban estacionarias se comentan a continuación:

- La reducción en tamaño de la fuente SPAC durante los eventos El Niño implica un menor transporte de humedad hacia Indonesia en comparación con el transporte de humedad cuando la fuente se considera estacionaria.
- Durante La Niña se produce una reducción en el tamaño de la fuente CORALS y se observa un confinamiento del transporte de humedad hacia el Pacífico occidental, que extiende su influencia hacia Indonesia y el Pacífico Central.

- Se detecta un desplazamiento hacia el norte de MEXCAR durante La Niña y una reducción asociada en el transporte de humedad hacia la ITCZ del Pacífico.
- Se observa una expansión de la fuente de ARAB hacia la costa de África oriental durante La Niña asociado con un incremento en el transporte de humedad hacia el Océano Índico, en particular durante los meses de DEFM.

Modo Anular del Norte (NAM)

La huella de NAM en el transporte de humedad desde las principales fuentes oceánicas se evaluó mediante las diferencias entre los “*composites*” mensuales de los seis episodios con el índice más alto y bajo del modo. Se analiza el semiaño invernal para el hemisferio norte, es decir, de noviembre a abril (NDEFMA).

Considerando las fuentes principales de humedad oceánicas estacionarias se observa que:

- Para la fuente del Pacífico Norte (NPAC) hay un incremento del transporte de humedad hacia el noreste de la propia cuenca oceánica para los valores bajos del índice NAM. Esto se debe al debilitamiento de las altas presiones del Pacífico y a los vientos del oeste más débiles en latitudes polares. Bajo estas condiciones, las trayectorias de las tormentas tienden hacia latitudes tropicales, afectando al noroeste de América del Norte.
- Para los valores altos del índice de NAM se espera una intensificación de las altas presiones en el Pacífico y, por lo tanto, el transporte de humedad desde NPAC se ve favorecido hacia el este de Asia. El monzón de Asia oriental que caracteriza el patrón de precipitación de la región no está favorecido durante el invierno, sin embargo, existe una interacción significativa con el alta de Siberia, la cual es modulada en intensidad por NAM. Por lo tanto, NAM juega un papel importante en los cambios de la alta Siberiana, a través de una correlación positiva en los valores bajos del índice de NAM (NAMI) relacionados con una menor intensidad de la alta siberiana. Este hecho favorece así la llegada de humedad del océano.
- Sobre la región del Océano Atlántico Norte los años con los valores más bajos de NAMI se caracterizan por presiones atmosféricas más bajas de lo normal y vientos del oeste débiles sobre el norte de Europa. Esta configuración incrementa

C. RESUMEN GENERAL

el transporte de humedad desde las fuentes del NATL, MEXCAR y MED hacia el sur de Europa y la cuenca mediterránea. Lo contrario ocurre para años con un alto índice de NAM, cuando la humedad es transportada hacia el Norte a través de Europa y, por lo tanto, pueden ocurrir eventos de sequías en la parte sur del continente europeo.

- La intensificación de las altas presiones del Atlántico y de los vientos alisios asociados a los años más intensos de NAM provocan un incremento en el transporte de humedad desde las fuentes NATL y MEXCAR hacia la región del Mar Caribe. El flujo es entonces intensificado, formando el chorro de niveles bajos del Caribe (CLLJ) que se divide en dos ramas, una sigue su camino hacia el oeste a través de América Central y la otra gira hacia el norte en dirección a América del Norte cruzando el Golfo de México. La señal observada en el campo de precipitación durante esta fase de NAM concuerda con la variabilidad del CLLJ y las características de los patrones de transporte de humedad sobre la zona. Por consiguiente, valores altos (bajos) de NAM se asocian con un incremento (debilitamiento) en el transporte de humedad que genera precipitación desde las fuentes del NATL y MEXCAR en América Central y del Norte a través del CLLJ.
- La intensificación o debilitamiento del sistema de altas presiones del Atlántico podría estar también relacionada con la variabilidad interanual encontrada para las fuentes de humedad del MED y del NATL cuando se analiza la divergencia de humedad integrada en la vertical.
- Debido a que los centros de actividad de NAM ocurren principalmente sobre las cuencas más grandes de los océanos del hemisferio norte y entorno a las latitudes medias y altas, las fuentes del Mar Rojo (REDS) y Mar Árabe (ARAB) parecen poco afectadas por las diferentes fases del modo.

Modo Anular del Sur (SAM)

El impacto de SAM se analizó para el período comprendido entre los meses de mayo y octubre, que corresponde con el invierno austral extendido (o semiaño austral). Se calcularon las diferencias entre los “*composites*” mensuales de los seis episodios de intensidad más altos y bajos. Cuando los límites de las fuentes principales de humedad se consideran estacionarias los resultados muestran que:

- Durante los valores más altos del índice de SAM, con sistemas de altas presiones más fuertes de lo normal, el cinturón de vientos del oeste y los alisios intensificados y la ITCZ posicionada más al norte, la humedad es transportada más hacia el sur y al este desde las fuentes de AGU, IND y SATL que durante la fase negativa del modo. Por lo tanto, en la parte sur de la cuenca del Océano Índico aparece una banda horizontal de precipitación con humedad originaria de la fuente AGU, y pequeñas áreas con origen en la fuente IND.
- Sobre Australia las fases positivas de SAM incrementan el aporte de humedad desde la fuente del Mar de Coral (CORALS) durante los meses finales del periodo de estudio.
- Los años de fase positiva del modo también se caracterizan por un incremento en la precipitación sobre la región del “*warm pool*” del Océano Índico y Pacífico Occidental desde las fuentes de CORALS y SPAC.
- Durante las fases positivas de SAM, la configuración de altas presiones alrededor de Australia dirigen la humedad hacia el norte desde la fuente CORALS y luego los vientos alisios la advectan hacia el oeste con mayor intensidad. Los vientos alisios intensificados traen humedad hacia la región desde la fuente SPAC, que desaparece para los valores más bajos del índice de SAM cuando los vientos alisios son menos intensos.
- Sobre el Océano Atlántico Sur cuando las altas presiones están intensificadas la fuente SATL mantiene el flujo de humedad hacia la Zona de Convergencia del Atlántico Sur (SACZ) y a la ITCZ. Se observa que durante los primeros meses del periodo de análisis los vientos alisios, que están intensificados, se introduce humedad al interior del continente (esta señal también es reconocible en el Pacífico, pero sólo sobre las islas) y la SACZ recibe más humedad durante los meses posteriores.
- El sureste de América del Sur recibe más humedad de las fuentes SATL, AGU y SPAC durante los años con menor índice de SAM. Estos resultados concuerdan con el movimiento de los ciclones hacia el norte durante esta fase de SAM y con que América del Sur sufre de una intensa actividad frontogenética asociada con anomalías positivas de precipitación sobre la parte sureste del continente.

C. RESUMEN GENERAL

- El debilitamiento de los vientos del oeste y de los vientos alisios para valores más bajos del índice de SAM favorece la llegada de humedad desde SATL durante el monzón en África.
- La variación de ZAN con SAM no parece relevante, tal vez debido al hecho de que se encuentra localizada sobre la región ecuatorial donde no llega la influencia del modo.

(6) *Fuentes de humedad para las regiones climáticas continentales*

Al final de esta investigación se analizan las fuentes de humedad de la manera más completa posible para dos conjuntos de regiones climáticas continentales (CCRs). La identificación y caracterización de las fuentes de humedad y su variabilidad será en los próximos años un punto de partida importante para las evaluaciones climáticas regionales y globales, incluidas las reconstrucciones paleoclimáticas y la interpretación de las salidas de los modelos de cambio climático. La realización de un análisis detallado para un número amplio de regiones climáticas servirá como una fuente sólida de información para estos estudios. La regionalización del primer conjunto de regiones climáticas analizadas (Figura 3.4) está basada en un cambio futuro homogéneo en la precipitación definida por Mahlstein y Knutti (2010) y la del segundo conjunto (Figura 3.5) está basada en el clima homogéneo actual establecido por Giorgi y Francisco (2000). Los resultados sobre las fuentes de humedad para todas las regiones climáticas están disponibles en forma de catálogo libremente “on-line” en la página web <http://ephyslab.uvigo.es/tramo/ccrs/>. Para cada región continental se analizan seis ítems para comprender las fuentes de humedad asociadas a cada una de ellas. A continuación se describe cada uno de estos ítems:

- (i) Se identifican las fuentes de humedad para cada región en base anual y estacional. Se presentan los campos de $(E - P)$ para cada día hacia atrás en el tiempo $(E - P)_n$, siendo $n=1$ a $n=10$, y el valor de $(E - P)$ integrado durante los 10 días de transporte analizados, $(E - P)_{1-10}$.
- (ii) Se evalúa la importancia de cada fuente de humedad detectada a lo largo de los 10 días de transporte hacia atrás en el tiempo. Se cuantifica día a día la serie de $(E - P)_n$ para ver la contribución diaria de la fuente sobre cada sumidero.

- (iii) Se presenta el ciclo anual de la contribución de las fuentes de humedad a la precipitación en las regiones destino. Se cuantifican las series $(E - P)$ de la contribución media mensual de cada fuente de humedad.
- (iv) Se analiza la variabilidad interanual de la contribución de las fuentes de humedad del campo $(E - P)$ para las regiones destino.
- (v) Se evalúa el rol de los principales modos de variabilidad climática global. El catálogo ofrece un análisis del papel de El Niño-Oscilación del Sur (ENSO) y los Modos Anulares del Norte y del Sur (NAM y SAM). Para esto se calculan las diferencias entre los “*composites*” de los ocho años extremos de cada modo.
- (vi) Se identifican las zonas oceánicas que se verán influidas más por los cambios climáticos futuros en evaporación menos precipitación y que afectan a la región climática continental en concreto. Sólo se seleccionan aquellas HSSRs que afectan a cada región destino para detectar las áreas continentales potencialmente vulnerables ante cambios futuros y ver cómo éstas pueden afectarla.

References

- Adler, R. F., Huffman, G. J., Chang, A., Ferraro, R., Xie, P.-P., Janowiak, J., Rudolf, B., Schneider, U., Curtis, S., Bolvin, D., et al. (2003). The version 2 global precipitation climatology project (GPCP) monthly precipitation analysis (1979-present). *Journal of Hydrometeorology*, 4(6):1147–1167, doi:http://dx.doi.org/10.1175/1525-7541(2003)004<1147:TVGPCP>2.0.CO;2.
- Bengtsson, L., Hagemann, S., and Hodges, K. I. (2004). Can climate trends be calculated from reanalysis data? *Journal of Geophysical Research*, 109(D11111), doi:10.1029/2004JD004536.
- Benton, G. S. and Estoque, M. A. (1954). Water vapor transfer over the North American continent. *Journal of Meteorology*, 11(6):462–477, doi:http://dx.doi.org/10.1175/1520-0469(1954)011<0462:WVTOTN>2.0.CO;2.
- Bosilovich, M. G. and Schubert, S. D. (2002). Water vapor tracers as diagnostics of the regional hydrologic cycle. *Journal of Hydrometeorology*, 3(2):149–165, doi:http://dx.doi.org/10.1175/1525-7541(2002)003<0149:WVTADO>2.0.CO;2.
- Brubaker, K. L., Dirmeyer, P. A., Sudrajat, A., Levy, B. S., and Bernal, F. (2001). A 36-yr climatological description of the evaporative sources of warm-season precipitation in the Mississippi River basin. *Journal of Hydrometeorology*, 2(6):537–557, doi:http://dx.doi.org/10.1175/1525-7541(2001)002<0537:AYCDOT>2.0.CO;2.
- Brubaker, K. L., Entekhabi, D., and Eagleson, P. (1993). Estimation of continental precipitation recycling. *Journal of Climate*, 6(6):1077–1089, doi:http://dx.doi.org/10.1175/1520-0442(1993)006<1077:EOCPR>2.0.CO;2.

REFERENCES

- Budyko, M. I. (1974). *Climate and life*. 508 pp., Academic Press, New York.
- Burde, G. and Zangvil, A. (2001a). The estimation of regional precipitation recycling. Part I: Review of recycling models. *Journal of Climate*, 14(12):2497–2508, doi:[http://dx.doi.org/10.1175/1520-0442\(2001\)014<2497:TEORPR>2.0.CO;2](http://dx.doi.org/10.1175/1520-0442(2001)014<2497:TEORPR>2.0.CO;2).
- Burde, G. and Zangvil, A. (2001b). The estimation of regional precipitation recycling. Part II: A new recycling model. *Journal of Climate*, 14(12):2509–2527, doi:[http://dx.doi.org/10.1175/1520-0442\(2001\)014<2509:TEORPR>2.0.CO;2](http://dx.doi.org/10.1175/1520-0442(2001)014<2509:TEORPR>2.0.CO;2).
- Castillo, R., Nieto, R., Drumond, A., and Gimeno, L. (2014a). Estimating the Temporal Domain when the Discount of the Net Evaporation Term Affects the Resulting Net Precipitation Pattern in the Moisture Budget Using a 3-D Lagrangian Approach. *PloS one*, 9(6):e99046, doi:10.1371/journal.pone.0099046.
- Castillo, R., Nieto, R., Drumond, A., and Gimeno, L. (2014b). The role of the ENSO cycle in the modulation of moisture transport from major oceanic moisture sources. *Water Resources Research*, 50(2):1046–1058, doi:10.1002/2013WR013900.
- Coplen, T. B., Neiman, P. J., White, A. B., Landwehr, J. M., Ralph, F. M., and Dettinger, M. D. (2008). Extreme changes in stable hydrogen isotopes and precipitation characteristics in a landfalling Pacific storm. *Geophysical Research Letters*, 35(L21808), doi:10.1029/2008GL035481.
- D’Abreton, P. and Tyson, P. (1995). Divergent and non-divergent water vapour transport over southern Africa during wet and dry conditions. *Meteorology and Atmospheric Physics*, 55(1-2):47–59, doi:10.1007/BF01029601.
- Davison, A. C. and Hinkley, D. V. (1997). *Bootstrap methods and their application*. Vol. 1, 594 pp., Cambridge University Press.
- Dee, D., Uppala, S., Simmons, A., Berrisford, P., Poli, P., Kobayashi, S., Andrae, U., Balmaseda, M., Balsamo, G., Bauer, P., Bechtold, P., Beljaars, A., van de Berg, L., Bidlot, J., Bormann, N., Delsol, C., Dragani, R., Fuentes, M., Geer, A., Haimberger, L., Healy, S., Hersbach, H., Hólm, E., Isaksen, L., Kållberg, P., Köhler, M., Matri-cardi, M., McNally, A., Monge-Sanz, B., Morcrette, J.-J., Park, B.-K., Peubey, C., de Rosnay, P., Tavolato, C., Thépaut, J.-N., and Vitart, F. (2011). The ERA-Interim

REFERENCES

- reanalysis: Configuration and performance of the data assimilation system. *Quarterly Journal of the Royal Meteorological Society*, 137(656):553–597, doi:10.1002/qj.828.
- Dirmeyer, P. A. and Brubaker, K. L. (1999). Contrasting evaporative moisture sources during the drought of 1988 and the flood of 1993. *Journal of Geophysical Research*, 104(D16):19383–19397, doi:10.1029/1999JD900222.
- Dirmeyer, P. A. and Brubaker, K. L. (2006). Evidence for trends in the Northern Hemisphere water cycle. *Geophysical Research Letters*, 33(L14712), doi:10.1029/2006GL026359.
- Dirmeyer, P. A. and Brubaker, K. L. (2007). Characterization of the global hydrologic cycle from a back-trajectory analysis of atmospheric water vapor. *Journal of Hydrometeorology*, 8(1):20–37, doi:http://dx.doi.org/10.1175/JHM557.1.
- Dominguez, F., Kumar, P., Liang, X.-Z., and Ting, M. (2006). Impact of atmospheric moisture storage on precipitation recycling. *Journal of Climate*, 19(8):1513–1530, doi:http://dx.doi.org/10.1175/JCLI3691.1.
- Drumond, A., Nieto, R., Gimeno, L., and Ambrizzi, T. (2008). A Lagrangian identification of major sources of moisture over Central Brazil and La Plata Basin. *Journal of Geophysical Research*, 113(D14128), doi:10.1029/2007JD009547.
- Durán-Quesada, A. M., Gimeno, L., Amador, J., and Nieto, R. (2010). Moisture sources for Central America: Identification of moisture sources using a Lagrangian analysis technique. *Journal of Geophysical Research*, 115(D05103), doi:10.1029/2009JD012455.
- Efron, B. (2003). Second thoughts on the bootstrap. *Statistical Science*, 18(2):135–140, doi:10.1214/ss/1063994968.
- Efron, B. and Tibshirani, R. J. (1994). *An introduction to the bootstrap*. Vol. 57, 436 pp., CRC Press, London.
- Eltahir, E. A. and Bras, R. L. (1994). Precipitation recycling in the Amazon basin. *Quarterly Journal of the Royal Meteorological Society*, 120(518):861–880, doi:10.1002/qj.49712051806.

REFERENCES

- Gat, J. and Carmi, I. (1970). Evolution of the isotopic composition of atmospheric waters in the Mediterranean Sea area. *Journal of Geophysical Research*, 75(15):3039–3048, doi:10.1029/JC075i015p03039.
- Gimeno, L., Drumond, A., Nieto, R., Trigo, R. M., and Stohl, A. (2010a). On the origin of continental precipitation. *Geophysical Research Letters*, 37(L13804), doi:10.1029/2010GL043712.
- Gimeno, L., Nieto, R., Drumond, A., Castillo, R., and Trigo, R. (2013). Influence of the intensification of the major oceanic moisture sources on continental precipitation. *Geophysical Research Letters*, 40(7):1443–1450, doi:10.1002/grl.50338.
- Gimeno, L., Nieto, R., Trigo, R. M., Vicente-Serrano, S. M., and López-Moreno, J. I. (2010b). Where does the Iberian Peninsula moisture come from? An answer based on a Lagrangian approach. *Journal of Hydrometeorology*, 11(2):421–436, doi:http://dx.doi.org/10.1175/2009JHM1182.1.
- Gimeno, L., Stohl, A., Trigo, R. M., Dominguez, F., Yoshimura, K., Yu, L., Drumond, A., Durán-Quesada, A. M., and Nieto, R. (2012). Oceanic and terrestrial sources of continental precipitation. *Reviews of Geophysics*, 50(RG4003), doi:10.1029/2012RG000389.
- Giorgi, F. and Francisco, R. (2000). Uncertainties in regional climate change prediction: A regional analysis of ensemble simulations with the HADCM2 coupled AOGCM. *Climate Dynamics*, 16(2-3):169–182, doi:10.1007/PL00013733.
- Gong, D. and Wang, S. (1999). Definition of Antarctic oscillation index. *Geophysical Research Letters*, 26(4):459–462, doi:10.1029/1999GL900003.
- Held, I. M. and Soden, B. J. (2006). Robust responses of the hydrological cycle to global warming. *Journal of Climate*, 19(21):5686–5699, doi:http://dx.doi.org/10.1175/JCLI3990.1.
- Ho, M., Kiem, A., and Verdon-Kidd, D. (2012). The Southern Annular Mode: A comparison of indices. *Hydrology and Earth System Sciences*, 16(3):967–982, doi:10.5194/hess-16-967-2012.

REFERENCES

- Huffman, G. J., Adler, R. F., Bolvin, D. T., and Gu, G. (2009). Improving the global precipitation record: GPCP version 2.1. *Geophysical Research Letters*, 36(L17808), doi:10.1029/2009GL040000.
- Hurrell, J. W. (1995). Decadal trends in the North Atlantic Oscillation: Regional temperatures and precipitation. *Science*, 269(5224):676–679, doi:10.1126/science.269.5224.676.
- Hurrell, J. W. et al. (2013). The Climate Data Guide: Hurrell North Atlantic Oscillation (NAO) Index (Station Based). Retrieved from <https://climatedataguide.ucar.edu/climate-data/hurrell-north-atlantic-oscillation-nao-index-station-based>.
- Joussaume, S., Sadourny, R., and Jouzel, J. (1984). A general circulation model of water isotope cycles in the atmosphere. *Nature*, 311(5981):24–29, doi:10.1038/311024a0.
- Kalnay, E., Kanamitsu, M., Kistler, R., Collins, W., Deaven, D., Gandin, L., Iredell, M., Saha, S., White, G., Woollen, J., Zhu, Y., Leetmaa, A., Reynolds, R., Chelliah, M., Ebisuzaki, W., Higgins, W., Janowiak, J., Mo, K., Ropelewski, C., Wang, J., Jenne, R., and Joseph, D. (1996). The NCEP/NCAR 40-year reanalysis project. *Bulletin of the American Meteorological Society*, 77(3):437–471, doi:http://dx.doi.org/10.1175/1520-0477(1996)077<0437:TNYRP>2.0.CO;2.
- Knippertz, P., Wernli, H., and Gläser, G. (2013). A global climatology of tropical moisture exports. *Journal of Climate*, 26(10):3031–3045, doi:http://dx.doi.org/10.1175/JCLI-D-12-00401.1.
- Koster, R., Jouzel, J., Suozzo, R., Russell, G., Broecker, W., Rind, D., and Eagleson, P. (1986). Global sources of local precipitation as determined by the NASA/GISS GCM. *Geophysical Research Letters*, 13(2):121–124, doi:10.1029/GL013i002p00121.
- Li, J. and Wang, J. X. (2003). A modified zonal index and its physical sense. *Geophysical Research Letters*, 30(12):1632, doi:10.1029/2003GL017441.
- Lorenz, C. and Kunstmann, H. (2012). The hydrological cycle in three state-of-the-art reanalyses: Intercomparison and performance analysis. *Journal of Hydrometeorology*, 13(5):1397–1420, doi:http://dx.doi.org/10.1175/JHM-D-11-088.1.

REFERENCES

- Mahlstein, I. and Knutti, R. (2010). Regional climate change patterns identified by cluster analysis. *Climate Dynamics*, 35(4):587–600, doi:10.1007/s00382-009-0654-0.
- Marshall, G. J. (2003). Trends in the Southern Annular Mode from observations and reanalyses. *Journal of Climate*, 16(24):4134–4143, doi:http://dx.doi.org/10.1175/1520-0442(2003)016<4134:TITSAM>2.0.CO;2.
- Massacand, A. C., Wernli, H., and Davies, H. C. (1998). Heavy precipitation on the alpine southside: An upper-level precursor. *Geophysical Research Letters*, 25(9):1435–1438, doi:10.1029/98GL50869.
- Meehl, G. A., Covey, C., Taylor, K. E., Delworth, T., Stouffer, R. J., Latif, M., McAvaney, B., and Mitchell, J. F. (2007). The WCRP CMIP3 multimodel dataset: A new era in climate change research. *Bulletin of the American Meteorological Society*, 88(9):1383–1394, doi:http://dx.doi.org/10.1175/BAMS-88-9-1383.
- Nan, S. and Li, J. (2003). The relationship between the summer precipitation in the Yangtze River valley and the boreal spring Southern Hemisphere annular mode. *Geophysical Research Letters*, 30(24):2266, doi:10.1029/2003GL018381.
- Nieto, R., Castillo, R., and Drumond, A. (2014a). The modulation of oceanic moisture transport by the hemispheric annular modes. *Frontiers in Earth Science*, 2(11), doi:10.3389/feart.2014.00011.
- Nieto, R., Castillo, R., Drumond, A., and Gimeno, L. (2014b). A catalog of moisture sources for continental climatic regions. *Water Resources Research*, 50(6):5322–5328, doi:10.1002/2013WR013901.
- Nieto, R., Durán-Quesada, A. M., and Gimeno, L. (2010). Major sources of moisture for Antarctic ice-core sites identified through a Lagrangian approach. *Climate Research*, 40:45–49, doi:10.3354/cr00842.
- Nieto, R., Gallego, D., Trigo, R., Ribera, P., and Gimeno, L. (2008). Dynamic identification of moisture sources in the Orinoco basin in equatorial South America. *Hydrological Sciences Journal*, 53(3):602–617, doi:10.1623/hysj.53.3.602.

REFERENCES

- Nieto, R., Gimeno, L., and Trigo, R. M. (2006). A Lagrangian identification of major sources of Sahel moisture. *Geophysical Research Letters*, 33(L18707), doi:10.1029/2006GL027232.
- Numaguti, A. (1999). Origin and recycling processes of precipitating water over the Eurasian continent: Experiments using an atmospheric general circulation model. *Journal of Geophysical Research*, 104(D2):1957–1972, doi:10.1029/1998JD200026.
- Oki, T. (2005). The hydrologic cycles and global circulation. In *Encyclopedia of Hydrological Sciences*. Vol. 1, 656 pp., John Wiley and Sons Ltd., doi:10.1002/0470848944.hsa001.
- Ordóñez, P., Ribera, P., Gallego, D., and Peña-Ortiz, C. (2012). Major moisture sources for Western and Southern India and their role on synoptic-scale rainfall events. *Hydrological Processes*, 26(25):3886–3895, doi:10.1002/hyp.8455.
- Peixoto, J. P. and Oort, A. H. (1992). *Physics of climate*. 520 pp., American Institute of Physics, New York.
- Persson, A. and Grazzini, F. (2007). User Guide to ECMWF forecast products. *Meteorological Bulletin*, 3:153.
- Rozanski, K., Sonntag, C., and Münnich, K. (1982). Factors controlling stable isotope composition of European precipitation. *Tellus*, 34(2):142–150, doi:10.1111/j.2153-3490.1982.tb01801.x.
- Salati, E., Dall'Olio, A., Matsui, E., and Gat, J. R. (1979). Recycling of water in the Amazon basin: An isotopic study. *Water Resources Research*, 15(5):1250–1258, doi:10.1029/WR015i005p01250.
- Seager, R., Naik, N., and Vecchi, G. A. (2010). Thermodynamic and Dynamic Mechanisms for Large-Scale Changes in the Hydrological Cycle in Response to Global Warming*. *Journal of Climate*, 23(17):4651–4668, doi:http://dx.doi.org/10.1175/2010JCLI3655.1.
- Seibert, P. (2001). Inverse Modelling with a Lagrangian Particle Dispersion Model: Application to Point Releases Over Limited Time Intervals. In *Air Pollution Modeling and its Application XIV*, pages 381–389. Springer, doi:10.1007/0-306-47460-3_38.

REFERENCES

- Seibert, P. and Frank, A. (2004). Source-receptor matrix calculation with a Lagrangian particle dispersion model in backward mode. *Atmospheric Chemistry and Physics*, 4(1):51–63, doi:10.5194/acp-4-51-2004.
- Smith, T. M., Reynolds, R. W., Peterson, T. C., and Lawrimore, J. (2008). Improvements to NOAA's historical merged land-ocean surface temperature analysis (1880-2006). *Journal of Climate*, 21(10):2283–2296, doi:http://dx.doi.org/10.1175/2007JCLI2100.1.
- Starr, V. P. and Peixoto, J. P. (1958). On the global balance of water vapor and the hydrology of deserts. *Tellus*, 10(2):188–194, doi:10.1111/j.2153-3490.1958.tb02004.x.
- Stohl, A., Cooper, O., Damoah, R., Fehsenfeld, F., Forster, C., Hsie, E.-Y., Hübler, G., Parrish, D., and Trainer, M. (2004). Forecasting for a Lagrangian aircraft campaign. *Atmospheric Chemistry and Physics Discussions, European Geosciences Union (EGU)*, 4(3):2405–2433.
- Stohl, A., Forster, C., Frank, A., Seibert, P., and Wotawa, G. (2005). Technical note: The Lagrangian particle dispersion model FLEXPART version 6.2. *Atmospheric Chemistry and Physics*, 5(9):2461–2474, doi:10.5194/acp-5-2461-2005.
- Stohl, A., Forster, C., and Sodemann, H. (2008). Remote sources of water vapor forming precipitation on the Norwegian west coast at 60°N—a tale of hurricanes and an atmospheric river. *Journal of Geophysical Research*, 113(D05102), doi:10.1029/2007JD009006.
- Stohl, A., Hittenberger, M., and Wotawa, G. (1998). Validation of the Lagrangian particle dispersion model FLEXPART against large-scale tracer experiment data. *Atmospheric Environment*, 32(24):4245–4264, doi:10.1016/S1352-2310(98)00184-8.
- Stohl, A. and James, P. (2004). A Lagrangian analysis of the atmospheric branch of the global water cycle. Part I: Method description, validation, and demonstration for the August 2002 flooding in central Europe. *Journal of Hydrometeorology*, 5(4):656–678, doi:http://dx.doi.org/10.1175/1525-7541(2004)005<0656:ALAOTA>2.0.CO;2.

REFERENCES

- Stohl, A. and James, P. (2005). A Lagrangian analysis of the atmospheric branch of the global water cycle. Part II: Moisture transports between Earth's ocean basins and river catchments. *Journal of Hydrometeorology*, 6:961–984, doi:http://dx.doi.org/10.1175/JHM470.1.
- Stohl, A. and Thomson, D. J. (1999). A density correction for Lagrangian particle dispersion models. *Boundary-Layer Meteorology*, 90(1):155–167, doi:10.1023/A:1001741110696.
- Stohl, A., Wotawa, G., Seibert, P., and Kromp-Kolb, H. (1995). Interpolation errors in wind fields as a function of spatial and temporal resolution and their impact on different types of kinematic trajectories. *Journal of Applied Meteorology*, 34(10):2149–2165, doi:http://dx.doi.org/10.1175/1520-0450(1995)034<2149:IEIWFA>2.0.CO;2.
- Sun, B. and Wang, H. (2014). Moisture sources of semiarid grassland in China using the Lagrangian particle model FLEXPART. *Journal of Climate*, 27(6):2457–2474, doi:http://dx.doi.org/10.1175/JCLI-D-13-00517.1.
- Thompson, D. W. and Wallace, J. M. (2000). Annular modes in the extratropical circulation. Part I: Month-to-month variability*. *Journal of Climate*, 13(5):1000–1016, doi:http://dx.doi.org/10.1175/1520-0442(2000)013<1000:AMITEC>2.0.CO;2.
- Trenberth, K. E., Fasullo, J. T., and Mackaro, J. (2011). Atmospheric moisture transports from ocean to land and global energy flows in reanalyses. *Journal of Climate*, 24(18):4907–4924, doi:http://dx.doi.org/10.1175/2011JCLI4171.1.
- Trenberth, K. E. and Guillemot, C. J. (1998). Evaluation of the atmospheric moisture and hydrological cycle in the NCEP/NCAR reanalyses. *Climate Dynamics*, 14(3):213–231, doi:10.1007/s003820050219.
- Uppala, S. M., Kållberg, P., Simmons, A., Andrae, U., Bechtold, V., Fiorino, M., Gibson, J., Haseler, J., Hernandez, A., Kelly, G., et al. (2005). The ERA-40 reanalysis. *Quarterly Journal of the Royal Meteorological Society*, 131(612):2961–3012, doi:10.1256/qj.04.176.
- Visbeck, M. (2009). A station-based southern annular mode index from 1884 to 2005. *Journal of Climate*, 22(4):940–950, doi:http://dx.doi.org/10.1175/2008JCLI2260.1.

REFERENCES

- Viste, E. and Sorteberg, A. (2013). Moisture transport into the Ethiopian highlands. *International Journal of Climatology*, 33(1):249–263, doi:10.1002/joc.3409.
- Wei, J., Dirmeyer, P. A., Bosilovich, M. G., and Wu, R. (2012). Water vapor sources for Yangtze River Valley rainfall: Climatology, variability, and implications for rainfall forecasting. *Journal of Geophysical Research*, 117(D05126), doi:10.1029/2011JD016902.
- Wernli, H. (1997). A lagrangian-based analysis of extratropical cyclones, II: A detailed case study. *Quarterly Journal of the Royal Meteorological Society*, 123(542):1677–1706, doi:10.1002/qj.49712354211.

Declaration

I herewith declare that I have produced this work without the prohibited assistance of third parties and without making use of aids other than those specified; notions taken over directly or indirectly from other sources have been identified as such. This work has not previously been presented in identical or similar form to any examination board.

The dissertation work was conducted from September 2011 to January 2015 under the supervision of Raquel Olalla Nieto Muñiz PhD and Luis Gimeno Presa PhD at the University of Vigo.

Ourense,



This dissertation was finished writing in Ourense on Thursday 22nd January, 2015

